

THE UNIVERSITY OF MICHIGAN
INDUSTRY PROGRAM OF THE COLLEGE OF ENGINEERING

HEAT AND MASS TRANSFER IN CLOSED, VERTICAL, CYLINDRICAL
VESSELS WITH INTERNAL HEAT SOURCES FOR
HOMOGENEOUS NUCLEAR REACTORS

Frederick G. Hammitt

This dissertation was submitted in partial fulfillment of the requirements for the degree of Doctor of Philosophy in the University of Michigan, 1958.

December, 1957

IP-259

ACKNOWLEDGEMENTS

I would like to acknowledge with sincere thanks the guidance and helpful suggestions of the members of the doctoral committee in the formulation and the conducting of the work upon which this dissertation is based. I would like to thank especially Dr. H. A. Ohlgren, chairman of the doctoral committee, for his many suggestions and unfailing encouragement and enthusiasm. I also want to express my gratitude to the other committee members: Professors R.C.F. Bartels, R. G. Folsom, H. J. Gomberg, and J. S. McNown, and Associate Professors D. V. Ragone and C. S. Yih.

I would also like to thank Mr. Bruce Arden, Research Associate, for his advice and guidance in programming the theoretical solution for the digital computer.

I would also like to acknowledge sincerely the advice and helpful suggestions of my various colleagues in the Engineering Research Institute projects associated with this investigation: Messrs. A. Anderson, E. M. Brower, A. E. Brown, P. Chu, Wm. Claucherty, R. P. Hanson, Y. Hwang, and K. Zyber.

I want to thank the Industry Program of The University of Michigan for its assistance in the reproduction of this thesis. I would also like to acknowledge with thanks the financial assistance of the Chrysler Corporation in the procurement of the research facilities which were utilized for the study.

Finally I owe sincere appreciation to my wife and family for their moral support and patience with my scholastic efforts during the past several years, and also assistance in the preparation of this thesis.

TABLE OF CONTENTS

	<u>Page</u>
ACKNOWLEDGMENTS.....	ii
LIST OF TABLES.....	vi
LIST OF FIGURES.....	vii
NOMENCLATURE.....	xiii
CHAPTER	
I. INTRODUCTION.....	1
Application to Nuclear Reactors.....	1
Scope of Present Investigation.....	3
II. REVIEW OF LITERATURE.....	5
Applicable Analytical Studies.....	6
Flat Plate Solutions (With and Without Heat Source).....	6
Closed Tubes Without Internal Heat Source.....	6
Closed Tubes With Internal Heat Source.....	7
Applicability of Previous Studies to Present Case.....	7
Applicable Experimental Investigations.....	8
Flat Plate Investigations.....	8
Closed Tubes Without Internal Heat Source.....	9
Closed Tubes With Internal Heat Source.....	9
Vertical Channel Experiments with Internal Heat Source.....	10
Applicability of Previous Experimental Investigations to Present Study.....	11
III. EXPERIMENTAL FACILITIES.....	13
General Requirements.....	13
Types of Research Facilities Constructed.....	14
Parameters Controlled.....	16
Required Measurements.....	17
Description of Facilities.....	19
Air-Cooled Facilities.....	19
Water-Cooled Facility.....	25
General Operation of Facilities.....	36
Modes of Operation.....	36

TABLE OF CONTENTS CONT'D

	<u>Page</u>
IV. RESULTS OF EXPERIMENTAL PROGRAM.....	61
General Expectations.....	61
General Character of Flow From Experimental Observations.....	62
Measured Flow Behavior From Experimental Runs.....	66
Boundary Layer Effect.....	66
Axial Temperature Gradients.....	74
Radial Temperature Gradients.....	89
Wall Conduction Heat Flux Distributions.....	91
Velocity Measurements.....	97
Overall Temperature Differential, Heat Source Relations.....	101
Effects of Length to Diameter Ratio and Absolute Dimensions of Test Section.....	107
Summarization of Experimental Runs.....	108
V. ANALYTICAL APPROACH.....	111
General Scope of Analysis.....	111
Analysis of Problem.....	113
Lighthill Approach.....	113
Modification for Volumetric Heat Source and Arbitrary Axial Wall Temperature Distribution..	117
Difference Equations for Arbitrary Wall Temper- ature and Heat Source Axial Distributions.....	122
Calculating Procedure.....	125
Digital Computer Program.....	125
VI. RESULTS OF THEORETICAL ANALYSIS.....	131
Configurations Covered by Theoretical Analysis.....	131
Lighthill Analogy.....	132
Linearly Variable Axial Wall Temperature, Uniform Heat Source.....	133
Parabolic Variable Axial Wall Temperature, Uniform Heat Source.....	134
Summarization of Theoretical Configurations.....	135
Detailed Results of Calculations.....	135
Boundary Layer Thickness.....	136
Axial Temperature Gradients in Fluid.....	142
Radial Temperature Differentials.....	146
Wall Conduction Heat Flux Distribution.....	150
Velocity Profiles and Magnitudes.....	162

TABLE OF CONTENTS CONT'D

	<u>Page</u>
VII. COMPARISON BETWEEN THEORETICAL AND EXPERIMENTAL RESULTS.	181
Possible Causes for Discrepancies Between Theoretical and Experimental Results.....	181
Effect of Turbulence.....	181
Assumption of Axial Symmetry.....	183
Effect of Center Probe.....	183
Effect of End-Section Heat Losses.....	185
Effect of Experimental and Theoretical Inaccuracies.....	186
Theoretical Considerations.....	188
Detailed Comparisons Between Experimental and Theoretical Data.....	189
Radial Temperature Profiles (Boundary Layer Behavior).....	191
Axial Temperature Profiles.....	192
Normalized Wall Conduction Heat Flux.....	193
Velocity Magnitudes.....	194
Summarization of Comparisons Between Experiment and Theory.....	195
VIII. METHODS OF SOLUTION FOR OVERALL PROBLEM.....	197
Statement of Overall Problem.....	197
General Method of Solution.....	198
Specific Examples.....	199
Non-Infinite Coolant Flow Rates; Co-Flow and Counter-Flow.....	200
Constant Wall Heat Flux.....	203
Approximate, Simplified Relations.....	204
IX. RECOMMENDED SUBSEQUENT INVESTIGATIONS.....	207
X. CONCLUSIONS.....	209
APPENDIX.....	213
BIBLIOGRAPHY.....	225

LIST OF TABLES

<u>Table</u>		<u>Page</u>
I	Summarization of Experimental Run Characteristics....	110
II	Approximate Relationships for Natural Convection Flow in Closed Vertical Cylinder with Internal Heat Genera- tion - Aqueous Fluids.....	205
A-I	Calculation Summary Sheet - Constant Wall Tempera- ture.....	218
A-II	Calculation Summary Sheet - Variable Wall Tempera- ture, Uniform q_v	219
A-III	Calculation Summary Sheet - Variable Wall Tempera- ture, Uniform q_v , Concluded.....	220
A-IV	Experimental Data Summary Sheet I, Water-Cooled Full Length Run.....	221
A-V	Experimental Data Summary Sheet II, Water-Cooled Reduced Length Runs.....	222
A-VI	Experimental Data Summary Sheet III, Water-Cooled Reduced Length and AEC Runs.....	223
A-VII	Experimental Data Summary Sheet IV,- Air-Cooled Runs.	224

LIST OF FIGURES

<u>Figure</u>		<u>Page</u>
1	Photograph of Preliminary Air-Cooled Facility.....	20
2	Photograph of Final Air-Cooled Facility.....	22
3	Photograph of Thermocouple Rod and Dye Injector for Air-Cooled Facility.....	23
4	Photograph of Water-Cooled Facility, Preliminary Arrangement.....	26
5	Photograph of Final Water-Cooled Facility.....	27
6	Photograph of Final Water-Cooled Facility, Reduced Length Test Section.....	28
7	Layout Drawing of Water Facility.....	29
8	Photograph of Thermocouple Dye-Injection Head for Water-Cooled Facility.....	32
9-a	Solution Physical Properties, Normality vs. Concentration.....	43
9-b	Solution Physical Properties, Normality vs. Boiling Point Elevation.....	44
9-c	Solution Physical Properties, Normality vs. Specific Heat at 20°C.....	45
9-d	Solution Physical Properties, Density vs. Temperature	46
9-e	Solution Physical Properties, Viscosity vs. Temperature.....	47
9-f	Solution Physical Properties, Thermal Conductivity vs. Temperature.....	48
9-g	Solution Physical Properties, Prandtl Number vs. Temperature.....	49
9-h	Solution Physical Properties, Electrical Conduct- ivity vs. Temperature.....	50
10	Rotameter Calibration Curve.....	54

LIST OF FIGURES CONT'D

<u>Figure</u>		<u>Page</u>
11	Proportionate Voltage Drop vs. Non-Dimensional Axial Position - Experimental Data.....	58
12-a	Radial Temperature Distribution - Experimental Data..	68
12-b	Radial Temperature Distribution - Experimental Data..	69
12-c	Radial Temperature Distribution - Experimental Data..	70
13-a	Non-Dimensional Boundary Layer Thickness vs. Overall/Radial Temperature Ratio - Experimental and Calculated Data.....	72
13-b	Non-Dimensional Boundary Layer Thickness vs. Overall/Radial Temperature Ratio - Experimental and Calculated Data.....	73
14	Non-Dimensional Boundary Layer Thickness vs. Non-Dimensional Axial Position.....	75
15-a	Non-Dimensional Wall Temperature vs. Overall/Radial Temperature Ratio, Experimental Data, $x/l = 0.25$	77
15-b	Non-Dimensional Wall Temperature vs. Overall/Radial Temperature Ratio, Experimental Data, $x/l = 0.50$	78
15-c	Non-Dimensional Wall Temperature vs. Overall/Radial Temperature Ratio, Experimental Data, $x/l = 0.75$	79
16-a	Non-Dimensional Centerline Temperature vs. Overall/Radial Temperature Ratio, Experimental Data, $x/l = 0.25$	82
16-b	Non-Dimensional Centerline Temperature vs. Overall/Radial Temperature Ratio, Experimental Data, $x/l = 0.50$	83
16-c	Non-Dimensional Centerline Temperature vs. Overall/Radial Temperature Ratio, Experimental Data, $x/l = 0.75$	84
17	Non-Dimensional Wall Temperature vs. Non-Dimensional Axial Position, Experimental Data.....	85

LIST OF FIGURES CONT'D

<u>Figure</u>		<u>Page</u>
18	Normalized Non-Dimensional Wall Temperature vs. Non-Dimensional Axial Position, Experimental Data....	86
19-a	Non-Dimensional Centerline Temperature vs. Non-Dimensional Axial Position, Experimental Data Compared to Linear and Parabolic Wall Temperature Distribution, $q_v \cong 10^8$	87
19-b	Non-Dimensional Centerline Temperature vs. Non-Dimensional Axial Position, Experimental Data Compared to Linear and Parabolic Wall Temperature Distribution, $q_v \cong 10^9$	88
20	Non-Dimensional Temperature Differential Centerline to Wall vs. Non-Dimensional Axial Position.....	90
21	Non-Dimensional Radial Temperature Profiles, Calculated Data, Constant Wall Temperature, Uniform q_v	92
22	Normalized Wall Conduction vs. Overall/Radial Temperature Ratio, Experimental Data.....	95
23	Non-Dimensional Boundary Layer and Core Velocity vs. Non-Dimensional Heat Source, Comparison of Experimental and Calculated Data.....	96
24	Non-Dimensional Overall Temperature Difference vs. Overall/Radial Temperature Ratio, Experimental Data..	103
25	Assumed Temperature and Velocity Profiles for Theoretical Analysis.....	115
26	Schematic Representation of Test Section as Used for Theoretical Analysis.....	116
27	Core Temperature Gradient Control Volume, Theoretical Analysis.....	121
28-a	Non-Dimensional Boundary Layer Thickness vs. Non-Dimensional Axial Position, Constant Wall Temperature Uniform Heat Source, Calculated Data.....	137
28-b	Non-Dimensional Boundary Layer Thickness vs. Non-Dimensional Axial Position, Comparison of Various Axial Heat Source Distributions, Calculated Data.....	140

LIST OF FIGURES CONT'D

<u>Figure</u>		<u>Page</u>
28-c	Non-Dimensional Boundary Layer Thickness vs. Non-Dimensional Axial Position, Uniform Heat Source Distribution, Linear and Parabolic, Calculated Data..	141
29-a	Non-Dimensional Centerline Temperature Distribution vs. Non-Dimensional Axial Position, Uniform q_v , Constant Wall Temperature, Calculated Data.....	143
29-b	Non-Dimensional Centerline Temperature Distribution vs. Non-Dimensional Axial Position, Constant Wall Temperature, Various Axial Heat Source Distributions.	145
29-c	Non-Dimensional Centerline Temperature Distribution vs. Non-Dimensional Axial Position, Uniform $q_v = 1 \times 10^6$ Variable, Linear Distribution of Overall/Radial Temperature Ratio, Calculated Data.....	147
29-d	Non-Dimensional Centerline Temperature Distribution vs. Non-Dimensional Axial Position, Uniform $q_v = 4 \times 10^7$, Variable, Linear Distribution of Overall/Radial Temperature Ratio, Calculated Data....	148
29-e	Non-Dimensional Centerline Temperature Distribution vs. Non-Dimensional Axial Position, Uniform $q_v = 2 \times 10^9$, Temperature Ratio, Calculated Data.....	149
30-a	Non-Dimensional Temperature Differential Centerline to Wall vs. Non-Dimensional Axial Position, $q_v = 1 \times 10^6$, Uniform, Calculated Data.....	151
30-b	Non-Dimensional Temperature Differential Centerline to Wall Vs. Non-Dimensional Axial Position, $q_v = 4 \times 10^7$, Uniform, Calculated Data.....	152
30-c	Non-Dimensional Temperature Differential Centerline to Wall vs. Non-Dimensional Axial Position, $q_v = 2 \times 10^9$, Uniform, Calculated Data.....	153
31	Normalized Wall Conduction vs. Overall/Radial Temperature Ratio, Linear Wall Temperature Distribution, Uniform Heat Source, Calculated Data.....	154
32-a	Normalized Wall Conduction vs. Non-Dimensional Axial Position, Constant Wall Temperature, Uniform Heat Source Distribution.....	155

LIST OF FIGURES CONT'D

<u>Figure</u>		<u>Page</u>
32-b	Normalized Wall Conduction vs. Non-Dimensional Axial Position, Constant Wall Temperature, Variable Axial Heat Source Distribution.....	156
32-c	Normalized Wall Conduction vs. Non-Dimensional Axial Position, Linear Wall Temperature Distribution, Uniform Heat Source.....	157
32-d	Normalized Wall Conduction vs. Non-Dimensional Axial Position, Linear and Parabolic Wall Temperature Distribution Comparison, Calculated and Experimental Data Comparison, Uniform Heat Source.....	158
33-a	Non-Dimensional Core and Boundary Layer Velocity vs. Non-Dimensional Axial Position, Uniform q_v , Constant Wall Temperature, Calculated Data.....	163
33-b	Non-Dimensional Core and Boundary Layer Velocity vs. Non-Dimensional Axial Position, Uniform q_v , Constant Wall Temperature, Calculated Data.....	164
33-c	Non-Dimensional Core and Boundary Layer Velocity vs. Non-Dimensional Axial Position, Various Axial q_v Distributions ($\bar{q}_v = 4 \times 10^7$), Constant Wall Temperature, Calculated Data.....	165
33-d	Non-Dimensional Core and Boundary Layer Velocity vs. Non-Dimensional Axial Position, Constant Wall Temperature, Calculated Data.....	166
33-e	Non-Dimensional Core and Boundary Layer Velocity vs. Non-Dimensional Variable Linear Distribution of Overall/Radial Temperature Ratio, Uniform $q_v = 1 \times 10^6$, Calculated Data.....	167
33-f	Non-Dimensional Core and Boundary Layer Velocity vs. Non-Dimensional Axial Position, Variable Linear Distribution of Overall/Radial Temperature Ratio, Uniform $q_v = 4 \times 10^7$, Calculated Data.....	168
33-g	Non-Dimensional Core and Boundary Layer Velocity vs. Non-Dimensional Axial Position, Variable Linear Distribution of Overall/Radial Temperature Ratio, Uniform $q_v = 2 \times 10^9$, Calculated Data.....	169

LIST OF FIGURES CONT'D

<u>Figure</u>		<u>Page</u>
34	Non-Dimensional Temperature Difference vs. Overall/ Radial Temperature Ratio, Linear Wall Temperature Distribution, Calculated Data.....	176
35	Non-Dimensional Heat Source vs. Non-Dimensional Overall Temperature Differential.....	177
36	Nusselt's Number vs. Non-Dimensional Heat Source, Experimental and Calculated Data.....	178
37	Test Section Nomenclature Schematic Diagram.....	211

NOMENCLATURE

T	Temperature
U	Dimensional velocity in axial direction
u	Non-Dimensional velocity in axial direction = $\frac{a^2}{\nu \kappa l} U$
X,x	Dimensional and non-dimensional coordinate in axial direction
R,r	Dimensional and non-dimensional coordinate in radial direction
l,a	Length and radius of tube
ρ	Density
c_v	Specific heat
k	Thermal conductivity
κ	Thermal diffusivity, $\kappa = k/\rho c_v$
ν	Kinematic viscosity
A_s	Area of tube wall
t	Non-dimensional temperature differential = $\frac{\alpha g a^4 \Delta T}{\nu \kappa l}$; particularly non-dimensional temperature difference between wall and fluid at any given axial position. Subscript o applies to top of tube at centerline. Subscript c applies to centerline (or core) in general.
t_w	Non-dimensional temperature differential between top and bottom of wall
$t_{\mathcal{L}o} = t_o + t_{w_o}$	Maximum non-dimensional temperature differential in the system = $Ra \cdot \frac{a}{l}$
$t_{\mathcal{L}}$	Non-dimensional temperature differential between fluid at centerline and wall at bottom

- Ra_a Rayleigh Number based on radius and maximum temperature differential = $\frac{\alpha g a^3 (T_{wall_{min}} - T_{fluid_{max}})}{\nu \kappa}$
- q_v Non-dimensional volumetric heat source = $\frac{Q_v a^6 \alpha g}{\rho \nu \kappa^2 l c_v}$
- Nu_a Nusselt Number based on radius = $\frac{h a}{k}$
- g Acceleration of gravity
- α Coefficient of volumetric expansion
- β Non-dimensional core thickness, $1-\beta$ is the non-dimensional boundary layer thickness and βR is the radius at which the boundary layer is terminated. See Figures 25 and 27.
- γ, γ' ,
- $F(\beta), G(\beta)$ Non-dimensional functions defined in text
- h Film coefficient for heat transfer

CHAPTER I

INTRODUCTION

The phenomenon of natural convection heat and mass transfer within closed vessels wherein the heat is generated internal to the fluid and removed through coolant passages surrounding or within the fluid vessel has assumed increasing importance recently in connection with homogeneous nuclear reactors. In such a case, the heat would be generated as a result of fissioning uranium or plutonium dissolved in aqueous or other fluids (such as liquid metals). The heat would be removed to the coolant and used as heat source for a heat engine cycle. The general natural convection phenomenon within closed vessels without internal heat generation is of considerable importance in numerous applications although to the present time it has not received extensive attention.

Application to Nuclear Reactors

The present investigation into natural convection flow within closed vessels wherein the heat is generated internal to the fluid was undertaken as a preliminary attempt to shed some light upon the mass and heat transfer phenomenon which might be expected to occur within a homogeneous nuclear reactor. Such reactors can be of several types. They can employ fluids either of the aqueous or molten metal type to suspend the fissile material either in solution or as a slurry. Also they can be internally cooled; i.e., the heat removed directly from the core by a suitable coolant fluid flowing through coolant passages within and/or surrounding the core; or they can employ a circulating system whereby the fissile material bearing fluid is pumped through a closed loop including

a heat exchanger which is external to the reactor core. In the case of internal cooling, it is conceivable that the fissioning fluid be contained within closed vessels surrounded by coolant or the coolant can be contained in tubes and the fuel in the surrounding space. In all cases, the reactor coolant will exchange heat with a heat engine system, either directly or through an intermediate loop arrangement.

For any combination of these arrangements, it becomes of extreme importance to obtain some knowledge of the velocity and temperature regimes within the reacting fluid. In those cases where the convection phenomenon replaces pure conduction to an appreciable extent, it appears likely that the temperature profiles within the fluid will be substantially altered, the maximum fluid temperature significantly changed, and the distribution of heat flux through the heat transfer surfaces affected as compared with the case of pure conduction. In addition there may be appreciable macroscopic fluid velocities which could, with the large temperature differences to be expected, cause a mass transport cycle from hot to cold regions and also possible velocity erosion of the heat transfer surfaces. The disposition of the gaseous fission products which will be formed during reactor operation will be affected by these velocities. This may involve their mode of evolution into bubbles if turbulence and vortices are created as well as their removal as possible films from the heat transfer surfaces. It may also grossly affect their distribution within the core as compared to the case where static diffusion would control.

In addition to the primary effects of the natural convection heat and mass transport mentioned above there may be an appreciable feed-back into the nuclear parameters in that local fluid density and

temperature will be altered from the static case. Also the possible appearance and motion of fission gas bubbles could seriously affect reactor operation and stability.

It is conceivable that such gases "plate out" to form continuous films over significant portions of the heat transfer surface causing an overloading of the unaffected sections with consequent rise of fuel temperature, consequent tube burn-out, and possible local nuclear reactivity effects due to the increased fuel temperatures. It is also possible that the moving voids created by the bubbles could affect nuclear reactivity and stability.

For all these reasons it appears most desirable that some understanding of the heat and mass flow phenomena be gained for those cases where natural convection or a combination of forced and natural convection obtain.

Scope of Present Investigation

The scope of the present investigation is a detailed examination of natural convection heat and mass transfer in a closed, vertical cylindrical vessel containing a fluid with Prandtl Number of the order of unity (i.e., aqueous fluids) wherein the heat is generated internal to the fluid (as with fissioning material in solution). As explained in detail in later sections, a further restriction is that the combination of volumetric heat source and length to diameter ratio as expressed by the non-dimensional heat source parameter, q_v , (see Nomenclature) be large. This range of heat source parameter was chosen for the investigation because it was believed to include the area of interest from the viewpoint of nuclear power reactors, where presumably the heat source density is very large.

The present investigation has been restricted to this particular geometry and type of fluid because it appeared to represent approximately the maximum degree of complication which would allow of mathematical treatment and was at the same time reasonably realistic and typical of the possible nuclear applications. It is anticipated that a basic understanding of the phenomena under these conditions, which may be attained as a result of this study, can be used to form order of magnitude estimates of the phenomena under more complicated conditions of geometry and fluid physical properties. Additional investigations, building upon the basis here obtained, can be conducted to broaden the scope of the experimental and analytical studies.

At the initiation of the present investigations, information regarding even the general nature of the velocity and temperature regimes to be anticipated was virtually non-existent. Consequently, a very broad approach was necessary to determine the existence of any correlation between a theory, which was to be originated, and experiment. It is felt that a very meritorious subsequent investigation would be the more precise determination of the degree of this correlation.

CHAPTER II

REVIEW OF LITERATURE

Up to the present time, there has been a very considerable number of investigations of natural convection heat and mass transfer under different conditions of geometry and different system arrangements. These have been both analytical and experimental in nature. In general these investigations have not considered an internal heat source or a closed vessel wherein the end effects play a substantial role. Due to the nature of the phenomenon of natural convection heat and mass transfer, the geometrical arrangement and the type of system exert a profound influence so that it is very difficult to estimate realistically the effects to be expected in an untried system from those found in a different system previously tested. This situation arises from the extremely complicated mathematics which are involved and the fact that it is necessary to make very restrictive simplifying assumptions in order to make mathematical treatment at all feasible. For this reason the solutions which are derived for a particular case are not readily transferrable to any other case where there are differences of geometry or system arrangement with respect to the manner of heating and cooling or system physical parameters. An extensive literature survey has indicated, however, that there are several previous analytical and/or experimental investigations reported in the literature which do have a bearing on the present study.

Applicable Analytical Studies

Flat Plate Solutions (Without and With Heat Source)

The case which is apparently most amenable to mathematical treatment and which has consequently received the most attention is that of a flat plate immersed in an infinite fluid and maintained at a temperature either above or below that of the fluid. The resulting flow is of the boundary layer type, either ascending or descending, depending upon whether the plate is heated or cooled. The laminar flow equations for this case have been solved in series by Pohlhausen for air (Prandtl Number = 0.733). The experiments of Schmidt and Beckmann⁽¹⁾ and later those of Saunders⁽²⁾ gave excellent agreement. Both sets of experiments involved flat plates in an infinite fluid. The work of Saunders involved turbulent boundary layer conditions and showed a substantial increase of heat transfer over the laminar calculations.

More recently, Ostrach⁽³⁾ has carried through the calculations for the flat plate in an infinite fluid for fluids of Prandtl Number ranging from 1000 to 0.01 using numerical solutions with high-speed digital computers. It is thus possible to form some idea of the effect of a Prandtl Number varying substantially from unity. In addition Ostrach has examined the case of two parallel vertical plates in an infinite sea of fluid with and without heat sources in the fluid with both constant and variable wall temperature, again using approximate numerical methods^(4,5).

Closed Tubes Without Internal Heat Source

The case of a tube, closed at one end and open at the other to an infinite fluid reservoir, where the tube walls are maintained at a constant temperature either greater than, or less than, the infinite

reservoir temperature is examined analytically by Lighthill⁽⁶⁾. No volumetric heat source is assumed. The case of a tube closed at both ends wherein the walls of one half are heated and those of the other half (axially) are cooled is also studied in the same paper. No attempt to include internal heat sources or variable wall temperature is made. The application which motivated this study was the liquid cooling of turbine blades rather than nuclear powerplants.

In a subsequent paper, Ostrach⁽⁷⁾ examines a geometrically similar case in which a constant wall temperature gradient is assumed.

Closed Tubes with Internal Heat Source

An analytical study of a vertical, closed tube with internal heat sources has been made by Murgatroyd⁽⁸⁾. This study covered fluids of Prandtl Number near unity (as aqueous fluids) and also very small Prandtl Number (as liquid metals), and considered laminar as well as turbulent conditions. Hence, the conditions of the study are quite close to those of the present instance except that the vessel considered by Murgatroyd is one of very large length to diameter ratio so that it is assumed that conditions do not change as a function of axial position. Thus, no consideration is made of the end effects. It was felt that these were essential to a realistic investigation as applied to homogeneous nuclear power reactors and, therefore, the Murgatroyd analysis could not be directly applied.

Applicability of Previous Studies to Present Case

The previous analytical studies of natural convection heat and mass transfer which appear to have some application to the present investigation have been listed in the previous sections. These are of

extreme value to the present study in that they lay the groundwork for the methods which were employed in the analysis. However, none are directly applicable since in all cases there are significant differences between the geometries and systems which were studied and that which is presently under investigation. As explained later, the methods used by Lighthill were expanded and adapted to the present purpose.

Applicable Experimental Investigations

A great variety of experimental studies have been made upon natural convection heat and mass transfer phenomena. However, the greatest number of these have been concerned with specialized geometrical configurations which were in general not tractable to mathematical analysis.. As a result the data cannot be meaningfully extrapolated to other geometrical arrangements or differing system and/or fluid property arrangements. There are, however, some previous experimental investigations which are very helpful in the present context.

Flat Plate Investigations

It has been previously mentioned that the experiments of Schmidt and Beckmann⁽¹⁾ and also those of Saunders⁽²⁾, both involving experimental studies of flat plates, either heated or cooled and maintained at constant temperature when immersed in an infinite sea of fluid, showed excellent agreement with the theoretical predictions of Pohlhausen and later Ostrach⁽³⁾. The Schmidt and Beckmann experiments were concerned with laminar conditions while those of Saunders involved also turbulent conditions. The theoretical work of Pohlhausen and Ostrach were upon laminar conditions. As might be expected, it was found by

Saunders that the heat transfer was considerably improved over the laminar expectations when turbulence was present.

Closed Tubes Without Internal Heat Source

As previously mentioned the case of a vertical tube, open at one end to an infinite reservoir or fluid and closed at the other, with walls maintained at constant temperature, either above or below that of the infinite reservoir was examined on theoretical grounds by Lighthill⁽⁶⁾. If the walls were cooled, then the top end of the tube would be closed and vice versa. Martin⁽⁹⁾ conducted a subsequent experimental study to attempt to validate the theoretical findings of Lighthill for this particular configuration. The order of magnitude agreement between experiment and theory in this instance was good although there were some deviations in detail. The types of flow regimes which were predicted by Lighthill (these will be discussed in great detail in a later section of this report) were confirmed. However, it was found that the heat transfer coefficients appeared to exceed those predicted by Lighthill by a factor of about 2.

Whether boundary layer was laminar or turbulent in these tests is uncertain. Incidentally, this excess of experimental over theoretical anticipation agrees with the results of the present study.

Closed Tubes With Internal Heat Source

A brief experimental investigation carried out by Haas and Langsdon⁽¹⁰⁾ under the sponsorship of the Atomic Energy Commission at the Oak Ridge National Laboratory duplicated quite closely in configuration the experimental facility constructed for the present study. (This reference was unfortunately not discovered until near the conclusion

of the experimental work for this study). The AEC facility consisted of a vertical glass tube (24 inches in length and 6 inches diameter), closed at both ends, containing an aqueous electrolyte solution in which heat was generated by ohmic resistance. The heat was removed by an external forced convection water annulus. Temperature profiles within the vessel were measured with a glass thermocouple rod, pivoted at the top and capable of being raised or lowered with respect to the vessel. Velocities were observed in a semi-quantitative manner by timing the motion of particles. Only three runs were made at roughly the same power level with similar conditions of coolant flow rate and direction. Thus, effectively a single point is obtained which has been added to the data from the present study. Unfortunately no theoretical analysis has accompanied the experiments.

Vertical Channel Experiments With Internal Heat Source

Various experimental and analytical studies involving natural convection heat and mass transfer in fluids having a volume heat source have been conducted at the Oak Ridge National Laboratory^(11,12,13). These have been concerned primarily with configurations involving one or more vertical flat plates, of large dimensions with respect to the distance between plates, so that the end effects are not considered. Internal heat generation was included, again using the ohmic resistance of aqueous solutions. The results obtained are not of primary interest in the present context since the end effects were not generally included. Interesting analytical solutions were obtained in some cases for specialized configurations including a constant axial gradient of wall temperature.

Applicability of Previous Experimental Investigations to Present Study

All of the previous experimental studies of natural convection heat and mass transfer which are mentioned in the preceding sections are of interest in connection with the present investigations in that they indicate applicable overall trends, suitable dimensionless parameters, types of experimental equipment, etc. However, only the experimental results from the AEC runs mentioned under "Closed Tubes With Internal Heat Source" are of direct application. The results obtained by Martin⁽⁹⁾ are also of interest since they apply to the Lighthill model of a tube open to an infinite reservoir at one end and closed at the other. As is explained later in this report, this is a special case of that with internal heat source, in that effectively it is analogous to an internal heat source supplied in an infinitely thin flat plate distribution (normal to the centerline) at the open end of the vessel.

CHAPTER III

EXPERIMENTAL FACILITIES

General Requirements

The primary objective of the present research is investigation of the natural convection heat and mass transfer phenomenon particularly as it applies to homogeneous nuclear power reactors. The scope of the investigation was limited to the investigation of the phenomenon in vertical, cylindrical passages, closed at both ends, with heat generation internal to the fluid and heat removed through an external cooling jacket. The fluids to be investigated were limited to those having a Prandtl Number of the order of unity (as aqueous solutions). Under these limitations it was desirable to design the equipment to duplicate as closely as feasible the conditions which might be expected within an aqueous, homogeneous power reactor core having internal heat transfer surface to a coolant. As is explained in later sections of this dissertation, analysis shows that the type of flow regime to be expected in a vertical closed tube, cooled through a surrounding annulus and heated by internal heat source, is controlled by a non-dimensional volumetric heat source parameter (here called q_v) which involves the volumetric heat source and also the dimensions of the vessel in such a way that a particular flow regime can be realized either through a large volumetric heat source or a small length to diameter ratio. The absolute magnitude of the tube radius is also of substantial importance; a large radius has an effect in the same direction as a large heat source rate. It is obvious that the rate of heat generation per unit volume to be expected in a nuclear power reactor is very large from conventional

standards. Consequently, it was felt that in general the range of interest would be that of large q_v even though the dimensions of passages within a reactor core might in some cases be small.

For the reasons cited in the preceding paragraph, it was felt that the design of the research facility should provide for large q_v . This could best be accomplished by utilizing as large a heat source generation rate as feasible, and providing a geometry of relatively small vessel length to diameter ratio and reasonably ample radius. This latter condition is also important from the viewpoint of adequate instrumentation capability. Since it appeared from the analysis that the flow regime should be uniquely controlled by the non-dimensional heat source parameter, it would be most desirable to obtain results under varying conditions of length to diameter ratio, absolute value of diameter, and also absolute volumetric heat source generation rate, but with q_v held constant.

Types of Research Facilities Constructed

It was decided to construct research facilities which provided the natural convection heat and mass transfer phenomenon within a closed-end, vertical, cylindrical vessel, with heat generated internal to a fluid of Prandtl Number of unity order and removed to an external coolant. The phenomenon should be produced with the non-dimensional heat source parameter sufficiently large to provide the type of flow regimes which might realistically be expected within the core of a homogeneous nuclear power reactor with internal cooling surface. In addition, the equipment should provide a maximum of flexibility to allow the widest variation of the significant parameters and the possible subsequent utilization of the equipment for related investigations. If

feasible, it was felt that these might include an eventual extension of the investigations into the field of liquid metals.

In order to obtain the required rates of internal heat generation, a system which offers a low external resistance to heat flow should be constructed. This implies the requirement of a forced-convection external jacket. Water, as a cooling medium in such a jacket, is used as a matter of convenience. A further requirement for the convenient study of the phenomenon is the ability to have visual observation. Thus, glass components are necessary. The maximum heat generation rate under steady-state conditions is fixed by the temperature gradient and radial thermal stresses across the glass. A facility of this general type was constructed.

In order to increase the scope of the investigation to lower values of the non-dimensional heat source parameter, q_v , and also to introduce a different type of wall cooling with the consequent changes in wall temperature distributions, a somewhat similar, but smaller air-cooled facility was also constructed. The construction of such a unit was especially attractive as a preliminary, low-cost facility for the testing of the instrumentation concepts and obtain some initial insight into the nature of the phenomenon.

In connection with the overall project, but beyond the scope of this dissertation, a liquid metal facility, similar in principle to the water-cooled aqueous facility mentioned in the preceding paragraphs, was also designed and constructed. The design envisioned the initial use of mercury as the test fluid, but was so arranged as to be suitable for bismuth or lead-bismuth alloys at temperatures up to 1000°F. This particular design is mentioned in the present report in that it influ-

enced significantly the design of the water-cooled aqueous facility which was used for this investigation. The aqueous facility was arranged in such a way that as many of the components as possible would be interchangeable between the aqueous and liquid metal facilities. In this way the aqueous tests could be regarded to some extent as preliminary testing of the type of equipment and instrumentation concepts preparatory to attempting similar tests with liquid metals. For this reason, the steel end-components of the aqueous facility were designed to be considerably heavier and more complicated than would have seemed necessary for a simple aqueous test. These particular components were visualized as eventually forming a portion of the liquid metal facility.

Parameters Controlled

The principal overall independent parameters controlled in the experimental investigation include

1. Non-dimensional heat source parameter, q_v
2. Distribution of non-dimensional heat source parameter
3. Distribution of wall temperatures
4. Heat flux through end sections
5. Vessel geometry
6. Physical properties of fluid

It is possible to maintain various constant levels of the non-dimensional heat source parameter under different conditions of the other independent parameters. For example, it is possible to vary the length to diameter ratio (and either length or diameter or both) of the test section and then to obtain some initial value of q_v by a suitable adjustment of the absolute volumetric heat source. It is also possible to

obtain different types of wall temperature distribution by changing from a forced-convection water coolant, as obtained in the water-cooled aqueous facility to a natural convection air coolant, as is obtained in the air-cooled facility. An additional change is effected if the direction of the coolant flow is reversed or the flow rate changed in the water-cooled facility. As will be explained in greater detail in later sections of this thesis, these different wall temperature distributions can be described in terms of the ratio of the temperature difference between the test section centerline at the top and the wall at the top, and the temperature difference between the top of the wall and the bottom of the wall. In addition, it is necessary to specify the type of gradient; i.e., linear, parabolic, etc.

It is also possible to maintain a constant non-dimensional heat source parameter for various fluid physical property conditions, even though the same aqueous solution be used for all the tests. This is possible through a variation of the temperature level which can be effected through an adjustment of the coolant flow rate. It thus seems most suitable that runs for constant values of non-dimensional heat source be made while the other parameters are varied. In this way it is possible to test the suitability of the analysis under a variety of different physical conditions, all leading to constant values of the non-dimensional parameter in terms of which some correlation between analysis and experiment should be possible.

Once the independent parameters described in the preceding paragraphs are set, the flow regime should theoretically be uniquely determined. In this case the dependent parameter is the non-dimensional

overall temperature difference, t_{ℓ_0} (see Nomenclature). This is related to the Rayleigh Number, the Prandtl Number, and the dimensions of the test section. As will be explained in later sections, the Nusselt's Number may be defined in terms of t_{ℓ_0} and q_v .

Consistent with the discussions of the above paragraphs, it seemed desirable that the facilities should be constructed in such a manner that constant q_v runs under varying conditions of the other independent parameters be possible.

Required Measurements

A list of the principal independent parameters is given in the last section. The principle dependent parameters are then non-dimensional temperature and/or Nusselt's Number. Additional dependent parameters which are of importance are the local wall temperatures, wall heat flux distribution, velocities, and condition of flow (laminar or turbulent).

It is desirable that the instrumentation be such that it is possible to measure all the dependent and independent variables which are of substantial importance. Included at the least are those listed in this and the preceding section. In order to determine the necessary quantities, it is required that the following measurements be made:

1. Temperature profiles within the fluid
2. Velocity magnitude, direction, and relative turbulence of flow throughout the test section
3. Wall heat flux including end sections
4. Heat input to the fluid and distribution thereof

From these measurements all the additional quantities which are required can be derived.

Description of Facilities

Two types of facilities were constructed. The initial facility utilized natural convection with atmospheric air as the coolant while the other used forced-convection water. Consequently, steady-state heat generation rates of considerably greater magnitude were possible in the second facility.

Air-Cooled Facility

The air-cooled facility, Figure 1, basically consisted of a vertical glass tube, closed at either end with suitable rubber stoppers, or other suitable closure, fitted with steel electrodes and provided with holes for the passage of the required instrumentation components. The length of the test section was a maximum of approximately 20 inches and the diameter $2\frac{5}{8}$ inches. Tests were conducted with the maximum length section as well as reduced length sections of approximately $\frac{2}{3}$ and $\frac{1}{3}$ of the original length.

The test fluid was an aqueous electrolyte with those physical properties of importance for heat transfer varying only by a negligible amount from ordinary water. Heat was generated within this fluid by the imposition of an alternating voltage along the axis so that an alternating current was induced within the electrolyte and heat generated according to the ohmic resistance of the solution. Under steady state conditions this heat was removed primarily by natural convection with the surrounding atmospheric air.

Heat input was measured electrically and controlled by means of a variable transformer.. No method for measuring the heat output of the facility to the air seemed feasible or necessary. It was possible

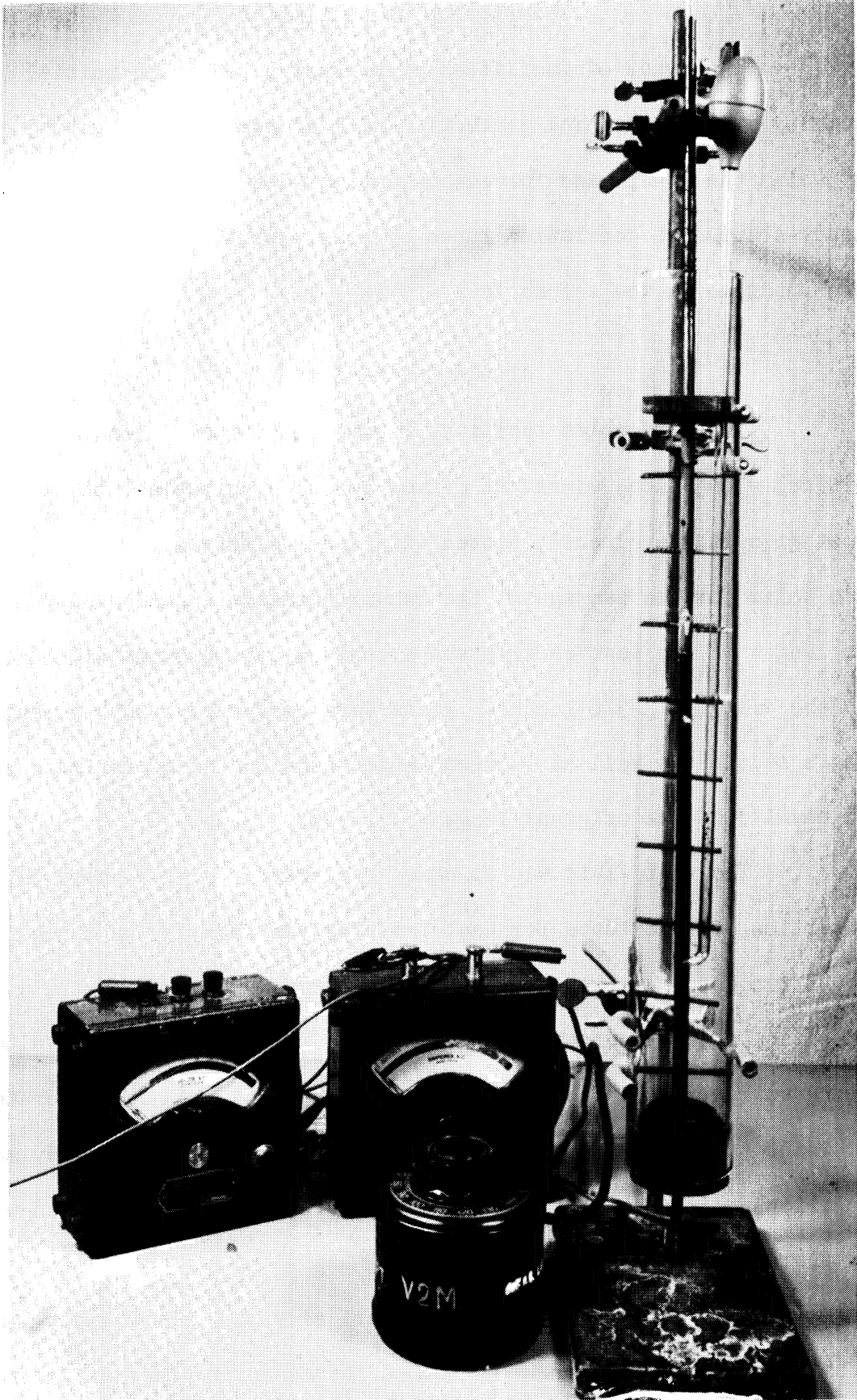


Figure 1. Photograph of Preliminary Air-Cooled Facility

to determine the relative values of heat conduction flux through the wall by noting the inside wall temperature and comparing with the outside wall or air temperature. In this connection it was found to be necessary to provide a tight seal at the top of the vessel to prevent evaporation heat loss which otherwise would account for a substantial (and relatively unknown) portion of the heat input. Figure 2 shows the facility revised with this additional feature. The sealing was accomplished by the substitution at the top of a rubber stopper for a wooden separator.

Internal temperature within the test section was measured with a glass "thermocouple rod"; i.e., a length of small bore glass tubing carrying thermocouple leads which terminate in a bead outside the glass (exposed to the fluid). The seal between glass and thermocouple rods was accomplished by fusing the glass around the wires and then in addition applying varnish to the joint. A typical "thermocouple rod" is shown in Figure 3.

In the initial arrangement, Figure 1, the position of the thermocouple bead within the fluid was determined by a "Christmas Tree" arrangement, consisting of a vertical wooden rod supporting horizontal "branches" at suitable intervals along the centerline. The branches were marked by threads at suitable distances from the wall. Close to the wall the intervals were of the order of $1/16$ inch. It was then possible to manually position the thermocouple bead at any desired elevation and distance from the wall.

In the subsequent arrangement, Figure 2, the thermocouple rod was positioned eccentrically with respect to the vessel centerline and maintained in a vertical position by a tight-fitting hole through the

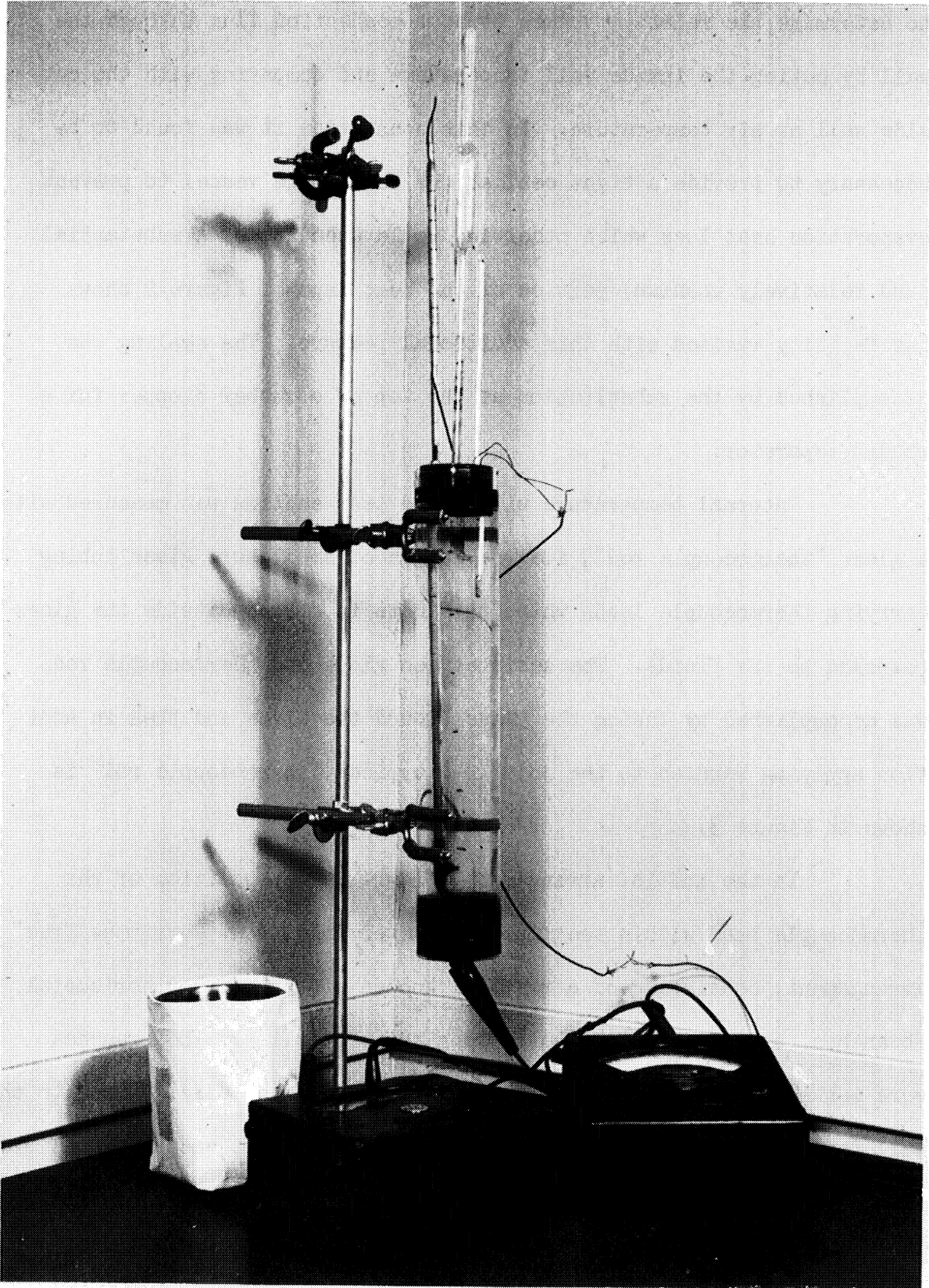


Figure 2. Photograph of Final Air-Cooled Facility

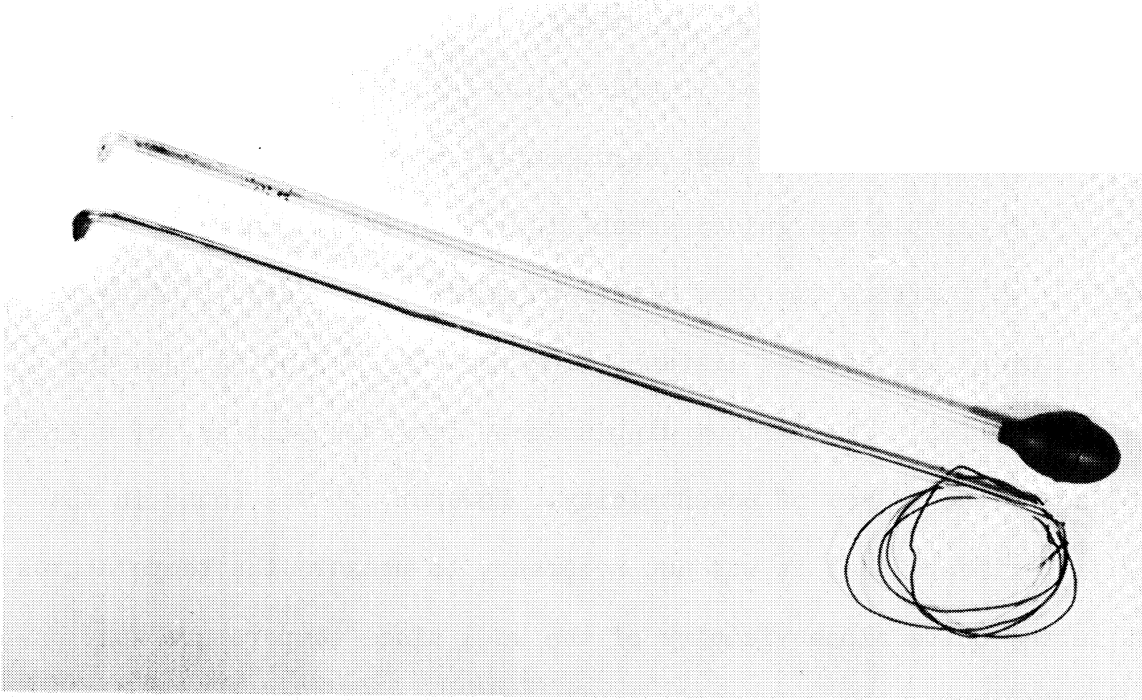


Figure 3. Photograph of Thermocouple Rod and Dye Injector
for Air-Cooled Facility

upper stopper. The guidance was improved by thin wooden discs placed on either side of the rubber and secured by small bolts. As the bolts were tightened the rubber would be displaced in the horizontal direction (i.e., diameter of rubber disc increased) so that a seal with both the glass test section and the glass thermocouple rod would be effected. With the thermocouple rod guided eccentrically in this manner, it would be possible to position the bead either adjacent to the test section inner wall or at any desired distance from the wall depending upon the degree of rotation. The maximum displacement from the wall is, of course, controlled by the degree of eccentricity. However, it was found in the initial experiments that it was not necessary to measure the temperatures except in the quite close vicinity of the wall since temperature was not a function of radius elsewhere. With the given arrangement it is, of course, also possible to measure the temperature at any desired elevation. Thermocouple voltage readings were measured by a precision potentiometer.

In addition to the thermocouple rod, other thermocouples were placed on the inner surface of the top and bottom electrodes and also along the outside of the glass test section.

Measurements of the velocity magnitude and direction, and observation of the degree of turbulence were to be effected by injecting dye through a small bore glass tube, Figure 3, positioned at any desirable location within the test section. The methods for positioning this component were the same as those used for the thermocouple rod in the two arrangements discussed in the preceding paragraphs. The dye injecting tubes may be seen in Figures 1, 2, and 3.

Water Cooled Facility

Construction Details of Test Facility Proper.--The water cooled facility is basically similar to the air cooled arrangement except that cooling is accomplished by forced-convection water flow through an annulus surrounding the test section. Photographs of the assembled facility are included as Figures 4, 5, and 6. In Figure 6 it has been adapted for reduced length test section runs.

As previously mentioned, the design was influenced to a substantial degree by the desirability of interchangeability of components between the water-cooled aqueous facility and a projected liquid metal facility. For this reason the steel end pieces are considerably heavier than would be necessary for aqueous testing only. As will be noted from a comparison of the photographs of Figures 4 and 5, the facility was somewhat simplified after the initial tests by the substitution of a simple steel plate closure for the bell arrangement originally used on the top. The original arrangement had been provided to allow for a continuous through-flow loop of which the natural-convection test section would have been only a portion.

A cross-sectional layout drawing of the facility with the bell closure and continuous loop piping provision is included as Figure 7. The construction features can be seen most readily from an examination of this drawing. The maximum length of test section used provided a cylindrical volume 22-3/8 inches in length. The drawing has been fore-shortened in this region but is otherwise in proportion. The test section diameter is approximately 3-7/8 inches and the wall thickness of the glass tube comprising the test section approximately 0.1 inches. Surrounding the test section is an annulus formed by the test section

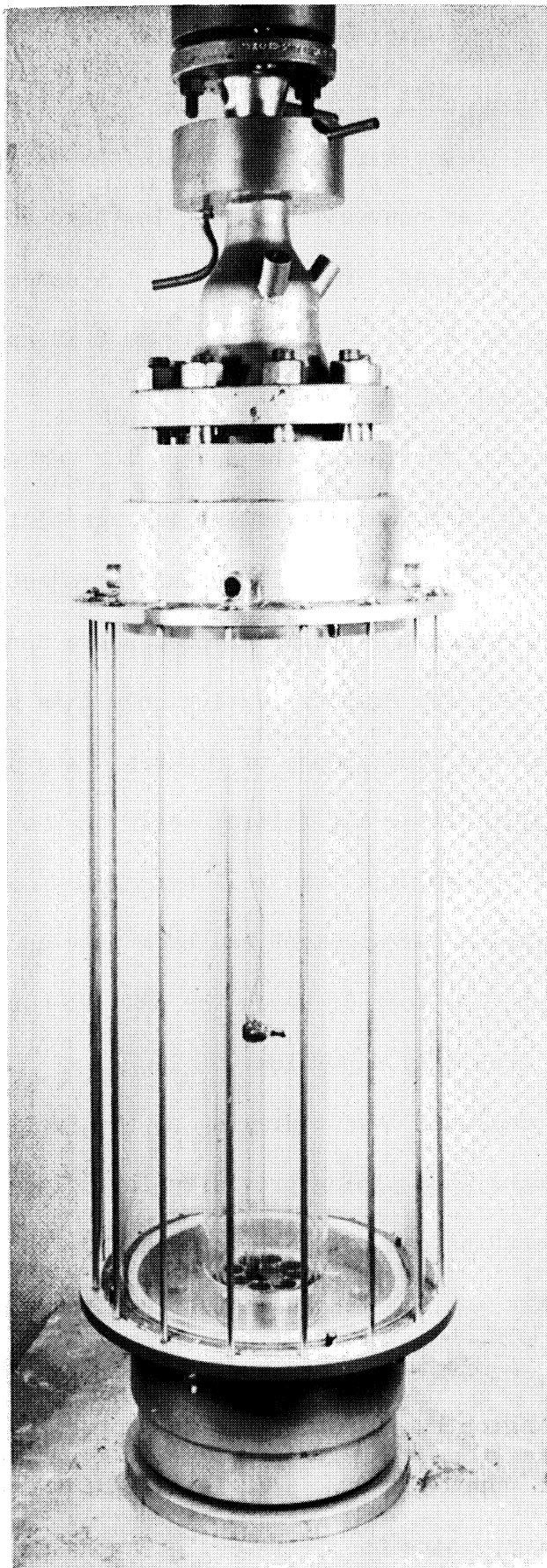


Figure 4. Photograph of Water-Cooled Facility,
Preliminary Arrangement

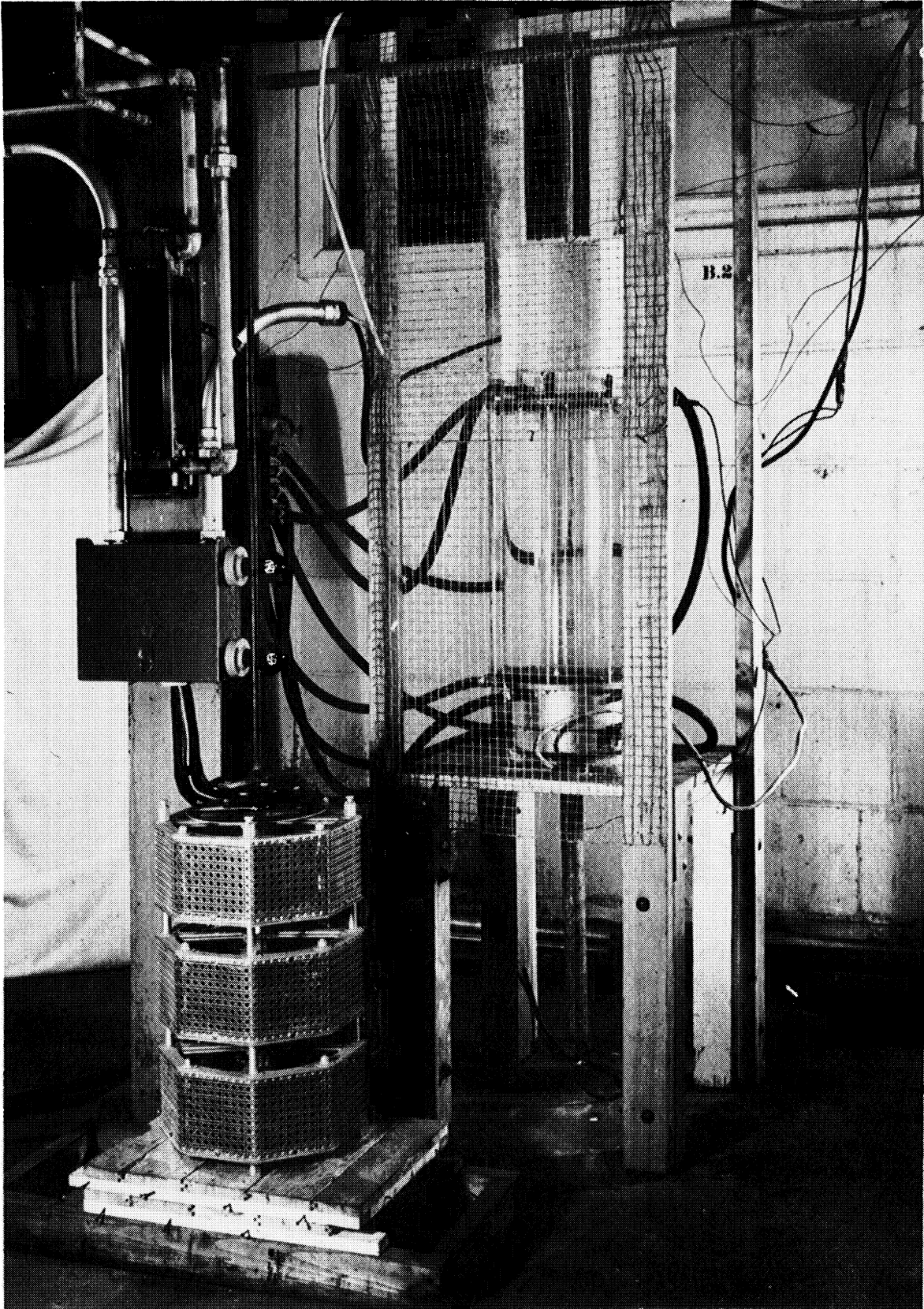


Figure 5. Photograph of Final Water-Cooled Facility

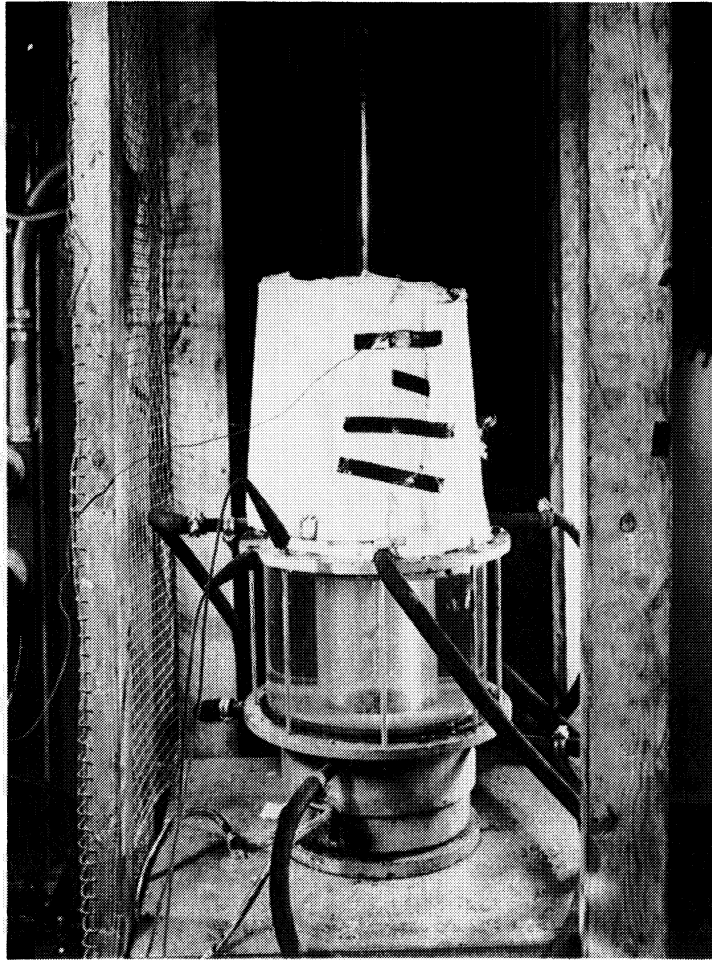


Figure 6. Photograph of Final Water-Cooled Facility,
Reduced Length Test Section

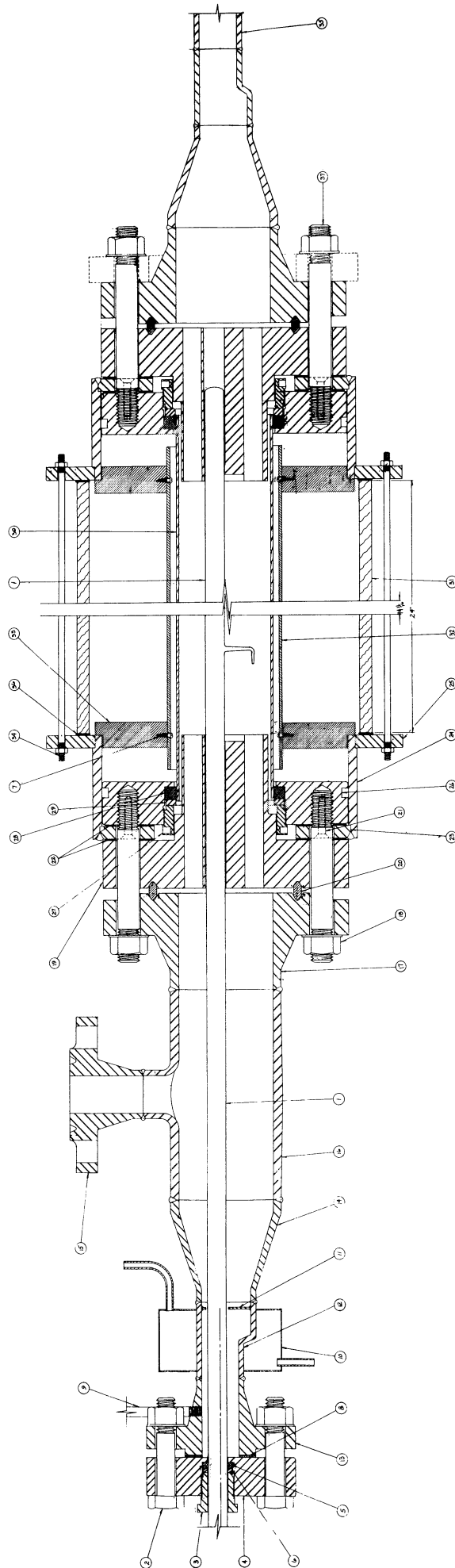


Figure 7. Layout Drawing of Water Facility

outside diameter and the inside diameter of a plexiglass tube (item 32 of drawing) which is positioned in plexiglass end baffle plates (item 33) to form a plenum chamber for the coolant at either end. The main support of the facility between the upper and lower sections is carried by a heavy glass cylinder (item 31) fabricated from a battery jar. The outer cylinder is maintained in compression to provide a seal on the gaskets at either end by steel through bolts (item 34) which are electrically insulated from the steel plate at the top end. The space between the plexiglass cylinder and the outer glass cylinder is filled with water under stagnant conditions since the seal between the plexiglass baffle plates and the steel members is only a restriction to prevent excessive circulation. The seal between the test fluid and the cooling water is maintained by a stuffing box at either end of the test section consisting of suitable rubber washers (item 28) and tightening nut (item 29). As will be noted, it is readily possible to substitute reduced length test sections by simply replacing the glass-ware with reduced length components.

The heat input to balance the loss through the cooling jacket and maintain steady state is provided by passing an alternating current axially through the facility between the top and bottom "electrodes." The electrodes (item 19) are heavy carbon steel components, tee-shaped in the cross-sectional drawing, provided with several axial holes drilled through in the axial direction. These holes are for the purpose of providing adequate flow area in the event it were desired to combine forced with natural convection. They also serve the purpose of providing a large surface area between the steel electrode and the fluid, so that the effect of any surface electrical resistance upon the heat source distribution would be minimized.

As in the preliminary version of the air-cooled facility, temperatures were measured by means of a thermocouple supported in an eccentrically-mounted vertical glass rod (item 1) which is positioned in bushings provided by the electrodes. This rod is capable of motion in the vertical direction and also of rotation. The thermocouple bead projects from a smaller bore glass tube affixed at right angles to the eccentric vertical rod. A seal is provided, as in the air-cooled facility, by fusing the glass around the thermocouple wires (iron-constantan was used). Varnish was applied as an aid in providing a satisfactory seal. Incidentally a seal at this location is a necessity because of the appreciable electrical conductivity of the solution. The thermocouple bead may be positioned at any desirable distance from the wall (maximum distance is controlled by the eccentricity of the vertical rod) depending upon the angle of rotation from that point at which it is adjacent to the wall. It may also be positioned at any desirable elevation.

In addition to the thermocouple leads, the vertical glass rod also encloses a small bore glass tube which projects from the surface of the vertical rod adjacent to the thermocouple probe. This tube is used for the injection of dye or bubbles at any desired location. It thus becomes possible to measure the velocity and temperature at the same location at the same time within the test section.

Figure 8 is a photograph of the thermocouple and dye-injection head. In this case, the vertical rod has been closed below these probes and is not carried down to the lower electrode bushing. This particular arrangement was used only for the reduced length test section runs where it was found that sufficient stiffness was provided by the upper electrode

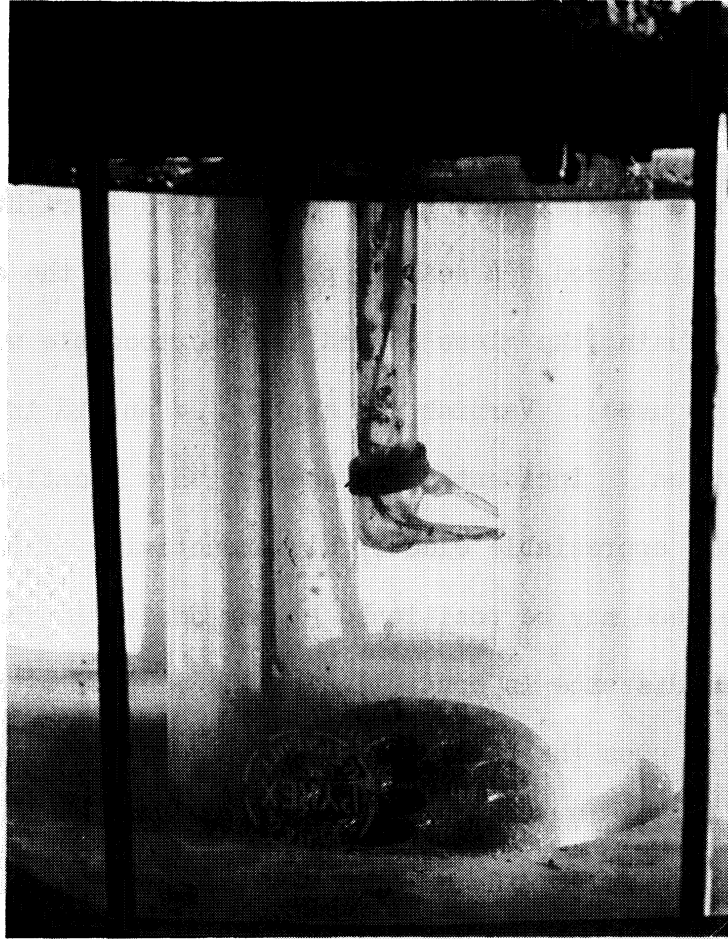


Figure 8. Photograph of Thermocouple Dye-Injection Head
for Water-Cooled Facility

bushing and the stuffing box surrounding the vertical glass rod as it projects from the facility at the top (items 3, 4, and 5 of the cross-sectional drawing of Figure 7). This removal of the lower support obviated problems of alignment which became troublesome in the reduced length arrangement. For the full length runs, the lower support proved necessary to provide sufficient guidance to the vertical glass tube. In this arrangement the probe assembly can be seen quite plainly in the photograph of Figure 4.

Limitations of Design.--The feasible power input rate to a facility of this sort is inherently limited by several of the construction features. In the first place the upper temperature limitation on the test fluid is set by the boiling point of water. Pressurization of the test section to a limited extent is possible but would involve numerous sealing complications. Within this maximum temperature limitation, the power limit is controlled by the temperature drop across the glass test section tube. In other words, there is approximately 130°F available between the maximum test fluid temperature and the temperature of the water coolant. This is substantially absorbed in the temperature differential across the glass wall of the test section. For this reason it is imperative that a test section of minimum wall thickness be employed. In the present design, a 3 mm. wall thickness has been used. The difficulty could, of course, be avoided if it were possible to use a material other than glass. No suitable material which provides the required transparency, the electrical resistivity, and the ability to withstand a temperature near the boiling point of water is, however, available.

In addition to the limitation on power level imposed by maximum available temperature differentials, there is also the possible limit of radial thermal stress in the glass test section tube. No information regarding the maximum allowable condition in this respect has been found, and no trouble of this nature was encountered with the present facility. However, a limitation due to the effect of the axial temperature gradient on the vertical thermocouple glass rod was noted in that too rapid movement of this component in the axial direction apparently did cause breakage on several occasions.

Auxiliary Instrumentation and Equipment Required.--In addition to the facility proper which has been discussed in the preceding sections, there is also the requirement of certain auxiliary equipment and instrumentation. The electrical power requirement is supplied through a 220 volt, 20 KVA variable transformer from a single-phase 220 volt alternating current line, Figure 5. The transformer is somewhat oversized for the aqueous application (about 5 KW maximum can be used) but was procured for the liquid metal facility. The electrical input is measured by a voltmeter-ammeter combination as well as a wattmeter in order to determine whether there is any deviation from unity power factor. None was observed in any of the experimental runs.

In order to determine the distribution of heat source generation, it is necessary to determine the direction and magnitude of the voltage gradient at all points. If, for example, no variation in voltage with radius at a given cross-section existed, then the power generation would vary as the voltage drop per unit axial distance, since the current would not be a function of axial position. Thus, it becomes desirable to measure the voltages in the fluid at all points. This can

be conveniently accomplished by measuring the potential difference between the travelling thermocouple bead and ground. It was found that a high-impedance voltmeter was required to obtain accurate data from the low conductivity electrolyte.

As has been previously stated, the heat is removed from the facility with a stream of coolant water. In order to verify that the electrical input is indeed removed in this manner and not, for example, substantially through conduction and radiation to the surrounding air and supporting members, it is desirable to measure the heat input to the water. This was accomplished by measuring the water flow rate and temperature rise. The flow rate was measured by a commercial rotameter which was calibrated with a weighing tank.

The rise in cooling water temperature as the water passed through the facility was determined by measuring the temperature in plenum chambers on the inlet and outlet lines by means of thermocouples.

To reduce heat loss to the surroundings, the top portion of the facility (Figure 6), was thermally insulated by wrapping with several inches of asbestos paper. As is explained in a later section, heat balance runs were made to determine the degree of heat transfer between the facility and the surrounding air. It was found to be quite negligible for most cases. Except for the top portion of the facility, there is very little temperature difference available to cause such heat transfer, since the exterior portions of the facility are at the temperature of the cooling water. This temperature never differed substantially from the ambient air temperature.

In addition to the auxiliary instrumentation described in the foregoing paragraphs, several other thermocouple positions were deemed desirable. These included a measurement of the top and bottom electrode temperatures, the temperature of the surface of the thermal insulation (to estimate possible heat transfer to the surrounding air), and room temperature. All these were led through a rotary switch so that any desirable measurement could be made through the precision potentiometer which was used. The cold junction was immersed in an ice bath maintained within a common thermos bottle.

General Operation of Facilities

The operation of the facilities, both air-cooled and water-cooled is similar in principle, although differing to some extent in detail. This is primarily a result of the fact that there are less degrees of freedom in the air-cooled operation. With the air-cooled type of facility the manner of cooling is limited to natural convection with the ambient air. Once the geometry of the system is fixed the only independent variable is the power input. This will uniquely fix the temperature values and profiles (for given ambient air conditions). In the case of the water-cooled facility, on the other hand, there is the possibility of altering the rate as well as direction of coolant flow. Thus there are various modes of operation possible with a given heat input rate.

Modes of Operation

Air-Cooled Facility.-The general mode of operation for either type of facility is simply the generation of heat internal to the test fluid by means of the ohmic resistance to an a.c. current, and the

obtaining of equilibrium conditions by the removal of an equal quantity of heat to the coolant; i.e., atmospheric air or water. In the case of the air-cooled facility with given test section dimensions, it is only possible to adjust the heat input which will determine uniquely the steady-state temperature conditions. It is thus only possible to conduct a series of experiments at differing power levels for a given test section. It is also possible to alter the test section dimensions and, thus, obtain additional series of experiments. In fact the experiments were run for three different length sections, all of the same diameter. It is possible, then, to duplicate the non-dimensional heat source parameter, q_v , for varying test section geometries, since, as previously discussed, q_v is proportional to volumetric heat source but is also very significantly a function of the test section dimensions.

Water-Cooled Facility.-With the water-cooled facility there are additional degrees of freedom in that the magnitude and direction of the coolant stream can be adjusted. Such adjustment affects the wall temperature distribution both in total axial difference from top to bottom and in the distribution of this difference. Therefore, it is possible to conduct experimental runs under varying conditions of wall temperature distribution but at the same value of the non-dimensional heat source parameter, q_v , with constant test section geometry. As in the case of the air-cooled facility it is also possible to conduct a series of groups of runs at various values of q_v . Each of these groups would presumably consist of runs at constant q_v but varying wall temperature distribution. A further degree of freedom is afforded by the possibility for altering the test section geometry. In matter of fact,

experiments were made for both a maximum length test section (about 22 inches) and a reduced length section (6.25 inches). It is possible to duplicate certain q_v values with both of these test section lengths and thus to afford a test of q_v as a suitably universal non-dimensional parameter for this particular application.

Water-Cooled Facility (AEC Tests).-The water-cooled facility used for the AEC tests⁽¹⁰⁾ has been previously described in this report and is indeed quite similar in concept to that constructed for the present investigations. The tests conducted with this facility utilized only a narrow range of heat source strengths and a single geometric configuration. As a result they effectively add a single point to the data. Fortunately this is in a range of non-dimensional heat source not thoroughly explored in the present test program and is taken with test section dimensions differing significantly from those of the present program. Also the ratio of wall temperature drop to temperature differential between centerline and wall is in a range not previously explored. Thus, a valuable addition to the data is afforded.

Experimental Procedures.-For either type of facility the experimental procedure, once equilibrium conditions with a given rate of heat input have been obtained, is similar. In all cases, the internal temperature profiles normal to the wall at fixed axial intervals are measured by the traversing thermocouple arrangements which were described in previous sections of this report. It was found in all cases that the axial temperature gradient steepened very rapidly as the bottom of the test section was approached and for this reason temperature measurements were made at considerably reduced axial spacing near the bottom. In

general it was found that the temperature was fairly constant near the top in the axial direction and decreased steadily in the central portion. It was always found that the temperature gradient was very steep adjacent to the wall, decreased rapidly at distances above approximately $3/16$ inches from the wall, and that virtually constant temperature, as measured in the radial direction, prevailed throughout the remainder of the cross-section. For this reason a much higher density of temperature readings progressing in the radial direction was necessary in the close vicinity of the wall.

In addition to the temperature measurements made with the travelling thermocouple, stationary thermocouple positions attached to the top and bottom electrodes were utilized in an attempt to determine the overall temperature differences prevailing within the test section. This procedure was more successful with the air-cooled facility than with the water-cooled equipment.

Velocity determinations throughout the test sections for given conditions of coolant flow and power input were attempted. This was accomplished by the injection of dye at any desired location throughout the test section. The type of equipment used in this connection has been previously explained. It was found that dye was far more suitable for the purposes of this investigation than oil bubbles. With the low velocities typical of these experiments, it was found nearly impossible to achieve a sufficiently close balance between the oil bubble and solution density. Such a balance was found to be extremely sensitive to temperature. With the temperature differences prevailing throughout the test section, it is doubtful that a suitable mixture could be found.

It was found that the dye was quite satisfactory in following even the small prevailing velocities. A determination of the state of the flow with respect to laminar or turbulent behavior could be made and also an indication of the direction and an approximation of the magnitude of the velocity was possible. Some difficulty was experienced in accurately determining the location of the dye injection since the injection velocity was necessarily appreciable with respect to the test fluid velocity. Thus, the dye stream would carry a significant distance before being affected by the test fluid velocity.

For the water-cooled facility, additional measurements necessary for each experiment included coolant water flow rate, temperature rise, thermal insulation temperature, and ambient temperature. For the air-cooled facility, the additional readings included air temperature, test fluid level (with the preliminary version wherein evaporation loss from the surface was a factor), and in some cases the outside wall temperature at several evenly spaced axial locations. For both facilities, a measurement of the voltage gradients, both axial and radial, within the test section were made. No radial voltage gradient could be detected within the degree of precision of the measurements.

Evaluation of Physical Properties of Test Fluid.--Most of the physical properties of the test fluid which are of interest from the viewpoint of the natural convection heat and mass transfer phenomenon are quite sensitive to temperature. However, it is not mathematically feasible to consider this temperature dependence. Consequently, it is virtually necessary that an arbitrarily defined "mean" temperature be selected and used as a basis for the evaluation

of the physical properties of the fluid. Theoretically, it is not at all clear what sort of a mean should be used. However, since measurements showed that the most substantial portion of the temperature gradient in the axial direction occurred near the bottom of the vessel, it was felt that the mean temperature should be defined as existing somewhat below the tube midpoint. Consequently, it was arbitrarily decided that the mean temperature should be measured at a point along the tube centerline at an elevation from the bottom of 0.45 of the total length. It is realized that the use of a mean temperature of this kind may be responsible for some of the inconsistencies between experimental data and calculations, especially when it is realized that the viscosity in particular, which undoubtedly exerts a significant influence upon the fluid behavior, varies by large amounts over small ranges of temperature.

As explained in the next section, the aqueous electrolyte which was chosen for the present tests is dilute sodium acetate solutions in water. It was found that a solution normality of about 0.35 provided sufficient electrical conductivity for the purpose. It then became necessary to evaluate the various physical properties which are of importance from the viewpoint of heat transfer for such solutions. This was accomplished through reference to the existing literature^(14,15,16). As mentioned in a later section, experiments were conducted to evaluate the electrical conductivity because of the possibly gross influence of the tap water for low conductivity solutions. It was also necessary to evaluate approximately the conductivity of the tap water in order to determine the possible current leakage through the coolant jacket. Such leakage was found to be negligible.

Curves for the physical properties as affected by solution strength and temperature are included in this report as follows:

1. Normality vs. Concentration (pounds of sodium acetate/gallon of water) - Figure 9-a
2. Normality vs. Boiling Point Elevation - Figure 9-b
3. Normality vs. Specific Heat at 20°C - Figure 9-c
4. Density vs. Temperature for Various Normalities - Figure 9-d
5. Viscosity vs. Temperature for Various Normalities - Figure 9-e
6. Thermal Conductivity vs. Temperature for Various Normalities - Figure 9-f
7. Prandtl Number vs. Temperature for Various Normalities - Figure 9-g
8. Electrical Conductivity vs. Temperature for Various Normalities - Figure 9-h

It is apparent from an examination of these curves that only viscosity and Prandtl Number are extremely sensitive to temperature. With the exception of electrical conductivity these are also most seriously affected by solution strength. It is noted that in most cases the physical properties of the solution vary only slightly from those of pure water.

Necessary Preliminary Test Programs.--It appeared desirable and necessary that certain minor preliminary test programs be conducted prior to the natural convection heat transfer experiments. These tests were concerned with the following subjects.

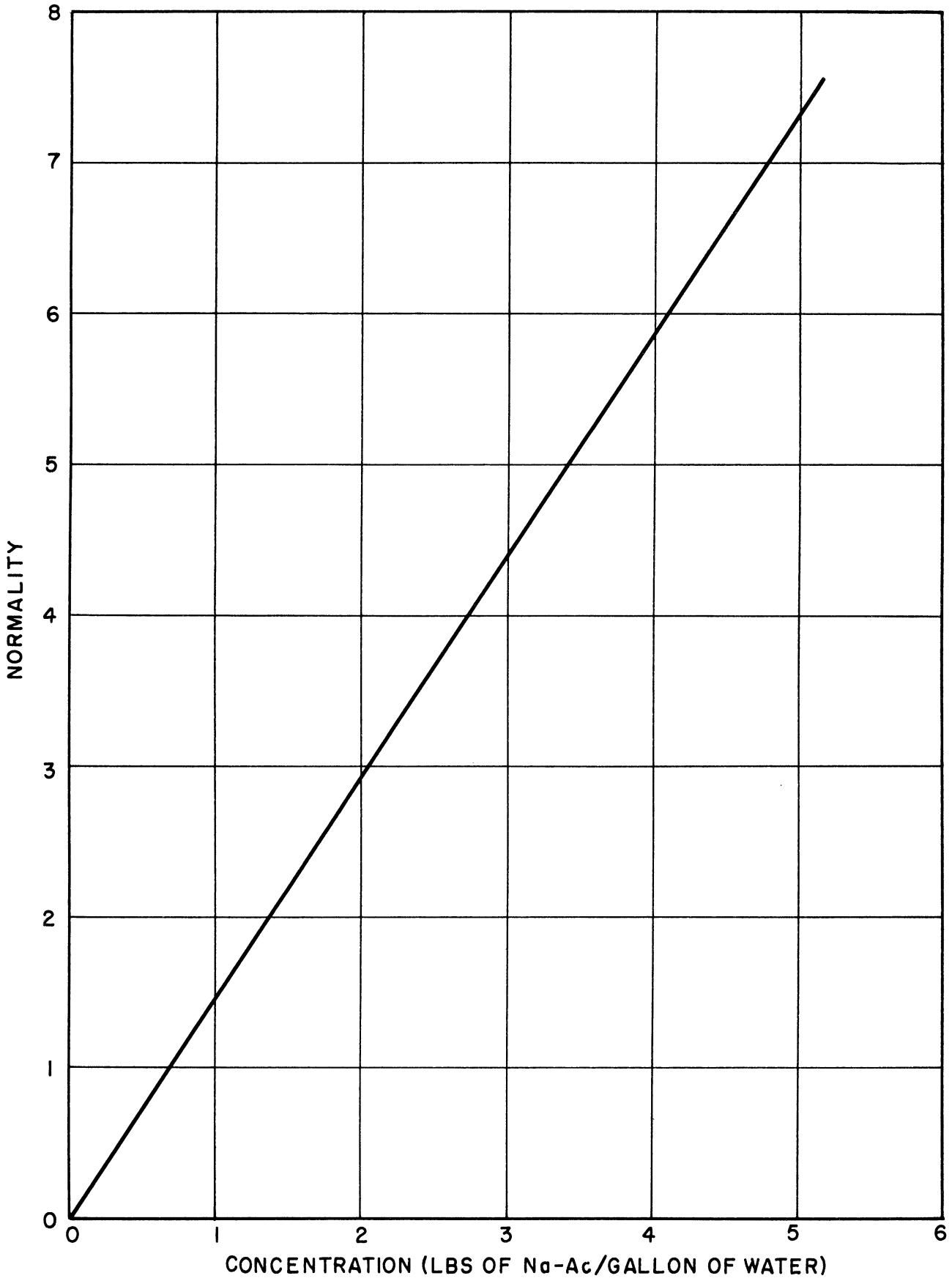


Figure 9-a. Solution Physical Properties, Normality vs. Concentration

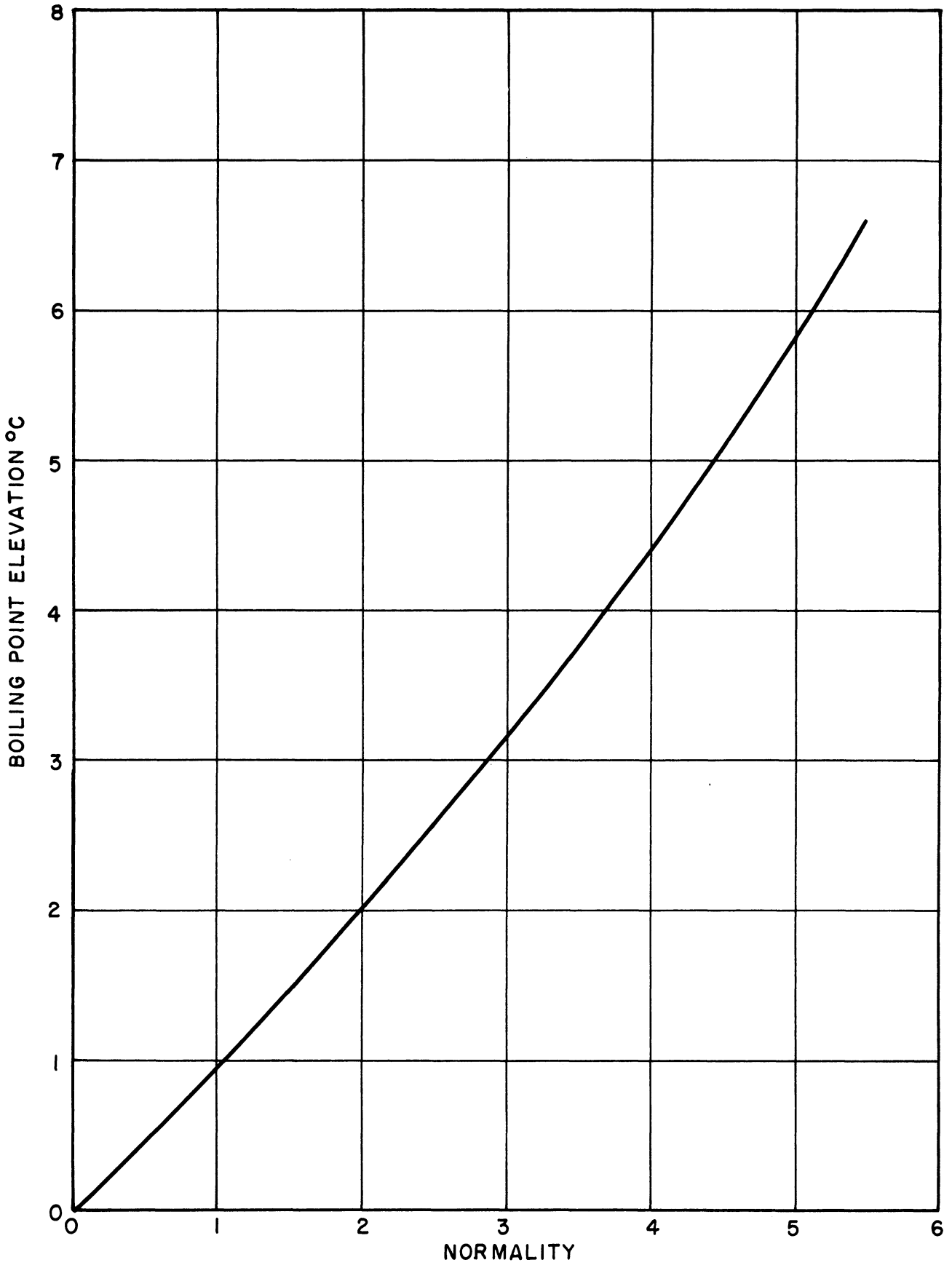


Figure 9-b. Solution Physical Properties, Normality vs. Boiling Point Elevation

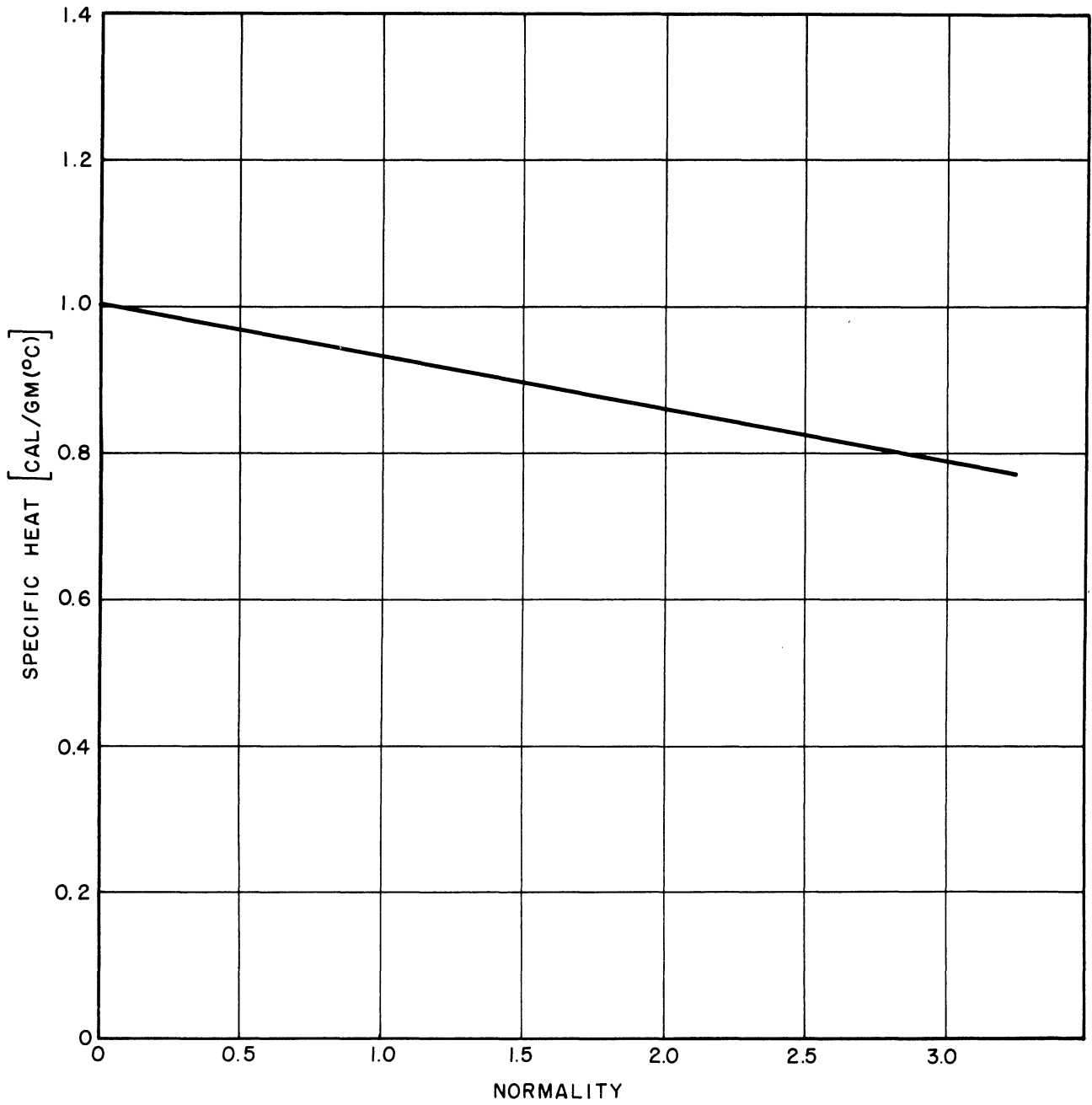


Figure 9-c. Solution Physical Properties, Normality vs. Specific Heat at 20°C

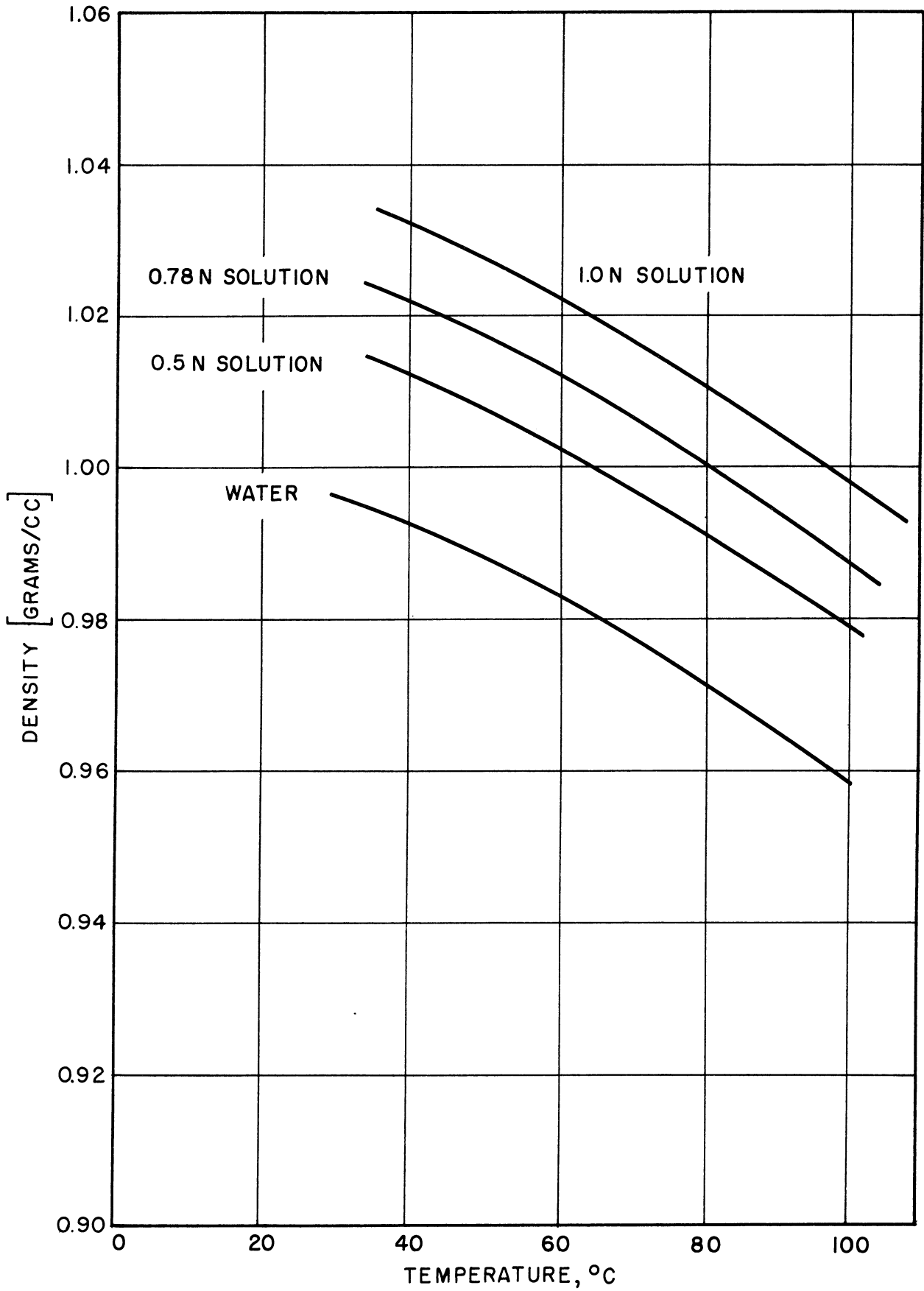


Figure 9-d. Solution Physical Properties, Density vs. Temperature

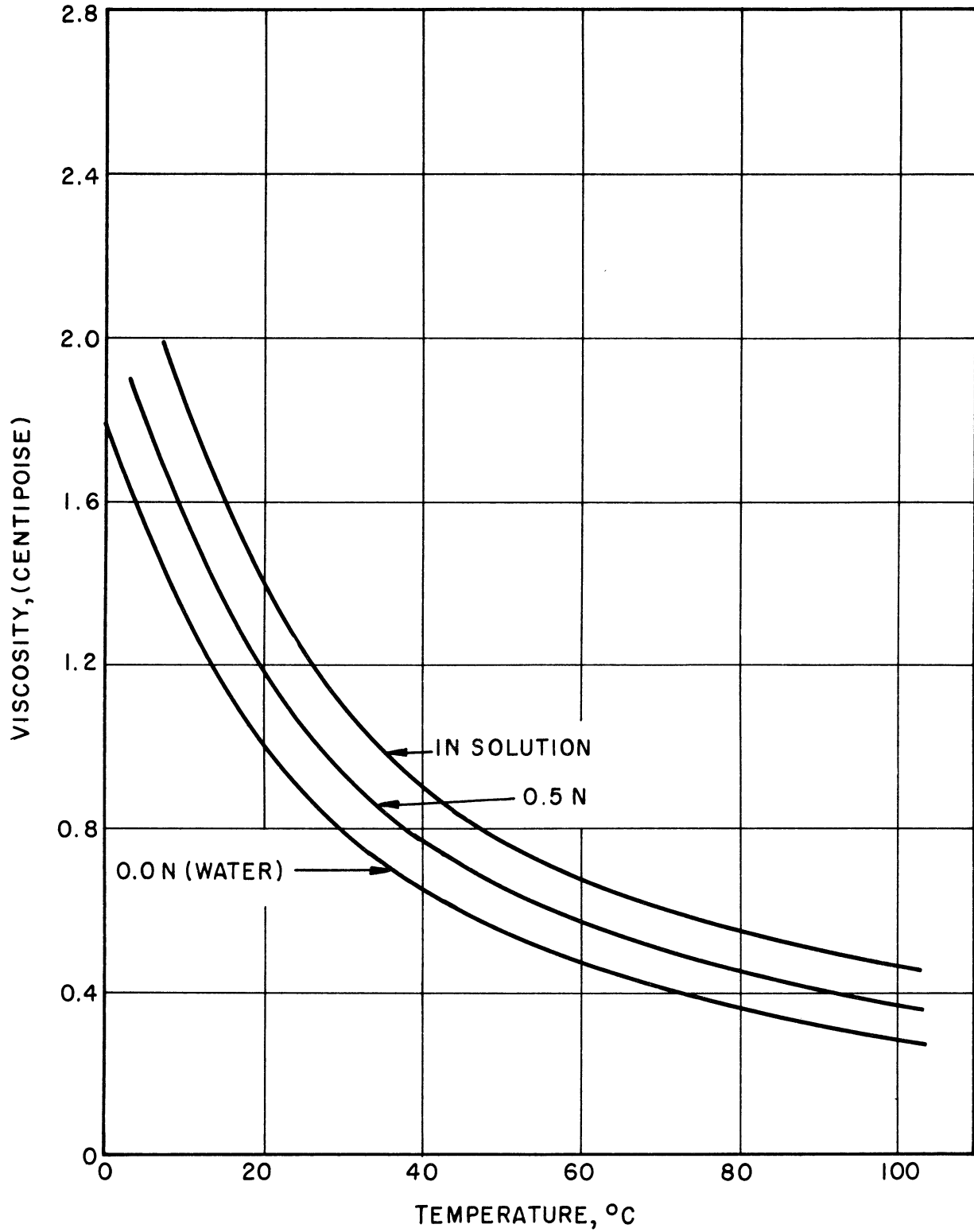


Figure 9-e. Solution Physical Properties, Viscosity vs. Temperature

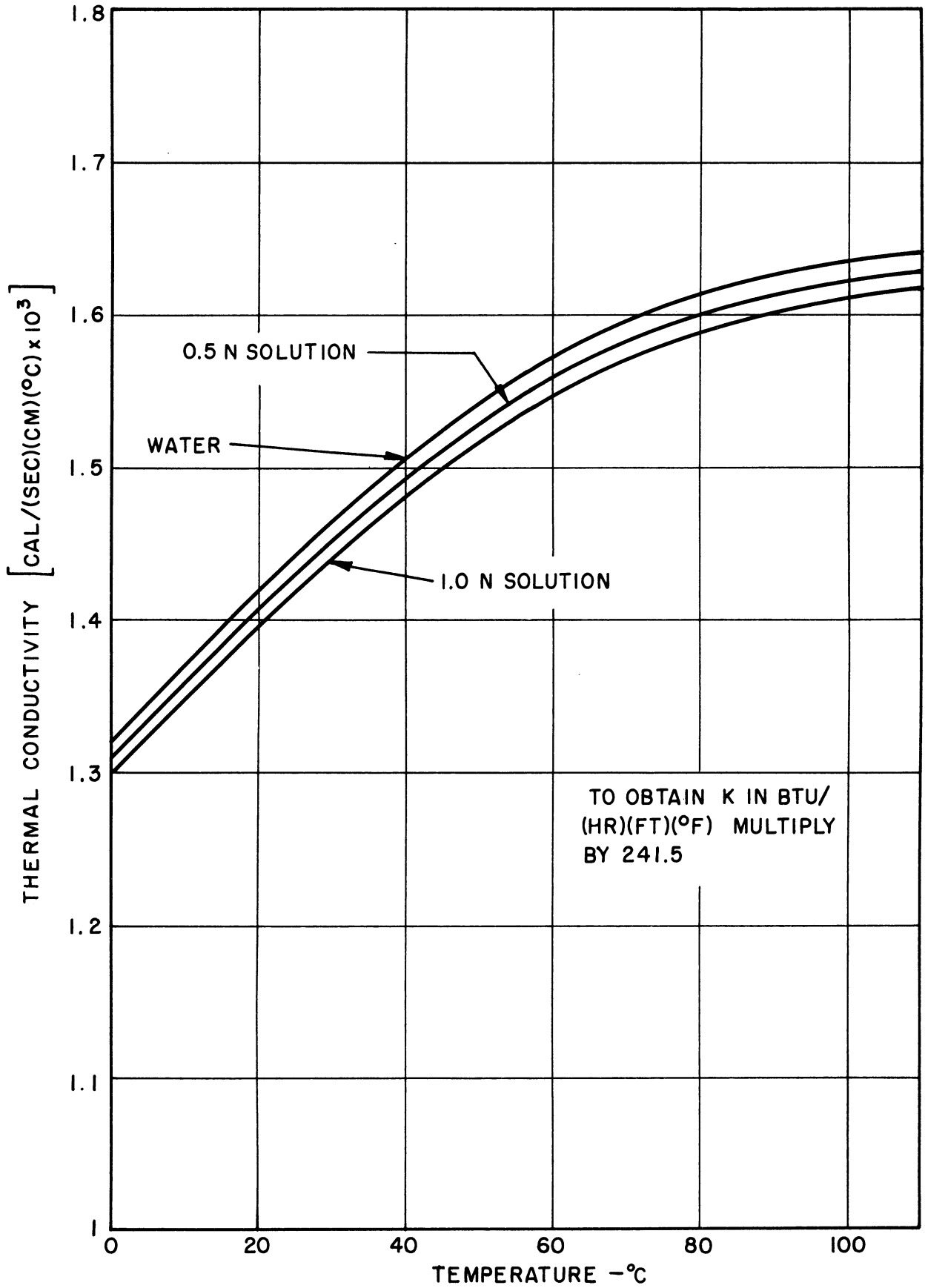


Figure 9-f. Solution Physical Properties, Thermal Conductivity vs. Temperature

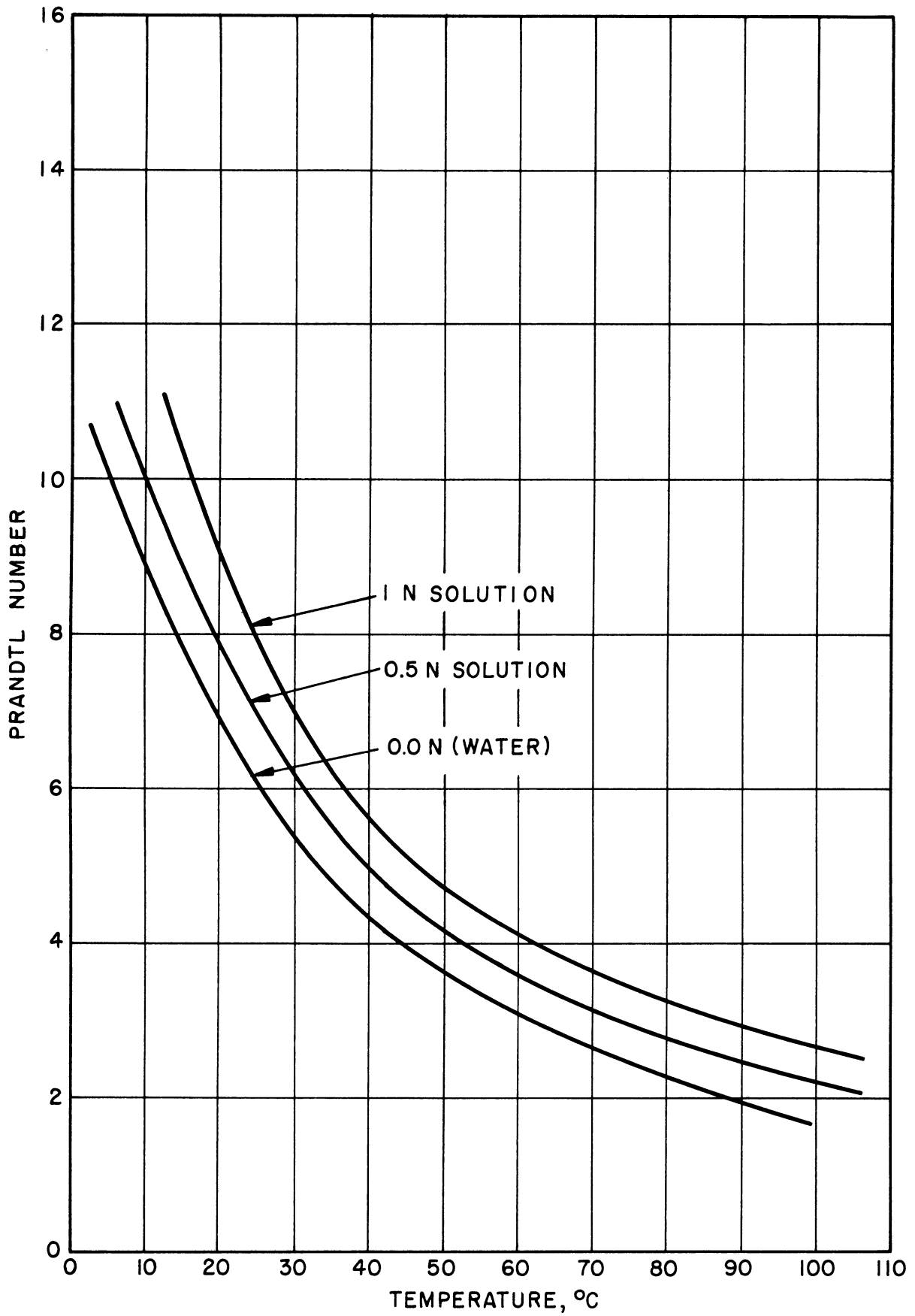


Figure 9-g. Solution Physical Properties, Prandtl Number vs. Temperature.

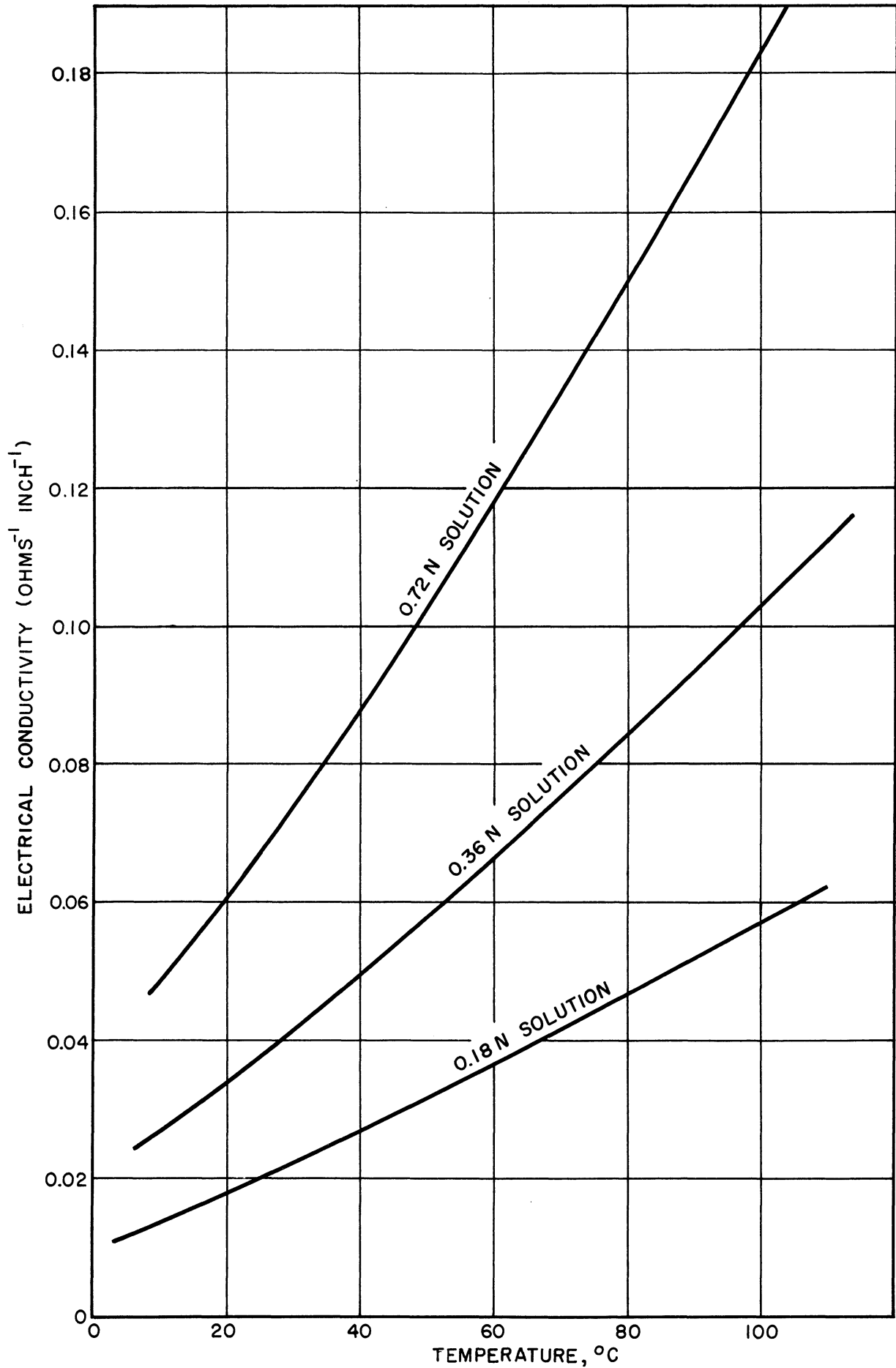


Figure 9-h. Solution Physical Properties, Electrical Conductivity vs. Temperature.

1. Effect of temperature upon electrical conductivity
2. Surface resistivity between electrode and fluid
3. Calibration of rotameter
4. Possible existence of non-unity power factor
5. Overall heat balance
6. Distribution of internal heat source
7. Effect of center thermocouple rod upon flow
8. Choice of suitable electrolyte.

Electrical Conductivity Temperature Dependence.-As mentioned in the foregoing section, most of the physical properties of the aqueous solution to be utilized as a test fluid were taken from the published literature. However, due to its possible effect upon internal heat source distribution and to the uncertain effects of the Ann Arbor tap water, the electrical conductivity of the solution to be used was evaluated experimentally. It should be mentioned that the absolute value of conductivity for a given strength of solution is only important for preliminary feasibility estimates, since the solution can be adjusted to give a suitable relation between the available voltage and the desired power. It is important to obtain some knowledge of the degree of dependence of conductivity upon fluid temperature.

Since the absolute value of the conductivity is not of prime importance but more the variation with temperature, it was felt that a rather crude experimental arrangement would suffice. A vertical, closed-end, glass tube, similar to the air-cooled test section was used. The "mean" temperature was measured at a point slightly below the midpoint as for the natural convection tests. Electrical conductivity was com-

puted from the known dimensions of the vessel and the current resulting from an axially imposed alternating voltage. The resulting relation between specific electrical conductivity and temperature for solutions of three typical normalities is shown in Figure 9-h. It is noted that the variation over a 10°C temperature change is of the order of 15%.

Surface Resistivity between Electrode and Fluid.-The existence of a possible surface resistivity between the steel electrodes and the fluid could become of importance if it were of sufficient magnitude to utilize a non-negligible portion of the total voltage drop. It was deemed necessary to conduct preliminary experimentation to determine whether or not such an effect was negligible when the actual test fluid, electrode material, and relation of electrode surface area to cross-sectional area of fluid normal to the electric current flow were considered.

A test using the air-cooled facility was made to determine the order of magnitude of this effect. Two separate runs were made: the surface area of the top electrode exposed to the fluid was doubled between the tests. Writing the relations between the current, voltage, and resistance, and inserting a term for the surface film resistance (if any) for each experiment, it becomes possible to solve for the surface film resistance. No change of overall resistance between the runs was noted. Considering the accuracy of the instrumentation, it was deduced that the specific surface resistance must be less than approximately 6 ohms-in.². In this case, the power consumed in the surface films would be less than 0.23 of the total heat generated for

the water-cooled facility, due to a large surface area in proportion to the test section diameter. For the air-cooled facility, the heat generated in each electrode surface film on this basis could be as large as approximately 6% of the total. However, subsequent voltage measurements taken in the solution at various axial positions during actual runs showed that the effect was negligibly small.

Calibration of Rotameter.-As stated in a previous section, the rotameter used for the measurement of cooling water flow rate was calibrated by means of timed flow into a weighing tank. The resulting calibration curve is included as Figure 10. It is noted that the variation from the readings of the scale attached by the manufacturer is only about 3%. This error becomes almost negligible in the heat balance calculations.

Power Factor Measurements.-In the preliminary tests with each facility, the power factor was determined by comparing the product of voltage and amperage readings with a wattmeter reading. Within the accuracy of the available instrumentation, no deviation from unity power factor was detected.

Overall Heat Balance.-No overall heat balance is possible for the air-cooled facility since the coolant is atmospheric air moving under natural convection. For the water cooled facility, however, it is possible to measure both heat input (electrically) and heat output through knowledge of the water flow rate and temperature rise. In this way, it should be possible to confirm that heat losses through the end

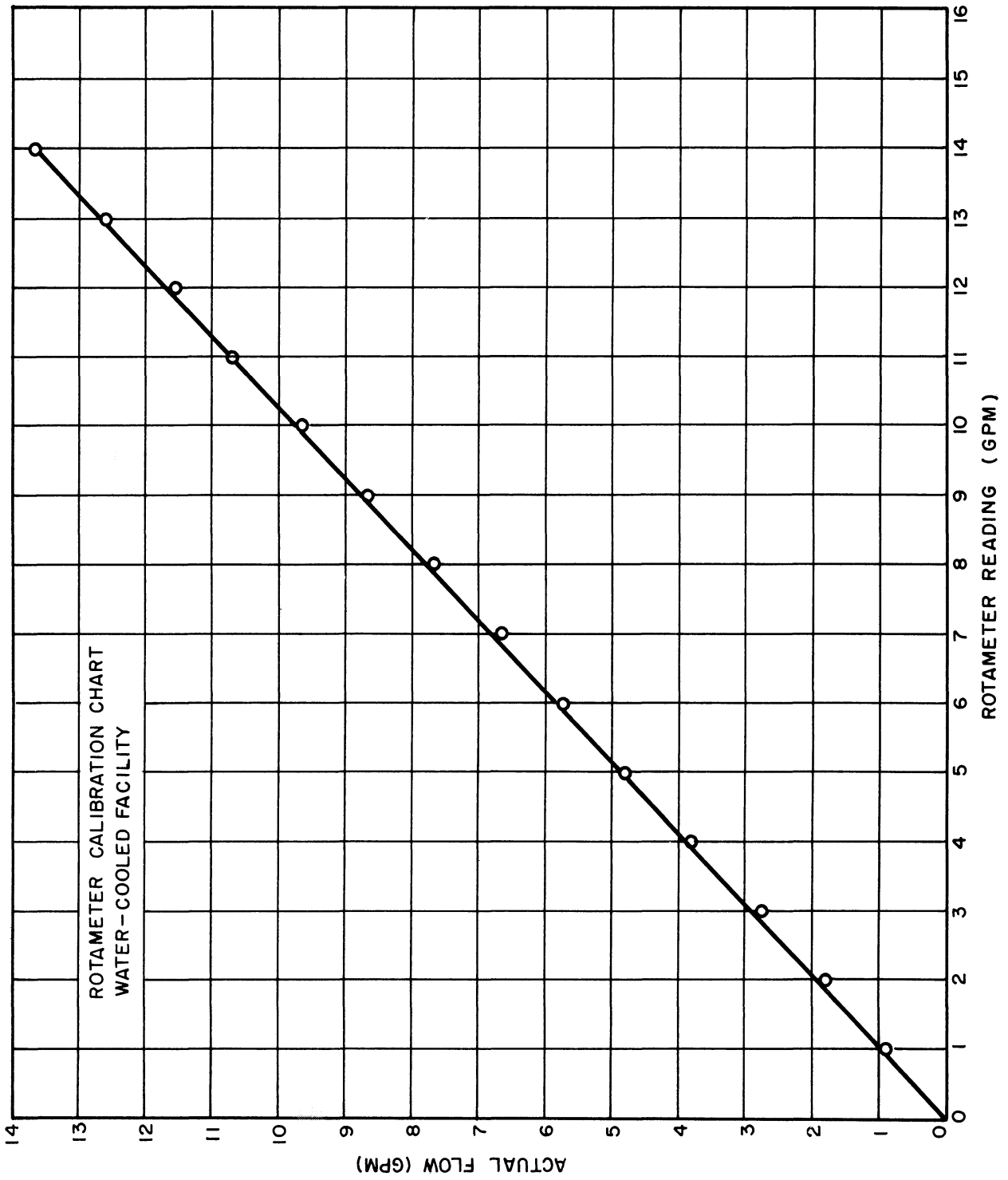


Figure 10. Rotameter Calibration Curve.

sections were small and also that there were no chemical reactions or electrolytic effects absorbing substantial quantities of heat.

Before attempting such a heat balance, it was first necessary to estimate the likely magnitude of heat transfer between the facility and the surroundings. A glance at the photographs of Figures 4 and 6 or the layout drawing of Figure 7 shows that except for the top portion, the external surface of the facility which is in contact with the surrounding air is in contact with the cooling water. Even the supporting metal table could hardly be at a temperature substantially different from that of the cooling water.

With no electrical input the temperature rise (or drop) of the coolant stream can be observed and from this a mean value of the product of film coefficient and surface area (BTU/hr.-°F) between air and facility deduced. In order to obtain a measurable temperature difference, it is desirable that as low a coolant flow rate as practicable from the instrumentation viewpoint be utilized. Such an experiment was conducted and it was determined that the rate of heat flow per unit temperature differential between those portions of the facility in contact with the coolant stream and the surroundings was approximately 20 BTU/hr.-°F. This is a small enough effect in most cases so that a large percentage error in its estimation would not be significant in the overall heat balance. Presumably the same value of facility to air film coefficient can be applied to the top portion of the facility, the only portion not in contact with the coolant. The temperature difference between the outside surface of the thermal insulation at this

location and the ambient air was measured for all experimental runs. It was found that the heat loss from this portion was negligible.

Overall heat balance calculations, applying suitable corrections as described in the preceding paragraphs, were made for all experimental runs with the water cooled facility. The results are displayed in the experimental summary sheets, Tables A-IV through A-VII in the Appendix. It is noted that there is a wide scatter, due principally to the inaccuracies inherent in the measurement of the small temperature rises of the coolant stream. However, for those cases where the power input is large and/or the coolant rate low, the accuracy is considerably improved. The average absolute error percentage is 13.4%. However, the algebraically averaged error percentage is only 2.1%. It does not appear from these results that there is any indication of a substantial discrepancy between the electrical input and the heat removal to the coolant.

As a further test to determine the existence of appreciable rates of electrolysis with the imposed a.c. current or other chemical reaction which might result in the release of gases, the sealed top portion above the liquid surface was vented continuously through a rubber hose which terminated below the liquid level in a water beaker. Over running periods up to 10 hours duration, no bubbling was observed. Simple calculations based on this observation show that no appreciable portion of the heat input could have been utilized in electrolysis.

Distribution of Internal Heat Source.-Voltage measurements between the thermocouple bead and the bottom electrode (ground potential) were made at various axial and radial positions throughout several of

the runs with both the water-cooled and air-cooled facilities. A high-impedance voltmeter was used so as not to disturb the potential distribution in the solution. No variation with radius, even in the proximity of the electrodes, was detected. The variation of voltage (including all the experimental points) in the axial direction as a function of non-dimensional axial position (x/l) is shown in Figure 11. It is noted that the relation is linear except for an increase of slope adjacent to either electrode. It is believed that this effect is due to the surface film resistance (as previously discussed) between electrode and fluid. It will be noted that that portion of the overall voltage drop which occurs adjacent to either electrode is no more than approximately 1 to 2% of the whole. It is thus not a sufficient departure from the straight line relation to be of importance. Assuming that there is no potential gradient in the radial direction, and that the axial gradient is substantially linear (as verified by the experimental results), then the existence of a substantially uniform internal heat generation term is verified. Apparently the variation of electrical conductivity with temperature is not sufficient, consistent with the temperature differentials existing in the facilities, to cause an appreciably non-uniform source generation term.

Effect of Center Thermocouple Rod Upon Flow.-The question naturally arises as to the effect of the center thermocouple rod of the water-cooled facility upon the flow and also of the "Christmas Tree" arrangement used in the preliminary air-cooled facility. From the theoretical viewpoint these pose boundary conditions of zero velocity along their surface. Such a boundary condition also exists, of course, along

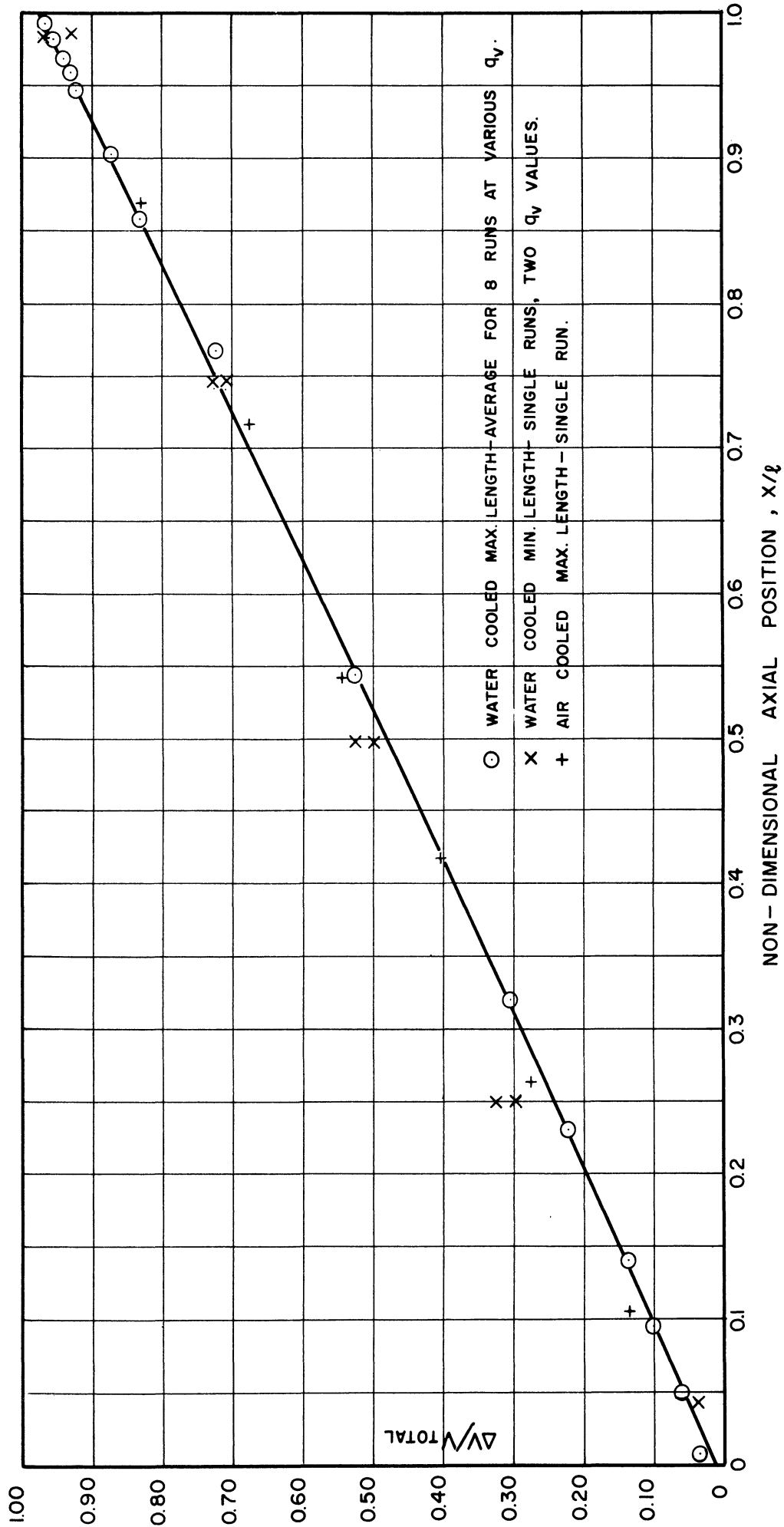


Figure 11. Proportionate Voltage Drop vs Non-Dimensional Axial Position - Experimental Data

the inner wall of the test section. Thus additional shear resistance is opposed to the fluid motion. However, this additional force is of the order of 10 - 20% of that imposed by the test section wall because of the ratio of the areas. Its importance is further reduced by the fact that the velocities along the centerline are considerably smaller than those adjacent to the cooled walls. From the viewpoint of blocking of flow area the effect is even less, being of the order of 1 to 4% of the total. Although it is doubted that these obstructions could cause any appreciable effect upon the gross heat and mass transfer behavior, it does seem probable that there might be some effect relative to the onset of turbulence. However, a detailed examination of this phenomenon was beyond the scope of the present investigation.

In the air-cooled facility in particular, tests were run both with and without the obstructions within the test section. No effect upon the overall heat transfer or the appearance of the velocity regime could be detected.

Choice of Suitable Electrolyte.-It was found from published data that electrical conductivities of the desired order of magnitude could be obtained with various types of reasonably dilute aqueous solutions. A dilute solution appeared particularly desirable in that the variation of the physical properties from those of pure water, for which detailed information is available, would be minimized. The selection rested then upon the lack of effect due to the passage of alternating current and lack of corrosivity. These conditions seemed well satisfied with sodium acetate and it was consequently selected.

CHAPTER IV

RESULTS OF EXPERIMENTAL PROGRAM

General Expectations

The experimental program, comprising results from both the air-cooled and the water-cooled facilities and considering in addition results from the water-cooled type of facility utilized by the AEC⁽¹⁰⁾, was intended to allow the attaining of some degree of insight into the mechanism of heat and mass flow under natural convection within a vertical closed tube with heat generated internal to the fluid and removed through the vessel walls. It was also expected that measurements could be made to allow the prediction of the overall temperature differentials which would be required to cause heat flows of a given magnitude under specified conditions of distribution of wall temperature and heat source, and of geometry. Results of this type might for example lead to the establishment of an empirical relation between non-dimensional heat source, and/or a modified version of Rayleigh's Number, and the Nusselt's Number. In addition to gross overall results of this sort, it was hoped that the internal temperature and velocity profiles might be measured to throw additional light upon the flow and heat transfer mechanisms. It was hoped that an analytical solution might be developed for the particular case under experimental study, and that this solution might then be applied to cases of differing geometry, and heat source and temperature distribution conditions. If the internal velocity and temperature regimes as well as the overall Nusselt's Numbers predicted by theory could be confirmed experimentally, then considerable reliance could be placed in the reliability of the theoretical solution and its

possible extrapolations. Generally speaking, as will be explained in detail in following sections of this report, such internal and overall correlations were indeed achieved.

General Character of Flow from Experimental Observations

Based upon all the experimental observations both of the present program and of the AEC experiments⁽¹⁰⁾, the flow within the tube, under conditions of internal heat generation throughout the fluid volume and heat removal to a coolant through the tube walls, is one of an ascending core in the central portion of the vessel surrounded by a descending layer adjacent to the vessel walls. Compared with the radius, the thickness of the descending layer is of the order of 0.1. It varies in thickness for different rates of heat input.

In all the tests conducted, regardless of the manner of cooling, there is a substantial drop in temperature along the inner surface of the test section wall from the top to the bottom. There is also a drop in temperature from top to bottom along the tube centerline. Although the temperature gradients along wall and tube centerline are not exactly similar, the temperature difference between wall and centerline is more or less the same for any axial position except near the tube bottom. In general this radial temperature difference is much smaller than the overall axial temperature difference. The radial temperature gradient is concentrated in the immediate vicinity of the test section wall, over an extent similar to that of the descending layer. The velocity profile measurements were not sufficiently precise to allow the conclusions that these temperature and velocity boundary layers are in fact of equal extent. On the other hand no evidence to the contrary was provided.

The existence of an axial temperature gradient both along the wall and the centerline is confirmed even for cases where the outside wall temperature is maintained substantially constant by the utilization of high coolant flow rates. From another viewpoint the temperature differential across the test section wall is greater at the top than at the bottom so that the heat flux through the wall per unit surface area is not uniform but greater at the top.

In all cases, there is a very rapid decrease of temperature in the lower perhaps 10% of the vessel so that the wall heat flux decreases very substantially near the bottom. The velocities are also decreased considerably in this area so that the flow appears quite stagnant. From a physical viewpoint, the existence of a stagnant region at the tube bottom implies that heat flow from this region must be largely the result of thermal conduction. Thus, although the wall heat fluxes in the area are relatively small, the temperature gradients are large.

Over the range of non-dimensional heat source, modified Rayleigh's Number (non-dimensional temperature), and test section geometry which it was possible to produce with the air-cooled and water-cooled facilities, it was possible to achieve either laminar or turbulent flow conditions. In general, turbulence appeared first in the core region near the top of the vessel. As the rate of power generation is increased, with other parameters held constant, the region of turbulence spreads toward the bottom of the vessel. At the highest power levels which were achieved, the degree of turbulence in the water-cooled rig seemed high. This was evidenced also by the temperature measurements which did not achieve steady-state under turbulent

conditions but exhibited a continuous fluctuation of several degrees Fahrenheit over a period of the order of 15 to 30 seconds. Instrumentation to provide a trace of temperature with time was not utilized in these experiments. It is felt that a further extension of the study might profitably attempt to correlate these temperature swings with the degree and initiation of turbulence.

It was not possible with heat sources sufficiently strong to produce relatively measureable temperature differences to obtain laminar conditions within the water-cooled facility for any of the lengths which were tested. In the smaller radius air-cooled facility, however, it was possible to obtain nearly laminar and also turbulent flow depending upon the rate of heat input. The approach to laminar conditions resulted, as will be explained in later sections of this report, in considerably greater temperature differentials required to extract a given quantity of heat (in terms of the non-dimensional heat source and temperatures). It should be noted that only small degrees of turbulence were obtained in the air-cooled facility as compared with the water-cooled facility even for the maximum feasible heat input to the air facility.

Those parameters which determine the onset of turbulence in a configuration of the type under investigation are not known. A detailed analysis of the question of flow stability is beyond the scope of the present investigation so that no attempt to delineate the non-dimensional parameters which are suitable in this regard was made. It is usually assumed in problems of natural convection that the Rayleigh's Number based upon axial distance is of primary importance. The values of this parameter are listed for the various runs in Tables A-IV - A-VII.

It is noted that they range from approximately 10^9 to 10^{12} for the water-cooled experiments and from 10^9 to 10^{11} for the air-cooled. Nevertheless, even for the water-cooled runs exhibiting the lowest length Rayleigh's Numbers a high degree of turbulence was noted, apparently in excess of that for the high Rayleigh's Number air-cooled runs. It thus appears, that in this type of configuration, the length Rayleigh's Number alone is not sufficient to define the degree of turbulence. The modified Rayleigh's Number, $t \phi_o$ (see Nomenclature for definition) may be more suitable in this regard. It is in the order of 0.5×10^7 to 2×10^8 for the water-cooled runs (see Tables A-IV through A-VII) and 10^6 to 10^7 for the air-cooled. The non-dimensional heat source parameter, q_v , ranges from 2×10^8 to 10^{10} for the water-cooled runs and from 0.5×10^7 to 10^8 for the air-cooled. From the observations of this particular test program, this latter parameter would appear to correlate most closely with the appearance of turbulence. It should be mentioned that the initiation of turbulence in this type of configuration differs from its initiation in the case of natural convection from a flat plate in an infinite fluid, for example, in that there is a feed-back of vortices generated in any portion of the vessel into all other portions. For example, if the flow leaving the descending boundary layer at the lower extremity of the vessel were turbulent, this would influence the ascending core since the fluid leaving the boundary layer becomes the fluid entering the core. Also if there were turbulence at the top of the vessel in the core, this would in turn influence the boundary layer. Turbulence in the boundary layer was not observed under conditions of laminar core flow.

Measured Flow Behavior From Experimental Runs

A general description of the flow phenomena which were observed from the experimental runs has been given in the foregoing section. The purpose of the present section will be the detailed exposition of the results of the experimental measurements. The data are presented in the form of various non-dimensional parameters the meanings of which are given in the Nomenclature section. These non-dimensional quantities are utilized to provide a base for as broad an application of the results as possible. To avoid confusion, Figure 37 is included, showing diagrammatically the various non-dimensional temperature differentials and velocities which are used.

Boundary Layer Effect

Visual observation of the flow obtained in the two facilities confirms qualitatively that there is a relatively thin outer layer of descending fluid adjacent to the cooled test section wall. Temperature profiles taken normal to the wall at different axial positions show that there is also a temperature boundary layer in that almost all the temperature drop between centerline and wall at a given axial position occurs very close to the wall. Because of the lack of precision of the velocity measurements it is not possible to confirm definitely that the radial extent of temperature and velocity boundary layers are equal. However, no evidence to the contrary was produced. It would be expected that they would be approximately equal for fluids wherein the ratio of thermal and momentum diffusivities is of the order of unity (i.e., Prandtl Number near one).. This condition is approximately satisfied by the aqueous test fluid.

The experimental radial temperature profiles which were obtained are shown along with the experimental points in Figure 12-a, b, and c. The ratio of the temperature difference between the fluid and the wall at the same axial position at a given point in the fluid to the temperature difference between the fluid along the centerline and the wall at the same axial position is plotted against the ratio of distance from the wall to the radius. Each curve sheet applies to an order of magnitude range of the ratio of differential between the temperature of the fluid along the centerline at the top to the minimum wall temperature (at the bottom) to the temperature difference between the fluid along the centerline at the top and the wall at the top. For the curve sheet 12-a this ratio t_{c_0}/t_o is approximately 5. This order of magnitude of the ratio is typical of the runs with the water-cooled facility when the coolant flow is in the upward direction. The second sheet, 12-b, is for values of this top-radial to overall temperature ratio of the order of 2.5. This is typical of the runs with the water-cooled facility when the coolant flow is directed in the downward direction. The final sheet, 12-c applies to values of the ratio in the order of 20. Such values apply to the air-cooled runs and to the water-cooled AEC runs. It was assumed in making these plots that the effect of the ratio was sufficiently small, that runs with slightly differing values of the ratio could be lumped together and applied to a mean value.

Each curve sheet shows three groups of curves which apply to different values of the non-dimensional axial position x/l . As marked, the upper group of curves applies to x/l of 0.25, the central group to x/l of 0.50, and the bottom group to x/l of 0.75. (i.e., near the

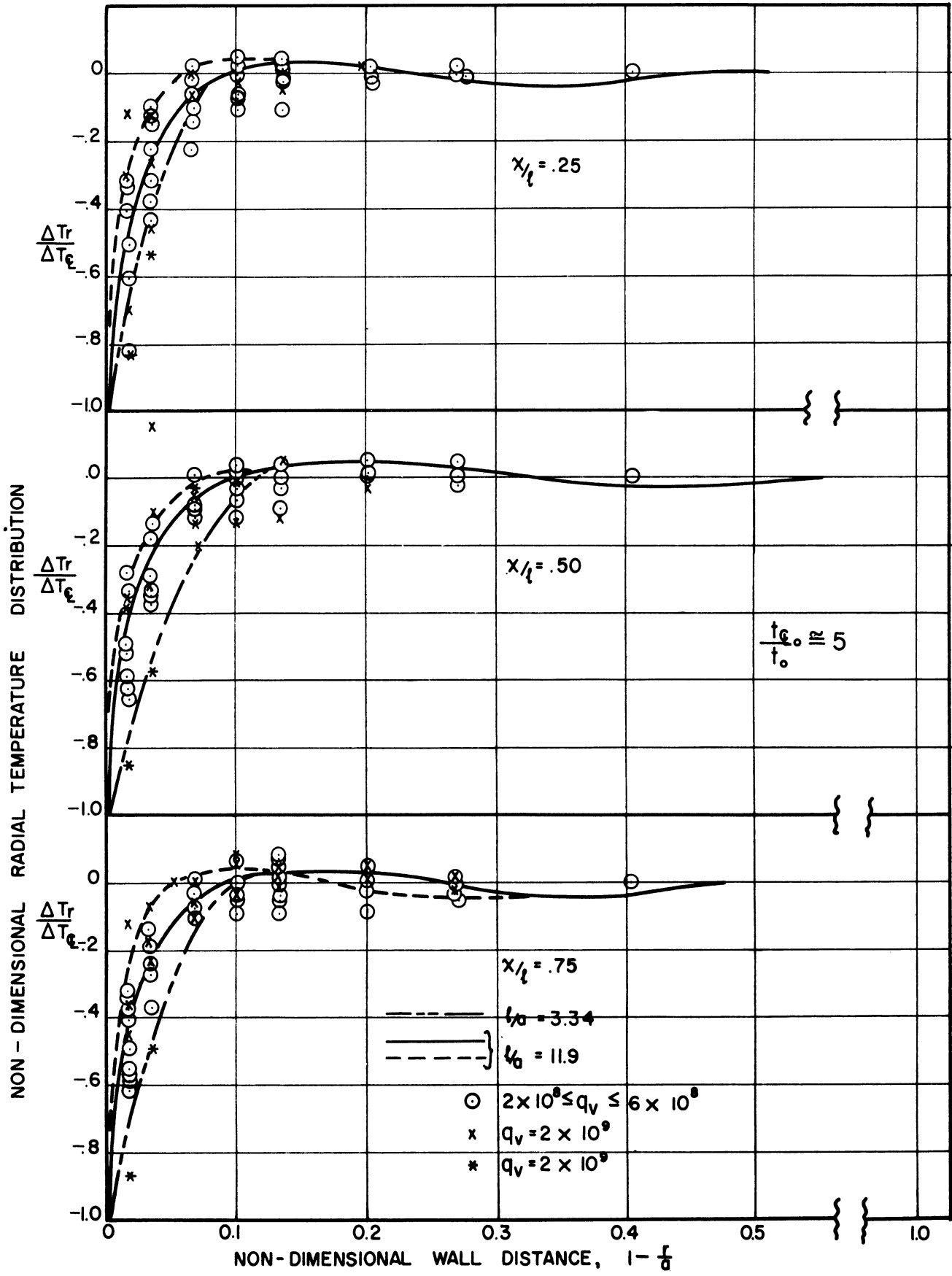


Figure 12-a. Radial Temperature Distribution - Experimental Data

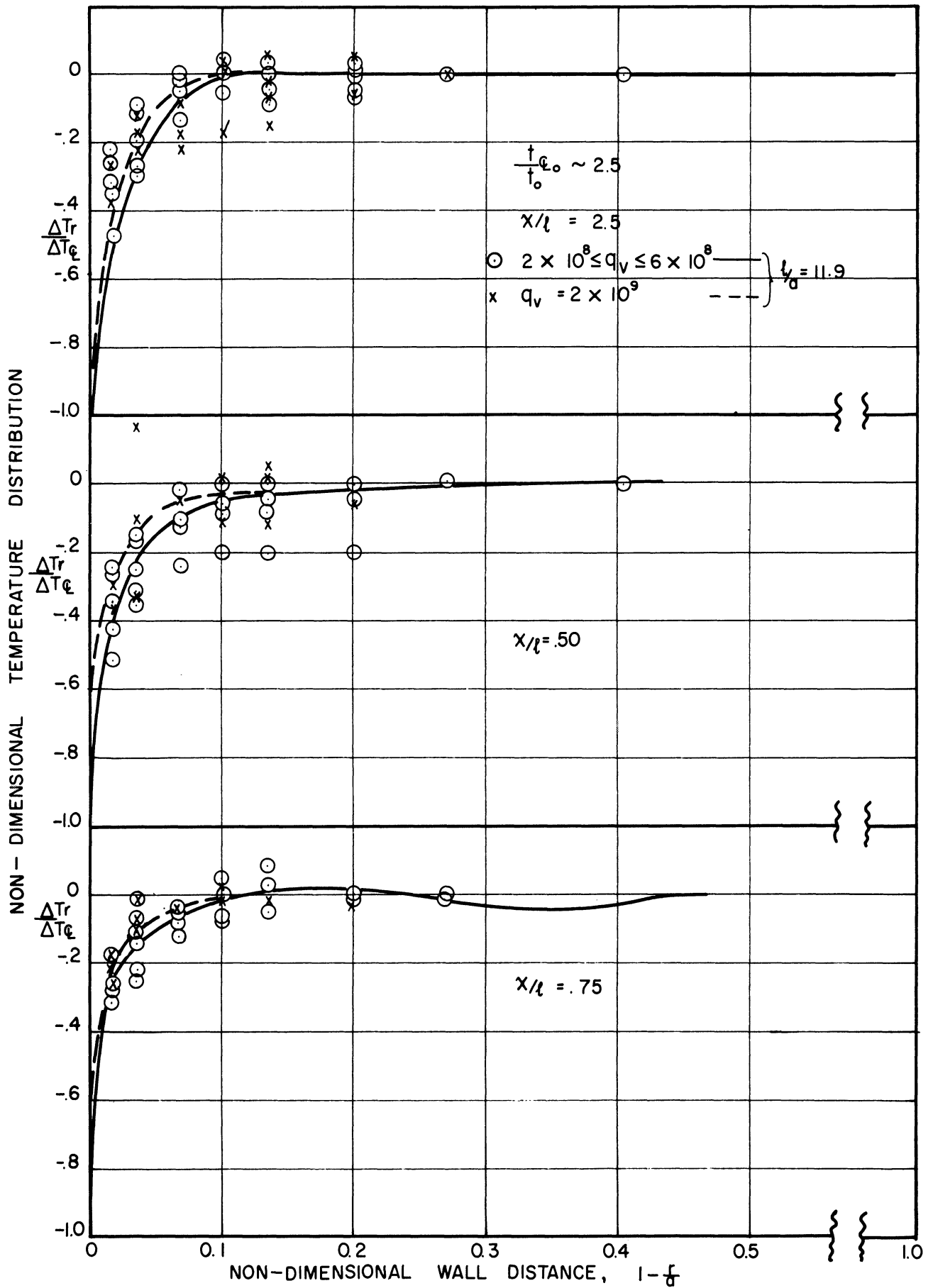


Figure 12-b. Radial Temperature Distribution - Experimental Data

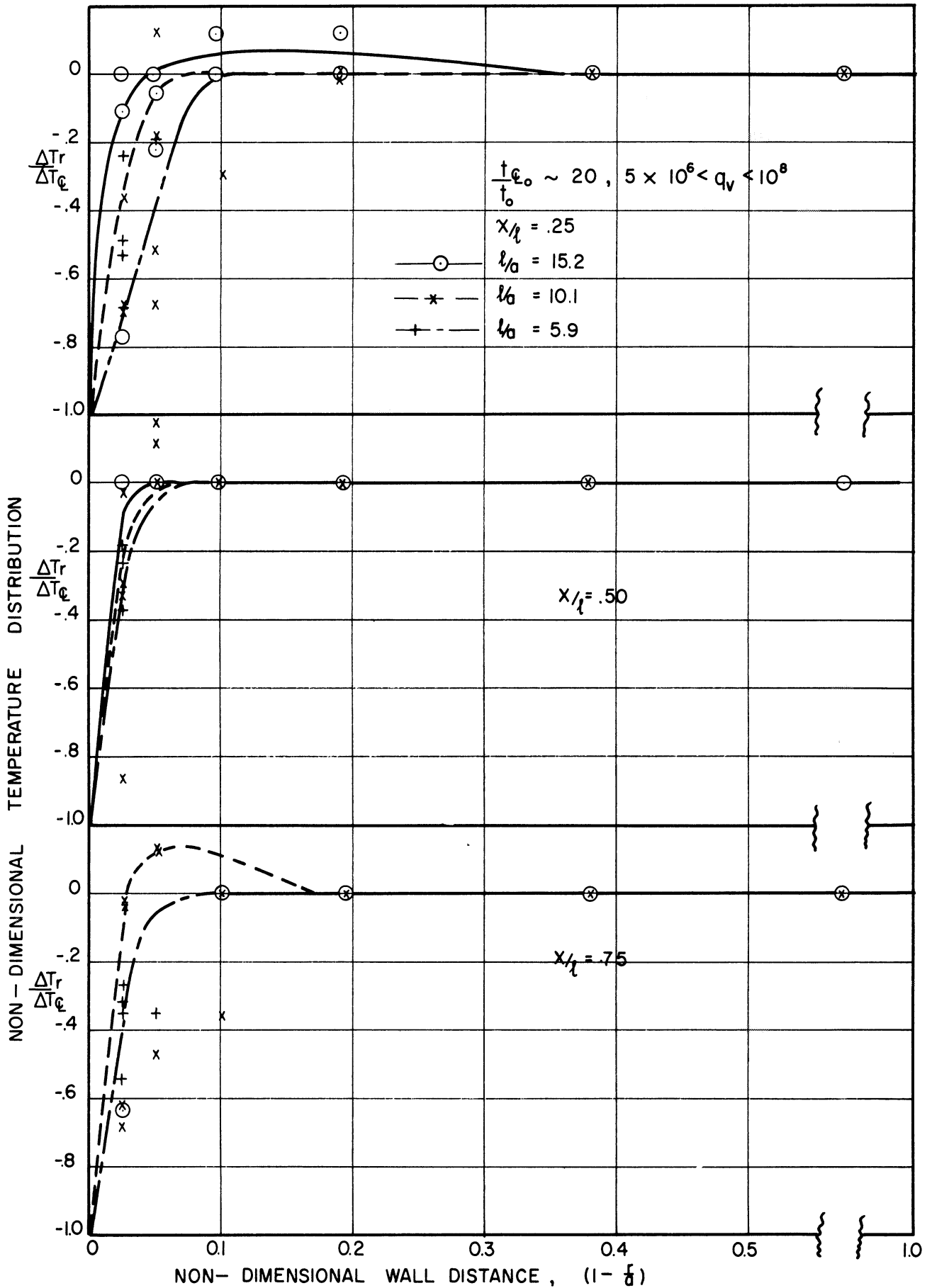


Figure 12-c. Radial Temperature Distribution - Experimental Data

bottom of the test section). As indicated in the legend for each curve sheet, the points are further divided according to the approximate value of the non-dimensional heat source parameter, q_v , and the length to radius ratio of the test section, l/a . Separate curves are drawn according to these various divisions.

It is noted that the character of all the curves are similar, differing mainly in the break point between the radial temperature gradient and the relatively constant temperature portion in the center of the test section. It is further noted that there appears to be a tendency for a saddle to form in the curve so that the maximum temperature exists not along the centerline but near the inner edge of the temperature boundary layer. This can be explained qualitatively on theoretical grounds as will be done in a later section of this report. The radial extent of the boundary layer can be approximated from these curves for the various experimental conditions. It is noted from an examination of Figure 12-c that there appears to be some tendency for a thickened boundary layer with the smaller l/a ratios. Otherwise, there appears to be a thickening of boundary layer with reduced non-dimensional heat source. This is consistent with the theoretical analysis as will be explained in a later section.

Assuming that the substantial variation of boundary layer thickness was only with non-dimensional heat source strength, the apparent temperature boundary layer thicknesses from Figure 12-a, b, and c have been cross-plotted as a function of the overall to radial temperature difference ratio t_{ℓ_o}/t_o . These plots are shown in Figures 13-a and b where experimental points are shown for the three previously used values of non-dimensional axial position, 0.25, 0.50, and 0.75 for

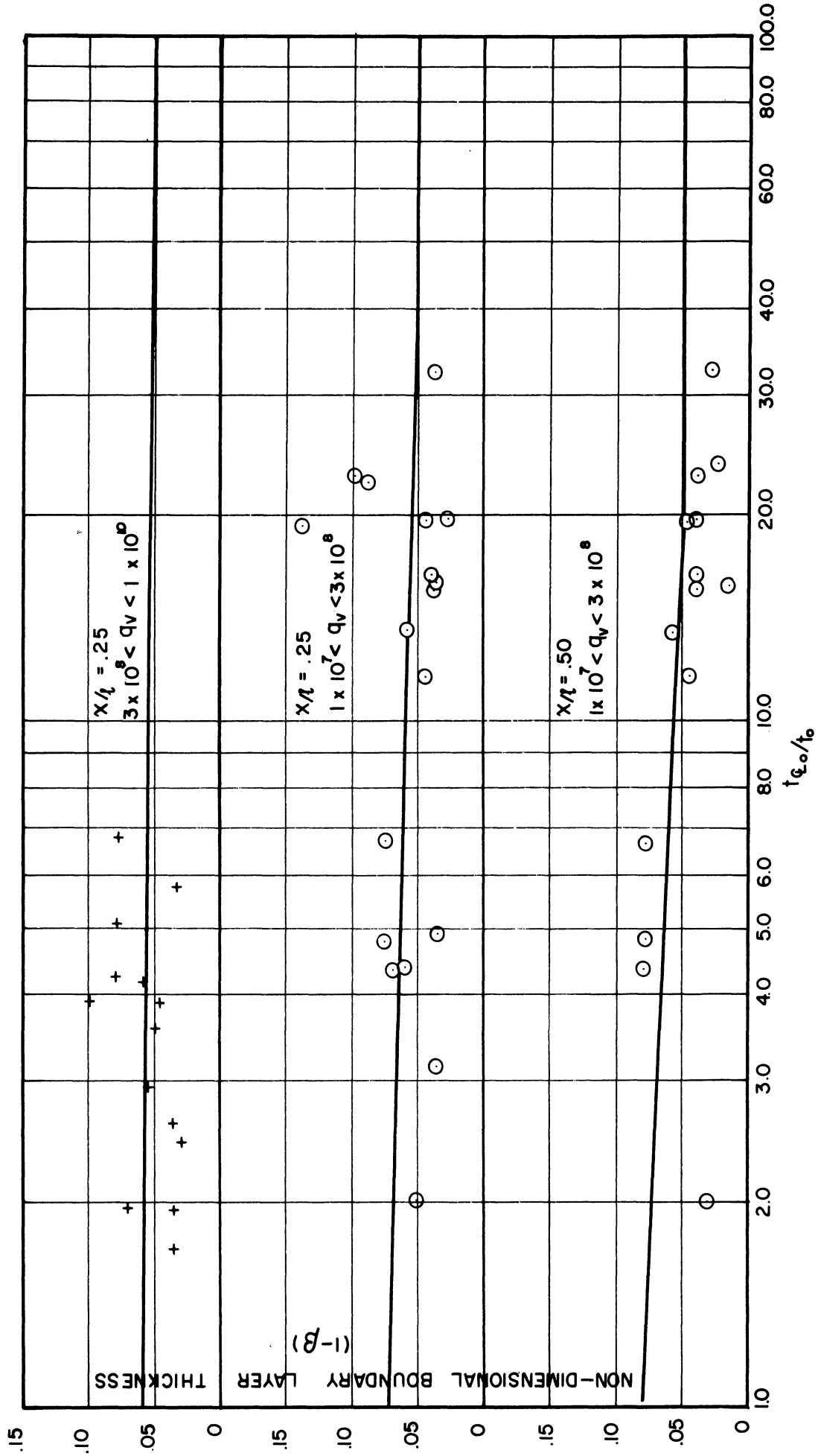


Figure 13-a. Non-Dimensional Boundary Layer Thickness vs. Overall Radial Temperature Ratio - Experimental and Calculated Data.

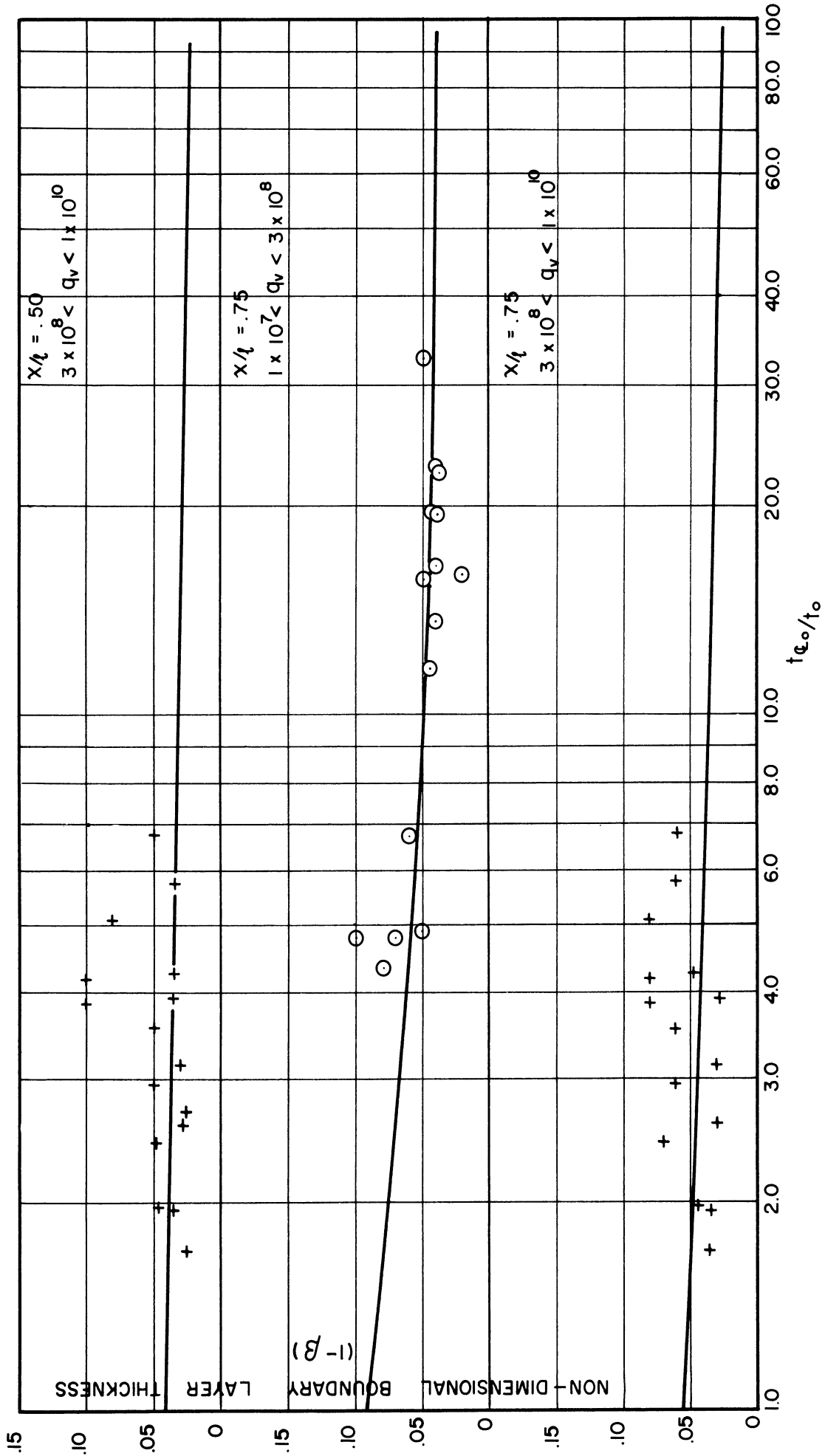


Figure 13-b. Non-Dimensional Boundary Layer Thickness vs. Overall Radial Temperature Ratio - Experimental and Calculated Data.

two ranges of q_v . It is noted that the boundary layer thickness is not strongly a function of t_{ξ_0}/t_0 .

A second cross-plot of this data is shown in Figure 14 where the boundary layer thickness is plotted as a function of the non-dimensional axial position, x/l . The experimental data, cross-plotted from Figure 13 for two overall/radial non-dimensional temperature ratios, is compared with the calculated data for a similar wall temperature distribution, for the same overall/radial temperature ratios. It is noted that the agreement is reasonably close and that the existence of a boundary layer type phenomenon, expected on theoretical grounds, is confirmed.

Axial Temperature Gradients

As previously mentioned, there exists a substantial axial temperature gradient both along the centerline and along the inner surface of the enclosing test section wall regardless of the method of wall cooling or the direction of the coolant flow. In all cases, the temperature decreases toward the lower end, with the rate of decrease accelerating as the bottom of the vessel is approached. The overall temperature difference between top and bottom of the test section, either along the centerline or along the wall, is greater by several times than the temperature differential between centerline and wall at a given axial position. The parameter overall/radial temperature ratio, t_{ξ_0}/t_0 , is in fact the ratio of the sum of temperature differentials between wall and centerline at the top of the vessel and the differential between wall top and bottom to the differential between centerline and wall at the top. This ratio ranged experimentally from approximately

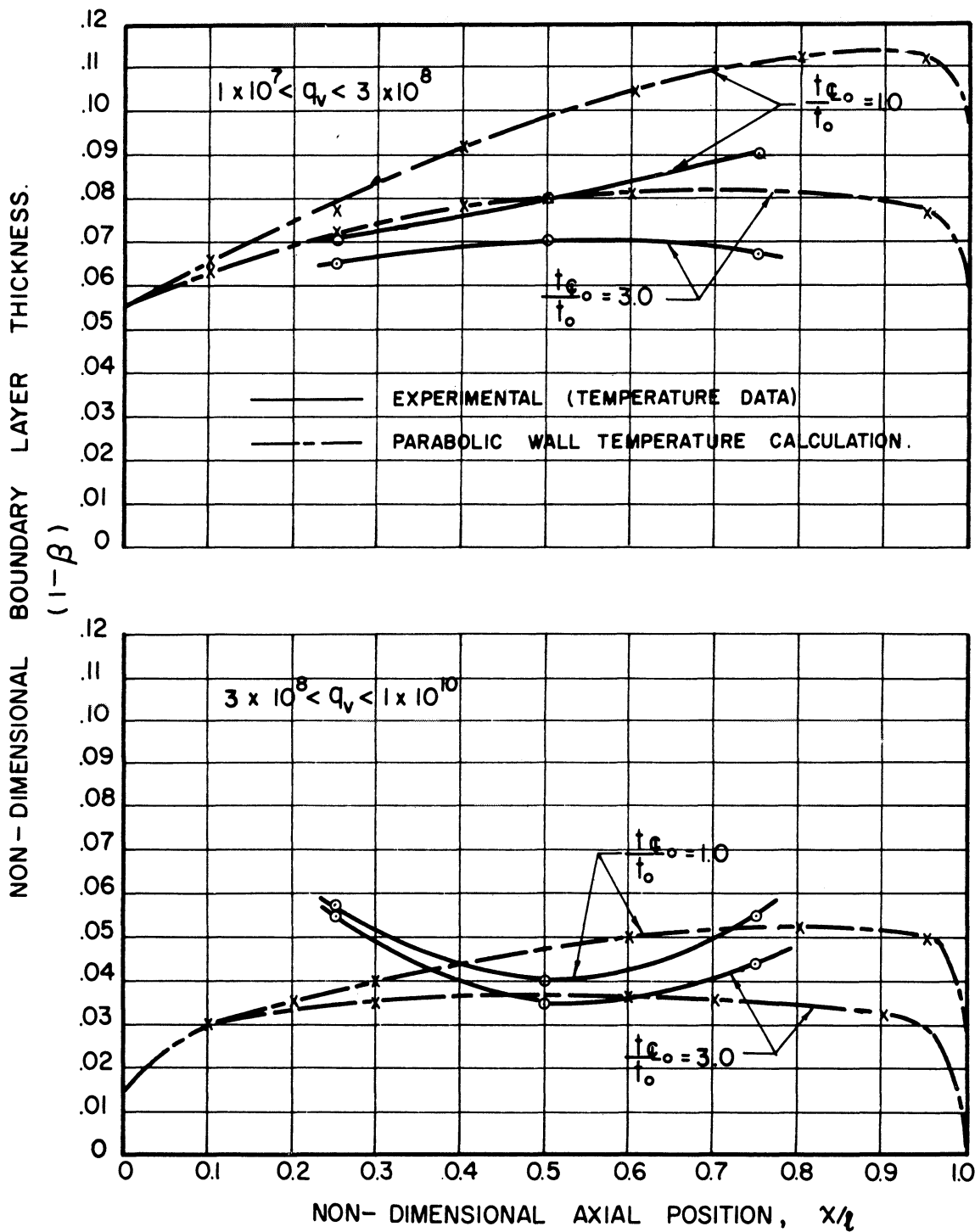


Figure 14. Non-Dimensional Boundary Layer Thickness vs. Non-Dimensional Axial Position

2.0 for the water-cooled facility runs in which the coolant flow was from top to bottom, to approximately 4.0 for the water-cooled facility runs in which the coolant flow was from bottom to top, up to 15 to 30 for the air-cooled facility. For the water-cooled AEC experimental runs⁽¹⁰⁾, the ratio was of the order of 40. It was found that minor variations in this ratio could be obtained by varying the rate of coolant flow for the water-cooled facility.

The experimental points for the ratio of non-dimensional wall temperature (differential from given axial position to bottom) to overall temperature (differential between centerline at top and wall at bottom - i.e., maximum differential existing in the facility) are plotted as a function of overall/radial non-dimensional temperature in Figures 15-a, b, and c. The first curve sheet, 15-a, applies to the non-dimensional axial position of 0.25, the second to 0.50, and the third to 0.75. The plotted points are those from the water-cooled facility at full and reduced length, with coolant flow preceding from top to bottom, and also in the reverse direction, for various coolant flow rates and values of non-dimensional volumetric heat source; those from the air-cooled facility at various power levels for full, 2/3, and 1/3 length; and finally those from the AEC runs. The legend printed on each sheet differentiates the points with respect to non-dimensional heat source parameter and also sets apart the AEC runs. The points for q_v less than 2×10^8 are those from the air-cooled facility.

By the definition of the ordinate and abscissa, the curve must pass through zero ordinate when the overall/radial temperature ratio is 1.0. The remainder of the curve is fairly well defined by

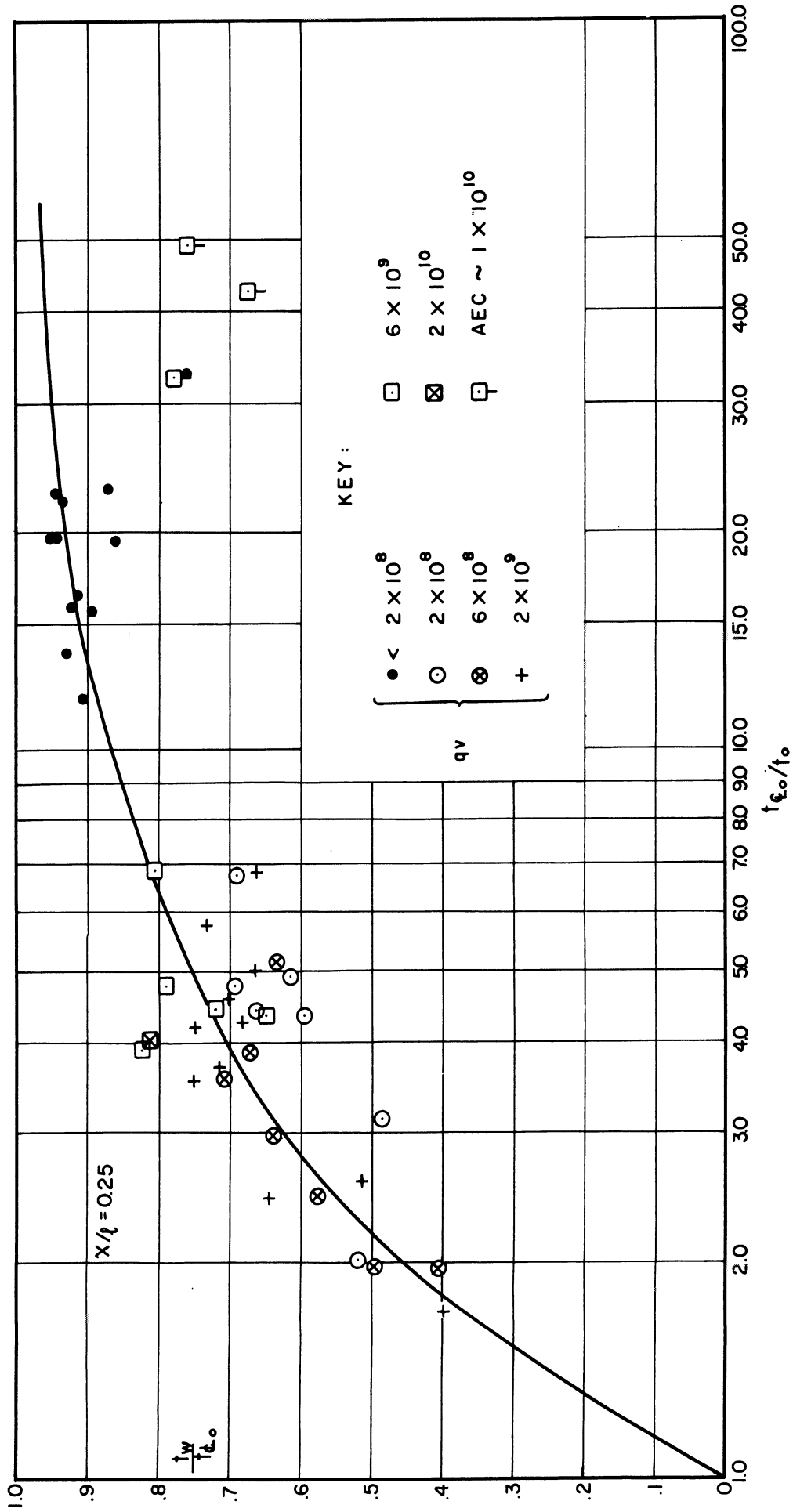


Figure 15-a. Non-Dimensional Wall Temperature vs. Overall/Radial Temperature Ratio, Experimental Data, $x/l = 0.25$

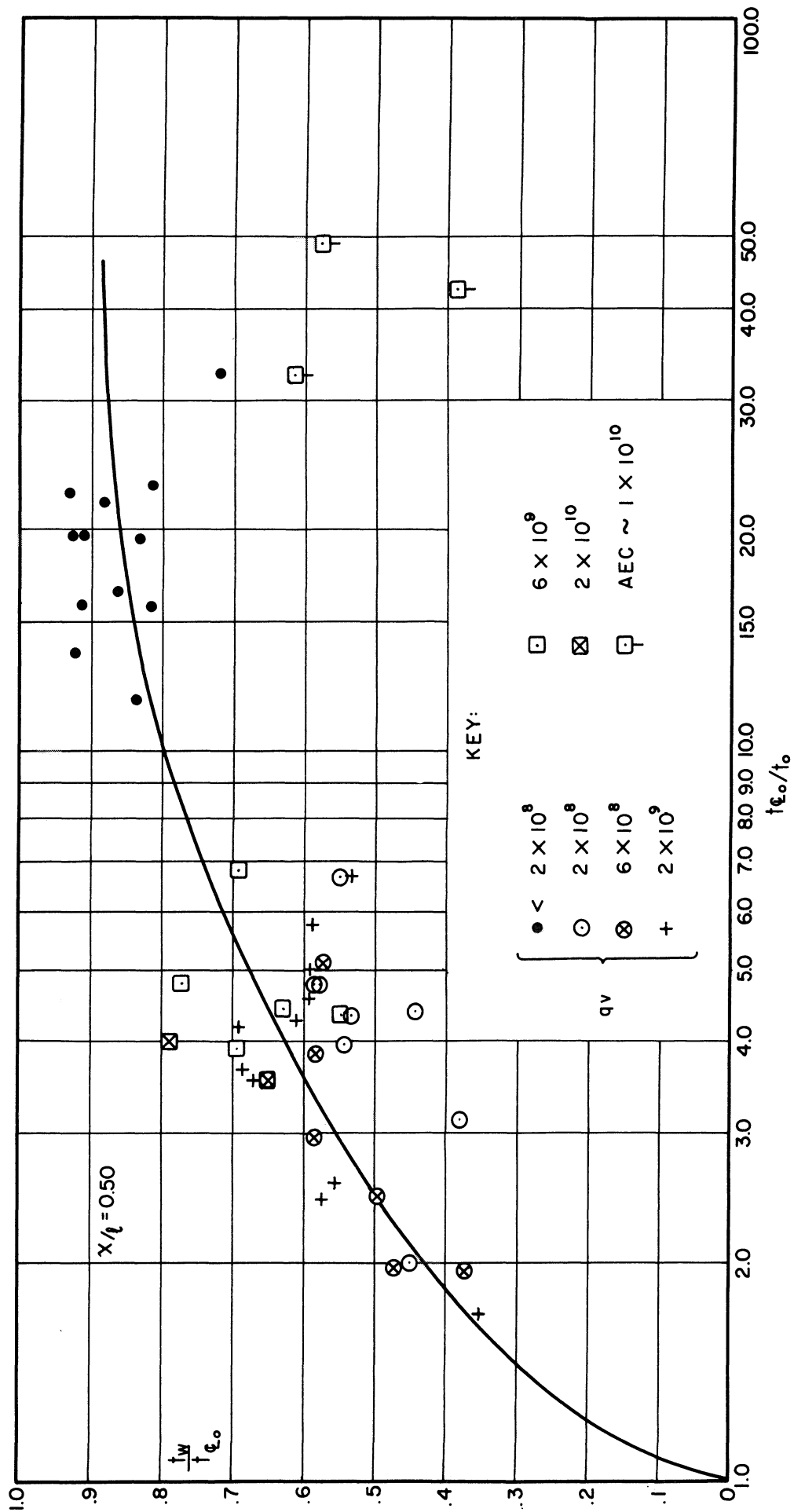


Figure 15-b. Non-Dimensional Wall Temperature vs. Overall/Radial Temperature Ratio, Experimental Data, $x/l = 0.50$

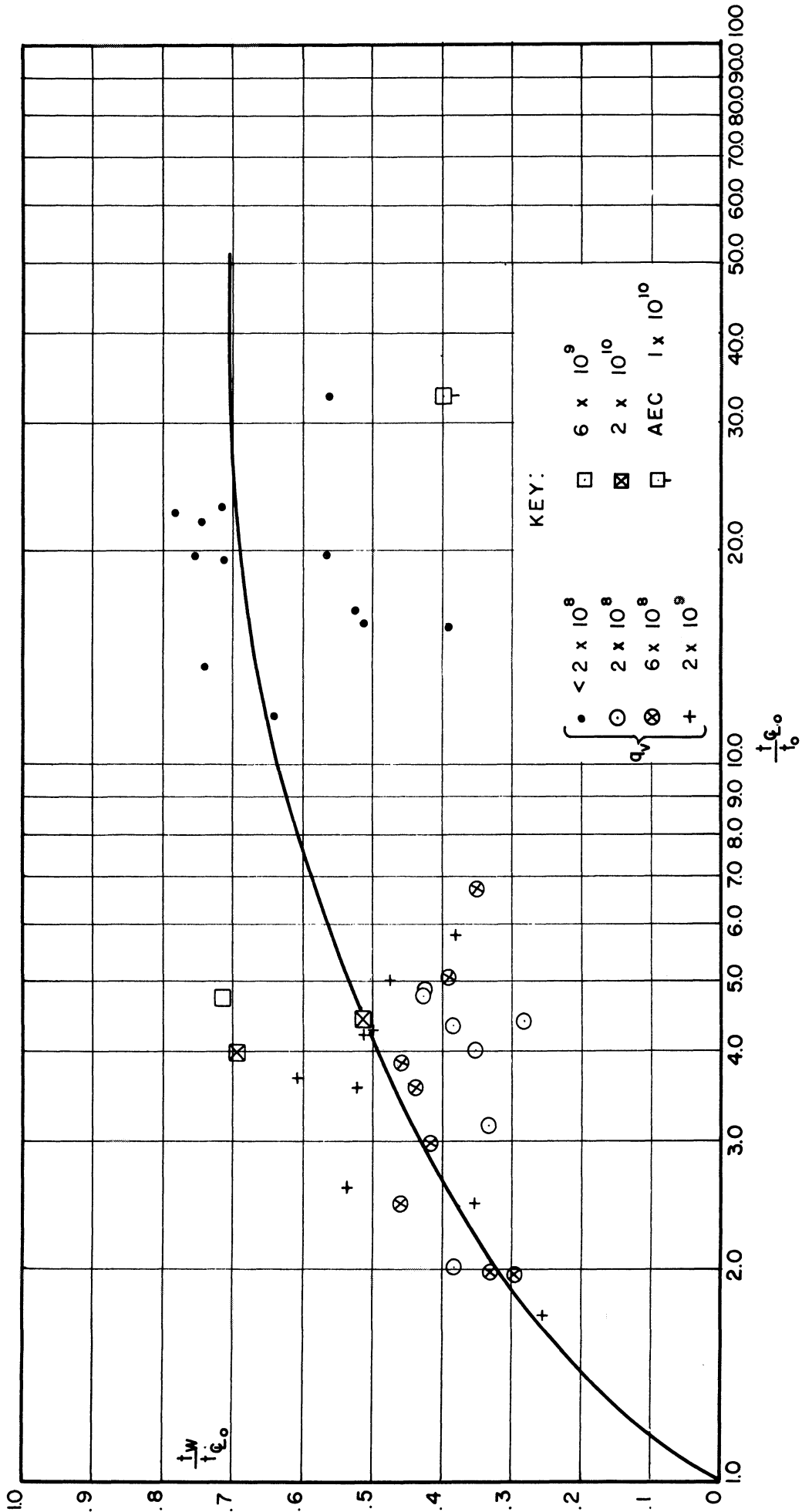


Figure 15-c. Non-Dimensional Wall Temperature vs. Overall/Radial Temperature Ratio, Experimental Data, $x/l = 0.75$

the experimental points for the various x/l positions with the exception of the AEC runs. It is believed that the inconsistency between the AEC runs and those of the present study is caused primarily by failure, in the case of the AEC runs, to measure the temperature sufficiently near the bottom of the facility. As previously mentioned, it was observed in all the runs of the present investigation, that the decrease in temperature very close to the lower extremity of the tube is severe. Thus, the wall temperature differential taken from the AEC runs is too low since it does not include this lower end drop. For this reason, the AEC points were not considered in the plotting of the experimental curves. There appears to be no theoretical basis for the assumption that the curves should drop for large overall/radial temperature ratio as is indicated by the AEC points.

Figures 16-a, b, and c are the plots of the experimental points for the ratio of temperature differential between fluid along the centerline at a given axial position and the bottom wall temperature to the differential between the fluid at the centerline at the top and the bottom wall temperature vs. the overall/radial temperature ratio for various x/l positions. Again the legend indicates the origin of the points and again points from the water-cooled, air-cooled, and AEC facility are included. Again the AEC points appear inconsistent with the remainder, and the reason is apparently as previously explained. A finite differentiation between the higher and lower ranges of non-dimensional volumetric heat source, q_v , appeared to exist so that separate experimental curves were drawn. By definition of the coordinates it is obvious that these curves should be asymptotic to 1.0 for infinite

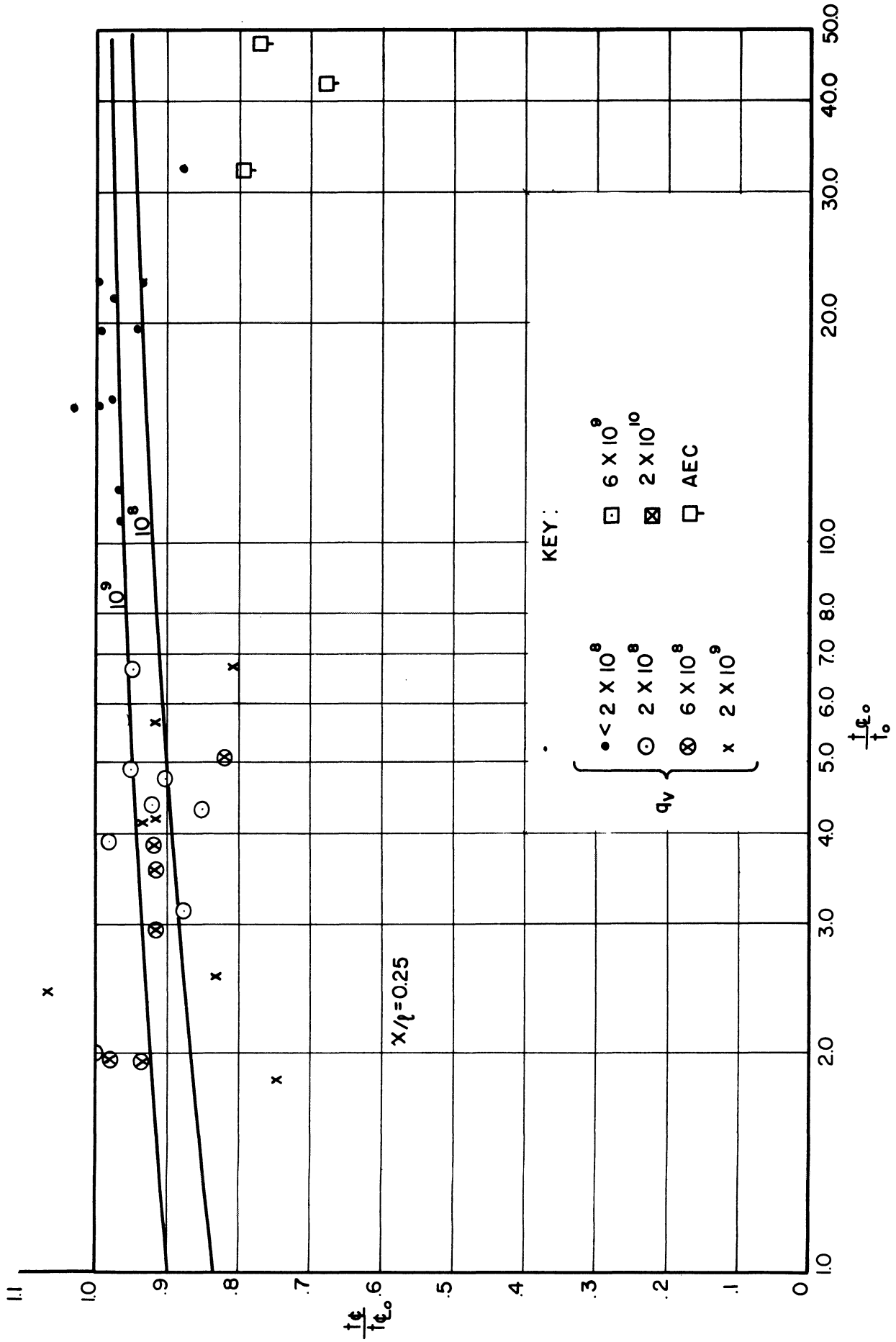


Figure 16-a. Non-Dimensional Centerline Temperature vs. Overall/Radial Temperature Ratio, Experimental Data, $x/l = 0.25$.

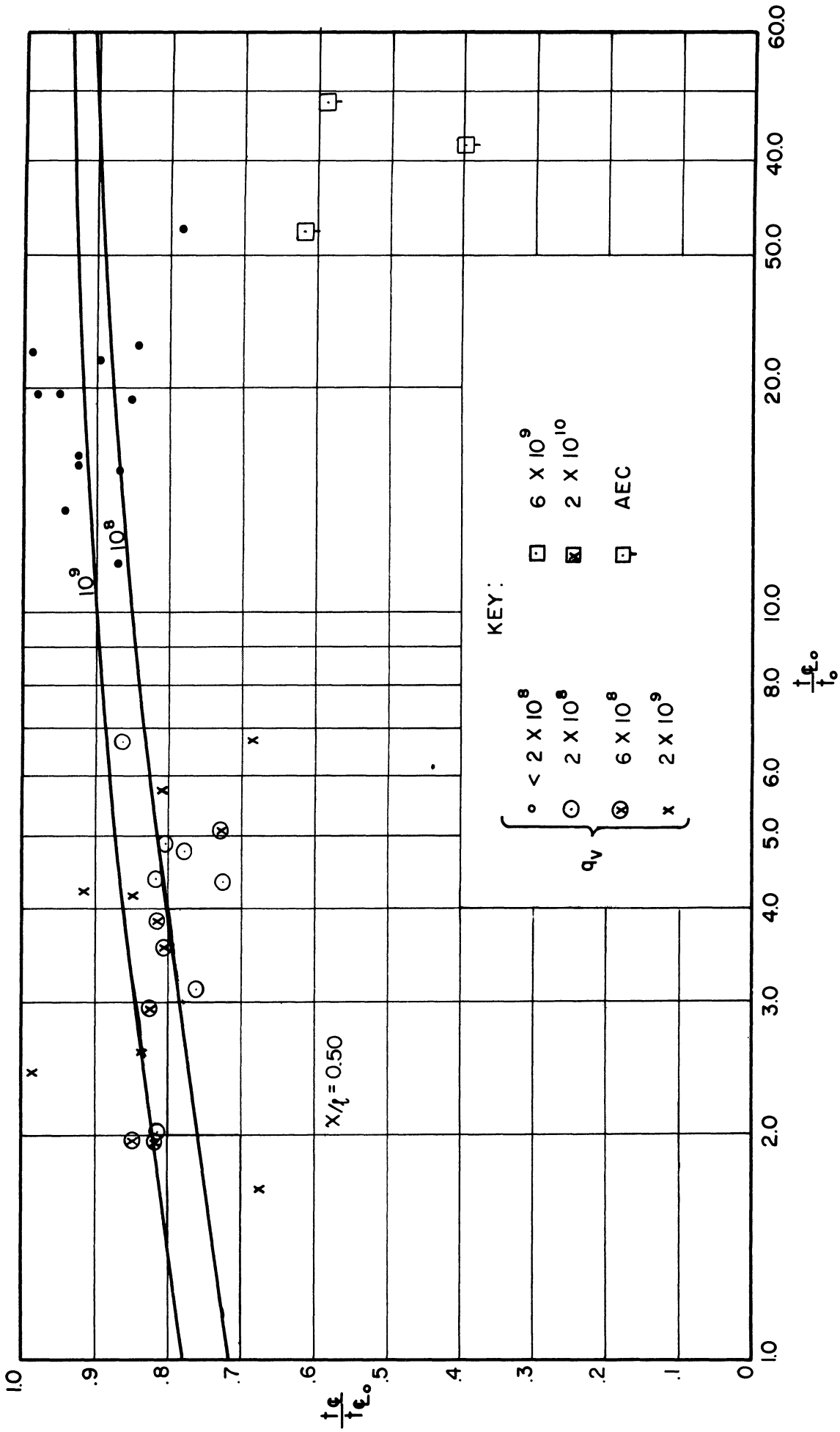


Figure 16-b. Non-Dimensional Centerline Temperature vs. Overall/Radial Temperature Ratio, Experimental Data, $x/l = 0.50$.

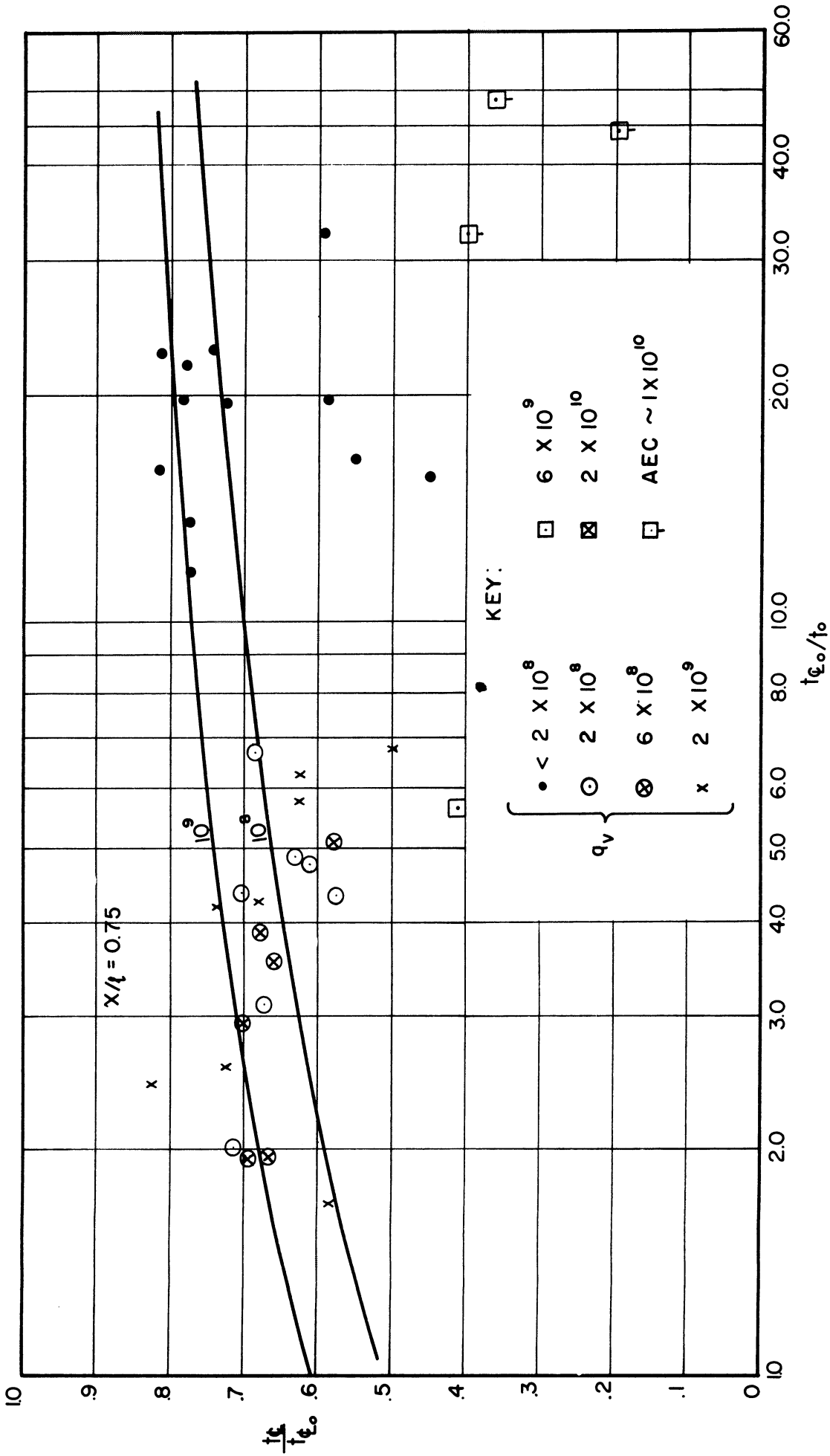


Figure 16-c. Non-Dimensional Centerline Temperature vs. Overall/Radial Temperature Ratio, Experimental Data, $x/l = 0.75$.

overall/radial temperature ratio. There is no obvious termination for unity value of this ratio.

Figure 17 is a cross-plot of these experimental curves showing the ratio of the non-dimensional wall temperature (differential from top to bottom) to the overall non-dimensional temperature (differential between centerline at top and wall at bottom) as a function of non-dimensional axial position. The parameter applying to the various curves is the overall/radial temperature ratio. It is noted that the curve for unity value of this ratio is the horizontal ordinate.

Figure 18 is a normalized version of the preceding Figure 17 in that the ratio of non-dimensional wall temperature at a given non-dimensional axial position to the overall non-dimensional wall temperature is shown as a function of non-dimensional axial position, x/l . It is shown that as the overall/radial temperature ratio is increased the proportion of the overall wall temperature drop concentrated near the bottom increases. The dotted straight line shows the linear wall temperature assumption on which the majority of the calculations were based (explained in detail in a later section).

Figures 19-a and b is a cross-plot of the experimental data from Figure 16, showing the ratio between the non-dimensional centerline temperature (differential from given axial position of centerline to wall at bottom) to the overall non-dimensional centerline temperature (differential between centerline at top and wall at bottom) as a function of non-dimensional axial position, x/l . The parameter distinguishing the curves is the overall/radial temperature ratio. The experimental curves are included for the non-dimensional heat source

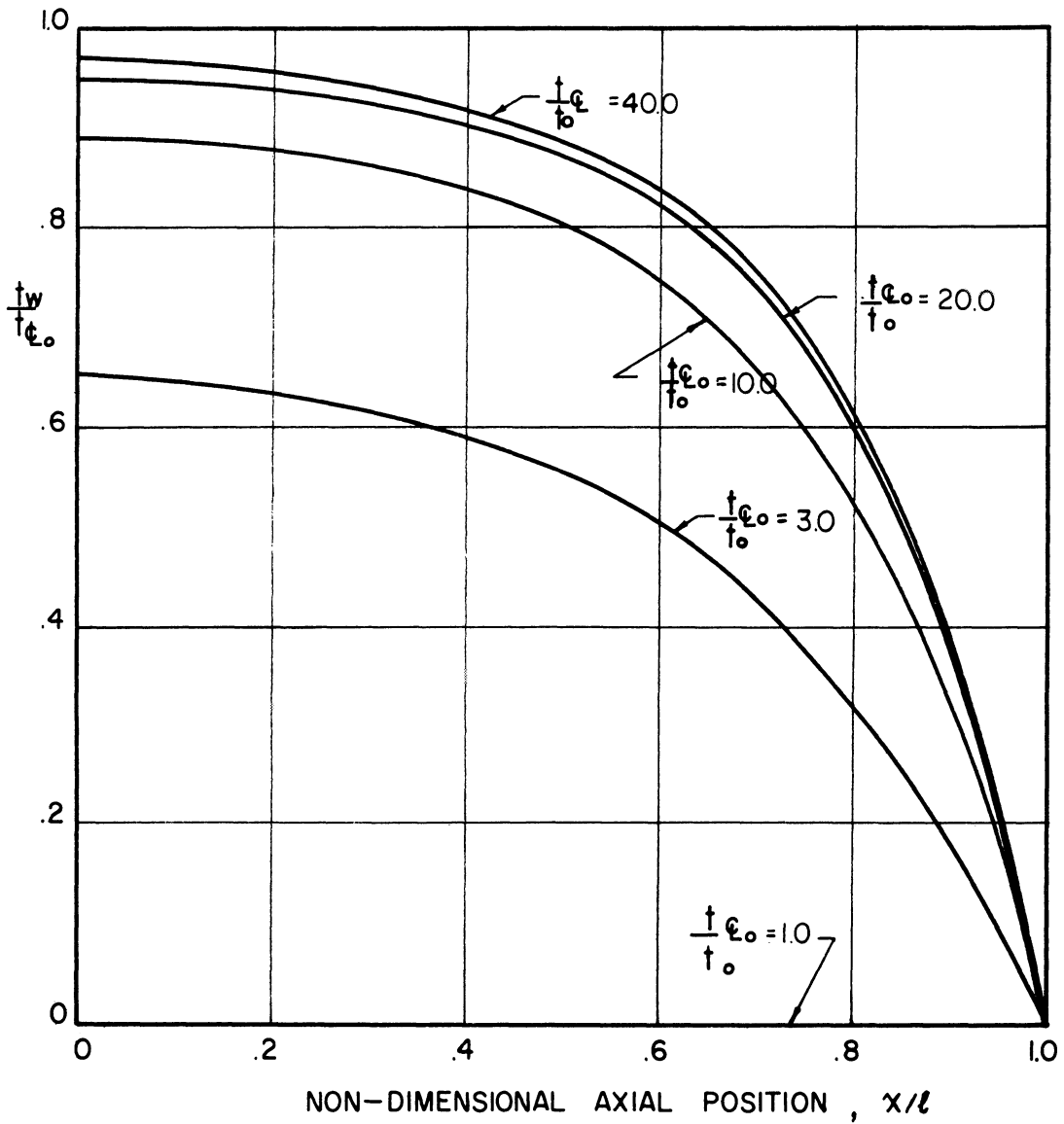


Figure 17. Non-Dimensional Wall Temperature vs. Non-Dimensional Axial Position, Experimental Data

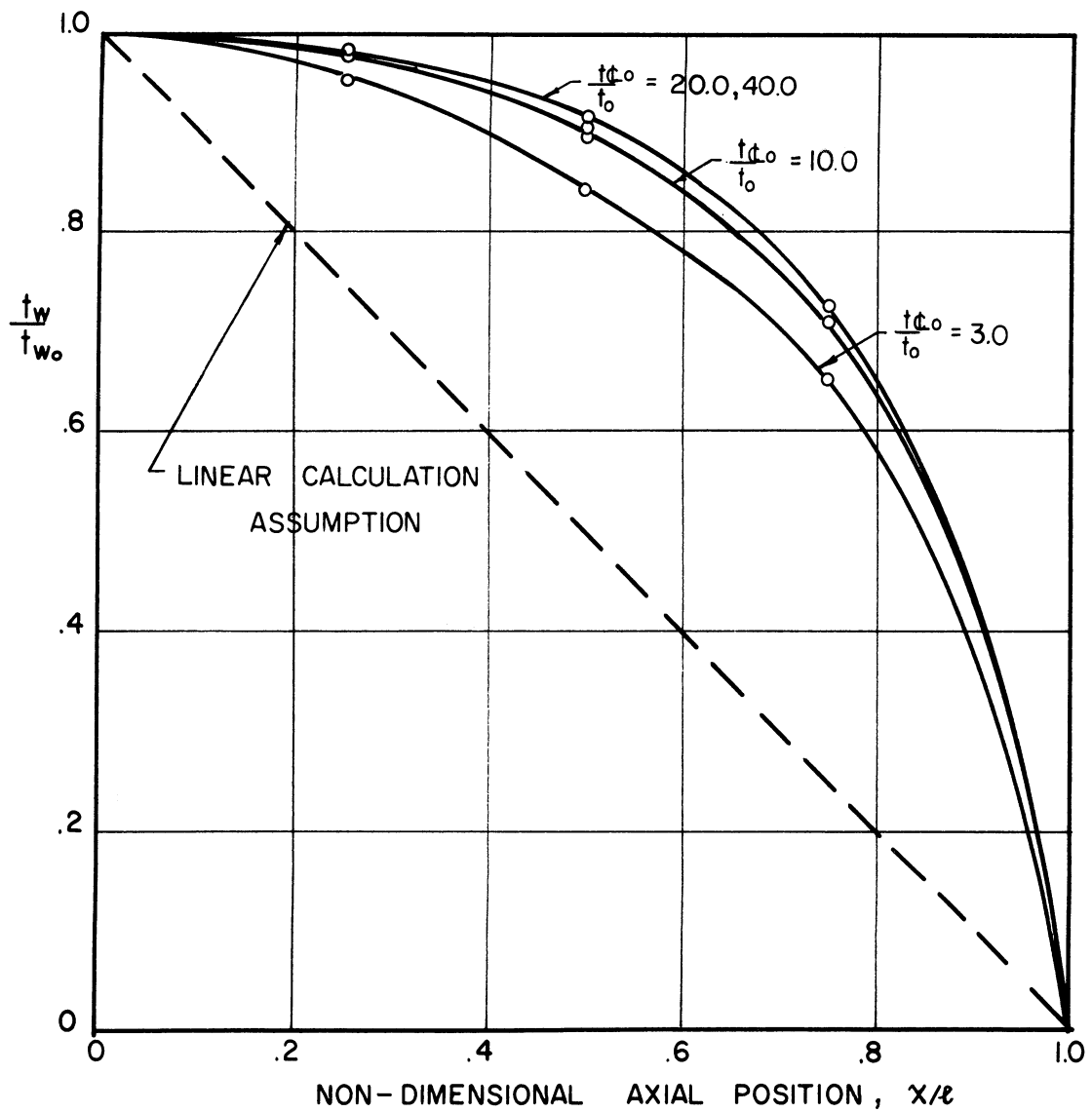


Figure 18. Normalized Non-Dimensional Wall Temperature vs. Non-Dimensional Axial Position, Experimental Data.

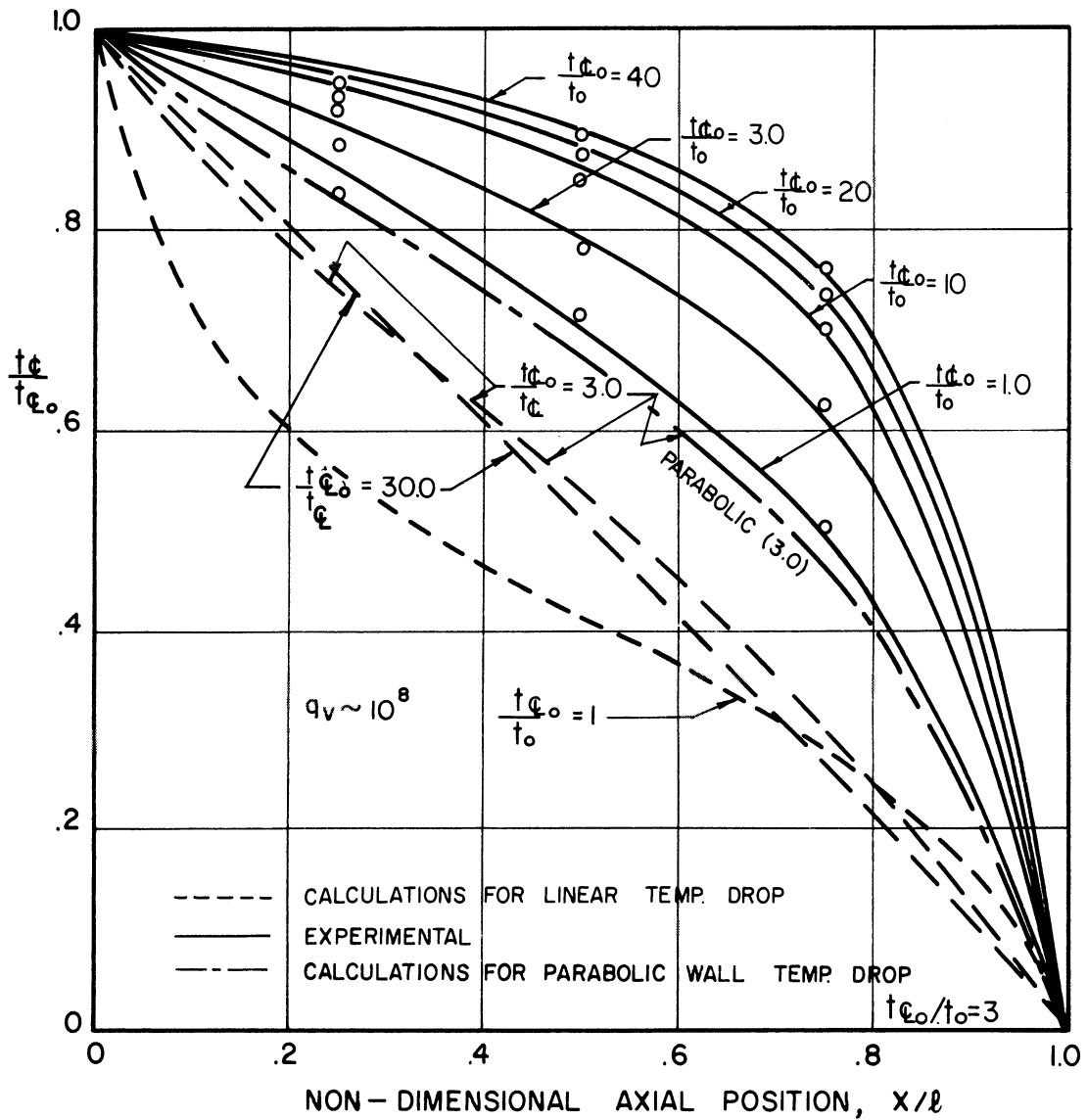


Figure 19-a. Non-Dimensional Centerline Temperature vs. Non-Dimensional Axial Position, Experimental Data Compared to Linear and Parabolic Wall Temperature Distribution, $q_v \approx 10^8$.

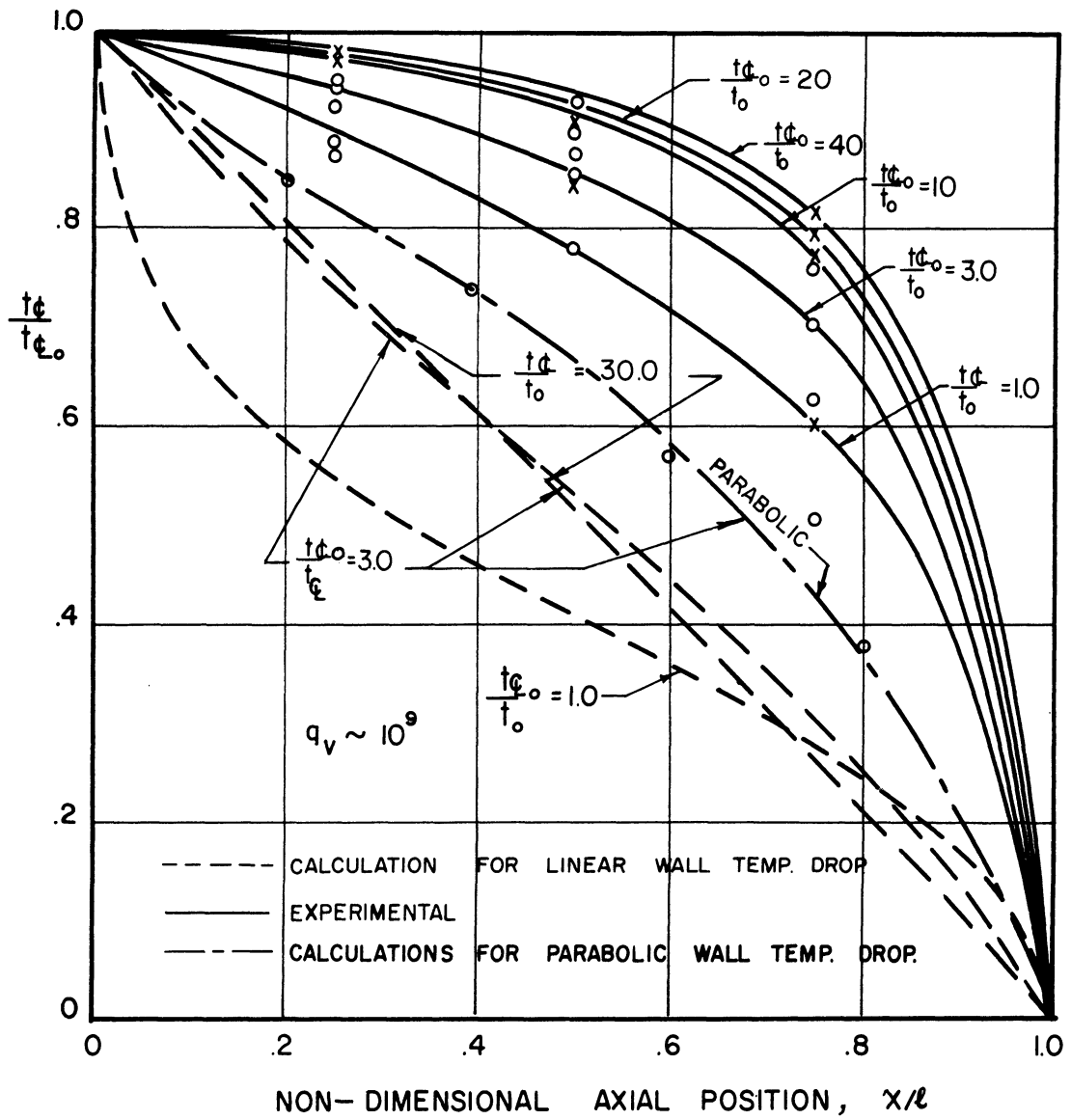


Figure 19-b. Non-Dimensional Centerline Temperature vs. Non-Dimensional Axial Position, Experimental Data Compared to Linear and Parabolic Wall Temperature Distribution, $q_v \approx 10^9$.

parameter, q_v of the order of 10^8 and 10^9 . The calculated curves, based upon the assumption of linear and parabolic wall temperature distribution are included for comparison. It is noted that the agreement with respect to type of curve and magnitude is quite good. The origin of these calculated curves will be explained in a later section.

Radial Temperature Gradients

The experimental radial temperature gradients at various non-dimensional axial positions were discussed under the section regarding boundary layer effects and are shown in Figures 12-a, b, and c. Figure 20 shows the variation of the temperature differential between centerline and wall at a given axial position for various ratios of the overall/radial temperature ratio. This is presented as a curve of the ratio of centerline to wall non-dimensional temperature differential at a given axial location to centerline at top to wall at bottom differential versus the non-dimensional axial position, x/l . It is noted that the differential between centerline and wall decreases in general toward the bottom of the tube with the rate of decrease becoming most pronounced toward the bottom. The decrease is most substantial for minimum ratios of overall/radial temperature ratio. For the case of constant wall temperature (i.e., overall/radial temperature ratio at top of unity), the drop toward the bottom is largest. It still exists for an overall/radial ratio of 3.0. In this case the differential is virtually constant for the entire length of the vessel except the section near the bottom where the differential decreases rapidly to zero. For the case of even larger ratios of overall to radial temperature differentials, it is noted that the experimental curves are quite flat with

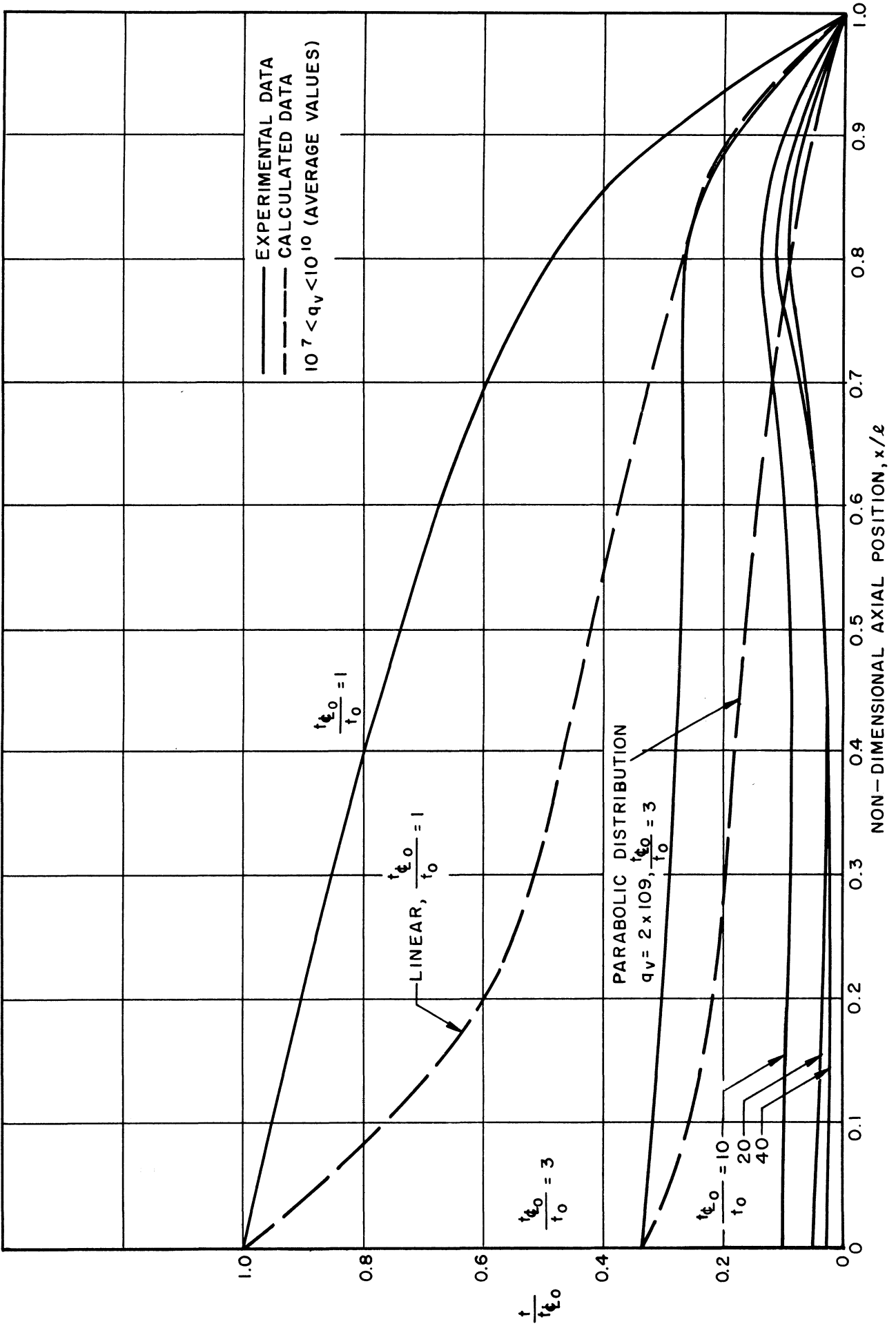


Figure 20. Non-Dimensional Temperature Differential Centerline to Wall vs. Non-Dimensional Axial Position.

axial position, showing a maximum toward the lower end of the test section before decreasing to zero at the bottom. The calculated curves for ratios of 3 and unity are shown for purposes of comparison. It is noted that the agreement between the experimental and calculated curves is quite good. The basis for the calculated curves will be explained in later sections of this dissertation. The experimental curves are the result of cross-plots from the experimental curves shown in Figures 12-a, b, and c. Although no experimental data are available for a unity value of the ratio of overall to radial temperature differential, the cross-plotted curves, Figures 15 and 16, were extrapolated to this value.

The idealized radial temperature gradients (assumed) for various values of the non-dimensional heat source parameter, q_v , resulting from the calculations and assumptions, are shown in Figure 21. It is noted that the boundary layer thickness at a specific axial position (the plots are based on an x/l of 0.40) increases as the non-dimensional heat source is decreased. Over the range of q_v between 2×10^9 and 10^5 it increases from approximately 0.04 to 0.30. The investigation was not carried to the determination of the non-dimensional heat source value for which the boundary layer would fill the entire tube.

Wall Conduction Heat Flux Distributions

The axial distribution of heat flux through the wall is of great practical importance in many applications. Consequently the variation of this quantity as a function of axial position was measured for many of the experimental runs. The resulting heat fluxes, normalized to a unity value for the test section midpoint ($x/l = 0.5$) are listed.

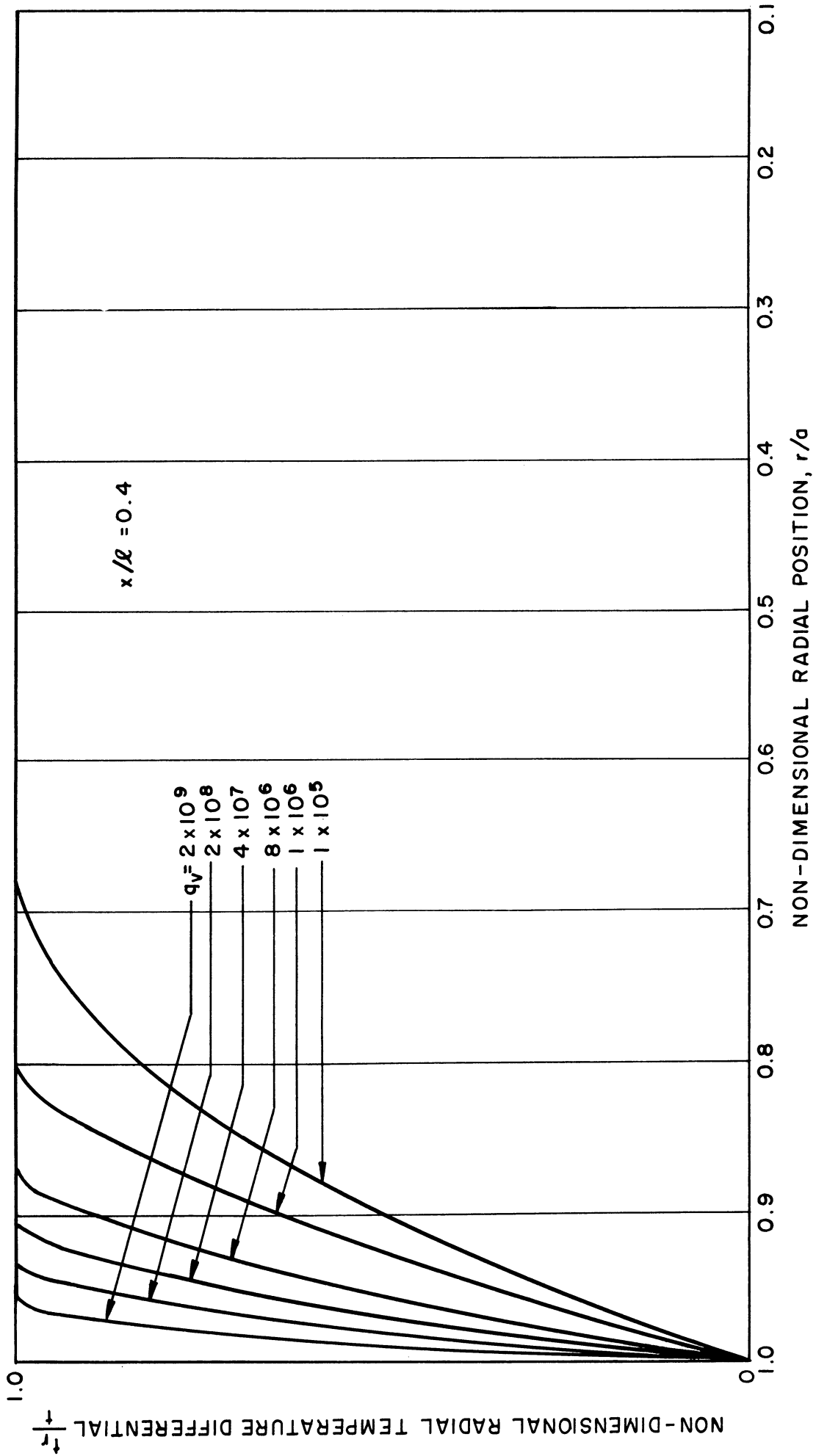


Figure 21. Non-Dimensional Radial Temperature Profiles, Calculated Data, Constant Wall Temperature, Uniform q_y

at 0.25 and 0.75 x/l in the summary sheets for the experimental runs, Tables A-IV through A-VII. The basis for the computation of these values from the experimental measurements is a measurement or estimation of the temperature differential across the glass test section. The temperature of the inner surface of the glass was measured at various axial positions by a travelling thermocouple probe as previously discussed. For the water-cooled facility the temperature of the outside of the glass test section tube was deduced from a knowledge of the inlet and outlet water temperatures. In most cases these do not differ by a significant amount as compared to the variation of the inner test section surface. The temperature differential between the outer surface of the glass test section and the water is small because of the existence of forced convection. It was assumed that the glass thickness and thermal conductivity does not change with position. For all these reasons the deduction of wall heat flux in this manner is not precise. However, the trends which are indicated by a large number of runs should not be substantially in error.

For the air-cooled facility the inner wall temperature was measured in the same manner as for the water facility. The outside wall temperature at various points along the length was also measured so that a direct determination of the temperature differential across the glass was possible. To deduce from these the relative values of the wall heat flux, it is again necessary to assume a constant wall thickness. This condition may be substantially in error so that the results would be affected.

The experimental points of wall conduction per unit area, normalized to the midpoint of the test section are plotted for various axial positions as a function of overall/radial temperature ratio, Figure 22. Points are shown for the water-cooled facility runs, the air-cooled runs, and also for the AEC runs. These latter were deduced from the reported coolant temperature and the inner wall temperatures which were listed in the same manner as previously described for the water-cooled facility. The use of experimental points from the three sources allows a representation over a range from 2 to 40 for the overall all/radial temperature ratio. It is noted from the curves that the variation from unity for the positions above and below the midpoint is most pronounced for the small overall/radial temperature ratios. At x/l of 0.25 and 0.75 there is a variation above and below the mean respectively, for all heat fluxes of the order of 20%. By definition the curve for x/l of 0.50 is a horizontal line at unity normalized heat flux.

The data from Figure 23 is cross-plotted for various values of the overall/radial temperature ratio giving normalized wall heat flux as a function of non-dimensional axial position, x/l , on the calculated data curve sheet, Figure 32-d, where it is compared with the normalized wall heat fluxes resulting from the theoretical calculations. The basis for these calculations is explained in a later section. The agreement between the experimental and the theoretical curves between the non-dimensional axial position extremes of 0.25 and 0.75 is good. It is noted that the theoretical curves indicate a many-fold increase near the top of the vessel. The experimental technique was not adequate to detect the existence of such a rise. If it had existed, the heat

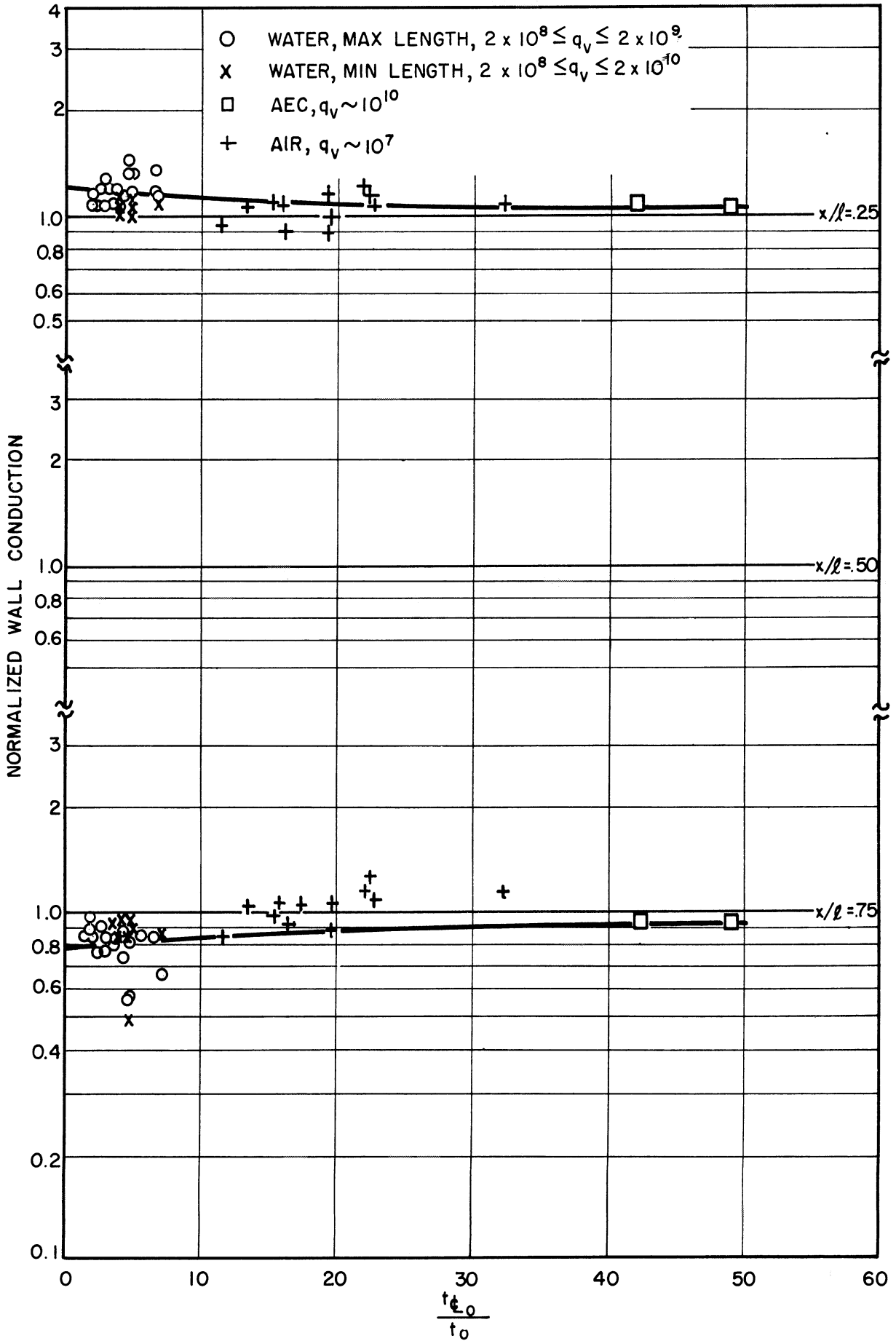


Figure 22. Normalized Wall Conduction vs. Overall/Radial Temperature Ratio, Experimental Data.

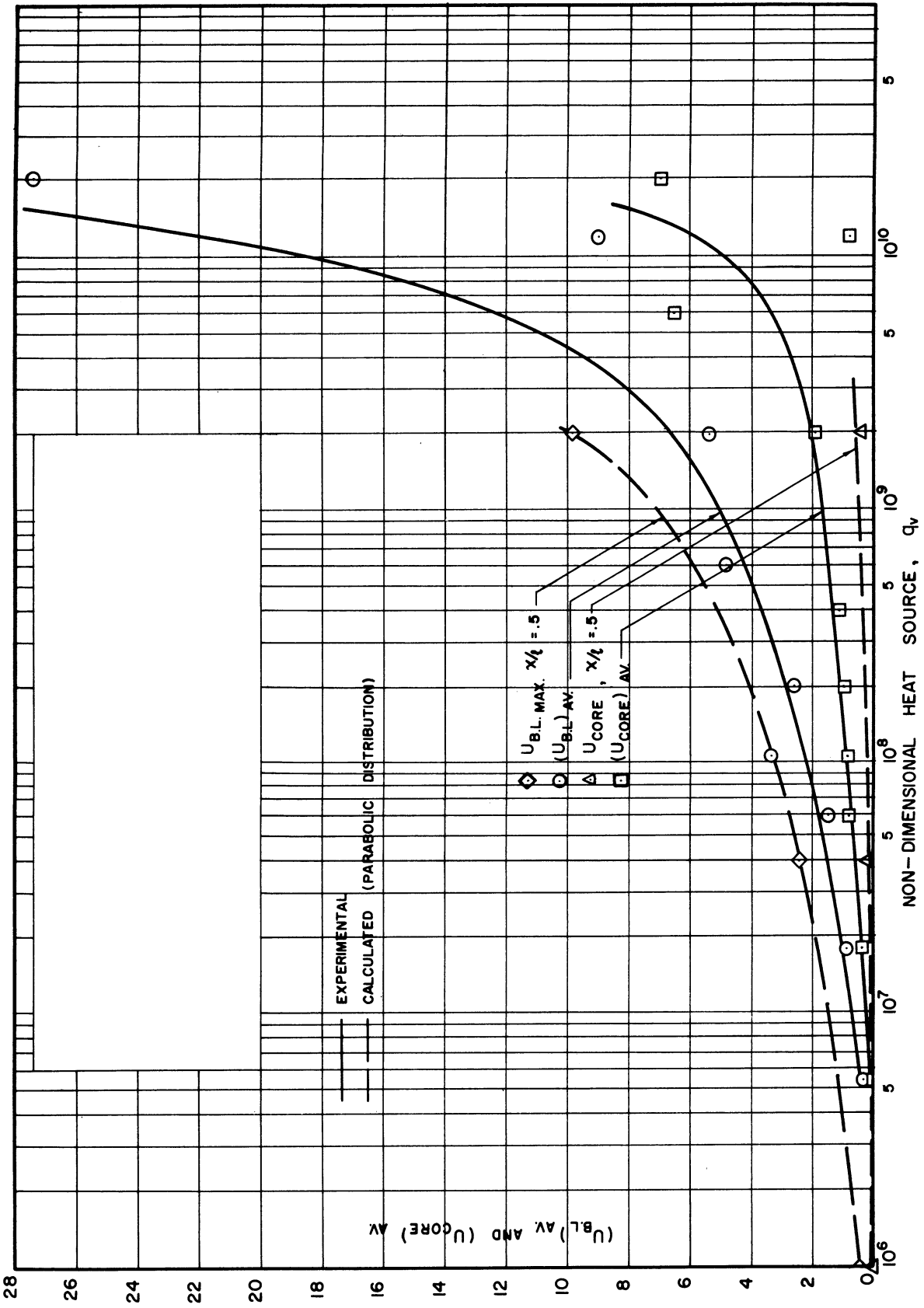


Figure 23. Non-Dimensional Boundary Layer and Core Velocity vs. Non-Dimensional Heat Source, Comparison of Experimental and Calculated Data.

flow through the glass test section in the axial position which would then occur would preclude its measurement. It is believed, however, that this large increase is mainly a function of the simplified model upon which the calculations were necessarily based and may have no physical significance.

It is noted that the theoretical wall heat fluxes tend to zero at the lower end. This situation was observed experimentally in that practically stagnant conditions were observed to exist at the bottom so that heat flow was mainly a result of only thermal conductivity. The heat flux measurements through the wall in this region of large axial gradients is obscured again by the possibility of axial heat flow in the wall.

Velocity Measurements

As was indicated in the Introduction, in many practical applications knowledge of the fluid velocity to be expected would be one of the most valuable attributes of a research program of this type. Knowledge of the velocity magnitudes and directions achieved in the various experiments here reported would also serve as a valuable check-point between the theoretical approach and the experimental results, since the theory provides detailed information regarding the anticipated velocity profiles under various conditions of heat source distribution and strength, and wall temperature distribution.

Unfortunately accurate measurement of the velocities existing within the test facilities is much more difficult than measurement of the temperatures. The velocities are not sufficiently large to allow the use of an impact tube (approximately 1 inch per second was the

largest encountered and the majority were considerably less). Hot-wire anemometers might be a possibility but their successful use seemed questionable in the electrically conducting solution. They also did not seem promising for use in liquid metals wherein the thermal conductivity as well as the electrical conductivity is high and elevated temperature conditions may be used. Since one of the original objectives of the aqueous program was the development of instrumentation suitable for a subsequent liquid metal program, the hot-wire anemometer was not given serious consideration.

Reliance in the measurement of velocity was placed instead in the visual observation of particles of dye and the timing of their motion. The general characteristics of the flow, the existence or lack of turbulence, and at least a semi-quantitative measurement of the direction and magnitude of the velocity at various locations within the test section could be attained in this way. As previously mentioned, it was found that dye was more successful in this regard than oil droplets. Actually dust, rust, and impurity particles within the fluid were also quite helpful.

The existence or lack of turbulence as affected by the other parameters of the tests has been discussed in a previous section. The general character of the flow, i.e., ascending core and descending boundary layer has also been discussed.

Velocity measurements for both the core and the boundary layer were made for several of the runs with both the water-cooled and the air-cooled facilities using visual observation and a stopwatch. Similar measurements were also reported for the AEC runs⁽¹⁰⁾. These have been converted to non-dimensional form and are summarized

in Tables A-IV through A-VII in the Appendix. See Nomenclature for the definition of the non-dimensional velocity term. Due to the uncertain nature of the measurements the exact axial location, power level, and overall/radial temperature ratio for the individual measurements is not of primary importance. Consequently, they have been averaged around mean power levels, all considered to exist at the tube mid-section, and the effect of overall/radial temperature ratio neglected. The resulting experimental points are plotted in Figure 23 as a function of non-dimensional heat source, q_v . Curves are shown for both the boundary layer and the core. These are compared with curves theoretically calculated for parabolic wall temperature distributions which closely match the actual wall temperature distribution, for an overall to radial temperature ratio of approximately 3. This is within the range of the water-cooled facility runs. However, the air-cooled runs have ratios of the order of 20 and the AEC runs of 40. The source of the calculated data will be explained in a later section.

Considering the various approximations and the large degree of experimental error for these particular measurements, it is felt that the matching between experimental and calculated data is very satisfactory. In addition to the points raised in the foregoing paragraphs there are the following sources of discrepancies:

1. The calculated boundary layer velocities apply to the maximum velocity of a parabolic profile. The observations are necessarily more of the nature of a mean.
2. The calculations are based on the absolute fluid viscosity. This is indeed the effective viscosity with laminar flow. However, there were conditions of turbulence present in

most of the experimental runs so that an effective eddy viscosity, which may be very much greater than the real viscosity, may apply. It is felt that this factor should result in experimental velocities less than those predicted by the laminar flow analysis which was used.

3. No account was taken of the effect of the overall/radial temperature ratio. All the experimental runs were compared with calculations based on a value of this ratio of about 3. As previously pointed out the true value of the ratio for some of the experiments was as great as 40. A glance at the calculated non-dimensional velocity curves for different values of this ratio, Figures 33-e, f, and g, shows that the expected velocity for a ratio of 40 is approximately only 60% of the value for a ratio of 3.

It is noted from an examination of Figure 23 that the measured boundary layer velocity is less than the theoretical expectation at a given value of q_v by perhaps 30%. Aside from experimental inaccuracy and the other factors mentioned above, it would seem that this discrepancy could be well explained as a result of the eddy viscosity and the fact that the calculated values apply to the maximum of a parabolic profile. The measured core velocity is, however, greater than the theoretical expectation by a large factor. This may be partly the result of the fact that the assumed core velocity profile was flat whereas the actual profile is probably more of parabolic nature. In this case, the observed velocity would exceed that anticipated from a flat profile.

Overall Temperature Differential, Heat Source Relations

Probably the most important result from a research program of the type which is described herein would be the ability to predict the overall temperature differential required within the fluid to transfer a given amount of heat under steady-state conditions. Experimental results of this type from the present study can be delineated through a relation between the overall temperature differential within the test section (centerline at top to wall at bottom) expressed in the suitable non-dimensional parameter to the non-dimensional heat source parameter, q_v . As is shown in the Appendix, there is a direct algebraic relation between q_v , t_{c_0} , and Nusselt's Number based on tube radius. It is thus equally permissible to present the heat transfer results as curves relating Nusselt's Number with either non-dimensional heat source or non-dimensional temperature. It was found from the theoretical analysis which gave rise to these non-dimensional parameters, that an additional parameter, the ratio between the overall temperature differential within the facility and the temperature differential between the fluid along the centerline at the top and the inner surface of the wall at the same axial position (overall/radial temperature ratio) was also necessary to specify the flow. It is noted that this ratio reflects the wall axial temperature gradient. It is also necessary to specify the form of this gradient, i.e., linear, parabolic, etc., in order that the problem may be completely specified. The theoretical considerations giving rise to these results will be discussed in much greater detail in later sections of this thesis.

The experimental points from the water-cooled and air-cooled facilities and the AEC runs are shown on Figure 24, where the non-

dimensional overall temperature difference t_{e} is plotted against the overall/radial temperature ratio t_{e}/t . Curves are shown for the various values of non-dimensional heat source parameter, q_v , for which the tests were made. In the particular cases of the air-cooled runs and the AEC runs, q_v was not held constant for a series of variations of the other applicable parameters. This was done for the water-cooled facility as explained in a previous section. Such a procedure was not possible for the air-cooled runs because there was no control of the coolant medium possible. Also it was not done for the AEC runs. As a result it was necessary that these particular runs be converted to consistent results at a given value of q_v which would be close to the mean for the group. This was done for both the air-cooled runs and the AEC runs by utilizing the relation between q_v and overall temperature differential which resulted from the theoretical analysis to prorate the runs to a common q_v value. These runs are the source of the $q_v = 5 \times 10^7$ and 2×10^{10} curves of Figure 24. The latter are from the AEC runs and the former from the air-cooled. The remaining lines are the result of the water-cooled runs.

An examination of the plots shows that the scatter of experimental points is not excessive and that the curves are quite well defined.

These curves are cross-plotted to Figure 35 which shows on logarithmic coordinates the relation between non-dimensional heat source, q_v , and overall temperature differential t_{e} , for different values of the parameter overall/radial temperature ratio. Also shown for purposes of comparison are the results of the theoretical calculations for the same conditions. Direct comparison should be possible between the parabolic wall temperature distribution calculation and the experimental

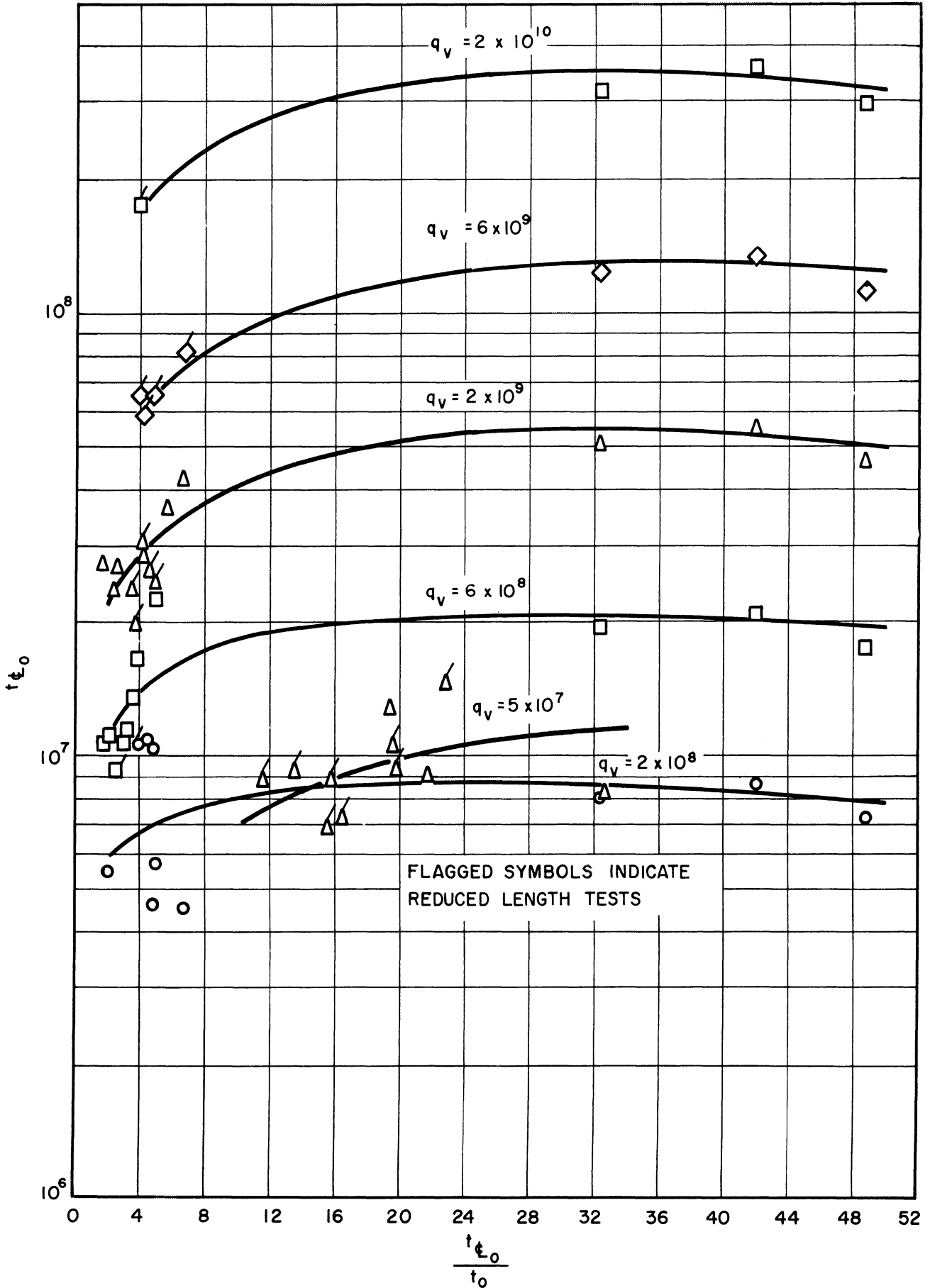


Figure 24. Non-Dimensional Overall Temperature Difference vs. Overall/Radial Temperature Ratio, Experimental Data.

curve for overall/radial temperature ratio of 3.0, and also between the calculated and experimental curves for overall/radial temperature ratio of unity (i.e., constant wall temperature). The experimental curve in this case is simply an extrapolation of the Figure 24 curve since no experimental points for the ratio less than about 2 were available. The parabolic wall temperature distribution curve utilized a wall temperature distribution which closely matched the experimental observations. The overall/radial temperature ratio for this case was approximately 3.0. It is noted that the parabolic curve closely approximates the linear curve for the same overall/radial temperature ratio. Parabolic calculations were not made at other values of this ratio. However, it is believed that the discrepancy between the linear and parabolic curves at other ratios would not be large. Therefore, a direct comparison between the calculated and experimental curves at values of the overall/radial ratio greater than 3 should also be possible.

An examination of Figure 35 discloses that the slope of the experimental and calculated curves on the logarithmic coordinates matches quite closely. In this regard there appears to be some tendency for the experimental slope to increase somewhat for the higher power levels. This is consistent with the observations made on a non-internal heat source closed tube experiment reported by Martin⁽⁹⁾. For the lower power levels and the higher values of the radial/overall temperature ratio, the slopes of experimental and calculated curves appear nearly identical. The experimental evidence for the slope in the lower power region is not complete. It is also noted that the slope of all the calculated curves, regardless of heat source strength or distribution, or overall/radial temperature ratio is the same. These facts can be

used to formulate approximate simplified equations relating q_v and t_{q_0} or Nusselt's Number. These are tabulated in a later section of this report.

In addition to the similarity between the slope of the experimental and theoretical curves on logarithmic coordinates, there is also the fact that the variation with a variation in overall/radial temperature ratio is in the same direction and of the same order of magnitude. For both theoretical and experimental results, it is indicated that a greater temperature differential is required to remove a given quantity of heat if the overall/radial temperature ratio is greater. In other words the minimum internal temperature differential is required when the wall temperature is maintained constant. While the theoretical results show this effect continuing even for values of the overall/radial ratio as great as 20 to 40, the experimental results show little variation beyond 20. They do show a substantial variation below 20 but not so great as the theory indicates.

It will be noted from an examination of Figure 35 that in all cases the overall temperature differential which is indicated experimentally for a given rate of heat removal (or generation) is considerably less than that anticipated theoretically. The factor involved is of the order of 2.5 for the higher q_v results, greater than approximately 10^8 . The discrepancy increases for still higher q_v because of the increased slope of the experimental curves. For q_v between 10^7 and 10^8 the discrepancy factor is of the order of 1.5. There appears to be a substantial discontinuity in q_v for t_{q_0} equal to about 6×10^6 (q_v between about 5×10^7 and 2×10^8). This is believed due to the change from nearly laminar to substantially turbulent flow which was observed in this range.

The phenomenon of turbulence as it appeared in the experimental facilities was discussed at length in a previous section of this report. It was mentioned that all the water-cooled runs (they were all taken at q_v in excess of 10^8) showed a high degree of turbulence. At the same time the air-cooled runs (all were below $q_v = 10^8$) showed little or no turbulence. It would be expected that the turbulent mixing would result in a reduction in the required temperature differential to remove a given quantity of heat. Since the lower power air-cooled runs also indicated an overall temperature differential substantially below the theoretical expectations (but **not** so much so as the water-cooled), it is felt that the influence of turbulent mixing at least in the area of transition between the descending boundary layer and the ascending core may have been present here too. It may be questionable whether this type of flow can exist under completely laminar conditions, since for low q_v the modified boundary layer model ceases to apply.

As has been previously mentioned there is an algebraic relation between q_v , $t_{c_{Lo}}$ and Nusselt's Number (as based on the radius of the test section):

$$\text{Nusselt's Number} = q_v / 2t_{c_{Lo}}$$

This is derived in the Appendix. It is possible to plot the information from Figure 35 on a curve sheet showing the relation between Nusselt's Number based on test section radius and q_v . Such curves are presented in Figure 36. It would also be a simple matter to construct a similar curve sheet relating Nusselt's Number and $t_{c_{Lo}}$. This has not been done as it would add no further information.

Effects of Length to Diameter Ratio
and Absolute Dimensions of Test Section

The experimental runs from which the information discussed in the foregoing sections has been derived, were made in test sections which varied not only in absolute magnitudes of length and diameter but also in the length to diameter ratio. The considerations upon which the theoretical analysis to which repeated reference has been made were based are such that the only effect of the dimensions upon the behavior of the fluid would be through the non-dimensional parameters. Consequently if results were presented in terms of these non-dimensional parameters there should be no differentiation between experimental points taken at differing length to diameter ratio or different absolute magnitude of either dimension, provided the other applicable parameters were varied in such a way that the non-dimensional quantities would not be affected.

With the water-cooled facility for example, it was possible to conduct runs at identical values of q_v but with a variation of test section length by a factor of 3 and with test section radius held constant. Under these conditions, no significant difference in the overall temperature differential (expressed in non-dimensional terms) was noted and also no observable difference in the degree of turbulence, i.e., both highly turbulent. In general, in the presentation of the experimental data it has not been found possible to detect any effect of the variation of dimensions or the ratio between dimensions provided the non-dimensional parameters relating to heat source strength and distribution and the ratio of overall/radial temperature differential were not affected. The one possible exception to this statement applies

to the radial temperature profiles, i.e., the temperature boundary layer thickness at a given axial location. It is possible from Figures 12-a and c to compare the temperature boundary layer thicknesses resulting in the water-cooled and air-cooled facilities respectively for different length test sections (maximum variation is by a factor of about 3) at different axial positions. It is noted in both cases that there appears to be a thicker boundary layer resulting from the shorter test sections even though q_v is maintained approximately constant.

In spite of the above-mentioned exception in the case of boundary layer thickness, it appears that the universality of the non-dimensional parameters with respect to dimensional changes, at least as regards overall heat transfer characteristics in a configuration of the type under test, within the experimental error, is established by this study.

Summarization of Experimental Runs

The various applicable data from the experimental runs is summarized in Tables A-IV through A-VII in the Appendix. Information given includes overall types of facility, method of cooling, direction and quantity of coolant flow, power input (electrical), power output to coolant (except for air-cooled facility), mean temperature of test fluid, non-dimensional heat source parameter, q_v , non-dimensional overall temperature differential, t_{e0} , overall/radial temperature ratio, Nusselt's Number as based on test section radius, test section dimensions and length to radius ratio, non-dimensional core and boundary layer velocity as observed at various axial positions, boundary layer

thickness as observed both from velocity and temperature viewpoints, degree of turbulence, normalized wall conduction, and error between electrical power input to test fluid and power input to coolant.

It is noted from an examination of the summary tables that there were 47 runs in all, and that a range of q_w covering nearly 4 decades was explored. The breakdown of these runs is as listed in Table I.

TABLE I. SUMMARIZATION OF EXPERIMENTAL RUN CHARACTERISTICS

RUN NUMBER	RUN CHARACTERISTICS
1 - 11	Water-cooled facility, upward coolant flow, full length test section. Coolant flow rate varying from 650 cc/min. to 10 GPM. q_v varying from 2×10^8 to 2×10^9 .
12 - 19	Water-cooled facility, downward coolant flow. Other parameters as runs 1 - 11 above.
20 - 26	Water-cooled facility, upward coolant flow, minimum length test section. Coolant flow rate varying from 650 cc/min. to 10 GPM. q_v varying from 2×10^8 to 6×10^9 .
27 - 32	Water-cooled facility, downward flow rate, other parameters as runs 20 - 26 above.
33 - 35	AEC runs, water-cooled, upward flow rate, constant dimensions, q_v about 10^{10} , approximately constant coolant rate.
36 - 39	Air-Cooled Facility, maximum length, q_v varying from 5×10^6 to 3×10^7 .
40 - 43	Air-Cooled Facility, moderate length, q_v from 1×10^7 to 6×10^7 .
44 - 47	Air-Cooled Facility, minimum length, q_v from 2×10^7 to 1×10^8 .

CHAPTER V

ANALYTICAL APPROACH

General Scope of Analysis

The problem of natural convection flow without internal heat sources in a tubular vessel with a single closed end (opposite end connected to an infinite reservoir) which is also of moderate length to diameter ratio has been considered in some detail by Lighthill⁽⁶⁾ for the case with constant wall temperature. The case of the similarity regime (defined later) in a vertical tubular vessel, closed at one end and connected with an infinite reservoir at the other as in the Lighthill case, but with a linear, axially-varying wall temperature, is examined by Ostrach⁽⁷⁾.

It is the purpose of this section to present a method of solution for the case of a vertical tubular vessel with both ends closed in which heat is generated in an arbitrary axial distribution of heat source strength and removed through walls which are under arbitrary temperature distribution. This case in particular has been examined because of the application to homogeneous nuclear reactors and in order to provide a correlation with the experimental results previously described. Since the heat source term in a power reactor is of an order of magnitude higher than conventional sources, it has been assumed that a modified boundary layer solution may be applied. It was pointed out by Lighthill⁽⁶⁾ for his case that the internal flow might be expected to fall within one of the following regimes, depending upon a parameter which is the product of the Rayleigh's Number and radius to length ratio for the tube:

1. Similarity Regime. The above parameter is small, i.e., Rayleigh's Number small or tube slender so that the temperature and velocity profiles are fully developed and their shapes (not magnitudes) do not vary with axial position. In other words, the boundary layer completely fills the tube.
2. Intermediate Regime. The boundary layer fills a substantial portion of the tube radius but the "fully developed" regime is not attained.
3. Boundary Layer Regime. If the above parameter is very large, i.e., large Rayleigh Number or short tube, the boundary layer does not have sufficient axial extent to grow into the central portion of the tube and thus occupies only a negligible portion of the radius. In the extreme case, the flow is completely analogous to a flat plate in an infinite fluid. However, the type of solution may be extended somewhat into the "intermediate regime" by utilizing partially arbitrary assumptions of temperature and velocity profile for the boundary layer and the central core.

The present analysis has not changed the validity of this general division. It is the last procedure described above which is extended in this report to the case with both ends closed, internal heat source, arbitrary axial wall temperature distribution. As stated by Lighthill⁽⁶⁾ the applicability of this type of solution depends upon the product of Rayleigh's Number and radius to length ratio being large. In terms of the present analysis, some of the following factors must apply in varying degrees if the modified boundary layer assumptions are to be used.

1. Absolute tube dimensions large, or
2. Heat source strong, or
3. Length to radius ratio of tube small, or
4. Thermal diffusivity and kinematic viscosity of fluid small.

If the application is to be to homogeneous nuclear power reactors, the heat source may be assumed strong, but the passage dimensions and length to radius ratio may be small. Also, if the fluid is a liquid metal, the thermal diffusivity may be relatively very large. However, as will be seen later, the assumptions which are made appear to limit the type of solution to fluids with a Prandtl Number of the order of unity. It has been assumed, and it appears generally correct, that the heat source term for aqueous homogeneous power reactors is sufficiently large so that the modified boundary layer type solution herein described is applicable. The analysis presented applies only for laminar flow. It is realized that turbulence may well exist for many applicable cases and, as previously mentioned, did exist for many of the experiments. However, the laminar analysis should be of interest in at least indicating the proper trends.

Although the present analysis appears limited to aqueous fluids, the trends which are indicated should apply also to some extent to liquid metals.

Analysis of Problem

Lighthill Approach⁽⁶⁾

According to the analysis of the Lighthill problem, if the product of Rayleigh's Number and radius to length ratio is sufficiently large, the flow is of the boundary layer type. If it is somewhat

smaller, it is necessary to consider the effect of the return velocity in the central portion of the tube. Under these conditions, he assumed that the return flow in the core would be at constant temperature since the influence of thermal conduction between the core and the boundary layer is small.

To analyze this situation, it is assumed that

1. The boundary layer approximations apply. (i.e., gradients in the axial direction are negligible as compared with radial gradients)*
2. Fluid inertial forces are small compared to buoyancy and shear. As Lighthill shows, this condition results if the Prandtl Number is large. (Thus, direct application to liquid metals appears unlikely.)
3. The radial extent of the temperature and velocity boundary layers is the same. (This appears to limit the applicability of the solution to Prandtl Number near unity.)

Further, a velocity and temperature profile as shown in Figure 25 are assumed. These are caused to satisfy the physical boundary conditions at the wall, the centerline, and at $r = \beta$ for the quantities and their first derivatives. Integral equations for the conservation of mass, momentum, and energy are written for each radial disc, Figure 26, i.e., these quantities are not satisfied point by point, but on an integrated basis.

* Boundary layer assumptions apply for all possible flow regimes. For large Rayleigh's Number, it is a boundary layer phenomenon by definition. For small Rayleigh's Number, there is very little change of any of the applicable parameters in the axial direction so that again the boundary layer assumptions apply.

TEMPERATURE AND VELOCITIES PROFILES

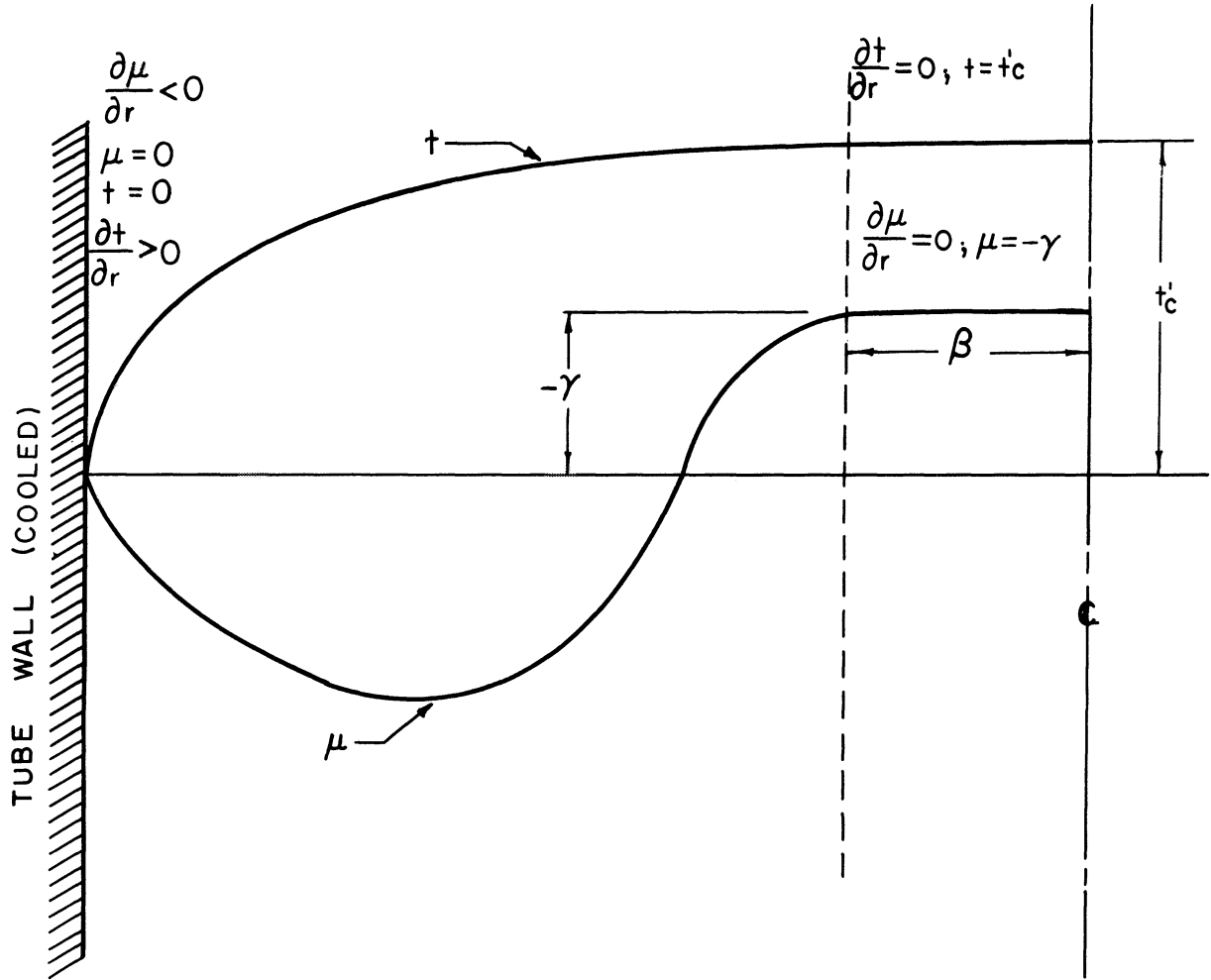


Figure 25. Assumed Temperature and Velocity Profiles for Theoretical Analysis

RADIAL DISC CONTROL VOLUME

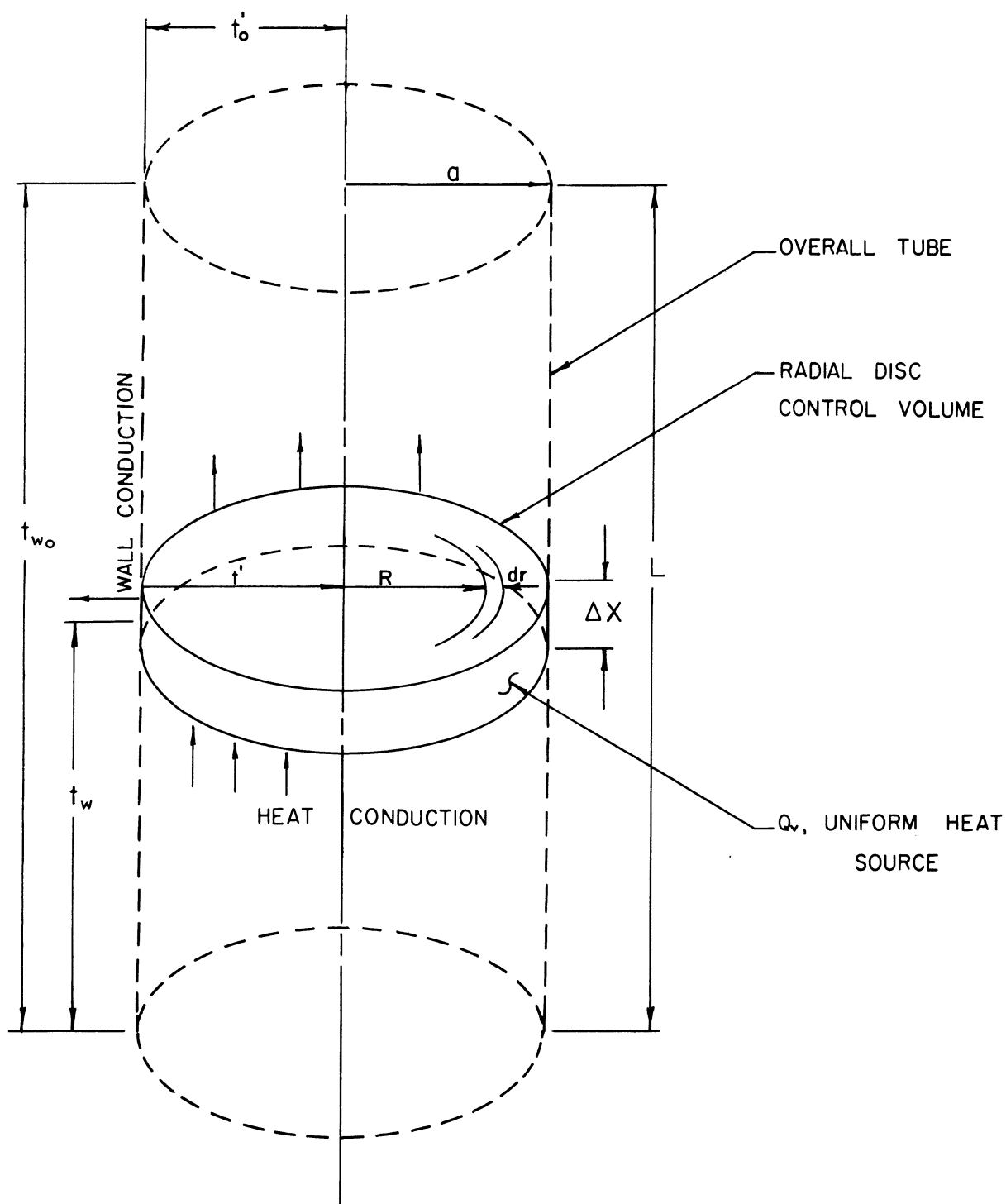


Figure 26. Schematic Representation of Test Section as Used for Theoretical Analysis

The velocity and temperature profiles assumed by Lighthill, in non-dimensional form are as below. The meanings of the symbols are given in Nomenclature. The parameters β , γ , and δ are functions of the axial position, x . However, the non-dimensional core temperature, t_1^* , is constant with x .

$$u = \begin{cases} -\gamma & \text{for } 0 < \beta < r \\ -\gamma \left[1 - \left(\frac{r - \beta}{1 - \beta} \right)^2 \left\{ 1 + \delta(r - 1) \right\} \right] & \text{for } \beta < r < 1 \end{cases} \quad (1)$$

$$t = \begin{cases} t_1 & \text{for } 0 < r < \beta \\ t_1 \left[1 - \left(\frac{r - \beta}{1 - \beta} \right)^2 \right] & \text{for } \beta < r < 1 \end{cases} \quad (2)$$

Modification for Volumetric Heat Source and Arbitrary Axial Wall Temperature Distribution

The procedure utilized for this study which includes the effects of the volume heat source and the arbitrary wall temperature distribution is similar to that of Lighthill except that the energy equation is modified to include the heat source term, and the assumed velocity and temperature profiles modified to allow a variation of core temperature in the axial direction. Under these conditions, the assumed profiles are:

$$u = \begin{cases} -\gamma & \text{for } 0 < \beta < r \\ -\gamma \left[1 - \left(\frac{r - \beta}{1 - \beta} \right)^2 \left\{ 1 + \delta(r - 1) \right\} \right] & \text{for } \beta < r < 1 \end{cases} \quad (1')$$

which is unchanged from the Lighthill relation (1) and

$$t = \begin{cases} t(x) & \text{for } 0 < \beta < r \\ t(x) \left[1 - \left(\frac{r - \beta}{1 - \beta} \right)^2 \right] & \text{for } \beta < r < 1 \end{cases} \quad (2')$$

* Non-dimensional temperature, t , is actually the product of Rayleigh's Number based on radius and the radius to length ratio. See Nomenclature.

The maximum fluid temperature will be attained at the top of the vessel in the core. In the non-dimensional quantities, this will be $(t_o + t_{w_o}) = t_{E_o}$ defined in terms of the temperature difference between fluid at centerline and wall at top plus the temperature difference between the top and bottom of the wall, as shown in Figure 26.

As given by Lighthill, the integrated forms of the equations expressing conservation of mass and momentum with boundary layer assumptions are:

$$\int_0^1 r u dr = 0 \quad (3)$$

$$\int_0^1 r t dr + \frac{1}{2}(t)_{r=0} + \left(\frac{\partial u}{\partial r}\right)_{r=1} = 0 \quad (4)$$

The integrated form of the energy relation, broadened over Lighthill's case to include the heat source term, is:

$$\frac{\partial}{\partial x} \int_0^1 r u t dr = \left(\frac{\partial t}{\partial r}\right)_{r=1} - \frac{q_v}{2} \quad (5)$$

where q_v is a non-dimensional heat source term which is proportional to the product of the local volumetric heat source and a grouping of the physical fluid quantities. The precise definition is given in the Nomenclature and the detailed derivation in the Appendix.

The assumed velocity and temperature profiles, (1') and (2'), are substituted into (3) and (4) as in the Lighthill analysis. Equation (3) yields δ as $\delta(\beta)$ exactly as in the Lighthill case. Equation (4), using the relation for δ from (3), yields γ as $\gamma(t, \beta)$. The expression is the same as that of Lighthill except that t_1 of Lighthill becomes $t(x)$. Thus,

$$\gamma = t(x) \frac{(3 + \beta)(3 + 2\beta)(1 - \beta)^3}{36(3 + 4\beta + 3\beta^2)} = t(x)G(\beta) \quad (6)$$

The relations (1'), (2'), and (6) are substituted into the energy relation (5), following the Lighthill procedure. The right side of the resultant relation will differ from Lighthill's case because of the presence of the heat source term. The left side, however, will also differ. The term in question is

$$\frac{\partial}{\partial x} \int_0^1 r u t dr$$

In the Lighthill analysis, t was a function of β multiplied by a constant, t_1 . Now, however, the multiplier temperature is a function of x .

As shown in the Appendix

$$\frac{\partial}{\partial x} \int_0^1 r u t dr = 2 \frac{d}{dx} [t^2(x)F(\beta)] \quad (7)$$

where $F(\beta)$ is as evaluated by Lighthill and is given in the Appendix.

Then the whole energy relation, integrated in an axial direction, is:

$$\int_{x_{N-1}}^{x_N} d[t^2(x)F(\beta)] = \int_{x_{N-1}}^{x_N} \frac{t(x)}{1-\beta} dx - \frac{q_v}{4} \int_{x_{N-1}}^{x_N} dx \quad (8)$$

$$\underbrace{[t^2(x)F(\beta)]_{x_{N-1}}^{x_N}}_{\text{Convection}} = \underbrace{\int_{x_{N-1}}^{x_N} \frac{t(x)}{1-\beta} dx}_{\text{Wall Conduction}} - \underbrace{\frac{q_v(x_N - x_{N-1})}{4}}_{\text{Heat Source}} \quad (9)$$

Equation (9) is essentially the energy relation for the radial disc shown in Figure 26. However, the relations for conservation of mass and momentum have also been used in the derivation.

There are two independent variables in (9), t and x . Consequently, it is necessary to formulate an additional relationship in order to allow a solution. The additional relation which has been used is that between axial position and the fluid temperature along the vessel centerline. Consider the control volume sketched in Figure 27. It is assumed that fluid transfer from the core to the boundary layer has only negligible effect on energy conservation for the core. It is also assumed that thermal conduction to or from the control volume is negligible. Order of magnitude calculations for those cases to which this type of modified boundary layer solution may be applied show that these assumptions are justified. Conservation of energy for the control volume gives:

$$q_v [\Delta x \pi (\beta R)^2] = c_v \rho \pi (\beta R)^2 \Delta x - \frac{dT_c}{dx} U_c \quad (10)$$

so that

$$\frac{dT_c}{dx} = - \frac{q_v}{\rho c_v U_c} \quad (11)$$

or in the non-dimensional quantities (see Appendix)

$$\frac{dt(x)}{dx} = \frac{q_v}{\gamma} \quad (12)$$

Thus,

$$[t(x)]_{x_{N-1}}^{x_N} = \frac{\bar{q}_v}{\gamma} (x_N - x_{N-1}) \quad (13)$$

The basic set of equations to be solved are then (9) and (13).

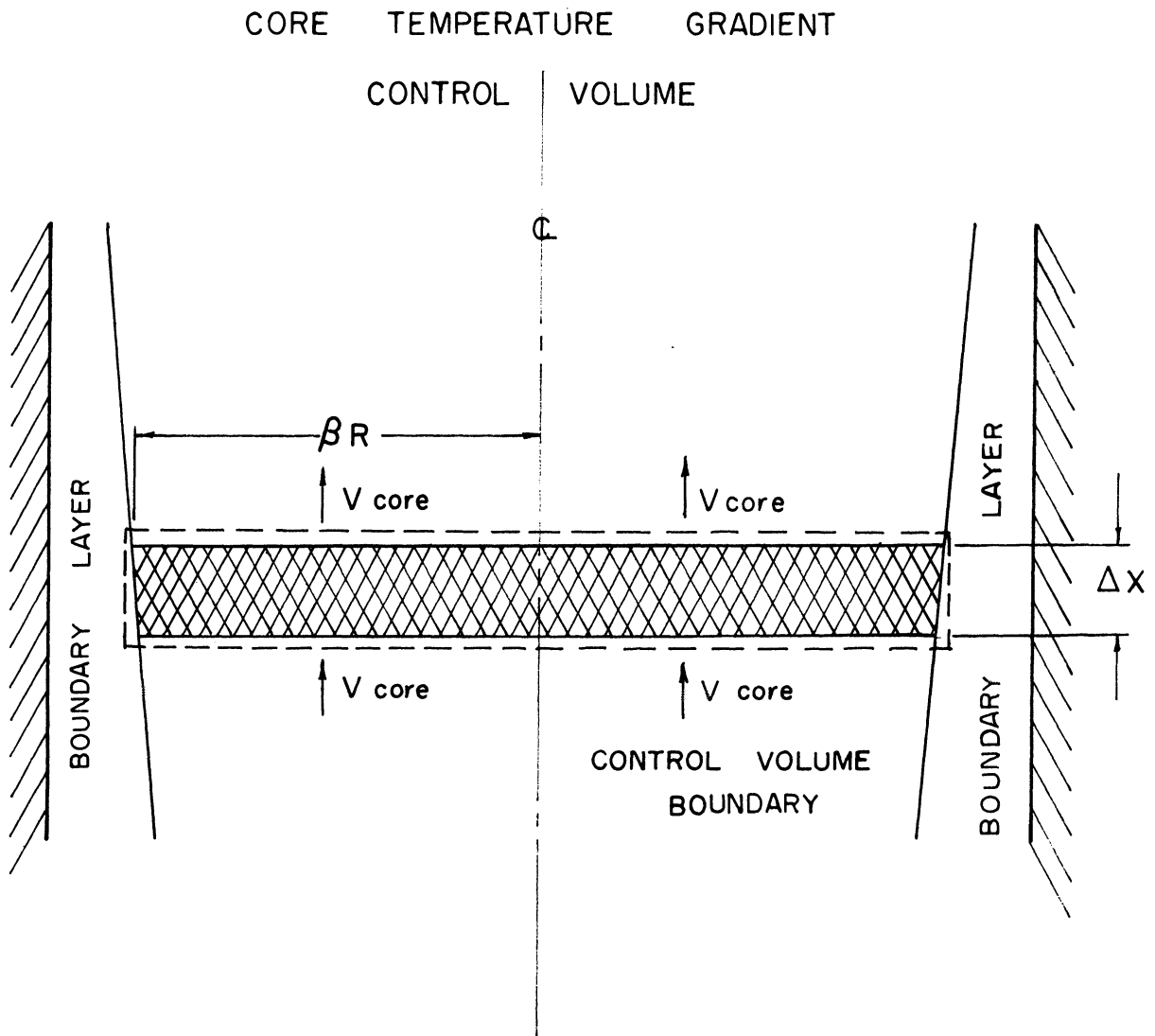


Figure 27. Core Temperature Gradient Control Volume,
Theoretical Analysis

Difference Equations for Arbitrary Wall Temperature
and Heat Source Axial Distribution

Rather than attempting to find analytic solutions for various specialized conditions of the boundary value problem it was considered more useful and practical to utilize an approximate numerical procedure and maintain a completely arbitrary specification of the axial distribution of wall temperature and heat source. The numerical procedure was designed for programming into a high-speed digital computer.

It is evident that the derivation for Equations (9) and (13) has considered a constant wall temperature where the t variable is related to the temperature difference between the fluid at any axial and radial position and the tube wall at that axial position. A change in variables is now made so that $t_{CL} = t + t_w$, where t is related to the temperature difference between wall and fluid at any axial position (for constant wall temperature it is not necessary to specify the wall axial position), and t_w is related to the temperature difference between the wall at any axial position and the wall at the bottom. The minimum temperature in the internal system is to be found at this location. As previously mentioned, Equations (9) and (13) are written for any of a series of radial discs, Figure 26, which together comprise the entire vessel. If a sufficient number of such discs are employed, it is permissible to consider the wall temperature constant for each disc. Then, Equation (9), which is basically the energy balance for a disc, does not involve the axial wall temperature gradient and is the same whether variable or constant wall temperature is considered. In other words, the t_w portion of t_{CL} makes no contribution.

On the other hand, Equation (13), expressing the fluid axial temperature distribution along the centerline, must consider the fluid

temperature as such, including both portions which make up the total, rather than just the temperature difference between the fluid and wall at a given axial position. The heat source term may be considered as a mean value for each disc, q_{vN} . Equation (9) is unchanged, and (13) becomes (14) below.

$$[t(x) + t_w(x)]_{x_{N-1}}^{x_N} = \frac{\bar{q}_v}{\gamma}(x_N - x_{N-1}) \quad (14)$$

As is shown in detail in the Appendix, these may be reduced to the approximate difference equations listed below.

$$\frac{t_N^2 F_N - t_{N-1}^2 F_{N-1}}{x_N - x_{N-1}} - \frac{t_N + t_{N-1}}{2 - \beta_N - \beta_{N-1}} + \frac{q_{vN}}{4} = \Delta \quad (15)$$

$$(t + t_w)_N = (t + t_w)_{N-1} \sqrt{1 - \frac{4q_{vN}(x_N - x_{N-1})}{(t + t_w)_{N-1}^2 (G_N + G_{N-1})}} \quad (16)$$

For a consistent solution, $\Delta \rightarrow 0$.

Boundary Conditions

The boundary conditions of zero slip on the walls, walls impervious to the fluid, wall temperature equal to the fluid temperature adjacent to the wall, heat flux through the wall equal to the conductive heat flux normal to the wall within the fluid and insulated end sections* are all implicit in the basic equations used and the assumed temperature and velocity profiles. The remaining conditions to be applied are concerned with the end effects. Physically, these may be

* It is possible to consider heat flow through the tube ends if desired by simply selecting a suitable q_v for each extreme discs.

stated in various ways. For example, if the tube as an entirety is considered, then the overall heat convection term in Equation (9) must vanish, and the total heat source must equal the total wall conduction. From another viewpoint, the mixed mean boundary layer effluent temperature at the bottom must equal the mixed mean temperature of the ascending core at that point. Also at the top, the mixed mean temperature of the core effluent must equal that of the boundary layer.

The latter statement can be satisfied with the assumed temperature profile only if

1. there is no radial temperature gradient at the tube ends, or
2. the boundary layer thickness at the ends is zero.

In this last case, assuming non-infinite velocities and considering conservation of mass, the core and boundary layer flows at the ends must be both zero. (The postulated over-simplified flow model is not capable of an examination of the detailed end conditions.) Since there is a temperature difference between the fluid at the tube centerline at the top and the wall at the top, it is necessary that the boundary layer thickness at the top be zero. This is physically necessary in any case from consideration of the basic boundary layer flow mechanism.

Examination of Equation (9) and the form of $F(\beta)$ given in the Appendix, shows that when β is 1.0 (i.e., zero boundary layer thickness), F is zero, and hence t^2F is zero. Since it is necessary that the overall convective term vanish for the tube, t^2F at the bottom must also be zero. This is accomplished if either the boundary layer thickness or the radial temperature gradient becomes zero at the bottom.

As the calculations show, the specification of either of these conditions carries with it the other. In this manner, all the boundary conditions are satisfied.

Calculating Procedure

The calculating procedure is a double iteration designed to satisfy the condition of zero boundary layer thickness at either end. Physically, if the wall temperature distribution and heat source are specified, the solution to the problem must be unique (assuming given physical properties of the fluid). Assuming that these quantities are specified, each radial disc, starting at the top, is considered separately. An initial estimate of $t_{c_{Lo}}$ at the top is made. It is then possible to compute, for an estimated β , the value of t_{c_L} at the bottom of the first disc from Equation (16). These values for t_{c_L} and β at either end of the first disc are substituted into Equation (15). If they are consistent, $\Delta = 0$. If not, an improved estimate for β is made. In this way, the calculation proceeds to the bottom of the tube. If $\beta = 0$ at the bottom, it is necessary to repeat with an improved estimate for the initial $t_{c_{Lo}}$.

Digital Computer Program

The trial and error procedure, a double iteration, described in the last section, was programmed for an IBM 650 high speed digital computer. For this purpose the tube was considered as divided into 11 radial discs as shown schematically in Figure 26. For each calculation the independent variables, which would be read into the machine via the data cards, were the non-dimensional heat source parameter, q_v , for each of the radial discs (in this way non-uniform heat source

distributions could be considered); and the non-dimensional wall temperature applying to each disc so that arbitrary variation of wall temperature could be considered. Values for the various dependent variables at the top of the tube, i.e., top side of the first radial disc, are read in by means of the data cards. In addition, an arbitrary guess for $t_{c_{L_0}}$ for the tube under the particular set of conditions is read in.

The program is so arranged that the machine proceeds to calculate the boundary layer thickness (in terms of non-dimensional core thickness, β) and the other applicable quantities at the bottom of the first disc. This is also an iterative process. An initial estimate of β at this point is read in with the data cards. Using this initial value, the machine computes Δ from equation (15). If Δ is greater than a prescribed suitable limit which is read in with the data cards, then a new value of β greater than the original by a prescribed constant (read in with data) is utilized for a second try. If Δ is still not within the prescribed limit, a linear extrapolation is used by the machine to estimate the next value for β . It is found that three or four iterations are sufficient to approximate the new β to a suitable degree of precision. At this point, the program is so arranged that the values of the various applicable parameters which have been computed for the bottom of the uppermost disc are substituted for the comparable parameters for the top of the second disc, and the iterative procedure to approximate β and the other parameters at the bottom of this disc is repeated.

In this way the computation moves down the tube to the bottom. By the previously discussed boundary conditions, β at the

bottom of the last disc should be 1.0. This will not be the case unless the initial guess of $t_{c_{Lo}}$ was sufficiently accurate. If the initial guess were too small, the non-dimensional core thickness will reach 1.0 before the bottom of the tube is reached; if the initial guess were too large, the boundary layer will still have a positive finite thickness at the bottom of the tube. This is physically reasonable from the following consideration. If too great a temperature differential had been assumed for a given heat source strength, then this heat could be removed with a boundary layer which was excessively thick. Therefore, the boundary layer will not have come to zero at the tube bottom.

As was previously stated, when β approaches 1.0, $F(\beta)$ approaches zero. It seemed more convenient in the machine program to base a correct solution on the degree of approach of $t^2F(\beta)$ from Equation (15) to zero rather than the approach of β to 1.0. A suitable limit for t^2F at the bottom was read in with the data cards. If t^2F were larger than this limit when the bottom of the tube were reached, the program would be returned to the top of the tube, and a second value for $t_{c_{Lo}}$ used and the entire procedure repeated. The second value would be larger than the first by a prescribed amount which would be read in with the data cards. If, on the first iteration, β became 1.0 before the bottom of the tube was reached, in most cases, a negative square root term would arise in the calculations. The program was arranged to start the procedure at the top of the tube again when this occurred. A new value for $t_{c_{Lo}}$ would be selected, larger than the first, as described above, by a prescribed amount.

The existence of a large t^2_F at the bottom of the tube is an indication, as previously mentioned, that $t_{C_{Lo}}$ is too large, and the attainment of $\beta = 1.0$ before reaching the bottom of the tube is an indication that $t_{C_{Lo}}$ is too small. However, no differentiation was made in the estimate of a second $t_{C_{Lo}}$ value, since the additional programming complication to accomplish this did not seem warranted. After the second iteration, if the previous tries had each resulted in a positive t^2_F at the bottom beyond the prescribed limit, a linear extrapolation was used to estimate $t_{C_{Lo}}$ more correctly. If one of the previous two tries had resulted in a return to the top of the tube because of a negative square root ($\beta = 1.0$ before bottom is reached), the extrapolation would not be used but rather the prescribed addition to $t_{C_{Lo}}$. In this way, eventually, $t_{C_{Lo}}$ would become large enough and positive t^2_F encountered.

These automatic provisions for the location of the proper $t_{C_{Lo}}$ were not entirely successful as they had been with the β iteration. Unless the initial guess of $t_{C_{Lo}}$ was very close, it was found that either the linear extrapolation would overshoot on the one hand, or the number of iterations necessary to cause the boundary layer to exist to the bottom of the tube would be excessive. An additional complication arose in that it was found that a solution with a negative boundary layer thickness existed mathematically and that in some cases of an excessively poor initial estimate of $t_{C_{Lo}}$ the machine would find this physically nonsensical solution rather than encounter the negative square root. For these reasons, it was found necessary to help the machine on occasion by improving manually the $t_{C_{Lo}}$ estimate after one or two iterations had been completed.

It was found that an iteration down the tube required something less than 10 minutes in most cases and that a solution for a given set of conditions could be attained with approximately 1/2 hour of machine time. The degree of precision required of the machine was such as to guarantee an accuracy in t_{e0} in excess of $\pm 2\%$. It was felt that this would be adequate for the present purpose. Higher precision could, of course, be attained with additional expenditure of machine time.

The effect of this possible slight inaccuracy in the overall heat transfer results may become more substantial in other aspects of the calculation. Since it has not been insisted that the boundary layer thickness at the bottom of the tube become precisely zero, there may be substantial uncertainty induced in the machine calculations for boundary layer thickness, velocity, wall heat flux, and temperature in the radial slice immediately adjoining the bottom. For this reason, the profiles computed near the top are virtually exact while those at the bottom may not be. However, it is estimated that the region of substantial error is limited to approximately the lower 5% of the tube length.

Because the boundary layer grows and decreases very steeply at either end of the tube, it was necessary to limit the radial slices at either end to an x/l of only 0.001. At the top the next position was set at 0.01, the next at 0.05, and the next at 0.20. At the bottom, the axial positions examined were at x/l values of 0.90, 0.96, 0.999. It was found that there was a substantial effect on the whole problem if less narrow divisions at the top were considered. Since conditions are not changing very rapidly with axial position near the central portion of the tube, larger increments were permissible.

CHAPTER VI

RESULTS OF THEORETICAL ANALYSIS

The theoretical analysis, which was described in detail in the last section, is such that detailed information covering not only the overall temperature differential for a given heat flow, but also anticipated temperature and velocity profiles throughout the test section and wall heat flux distribution, results. These various phases of the calculated results will be covered in this section. In addition those comparisons with the experimental data which are possible will be emphasized.

Configurations Covered by Theoretical Analysis

Various configurations of wall temperature distribution, and heat source parameter distribution and strength were covered by the IBM-650 digital computer program described in the last section.

Constant Wall Temperature, Uniform Heat Source

The simplest configuration is that of constant wall temperature and uniform heat source distribution. Calculations of this type were run over a range of non-dimensional heat source parameter, q_v , from 10^5 to 2×10^9 .

Constant Wall Temperature, Axial Heat Source Variation

A second series of computations involved variable distributions of the non-dimensional heat source parameter, q_v , also with constant wall temperature. As previously explained, it is possible to consider any

arbitrary axial distribution of q_v . However, the type of analysis does not permit the consideration of radial variation in q_v . The axial variations which were used included a sine distribution wherein the volumetric heat flux is zero at the test section ends and follows a sine curve distribution down the tube. The choice of this distribution was motivated by the fact that such a distribution is common in an unreflected nuclear reactor core. For example, if the test section were considered to be an aqueous fissionable fuel container running the length of a reactor core but located in the central portion with respect to the horizontal direction, then such a heat flux, or thermal neutron flux, distribution (sine along axis, uniform along radius) would be approximated

In addition to the sine distribution, triangular distributions, wherein the volumetric heat flux varied linearly from, in one case, a maximum at the top of the test section to zero at the bottom, and in another case, from zero at the top to a maximum at the bottom were also examined. These particular distributions have no specific application to nuclear reactor cores as such. However, it was felt that they would illustrate the trends attributable to a preponderance of volumetric heat flux either at the top or at the bottom.

Lighthill Analogy

The final constant wall temperature case examined was one which is of interest because it approximates the case of the Lighthill analysis⁽⁶⁾, wherein the vessel is open at the lower end to an infinite high temperature fluid reservoir (if walls are cooled) and there is no internal heat source. Since there is no heat source, the core is at

constant temperature. This configuration can be approached in a somewhat different manner, through the mechanism of the present internal heat source analysis. If it is considered that all the heat is generated within an infinitely thin radial disc at the bottom of the test section, so that the boundary layer effluent at the bottom is heated to the infinite reservoir temperature (from the Lighthill analysis), and that no further heat is added to the core fluid as it rises to the top of the tube, so the core temperature is constant, then the Lighthill conditions are realized. It was found that the program run on this basis did indeed produce results analogous to Lighthill's, which were of course achieved in a considerably different manner. This result is heartening in that it virtually eliminates the possibility of an algebraic error in the present analysis. Also it indicates the fruitful possibility of the further study of the physical configuration, which was considered by both Lighthill⁽⁶⁾ and Ostrach⁽⁷⁾ for constant and linearly variable wall temperature respectively, with the present machine program and completely arbitrary wall temperature distribution.

Linearly Variable Axial Wall Temperature, Uniform Heat Source

The third series of machine computations involved linearly variable axial wall temperature distribution with uniform heat source distribution. Aside from the non-dimensional heat source parameter, q_v , a second parameter is necessary to define uniquely the conditions existing for these runs. The parameter used for this purpose is the ratio of the sum of non-dimensional temperature differentials from the fluid

centerline to the wall at the top of the vessel and from the wall at the top to the wall at the bottom to the differential from centerline to wall across the top. In terms of the non-dimensional parameters used in the analysis, this may be written

$$\frac{t_o + t_w}{t_o} = \frac{t_{c_o}}{t_o}$$

It has been called overall/radial temperature differential on the curve sheets and the written material of this dissertation.

The effect of this parameter was examined over a range in excess of three decades of q_v as it varied from 1.0 (constant wall temperature) up to approximately 40. The results will be discussed in a later section.

Parabolic Variable Axial Wall Temperature, Uniform Heat Source

A fourth series of runs was made wherein an axial temperature distribution closely resembling that of the experimental runs was utilized. This has been called a parabolic distribution on the curve sheets and in this dissertation. It approximated a parabola but was actually taken from a curve representing the average of several experimental profiles. Calculations of this type over a q_v range in excess of three decades were made. For all cases the value of t_{c_o}/t_o was approximately 3 since this value was about typical of the water-cooled facility runs. The purpose of these calculations was of course to provide as direct a basis for comparison as possible between the theoretical and experimental results.

Summarization of Theoretical Configurations

All the pertinent data from these computations, including non-dimensional temperature differential between centerline and wall, non-dimensional core thickness, and non-dimensional wall heat flux, all at various axial positions, are tabulated in Tables A-I through A-III in the Appendix. In addition the values of q_v , $t_{c_{L0}}$ and $t_{c_{L0}} / t_o$ are listed for each run. The values of non-dimensional core and boundary layer velocity at each axial position can be computed from the given data but did not come directly from the machine program, as did the other quantities listed in these tables. The resulting velocity values are plotted, as will be discussed in succeeding sections.

Computations combining the effects of variable heat source and variable wall temperature were not made. It was felt that the proportional effects indicated by each separately as compared to the simplified case of constant wall temperature, uniform heat source, would be at least approximately additive. Additional computations in this direction, if information regarding a specific configuration were desired, could of course be made using the same machine program.

Detailed Results of Calculations

The general types of theoretical calculations which were made have been discussed in the previous sections. The purpose of this section will be the detailed delineation of the results which were obtained.

Boundary Layer Thickness

For the various configurations calculated (as explained in previous sections), the non-dimensional core thickness (1 - non-dimensional boundary layer thickness) is shown as a function of non-dimensional axial position in Figures 28-a, b, and c. Figure 28-a applies to constant wall temperature and uniform heat source distribution, Figure 28-b to constant wall temperature and various heat source distributions, and Figure 28-c to variable wall temperature distributions with uniform heat source.

Constant Wall Temperature, Uniform Heat Source--Examination of the constant wall temperature uniform heat source case (Figure 28-a) discloses a similar shape for the curves at various values of internal heat source. In all cases the boundary layer grows very rapidly initially, reaching a substantial portion of full width at x/l of only 0.01. This is more evident from examination of the tabulated values in Table A-I. Boundary layer thickness increases more gradually until almost the bottom of the tube, where it drops precipitously to zero.

The physical possibility of a decrease in boundary layer thickness seems uncertain. In normal boundary layer applications, such a result is possible for accelerating flow. However, an examination of Figures 33-a and b giving the non-dimensional core and boundary layer velocities for this particular case shows that both core and boundary layer velocities decrease toward the bottom of

the tube before the decrease in boundary layer thickness from Figure 28-a. Therefore, these calculations imply a decrease of mass flow rate in the boundary layer near the bottom. This result of the mathematical analysis of a simplified theoretical model may not have physical reality. However, since the region of decreasing boundary layer thickness is limited in general to the bottom $1/10$ of the length only, it is reasonable to assume that the effect upon the overall phenomenon is probably not substantial.

Limits of Analysis as Effected by Boundary Layer--A further examination of Figure 28-a shows the boundary layer thickness at any given axial position increases with a decrease of non-dimensional volumetric heat source. In this way the utility of the type of analysis is apparently limited to values of volumetric heat source sufficiently large to prevent the boundary layer from filling the entire cross-section. Such a result might occur if a q_v approximately 2 to 3 decades below the minimum considered were used. An analysis to determine the lower limit of applicability would be a useful extension to the present study. The upper limit is apparently $q_v = \text{infinity}$. However, the necessity of the complications of this approach beyond those of the flat-plate boundary layer analysis disappears as q_v is increased so that the portion of the cross-section occupied by the boundary layer becomes insignificant.

Figure 21 is a cross-plot of the data from Figure 28-a showing the extent of the boundary layer at x/l of 0.4 for various heat

source strengths. It is noted that even at the minimum q_v of 10^5 , in excess of $2/3$ of the radial extent is free of the boundary layer.

Constant Wall Temperature, Variable Heat Source--The curves for boundary layer thickness for constant wall temperature, variable heat source distributions are shown in Figure 28-b for three values of q_v : 10^6 , 4×10^7 , and 2×10^9 . The effects of uniform distributions are compared with a sine distribution; linear distributions with maximum at top and bottom respectively, and zero at opposite end; and the heat source concentrated in an infinitely thin radial disc at the bottom (analogous to Light-hill case as previously explained) are shown at q_v of 4×10^7 . Only the sine and uniform distribution are shown at the other q_v values. It is noted that the effect of the different heat source distributions on boundary layer thickness is relatively minor in all cases.

Variable Wall Temperature Distribution, Uniform Heat Source--Figure 28-a shows the boundary layer thickness curves for the cases of variable wall temperature and uniform heat source. Three families of curves are shown, one for each of the q_v values: 10^6 , 4×10^7 , and 2×10^9 . In each case solid curves are shown for the following t_{q_0}/t_0 (overall to radial temperature ratio) ratios: 1.0, 3.0, 10.0, 20.0, and 40.0. In addition, for each q_v a dotted curve representing the "parabolic" wall temperature distribution, taken from experimental distributions as previously mentioned, for t_{q_0}/t_0 of 3 is included. It is noted that the parabolic curve for the overall/radial ratio of 3 approximated the linear curve for 10. Also the boundary layer thickness at a given q_v is substantially decreased as the overall/radial temperature ratio is

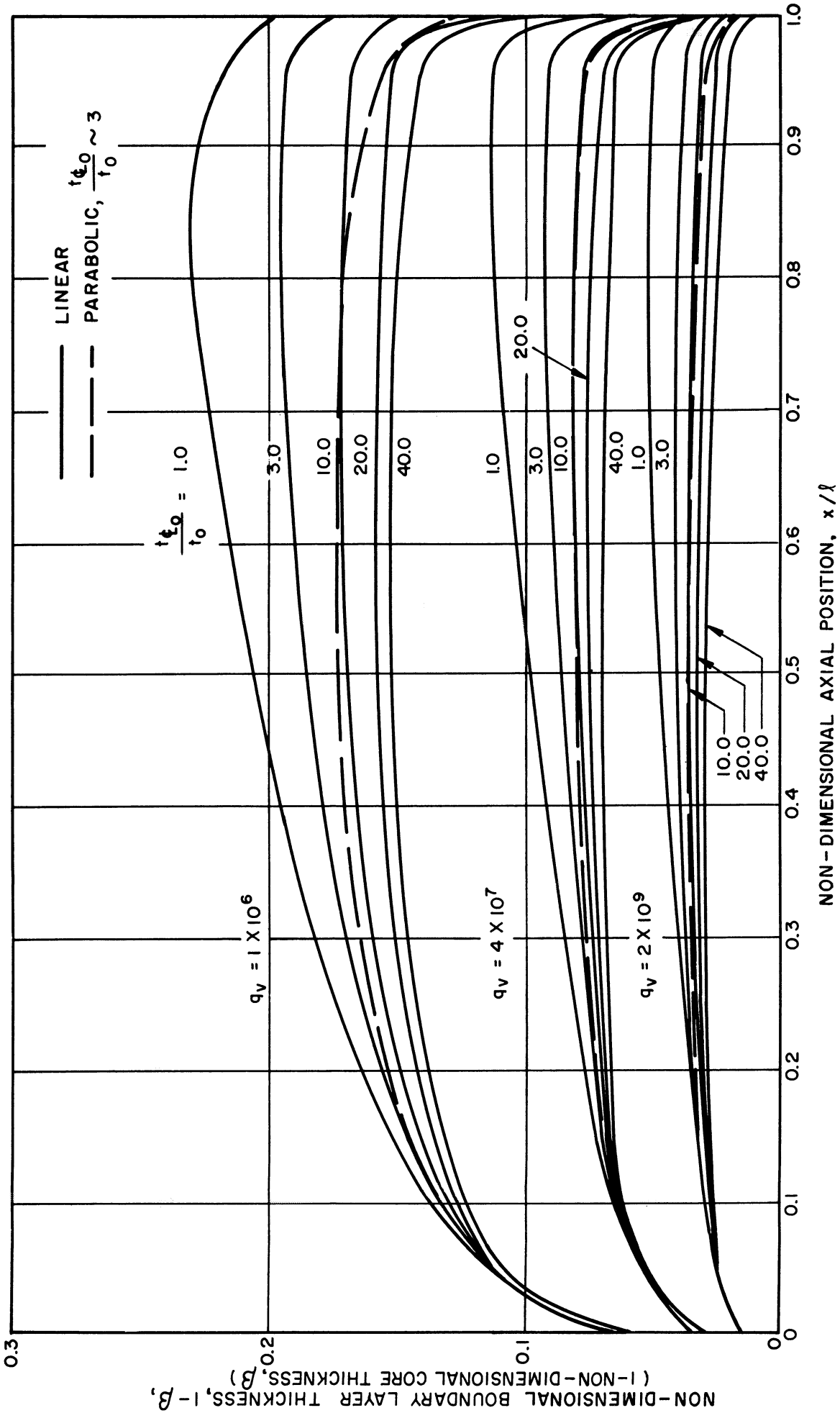


Figure 28-a. Non-Dimensional Boundary Layer Thickness vs. Non-Dimensional Axial Position, Constant Wall Temperature, Uniform Heat Source, Calculated Data.

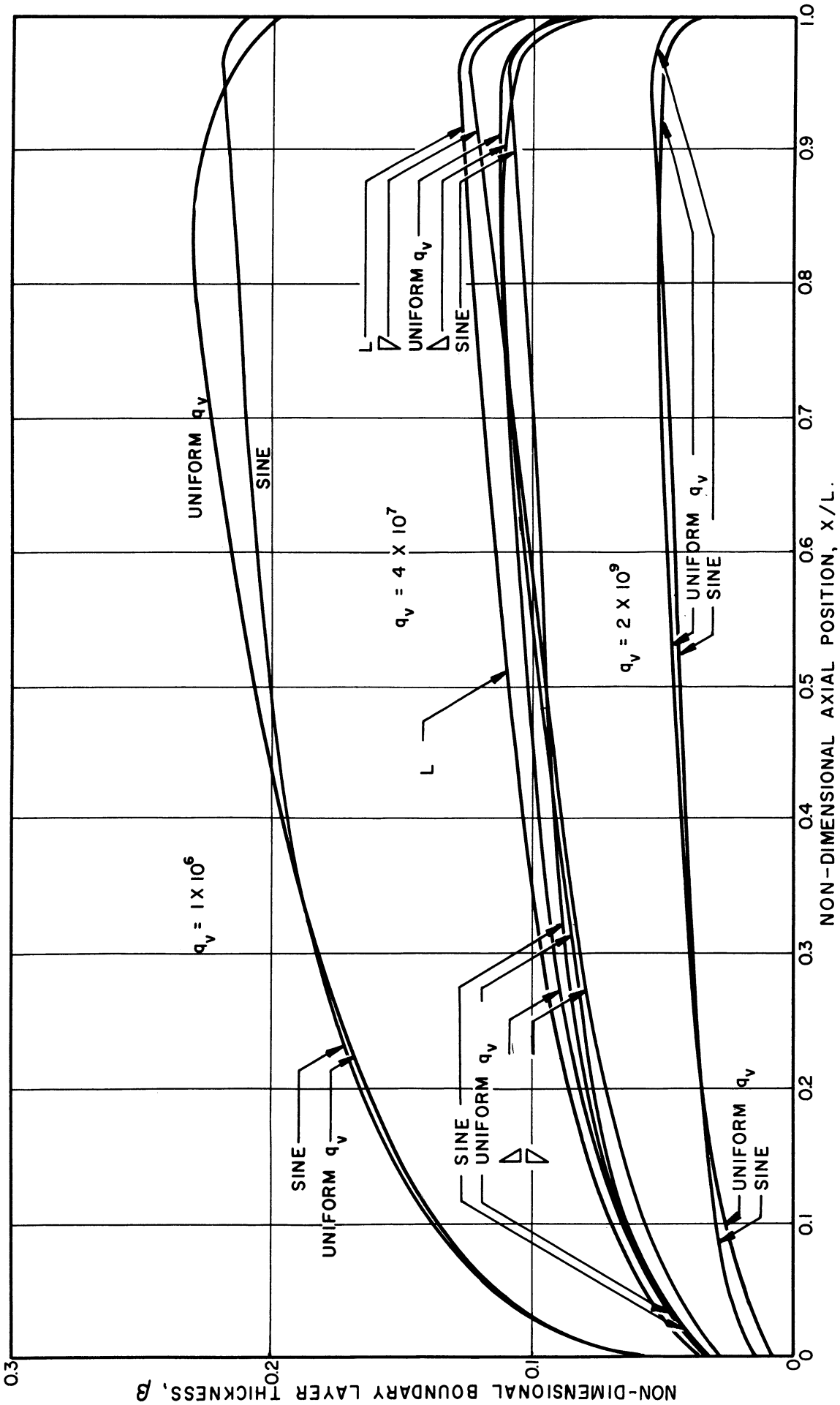


Figure 28-b. Non-Dimensional Boundary Layer Thickness vs. Non-Dimensional Axial Position, Comparison of Various Axial Heat Source Distributions, Calculated Data.

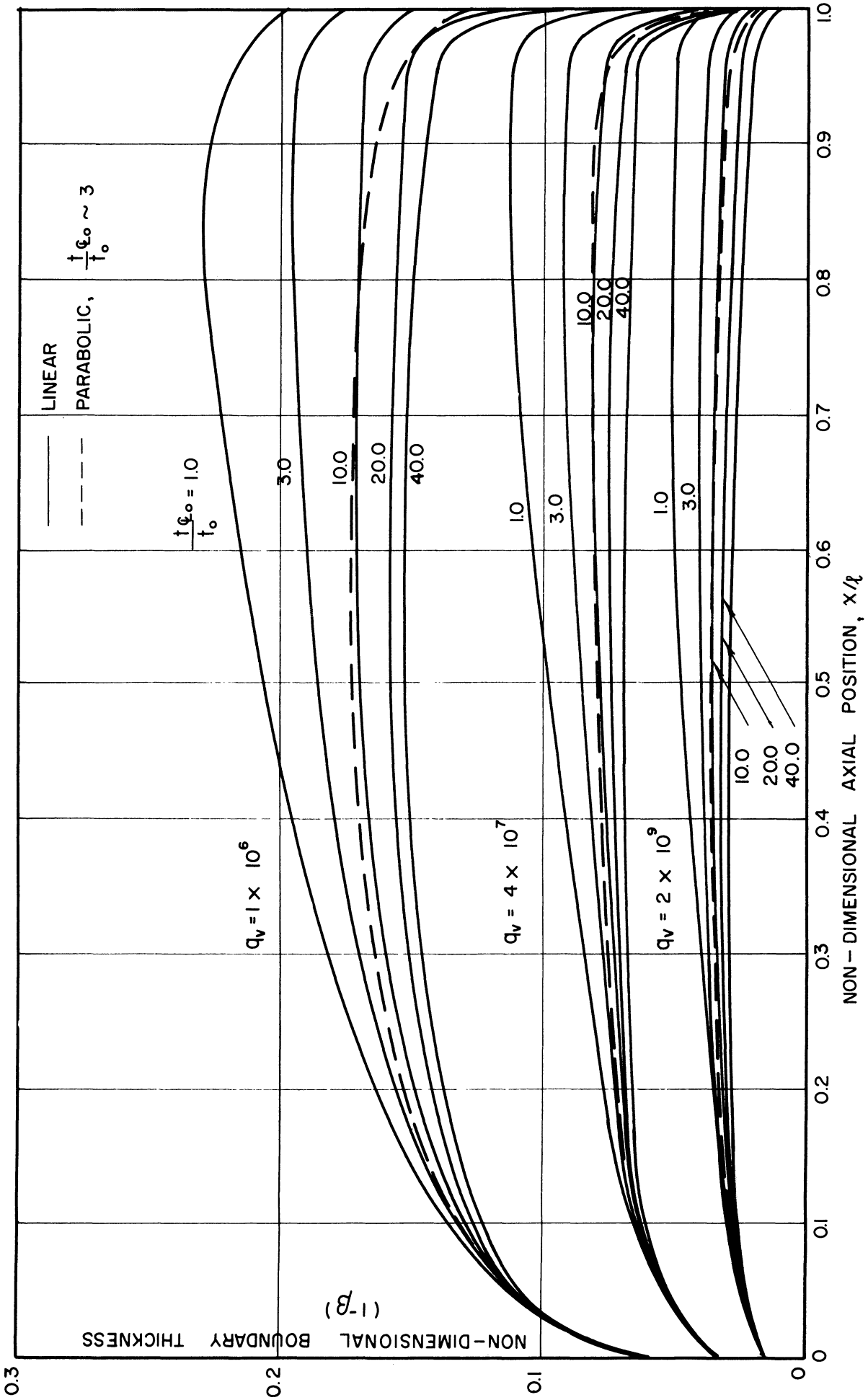


Figure 28-c. Non-Dimensional Boundary Layer Thickness vs. Non-Dimensional Axial Position, Uniform Heat Source Distribution, Linear and Parabolic, Calculated Data.

increased and the peak thickness is moved further from the bottom of the tube. The effect of the substitution of a parabolic for the linear distribution is apparently roughly the same as an increase in the overall/radial temperature ratio. It is of course realized that the $t_{c_0}/t_o = 1.0$ curve is the constant wall temperature curve by the definition of the symbols.

Axial Temperature Gradients in Fluid

One of the most outstanding differences between the present analysis and that of Lighthill is that, with internal volumetric heat source, there is a substantial axial temperature gradient with temperature decreasing from top to bottom. In general the axial temperature differences in the fluid along the centerline are considerably larger than the radial differences, even for the case of constant temperature of the inner surface of the test section wall. These gradients are examined in detail in this section.

Constant Wall Temperature, Uniform Heat Source--The ratio of the non-dimensional temperature differential between the vessel centerline at any axial position and the wall at the bottom and the differential between the centerline at top and wall at bottom is shown as a function of non-dimensional axial position in Figure 29-a for constant wall temperature, uniform heat source. Curves are plotted for the various q_v for which calculations were made, ranging from 10^5 to 2×10^9 . Even over so large a range there is little effect of the axial temperature distribution. In general the low q_v curves are slightly above those for higher q_v . The greatest temperature drops are concentrated near

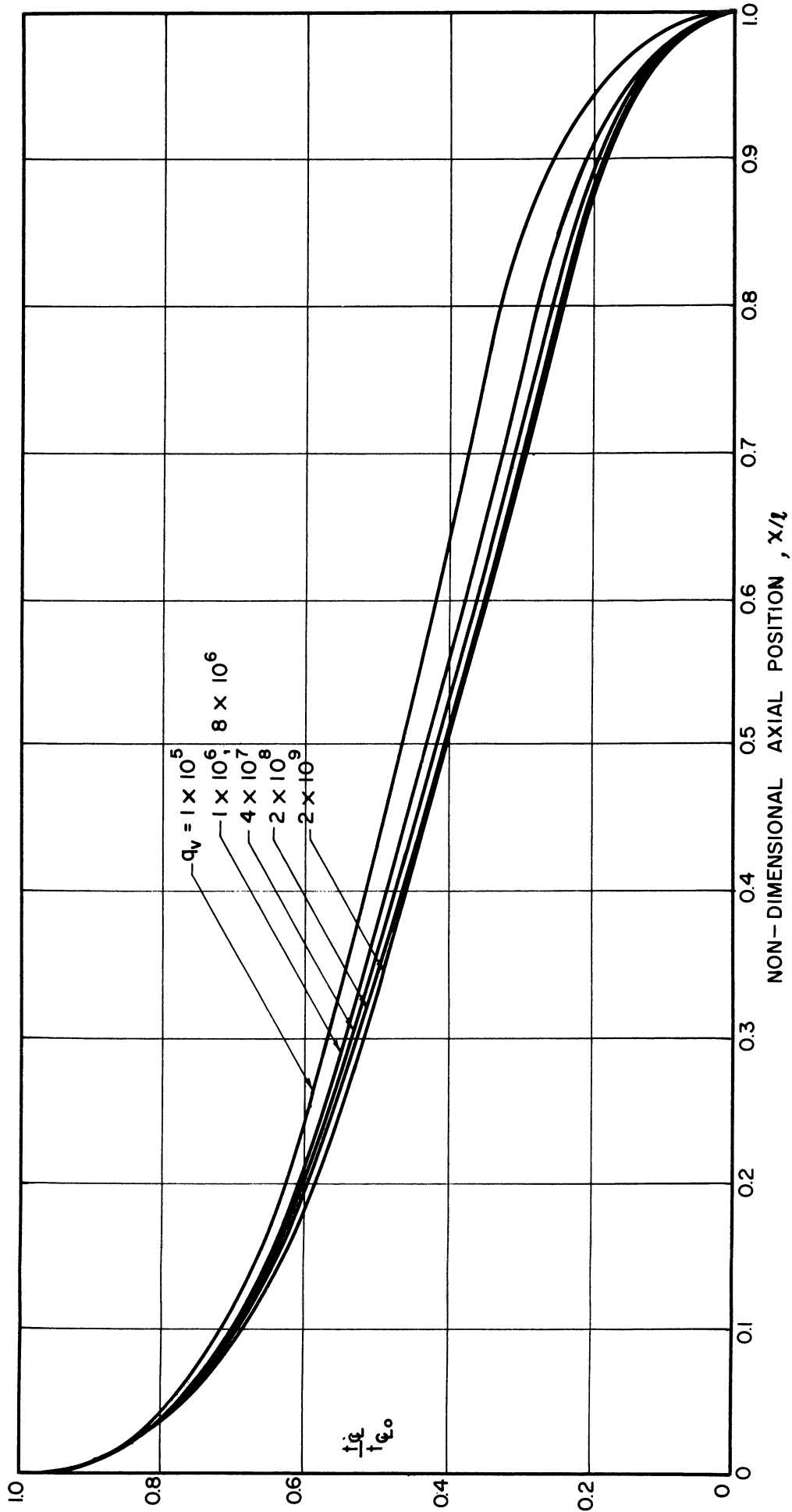


Figure 29-a. Non-Dimensional Centerline Temperature Distribution vs. Non-Dimensional Axial Position, Uniform q_w , Constant Wall Temperature, Calculated Data.

either end, with a more level portion in the center. As discussed further in a later section, the experimental runs showed a severe drop in temperature near the bottom and less near the top. This condition was more closely duplicated analytically when the experimental wall temperature ("parabolic") distribution was used.

Constant Wall Temperature, Variable Heat Source Distribution--The fluid centerline temperature distribution results for various heat source distributions but constant wall temperature are shown in Figure 29-b for a q_v of 4×10^7 . Results for other heat source strengths are not included since the axial temperature distribution is only slightly affected by heat source strength. The horizontal line marked applies to the heat source distribution concentrated in an infinitely thin radial disc at the bottom (Lighthill analogy as previously explained). This of course represents a constant centerline (or core) temperature. The next lowest curve represents a linear heat source distribution ranging from maximum at the bottom to zero at the top. The lowest curve is the reverse arrangement of linear distribution. The sine and uniform distribution curves are clearly marked. It is noted that the centerline axial temperature gradient is strongly affected by heat source distribution. In general the greater the preponderance of heat source strength near the bottom, the greater the proportion of the total temperature drop which occurs near the bottom. The sine distribution approaches a linear temperature drop of the core.

Linearly Variable Axial Wall Temperature, Uniform Heat Source--The fluid temperature centerline distributions resulting from the uniform

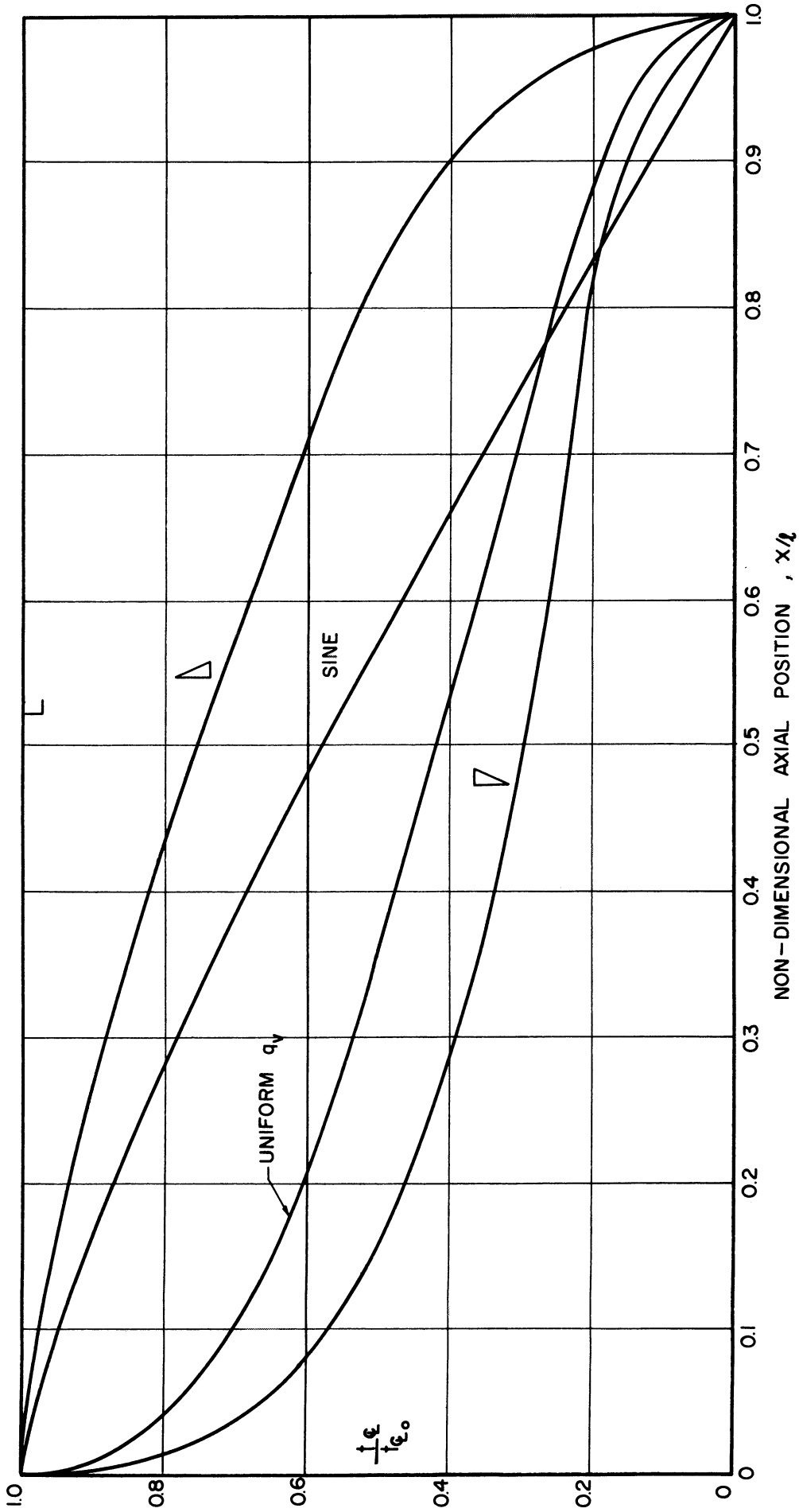


Figure 29-b. Non-Dimensional Centerline Temperature Distribution vs. Non-Dimensional Axial Position, Constant Wall Temperature, Various Axial Heat Source Distributions.

heat source, linear axial wall temperature variation calculations are shown in Figures 29-c, d, and e. Each applies to a different q_v ; these are 10^6 , 4×10^7 , and 2×10^9 respectively. It will be observed that the increase of radial/overall temperature ratio does not have a great effect on the distribution. In general, the concentration of drop near the top and bottom is reduced for the larger ratios and a closer approach to a linear centerline temperature distribution is made.

Parabolic Variation of Axial Wall Temperature, Uniform Heat Source--The figures mentioned in the preceding section, 29-c, d, and e show also the effect on centerline temperature distribution of a wall temperature distribution approximating the experimental results; i.e., an approximate parabola. As will be observed, the effect upon the centerline axial temperature distribution is significant. The portion of the overall temperature drop occurring near the bottom of the vessel is greatly increased so that little drop is evident near the top or for a considerable distance down the tube. As will be discussed in greater detail in a later section, these analytical results closely approximate the measured experimental temperature profiles.

Radial Temperature Differentials

The theoretical analysis assumed for the calculating model radial temperature profiles (Figure 25) consisting of a parabolic distribution in the boundary layer tangent to a horizontal core temperature at the juncture between boundary layer and core. The magnitude of the non-dimensional temperature differential between core and wall as a

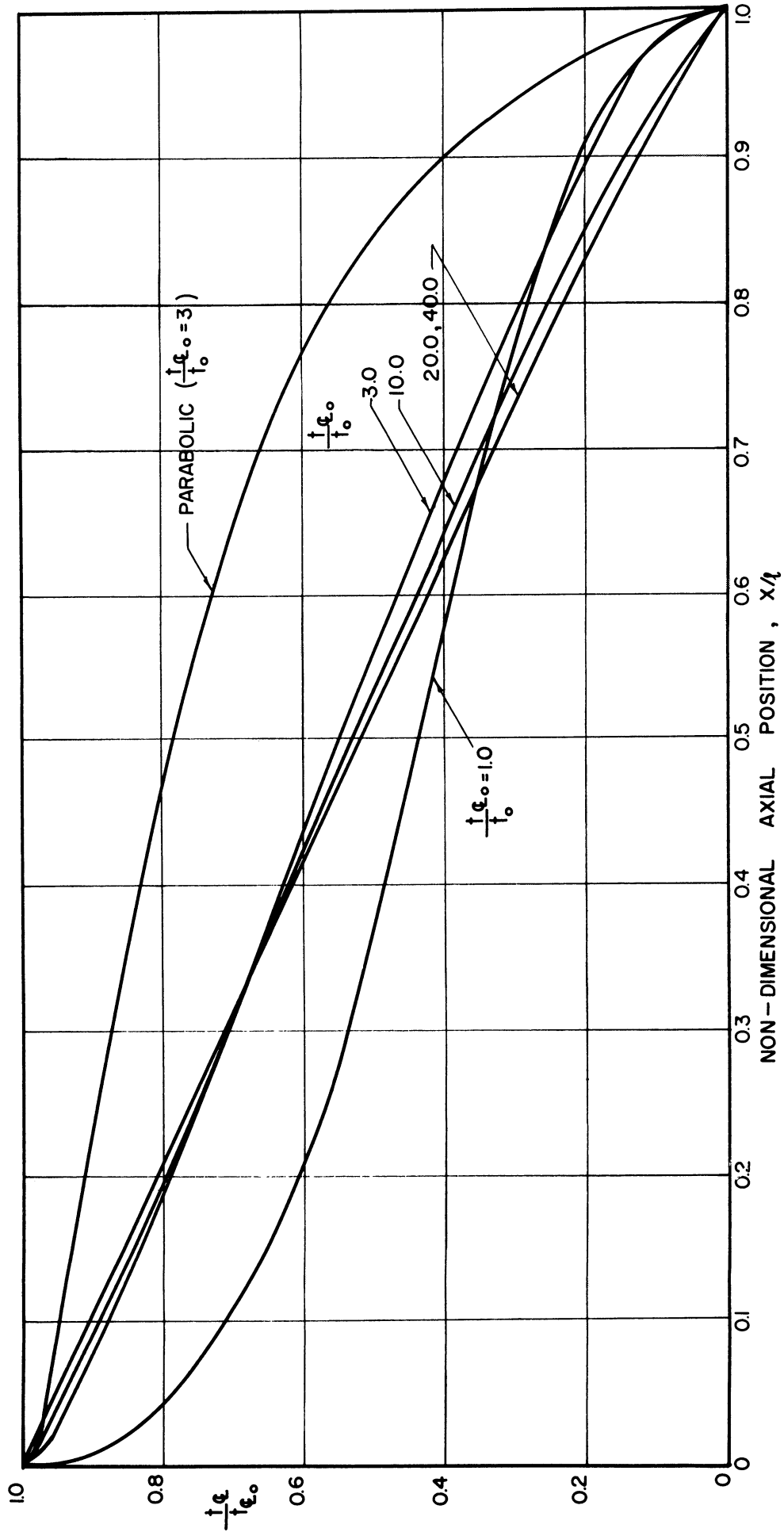


Figure 29-c. Non-Dimensional Centerline Temperature Distribution vs. Non-Dimensional Axial Position, Uniform $q_v = 1 \times 10^6$ Variable, Linear Distribution of Overall/Radial Temperature Ratio, Calculated Data.

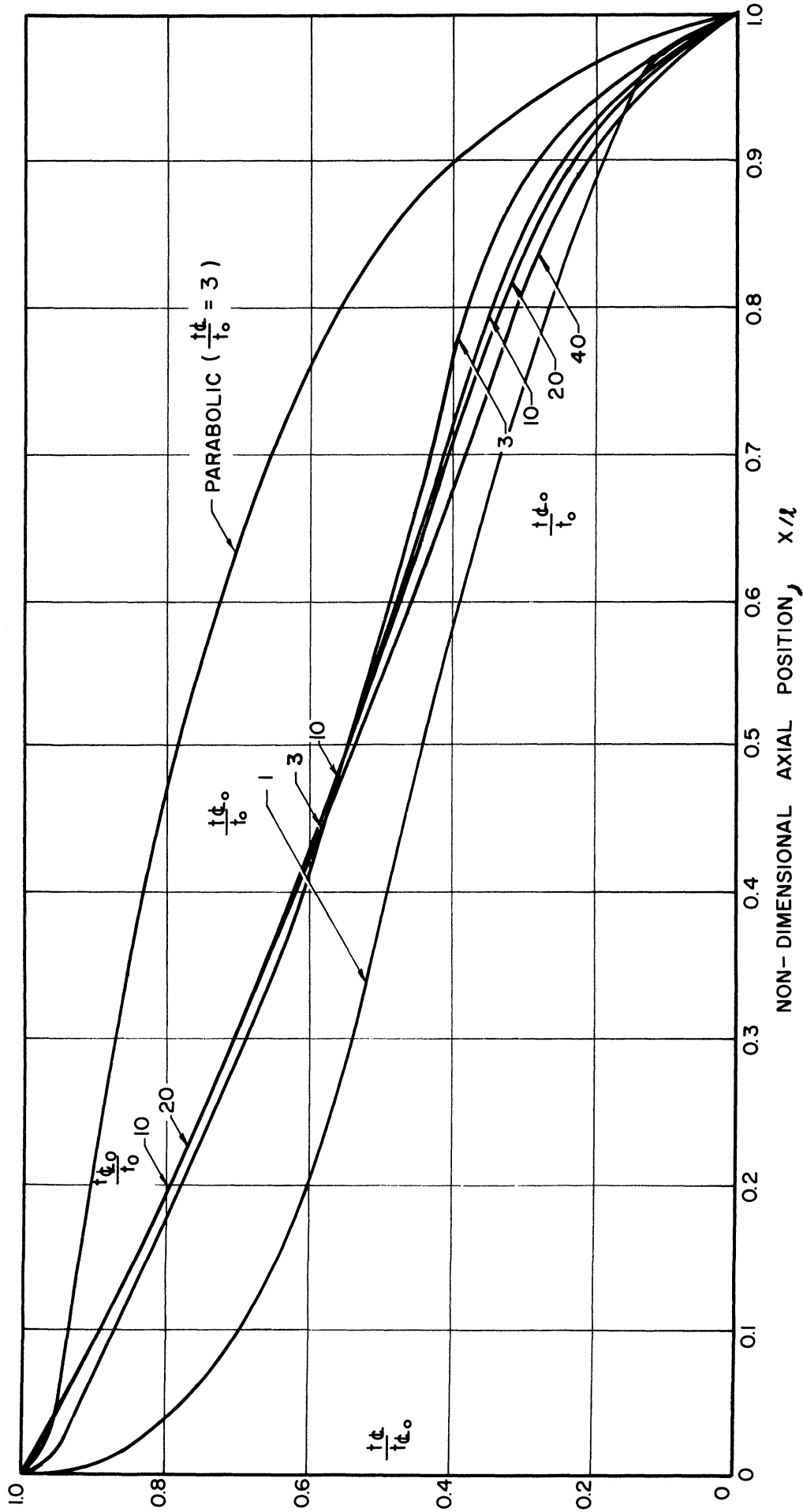


Figure 29-d. Non-Dimensional Centerline Temperature Distribution vs. Non-Dimensional Axial Position, Uniform $q_v = 4 \times 10^7$, Variable, Linear Distribution of Overall/Radial Temperature Ratio, Calculated Data.

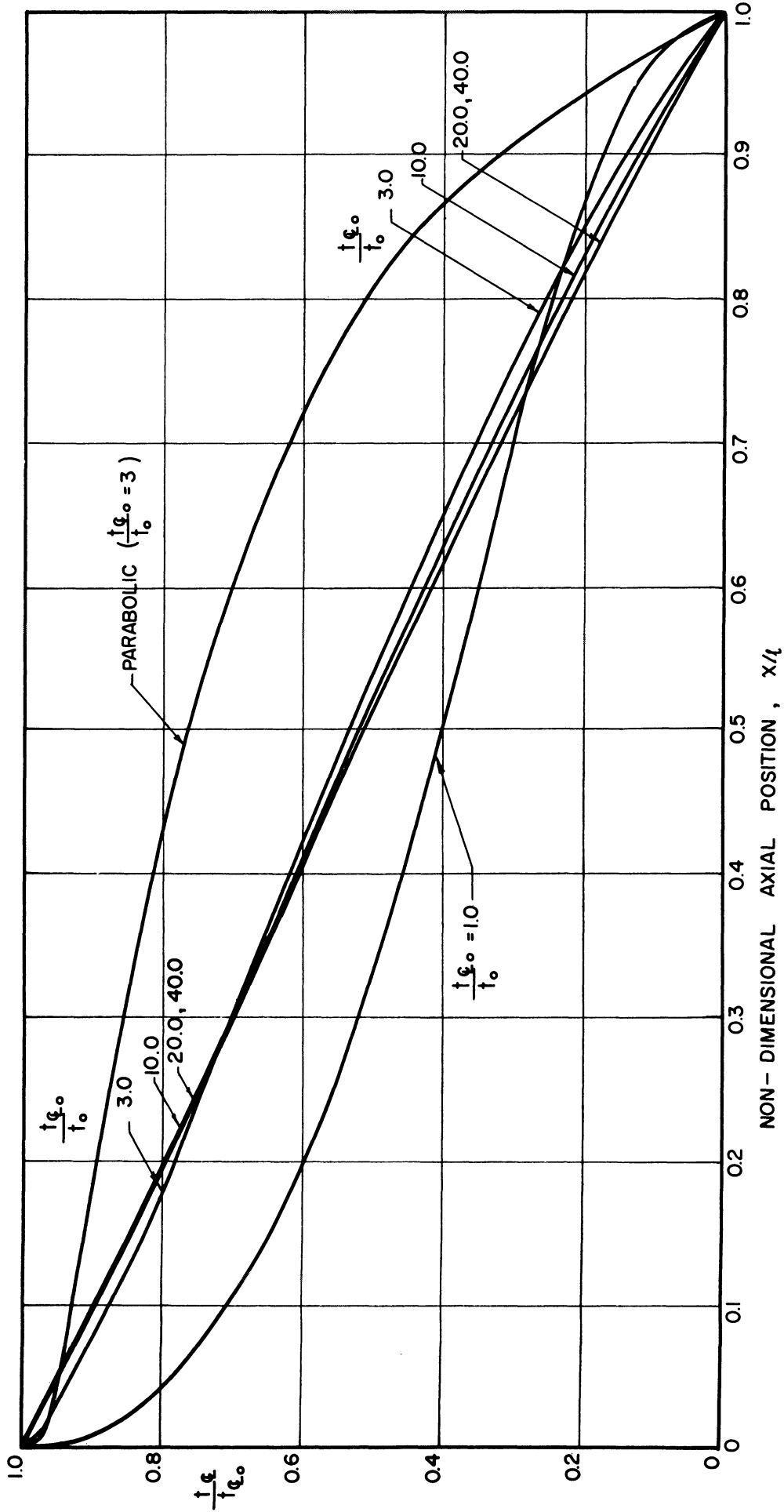


Figure 29-e. Non-Dimensional Centerline Temperature Distribution vs. Non-Dimensional Axial Position, Uniform $q_v = 2 \times 10^9$ Variable, Linear Distribution of Overall/Radial Temperature Ratio, Calculated Data.

function of non-dimensional axial position is the subject of this section.

Figures 30-a, b, and c show the ratio between non-dimensional temperature differential between centerline and wall at any axial position to non-dimensional temperature differential between centerline at top and wall at bottom as a function of non-dimensional axial position. The three curve sheets apply to q_v values of 10^6 , 4×10^7 , and 2×10^9 respectively. It should be mentioned that no curves are included with these figures for the cases of constant wall temperature. The information for these cases is given in the t_{G_0}/t_0 curves of Figures 29-a and b since $t = t_{G_0}$ for constant wall temperature. These curves have been discussed in a previous section.

The general effect of an increasing ratio of overall/radial temperature is a decrease in the centerline to wall differential as compared with the overall differential. In general, the curves are fairly horizontal except for the portion near the lower end of the tube where the centerline to wall differential goes rapidly to zero. The differential decreases consistently, however, throughout the run length, from the top toward the bottom. The parabolic wall temperature distribution curve for all cases closely follows the linear curve for the same overall/radial temperature ratio.

Wall Conduction Heat Flux Distribution

Constant Wall Temperature, Uniform Heat Source

The calculated data for wall heat flux as a function of axial position is presented for the various computations in Figures 32-a, b,

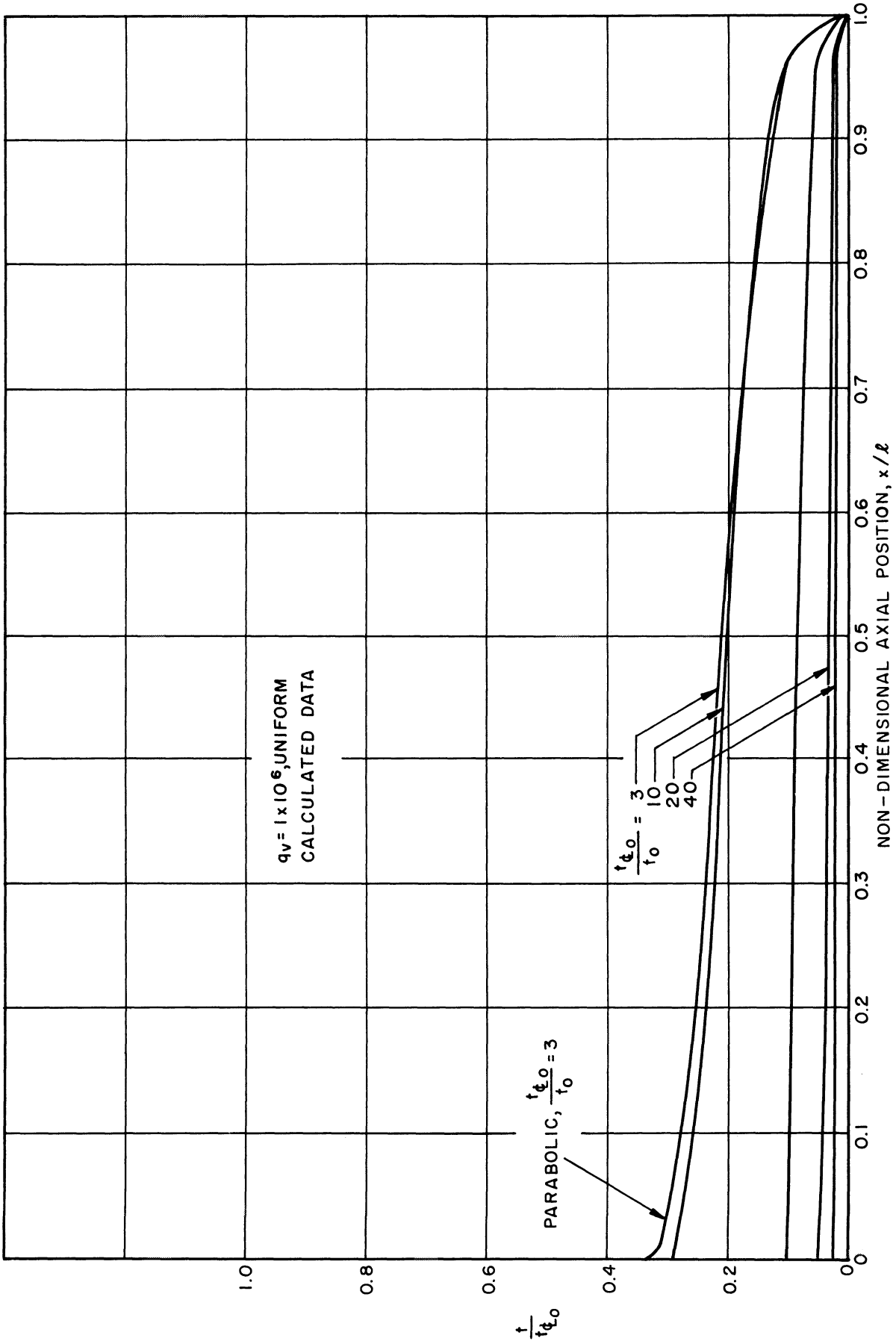


Figure 30-a. Non-Dimensional Temperature Differential Centerline to Wall vs. Non-Dimensional Axial Position, $q_v = 1 \times 10^6$ Uniform, Calculated Data.

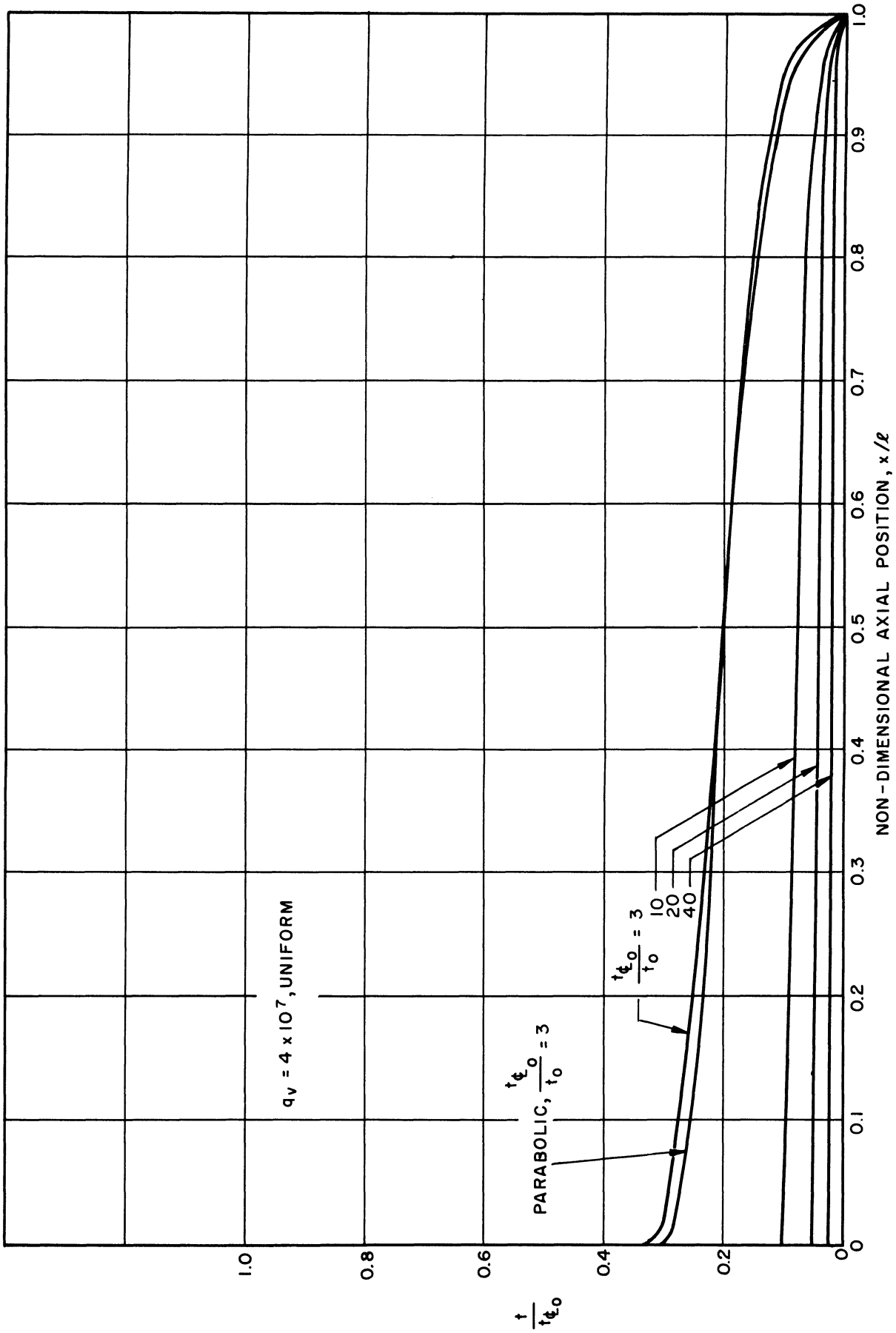


Figure 30-b. Non-Dimensional Temperature Differential Centerline to Wall vs. Non-Dimensional Axial Position, $q_v = 4 \times 10^7$, Uniform, Calculated Data.

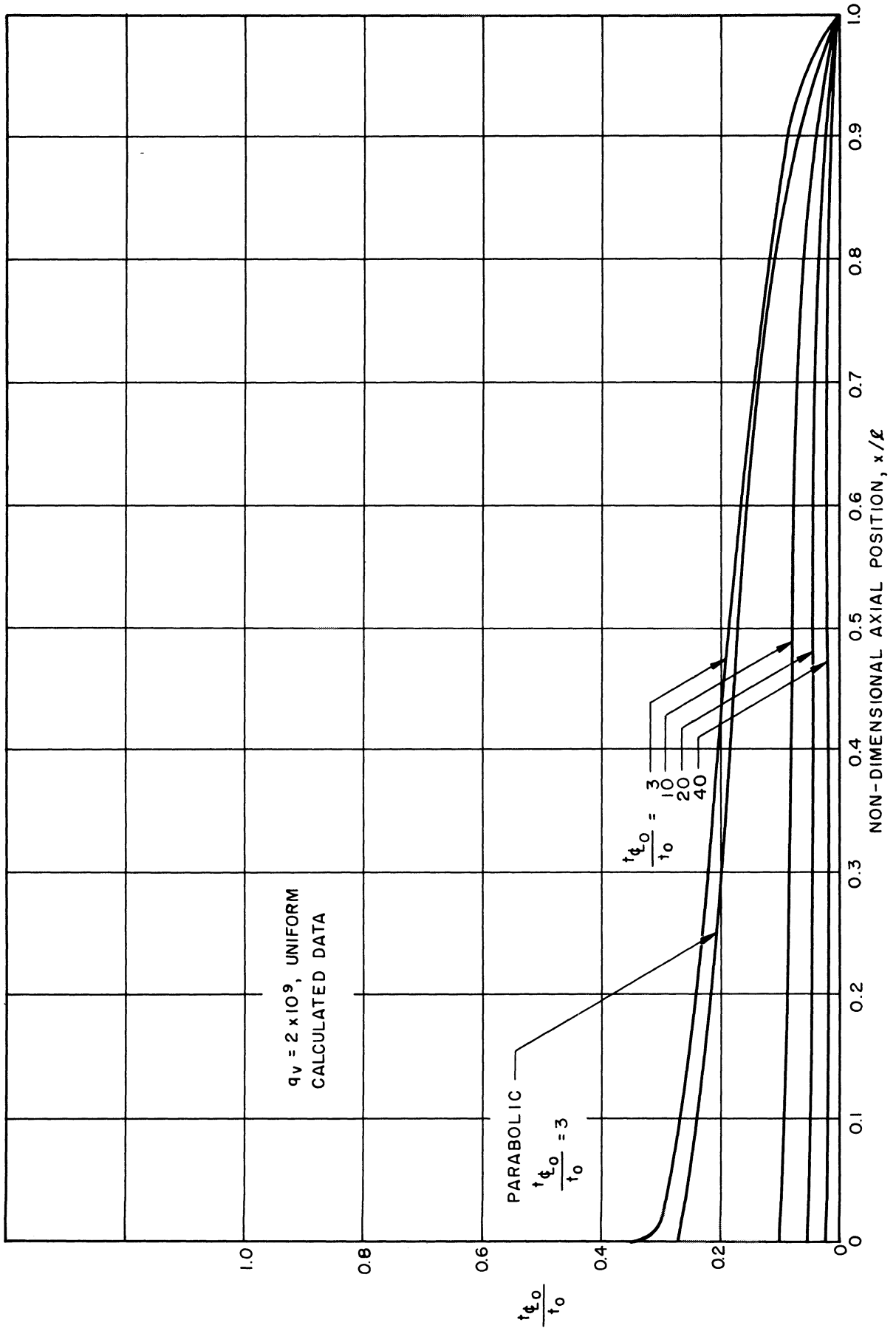


Figure 30-c. Non-Dimensional Temperature Differential Centerline to Wall vs. Non-Dimensional Axial Position, $q_v = 2 \times 10^9$, Uniform, Calculated Data.

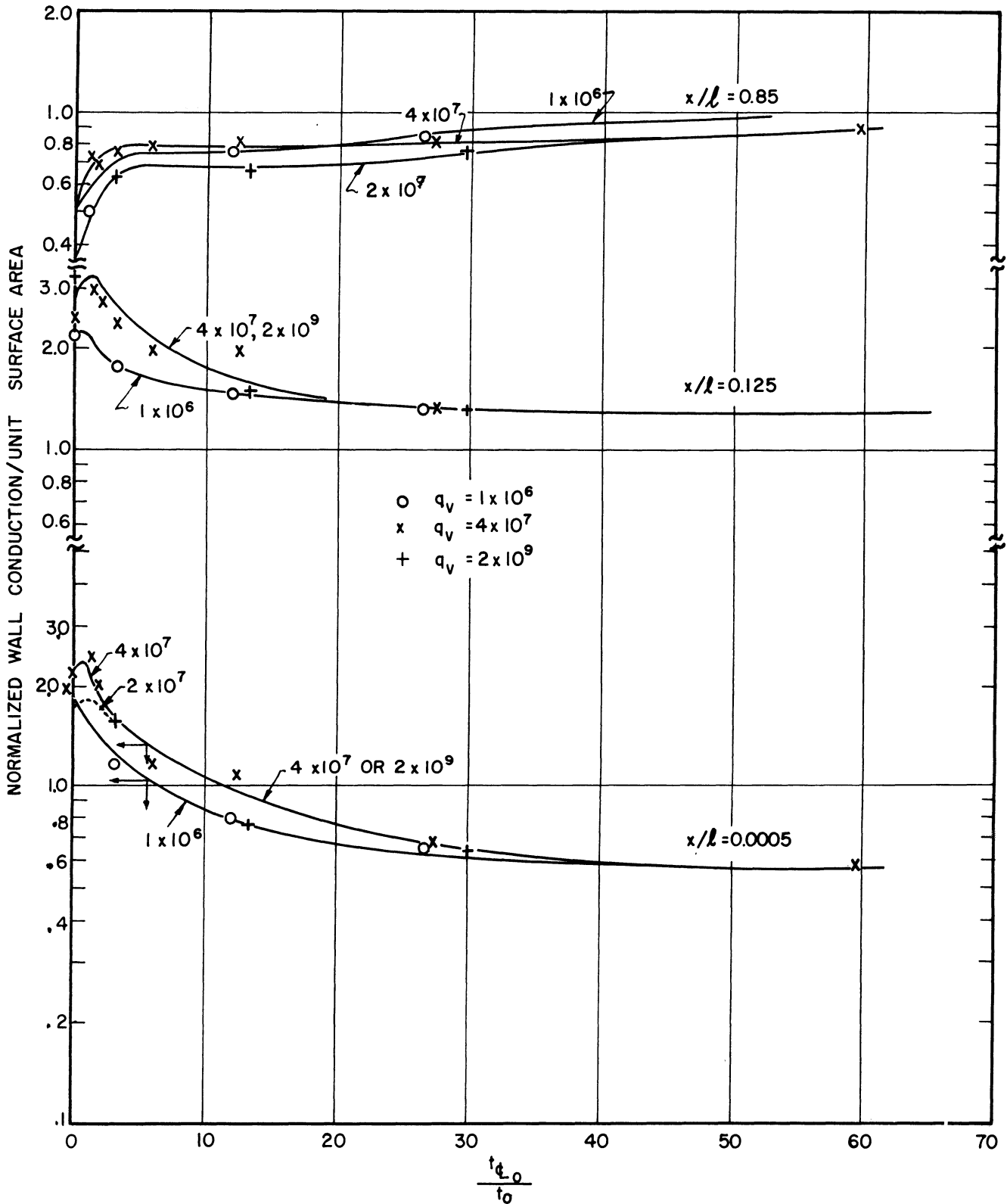


Figure 31. Normalized Wall Conduction vs. Overall/Radial Temperature Ratio, Linear Wall Temperature Distribution, Uniform Heat Source, Calculated Data.

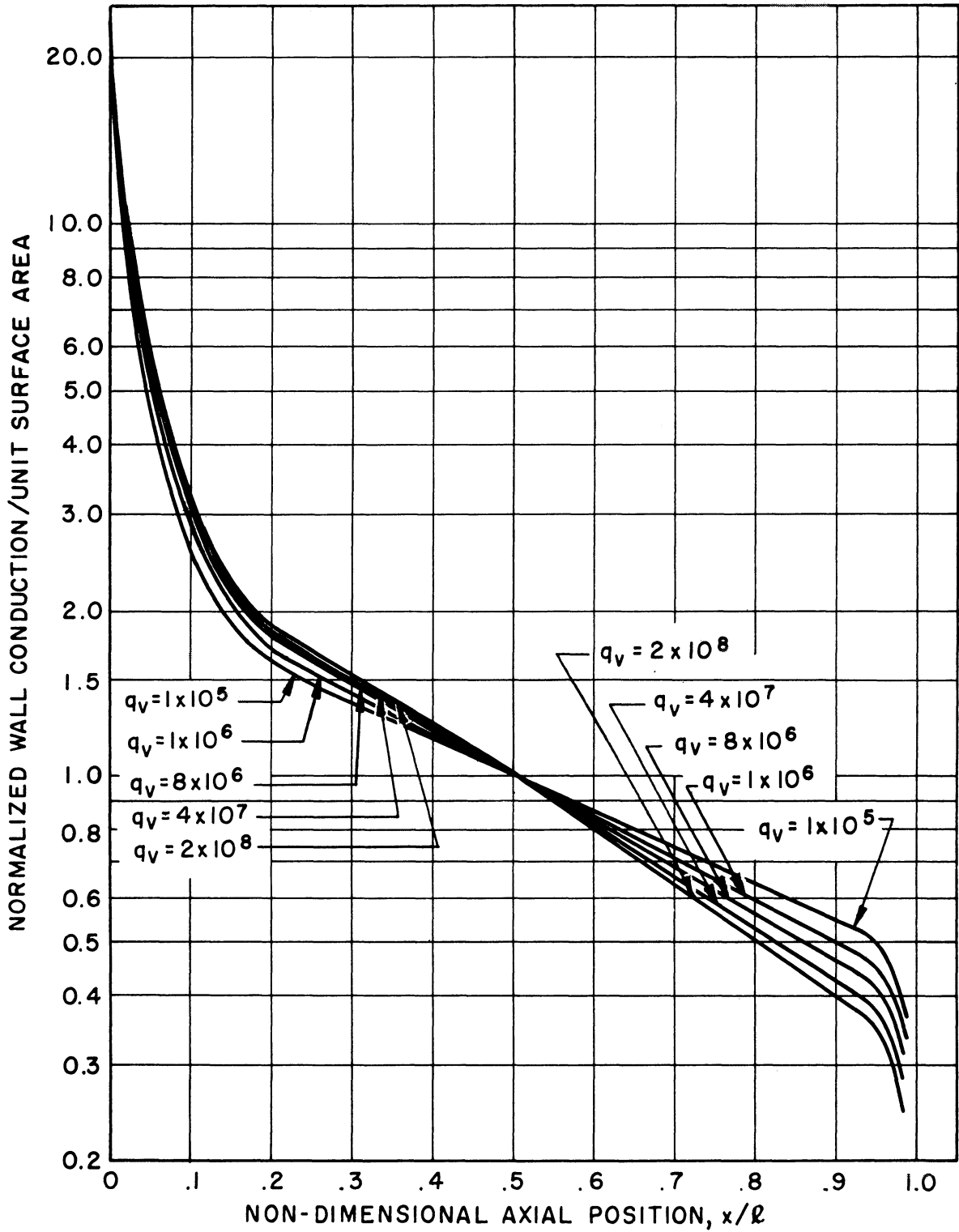


Figure 32-a. Normalized Wall Conduction vs. Non-Dimensional Axial Position, Constant Wall Temperature, Uniform Heat Source Distribution.

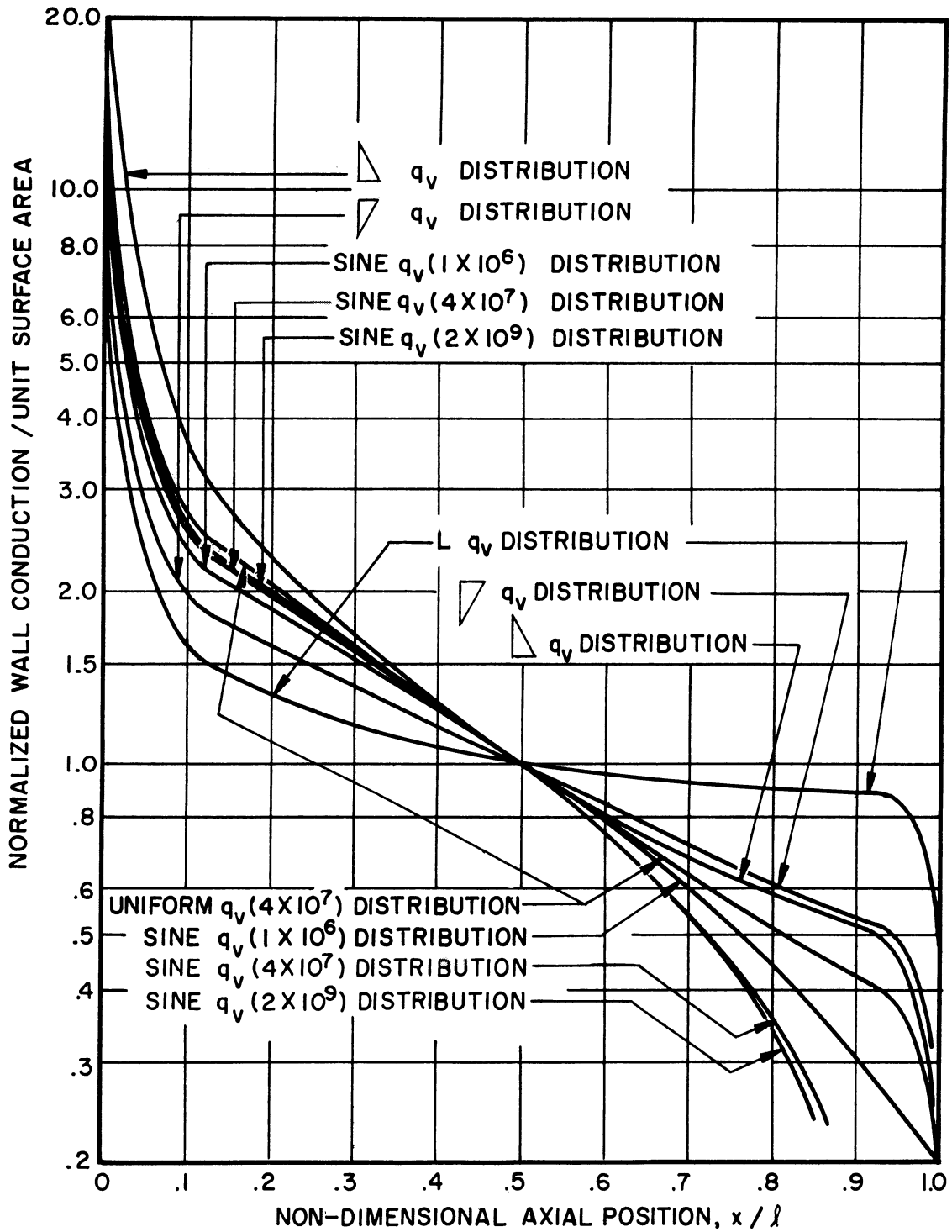


Figure 32-b. Normalized Wall Conduction vs. Non-Dimensional Axial Position, Constant Wall Temperature, Variable Axial Heat Source Distribution.

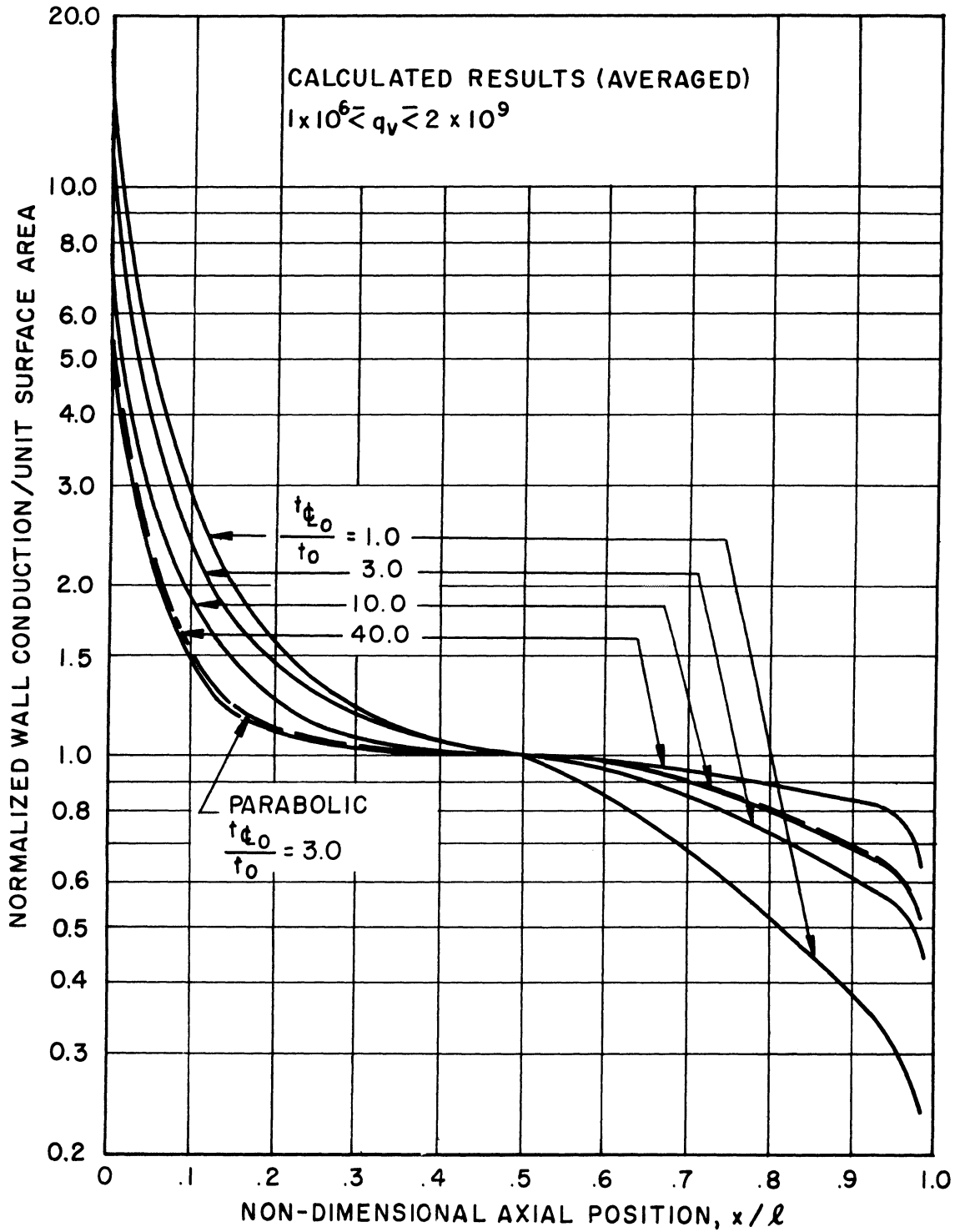


Figure 32-c. Normalized Wall Conduction vs. Non-Dimensional Axial Position, Linear Wall Temperature Distribution, Uniform Heat Source.

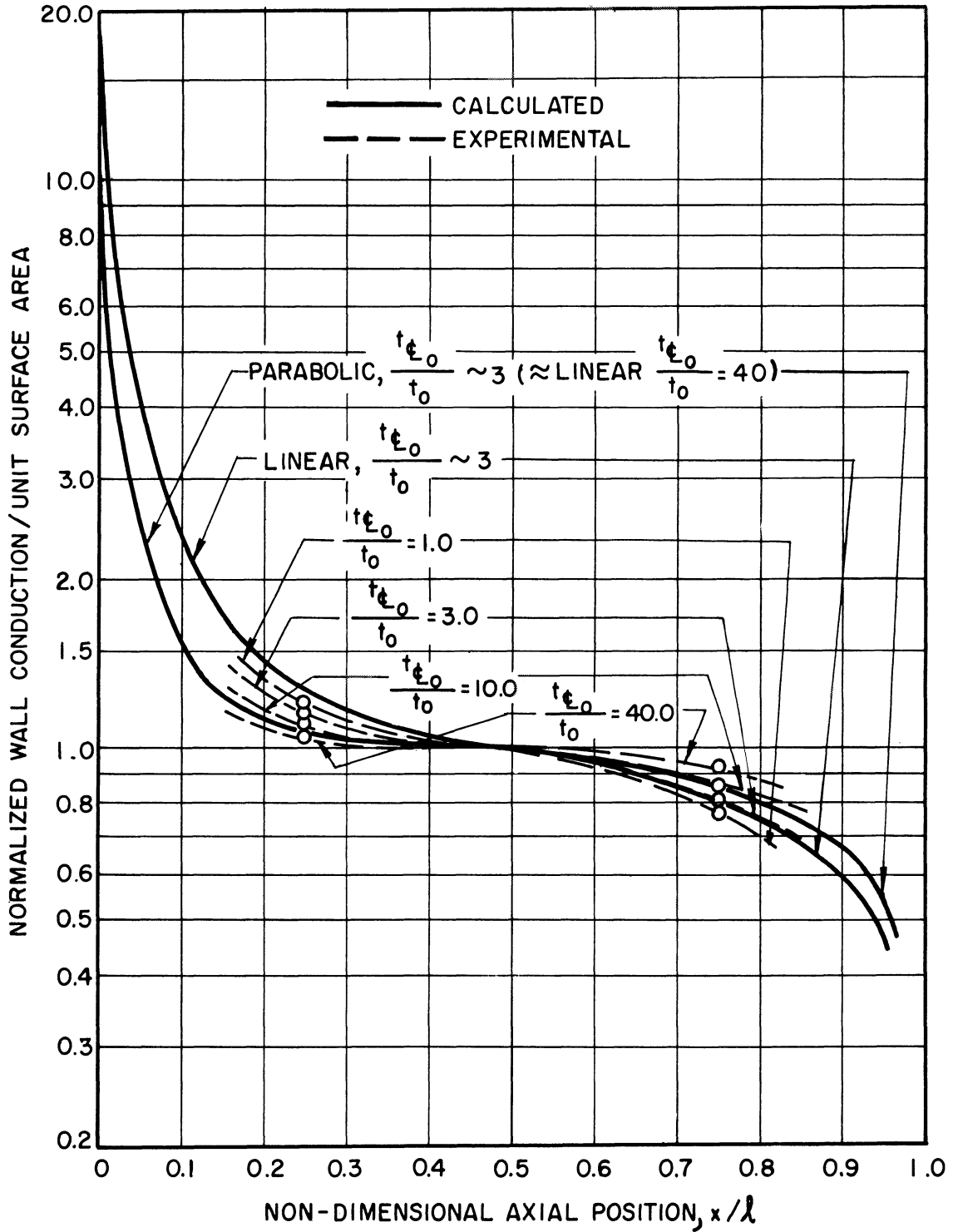


Figure 32-d. Normalized Wall Conduction vs. Non-Dimensional Axial Position, Linear and Parabolic Wall Temperature Distribution Comparison, Calculated and Experimental Data Comparison, Uniform Heat Source.

and c. Figure 32-d shows a comparison between the theoretical and calculated data. Figure 31 is a cross-plot of the normalized wall conduction at various x/l position for various ratios of the overall/radial temperature ratio. Such a cross-plot was necessary for the variable wall temperature calculations because they are not for the precise overall/radial ratios which have been used for the other results. It is noted that the computed points of the cross-plots do not form a completely smooth curve. This is a result of the fact that completely precise results were not demanded of the machine program. Apparently the resulting discontinuities are magnified in the case of the wall heat flux results. In addition to the x/l positions used for the cross-plots, it is known that all curves pass through 1.0 at x/l of 0.5 by the definition of the normalized wall heat flux.

Figure 32-a shows the local wall heat flux divided by the value at the tube mid-point plotted as a function of non-dimensional axial position, x/l , for constant wall temperature and uniform heat flux distribution. Separate curves are shown for q_v ranging from 10^5 to 2×10^9 . Under these conditions, the wall heat flux rises to approximately 20 times its average value at the uppermost portion of the tube, is of the order of twice its average value at approximately 15% of the total tube length down from the top, and decreases to the order of 0.4 times the average value at a point 5% of the total length up from the bottom. It decreases to zero at the bottom. The distribution is quite insensitive to the heat source strength within the range studied. However, the variation with heat source strength is such as to accelerate

the differences with higher heat flux.

Constant Wall Temperature, Variable Heat Source--Figure 32-b shows the effect upon normalized wall heat flux of different distributions of the internal heat source parameter, q_v , for conditions of constant wall temperature. The general relations are the same as mentioned for uniform heat source distribution in the preceding paragraph. There is a preponderance of wall heat flux at the top of the tube and a substantial decrease below the average value at the bottom. The higher rates of average heat flux result in relatively greater non-uniformity of wall flux. A preponderance of internal heat generation near the bottom of the tube (the extreme in this direction is reached in the Lighthill analogy where all the heat is added in an infinitely thin radial slice at the bottom) results in flattening of the wall distribution curve and a reduction of the peak near the top. A preponderance of heat addition near the top (a linear distribution with maximum at the top and zero at the bottom was considered) results in a curve flatter than that for uniform heat addition in the central portion of the test section, but, as would be expected, in an exaggerated peak value at the top. The sine distribution of internal heat flux results in a very close approximation to the curve for uniform distribution.

Linear and Parabolic Axial Wall Temperature Distribution, Uniform Heat Source

Effects upon the normalized wall heat flux distribution as a function of x/l for various ratios of overall/radial temperature differential for both linear and parabolic wall temperature distributions are shown in

Figure 32-c. In general the effect of an increasing ratio is a reduction in the non-uniformity of the wall flux distribution. As the ratio is increased from unity (constant wall temperature case) to 40, the peak flux at the top of the tube is reduced from about 20 times the average for the entire tube to about 6 times the average. Likewise, the rate of decrease toward the bottom of the tube is less for the large overall/radial ratio of 40 at the x/l of 0.95 point while it is reduced to approximately 0.14 of the average value for the constant wall temperature case at the same point. Also, the central portion of the tube shows virtually constant wall heat flux for the large temperature ratios. The curve sheet shows only values averaged over the range of q_w rather than separate q_w curves since for the constant wall temperature case, the effect of different heat source strengths is minor.

The parabolic axial wall temperature distribution calculation is also included on Figure 32-c. It is approximately the equivalent of the overall/radial temperature ratio linear curve of 10 although the ratio for the parabolic calculation was approximately 3. Thus it is apparent that wall temperature distributions shaded from the linear in the direction of a concave downward parabola would result in an evening out of the distribution of wall heat flux, in the same manner as an increase in the overall/radial temperature ratio.

Comparison with Experimental Results--Figure 32-d shows a comparison of the uniform heat source, linear and parabolic wall temperature distribution curves with experimental results. The experimental distribution for an overall/radial ratio of 3 lies between the calculated curves for

linear and parabolic wall temperature distributions. The shape of the experimental and calculated curves are similar. As will be discussed in a later section, there is no experimental evidence for the large variations from uniform heat flux predicted theoretically near either end.

Velocity Profiles and Magnitudes

General Profile Aspects--As explained in a previous section, arbitrary velocity profiles, which satisfied the physical boundary conditions along the wall, at the intersection between the descending fluid layer adjacent to the wall and the ascending core, and at the centerline were assumed. Schematically, the velocity profile at a given axial position is shown in Figure 25. The velocity is zero at the wall, attains a maximum in the downward direction at a position near the wall, and has a profile tangent to a horizontal line at the junction between boundary layer and core. It has a constant upward magnitude across the core, from boundary layer to boundary layer. The magnitudes of the profiles and the radial location of the maximum and zero points depend upon the axial position and the other problem parameters as explained previously. Under the general assumptions of the analysis it is impossible to compute the anticipated velocity at any location within the test section. It is the purpose of the present section to review the numerical data resulting from the machine computations for various values of the system parameters. The non-dimensional velocities, u , as a function of x/l , for the various system configurations are shown in Figures 33-a, b, c, d, e, f, and g.

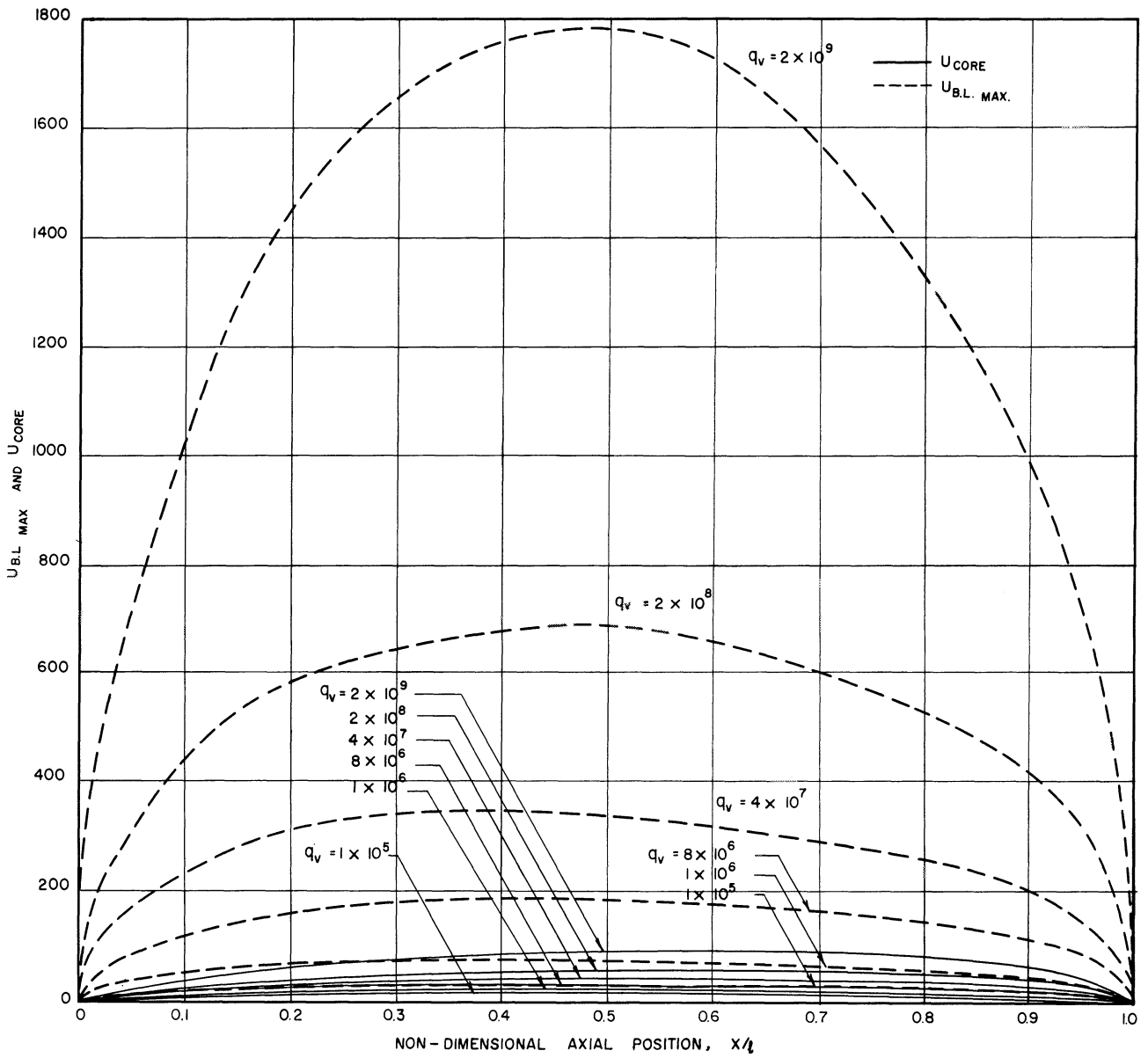


Figure 33-a. Non-Dimensional Core and Boundary Layer Velocity vs. Non-Dimensional Axial Position, Uniform q_v , Constant Wall Temperature, Calculated Data.

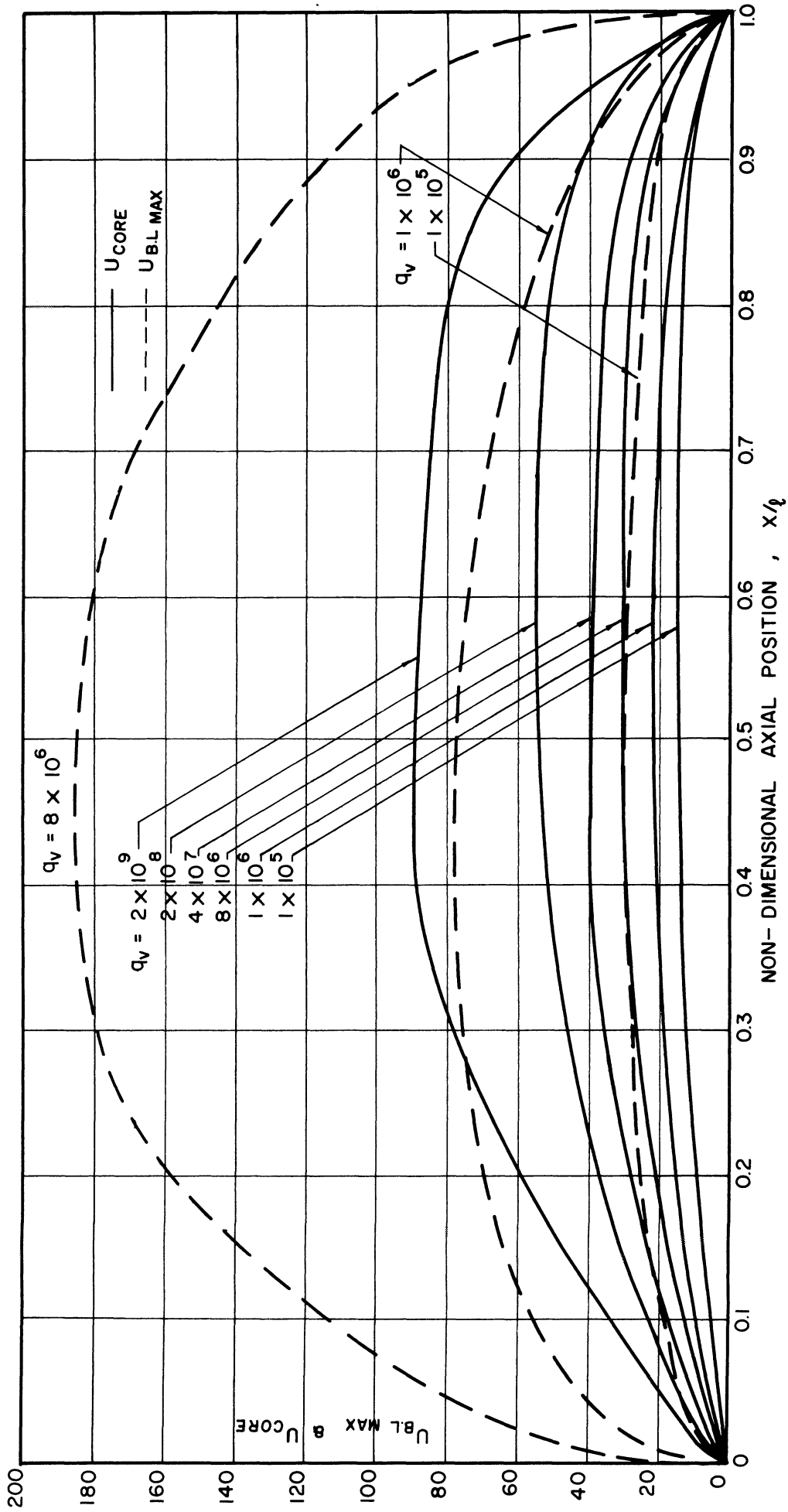


Figure 33-b. Non-Dimensional Core and Boundary Layer Velocity vs. Non-Dimensional Axial Position, Uniform q_w , Constant Wall Temperature, Calculated Data.

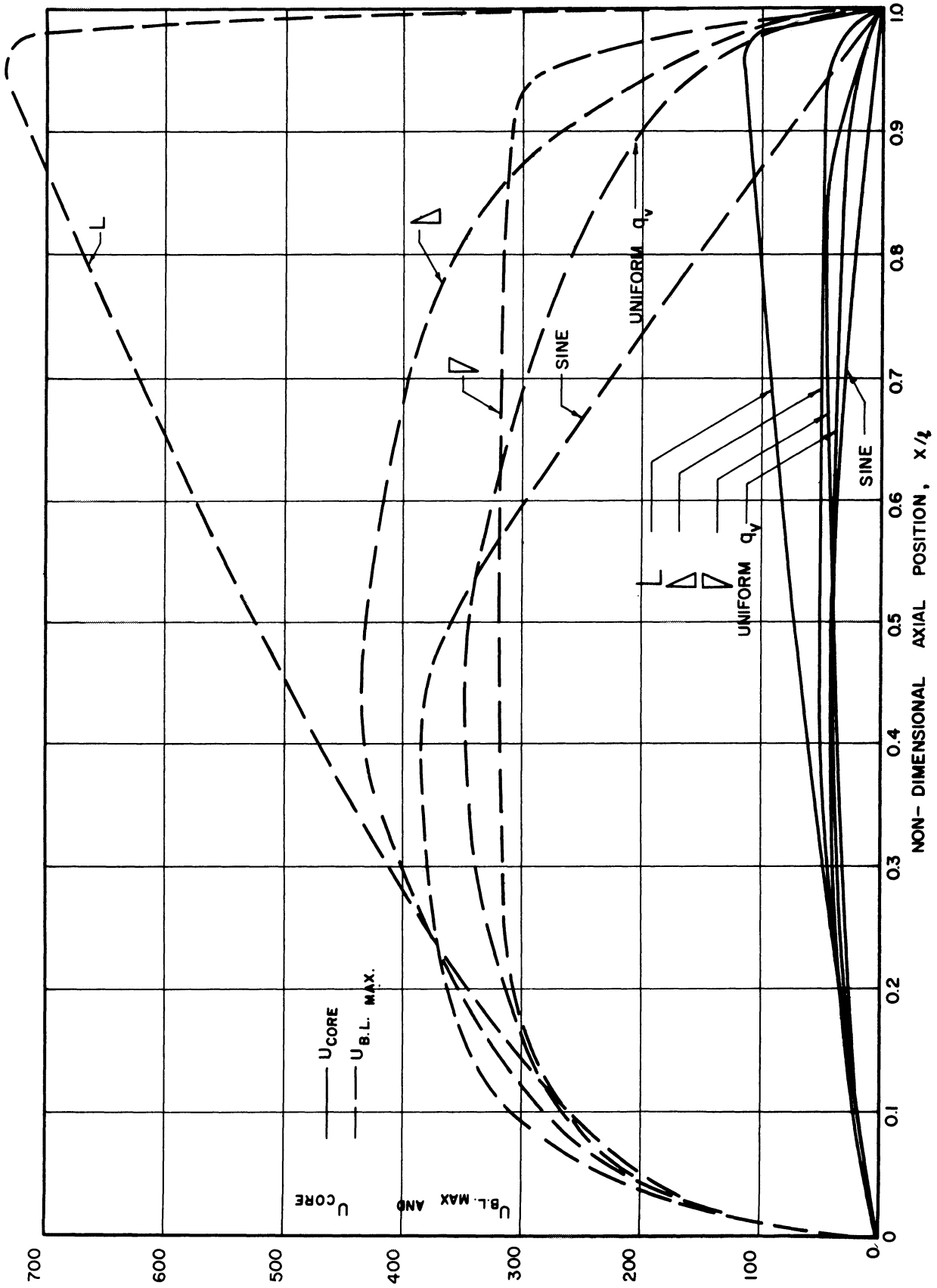


Figure 33-c. Non-Dimensional Core and Boundary Layer Velocity vs. Non-Dimensional Axial Position, Various Axial q_v Distributions ($\bar{q}_w = 4 \times 10^7$), Constant Wall Temperature, Calculated Data.

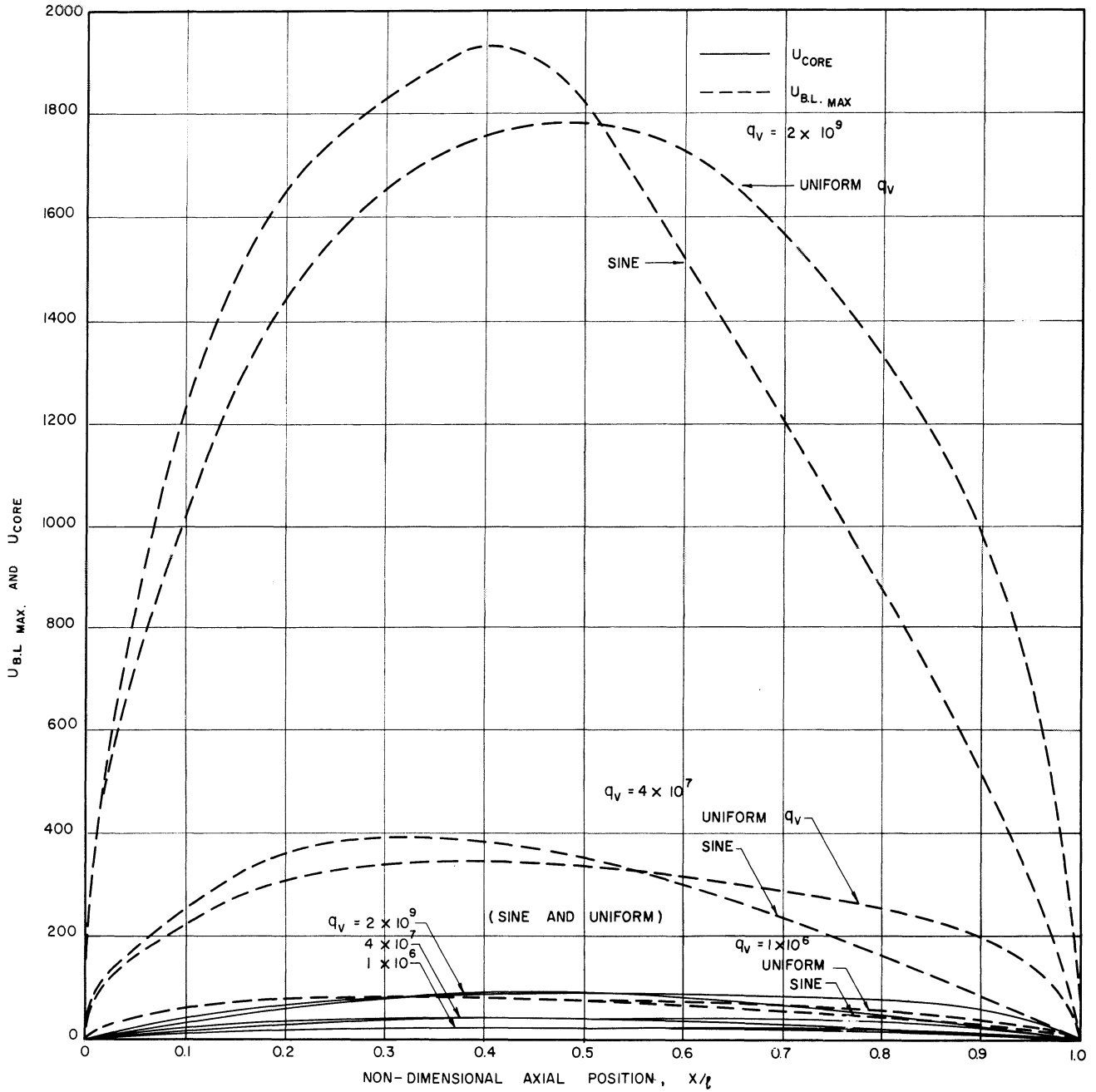


Figure 33-d. Non-Dimensional Core and Boundary Layer Velocity vs. Non-Dimensional Axial Position, Constant Wall Temperature, Comparison of Sine and Uniform q_v Distribution, Calculated Data.

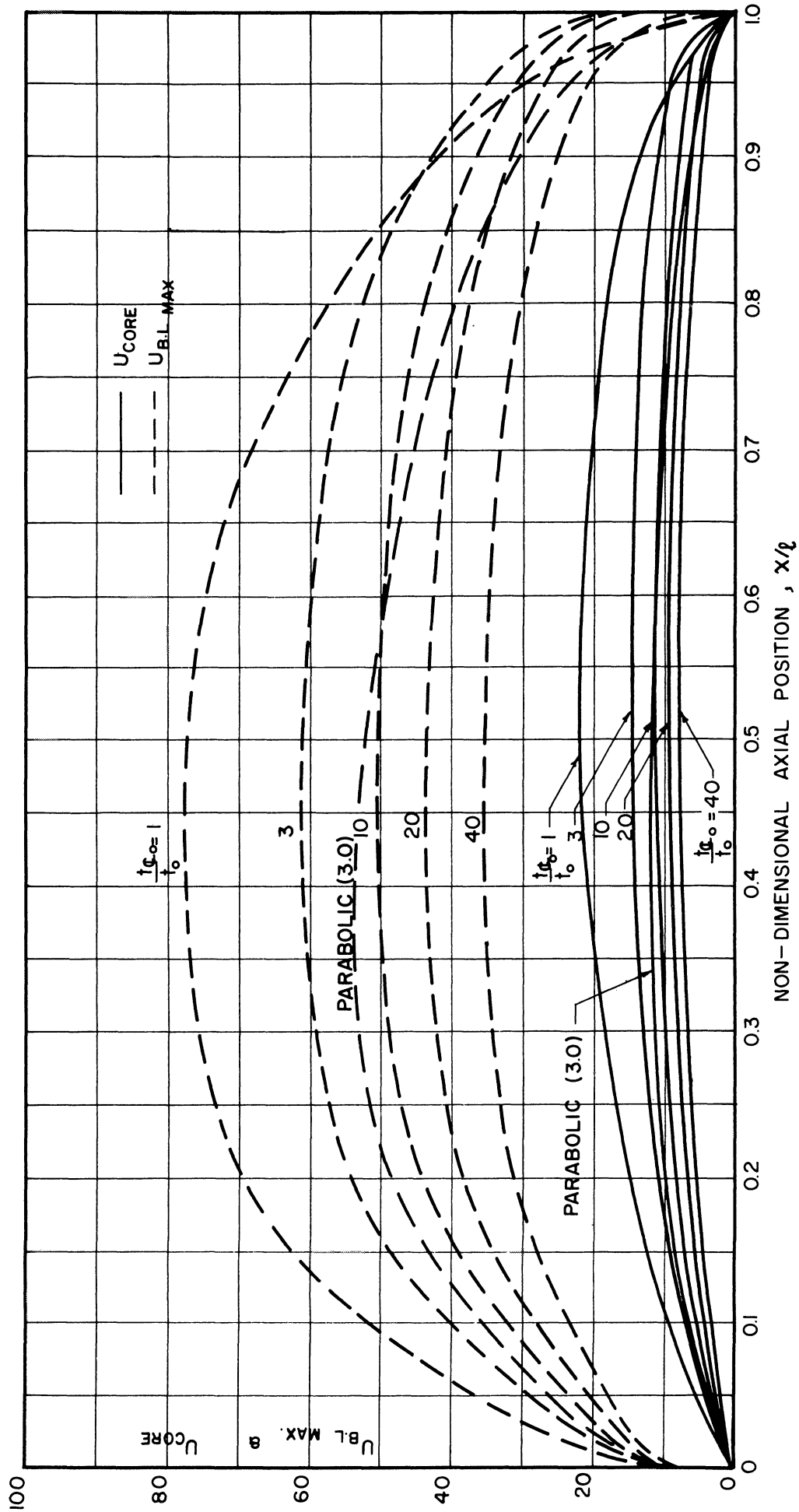


Figure 33-e. Non-Dimensional Core and Boundary Layer Velocity vs. Non-Dimensional Variable Linear Distribution of Overall/Radial Temperature Ratio, Uniform $q_v = 1 \times 10^6$, Calculated Data.

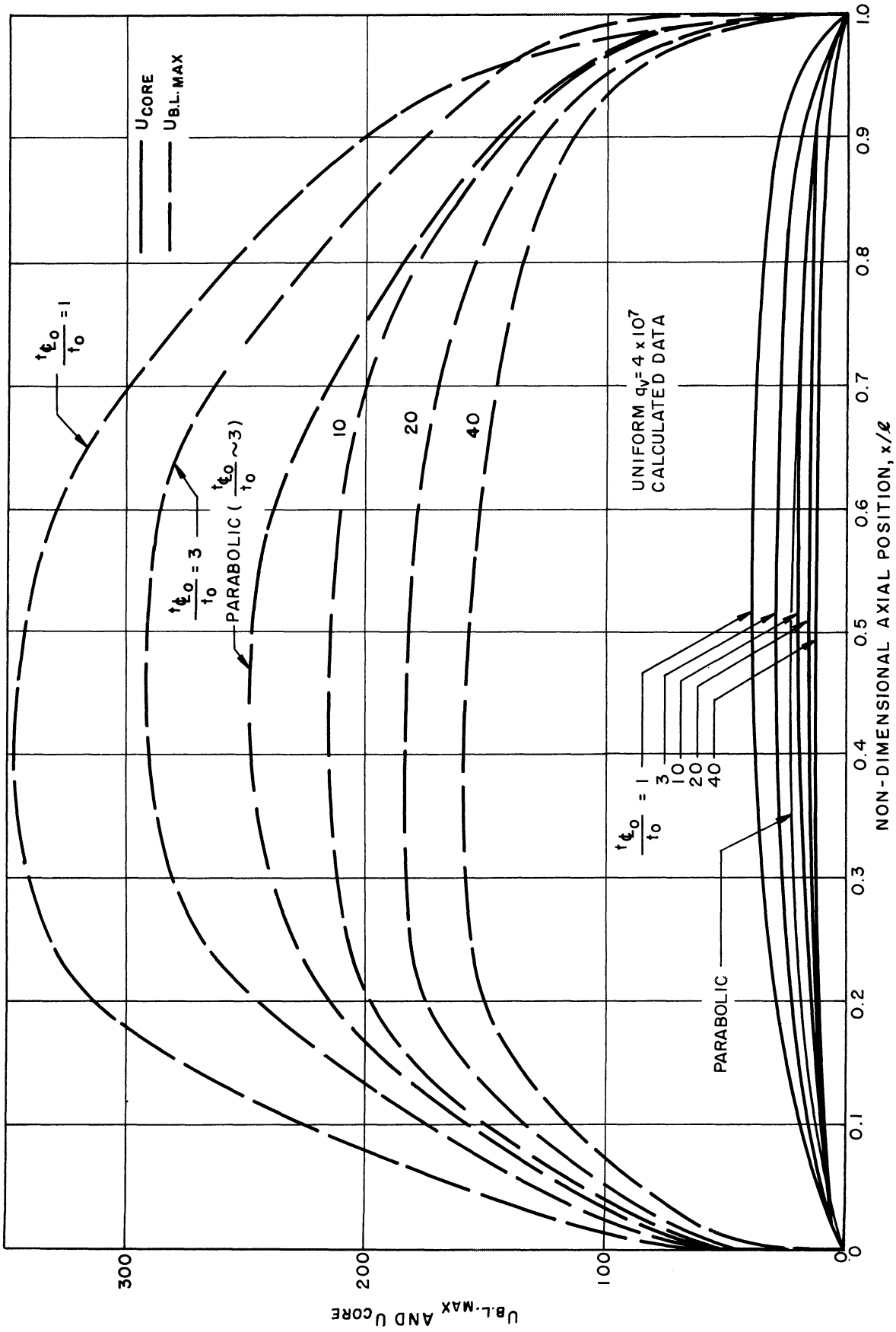


Figure 33-f. Non-Dimensional Core and Boundary Layer Velocity vs. Non-Dimensional Axial Position, Variable Linear Distribution of Overall/Radial Temperature Ratio, Uniform $q_w = 4 \times 10^7$, Calculated Data.

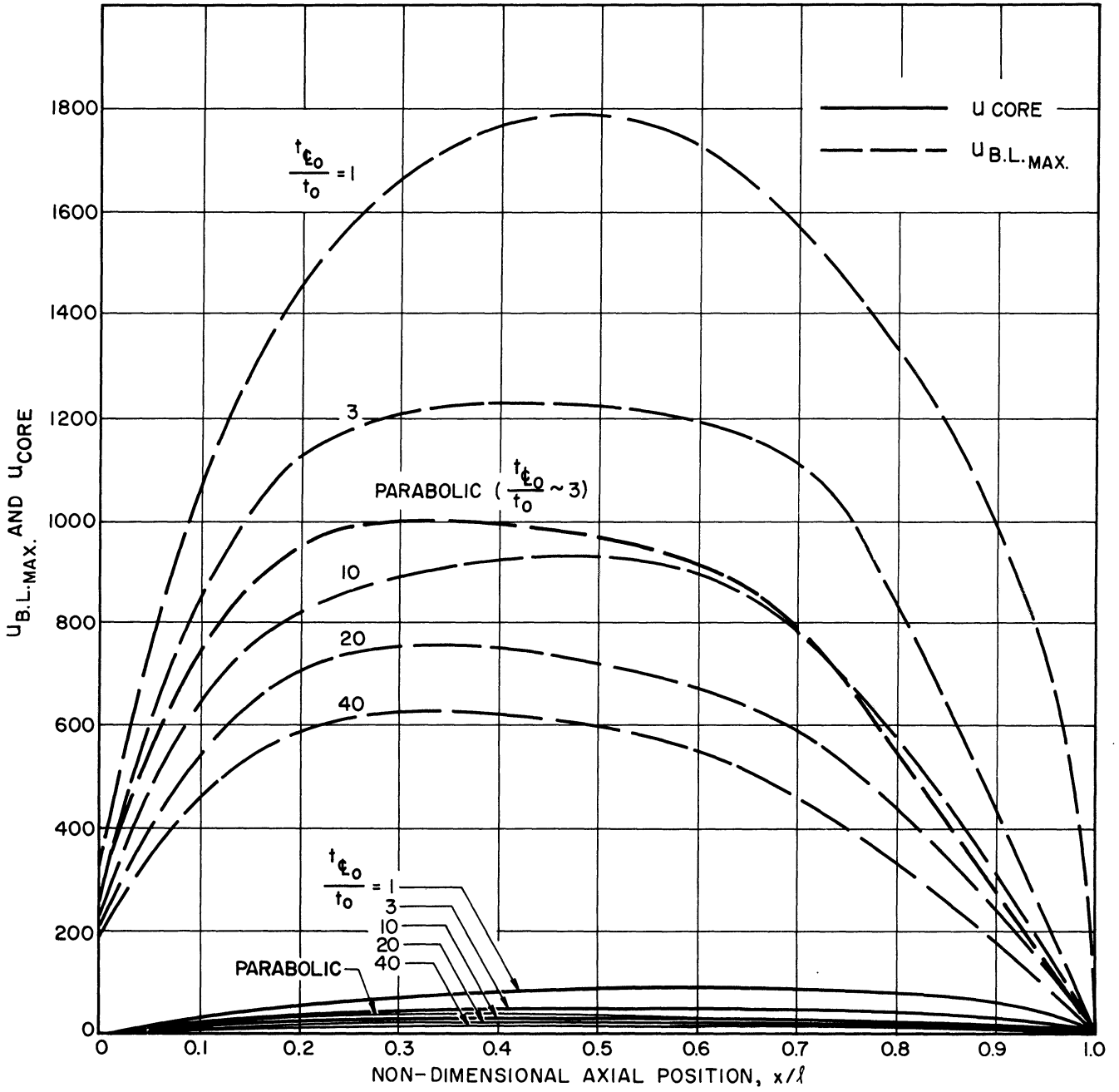


Figure 33-g. Non-Dimensional Core and Boundary Layer Velocity vs. Non-Dimensional Axial Position, Variable Linear Distribution of Overall/Radial Temperature Ratio, Uniform $q_v = 2 \times 10^9$, Calculated Data.

Constant Wall Temperature, Uniform Heat Source--The non-dimensional velocities, u , of both the boundary layer* and the core are shown in Figures 33-a and b as a function of x/l for the case of constant wall temperature and uniform heat source for the various values of q_v for which computations were made. In general both boundary layer and core velocities increase to a maximum near the midpoint of the test section and are zero at either end. They are approximately symmetrical about the tube midpoint as measured in the axial direction. The velocity magnitudes for both core and boundary layer increase for larger values of volumetric heat source. However, the proportionate discrepancy between boundary layer velocity (which is the greater by a fairly large factor in some cases) and core velocity decreases as the volumetric heat source strength is decreased. This is to be expected since the portion of the total tube cross-section occupied by the boundary layer is greater for the lower heat input rates (see previous discussions on boundary layer thickness). All the profiles, for q_v ranging from 10^5 up to 2×10^9 are shown in Figure 33-a. Figure 33-b is included to show an enlarged view of the lower q_v boundary layer velocity curves and all of the core velocity curves.

Constant Wall Temperature, Variable Heat Source Distribution--The non-dimensional boundary layer and core velocities for variable volumetric heat source distributions but constant wall temperature are shown in Figure 33-c. It is noted that the heat source distribution has a very significant effect upon the velocities. For clarity, only the curves

* Boundary layer velocity in this and succeeding sections refers to the maximum boundary layer velocity at a given axial position.

for $\bar{q}_v = 4 \times 10^7$ are shown. The uniform q_v distribution curve is shown for reference.

Preponderance of heat addition at the bottom of the tube results in a substantial increase in the peak core and boundary layer velocities as compared with the uniform distribution case. In the extreme case, the "Lighthill analogy", the peak velocities are approximately twice those of the uniform case and occur near the bottom of the tube (x/l of about 0.95) rather than near the midpoint as for the uniform distribution case. The linear distribution with maximum at the bottom has a similar although considerably less pronounced effect. The linear distribution with maximum at the top has the reverse effect in that the peak velocity is decreased by about 20% as compared with the uniform distribution case. In this particular case (linear), the velocity profile is nearly constant over the length of the tube with the exception of approximately 10% at either end wherein it decreases to zero. The sine distribution of heat source results in a velocity profile quite similar to the uniform distribution except that the peak velocity is slightly greater (about 10%) and its location is shifted toward the top of the tube to an x/l of about 0.35. Although the preceding discussion has been concerned mainly with the boundary layer velocity, similar trends are observed to apply to the core velocities.

Figure 33-d represents a comparison of the non-dimensional velocity magnitudes and distributions resulting from the uniform and sine distributions respectively of volumetric heat source. In this

case three q_v values were investigated: 10^6 , 4×10^7 , and 2×10^9 .

The comparison between the sine and uniform distributions was covered in the preceding paragraph for a single value of q_v . The trends are the same at the other q_v values investigated. As previously mentioned, the magnitude of both core and boundary layer velocity increases substantially with an increase of q_v .

Variable Wall Temperature, Uniform Heat Source--The effects upon non-dimensional boundary layer and core velocities due to both linear and parabolic wall temperature distributions with uniform heat source are shown in Figures 33-e, f, and g. Each curve sheet represents a separate value of q_v : 10^6 , 4×10^7 , and 2×10^9 . In general, the effect of an increase in the overall/radial temperature differential ratio at a given q_v is a reduction in both core and boundary layer velocity and a flattening of the profile (as plotted against axial position). The curve for unity value of this ratio is of course the constant wall temperature curve. The effect of the substitution of a parabolic wall temperature distribution for a linear distribution with the same value for the overall/radial temperature ratio is the same as an increase in the ratio. The parabolic curve for $t_{c0}/t_o = 3$ fairly closely approximates the linear curve for t_{c0}/t_o of 10. However, whereas the linear curves are quite symmetrical about the axial midpoint of the tube, the peak velocity with the parabolic curve is shifted toward the top of the tube. The preceding remarks apply equally to the three q_v values which were investigated. The difference between curves at different q_v but same overall/radial temperature ratio is mainly an increase of

velocity for larger q_v .

Overall Temperature Differential and Heat Source Relations

General Remarks--The relations between the overall temperature differential within the fluid and the heat source term are of the utmost practical importance in predicting the heat transfer characteristics to be expected from a given physical configuration with given internal heat generation and fluid physical property parameters. These overall characteristics result from the theoretical analysis along with the detailed aspects of the fluid behavior which have been reviewed in the foregoing sections.

Specific Results--The specific results of the theoretical calculations relating the overall maximum temperature differential required within the fluid to cause a removal of heat through the test section walls to the coolant equal to the volumetric heat source generation rate throughout the vessel are shown in Figures 35 and 36. Figure 35 is a plot on logarithmic coordinates of the overall non-dimensional heat source parameter, q_v , against the non-dimensional overall temperature differential $t_{G_{Lo}}$. As labeled, the various curves represent the different volumetric heat source distribution calculations which have been discussed in previous sections of this report with constant wall temperature and also the uniform heat source, variable wall temperature calculations. In addition, the comparable (as far as possible) experimental curves are shown.

On logarithmic coordinates, all the curves appear as virtually straight lines of the same slope over the range of non-dimensional heat source strength for which calculations were made, i.e: from 10^5 to 2×10^9 . This slope is approximately 1.25.

Effect of Variable Heat Source Distribution--The effect of a preponderance of heat source generation near the bottom of the vessel is a decrease in the overall temperature differential required to remove a given quantity of heat as compared with the case of uniform distribution. This is as expected on physical grounds since it means a greater temperature differential between centerline and wall throughout the length of the vessel, Figure 29-b. The extreme in this direction is of course the Lighthill analogy previously discussed which shows the minimum overall temperature differential required for a given heat source strength of all the cases which were investigated. The linear (zero at top) heat source distribution is next and is a compromise between the Lighthill case and the uniform heat source distribution. The linear distribution (zero at bottom and maximum at top) shows a larger required overall temperature differential than the uniform case. The sine distribution requires slightly less temperature differential (about 20% less) than the uniform distribution.

Effect of Variable Wall Temperature Distribution--The general effect of an increase in the ratio between overall and radial (at top) non-dimensional temperature differential i.e., proportionately greater wall drop from top to bottom, is an increase in the overall temperature

differential required to remove a given quantity of heat. In this respect the parabolic distribution and the linear wall temperature distribution, compared at the same value of overall/radial temperature ratio, are approximately equivalent as will be seen from an observation of the curves.

Figure 36 shows the relation between Nusselt's Number based on the test section radius to the non-dimensional heat source parameter, q_v . This is actually simply a replot of the non-dimensional temperature vs. heat source curves of Figure 35 since Nusselt's Number, q_v , and $t_{c_{Lo}}$ are related algebraically by the relation:

$$\text{Nusselt's Number} = q_v / t_{c_{Lo}}$$

The derivation is shown in the Appendix. It would of course be equally possible to construct curves relating non-dimensional temperature differential with Nusselt's Number. It is felt that these curves are not as instructive in presenting the basic relations as are the non-dimensional heat source vs. temperature differential curves.

Figure 34 is a cross-plot of the non-dimensional overall temperature differential against the overall/radial temperature differential ratio which was necessary in order to prepare the information shown in Figures 35 and 36. Such a preliminary cross-plot is necessitated by the fact that the overall/radial temperature ratio was a dependent variable in the machine calculations so that its values were not the predetermined round numbers convenient for comparative purposes. The calculated points for the parabolic wall temperature distribution

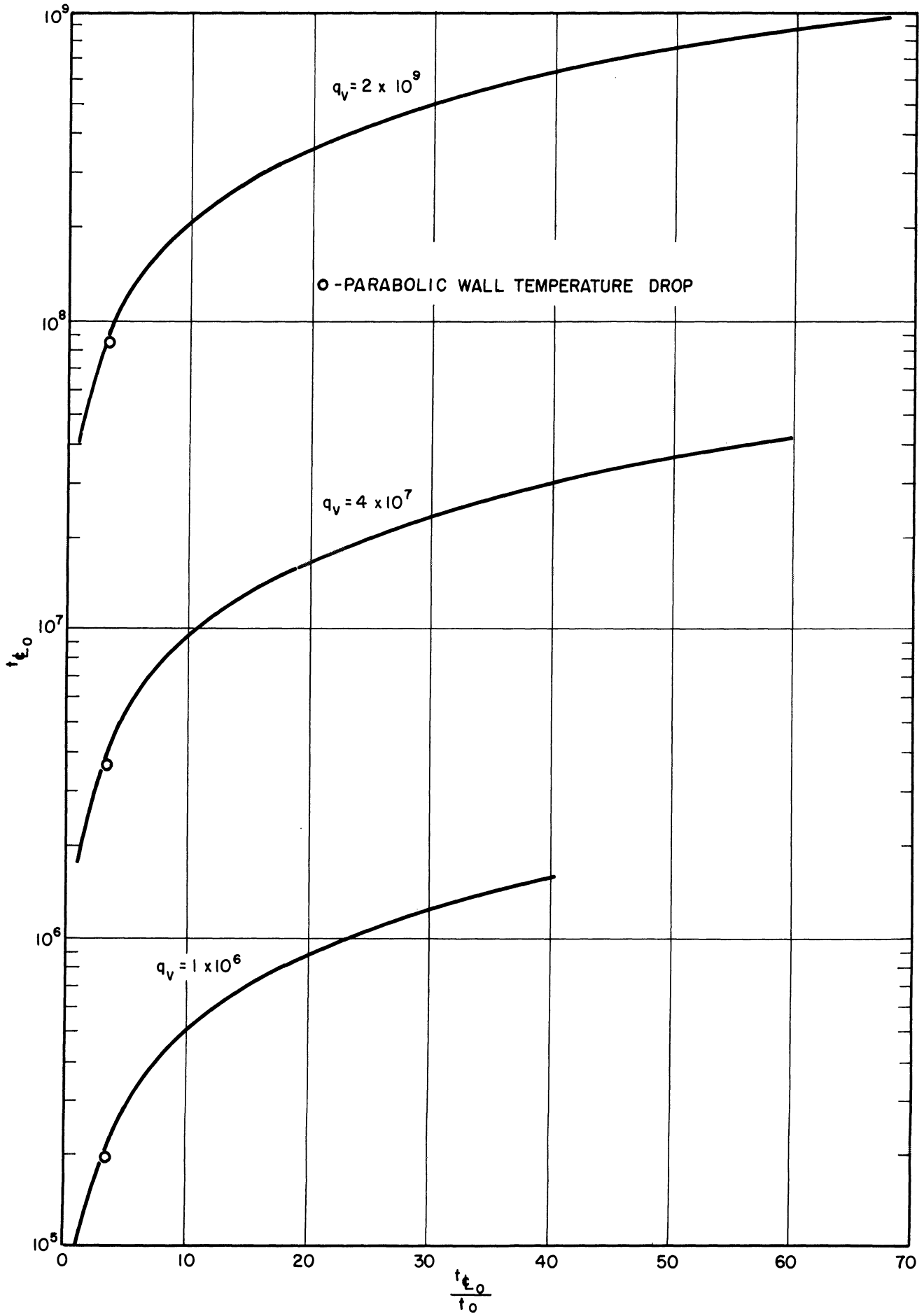


Figure 34. Non-Dimensional Temperature Difference vs. Overall/Radial Temperature Ratio, Linear Wall Temperature Distribution, Calculated Data.

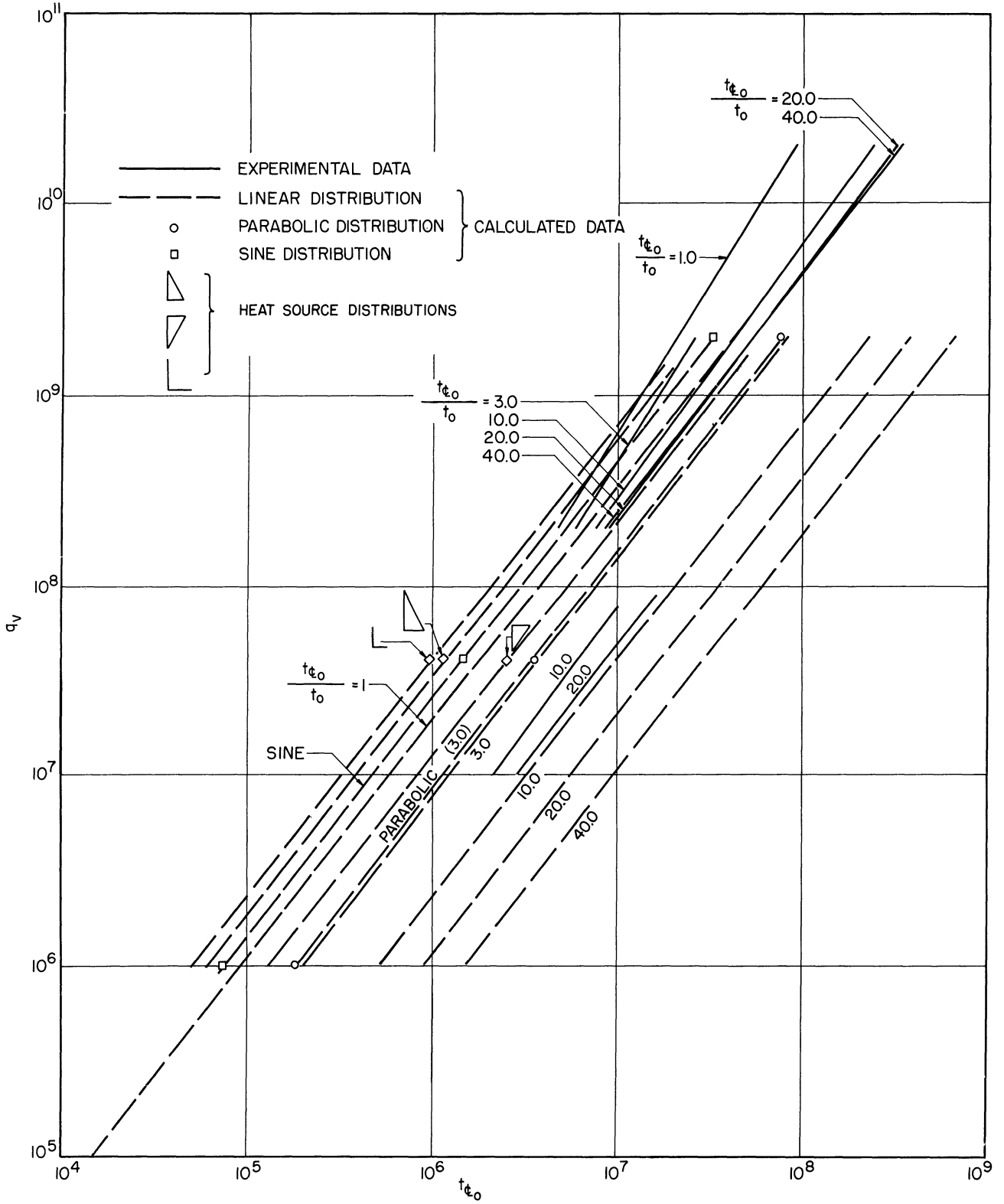


Figure 35. Non-Dimensional Heat Source vs. Non-Dimensional Overall Temperature Differential.

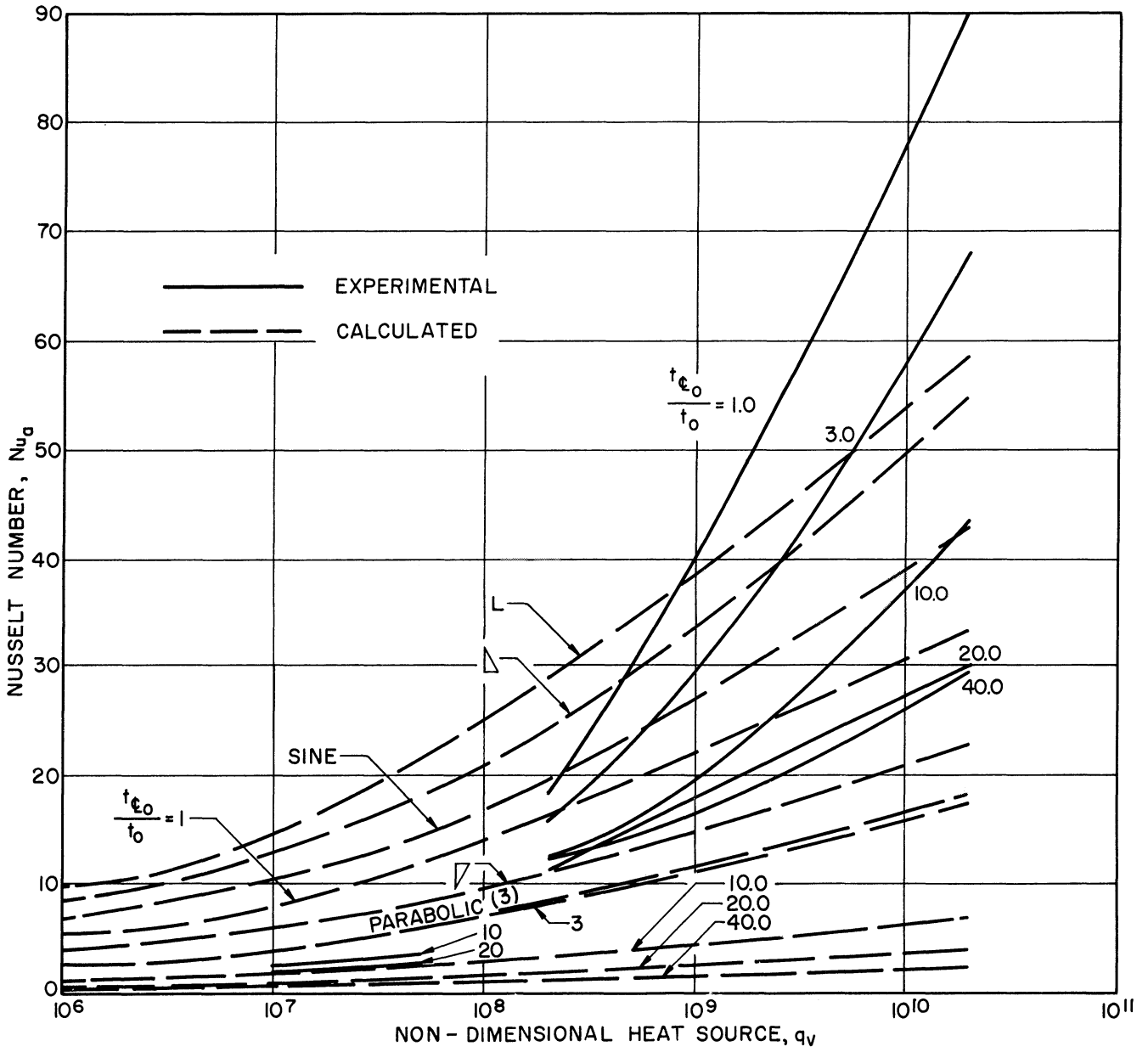


Figure 36. Nusselt's Number vs. Non-Dimensional Heat Source, Experimental and Calculated Data.

are included although the curves apply to the linear distribution. It is noted that the parabolic distribution calculation results in a slightly reduced overall temperature differential as compared with the linear distribution.

CHAPTER VII

COMPARISON BETWEEN THEORETICAL AND EXPERIMENTAL RESULTS

General Remarks

The results of an experimental research program on the phenomenon of natural convection heat and mass transfer in vertical closed tubes wherein the heat is generated internally and removed to a coolant through the walls of the test section vessel have been presented and explained in the preceding sections of this report. In addition, a theoretical analysis of the same system has been conducted. The details of this analysis have also been explained in detail in preceding sections. It is the purpose of the present section to examine the degree of correlation between the theoretical and experimental results and to discuss those features of the experimental and theoretical investigations which would be expected to produce discrepancies between theory and experiment.

Possible Causes for Discrepancies Between Theoretical and Experimental Results

There are various obvious factors both in the design of the experimental facilities and in the theoretical analysis, which would conceivably lead to discrepancies between the theoretical and experimental results. These various factors will be considered in some detail in the present section.

Effect of Turbulence

As previously mentioned, the analysis was based upon laminar flow, and considered shearing stress and thermal conductivity to be based upon the values of viscosity and conductivity obtaining under quiescant,

mean temperature conditions. When there is turbulent mixing, then the effective values of viscosity and conductivity are increased by the contributions of eddy viscosity and conductivity (referring to a commonly advanced concept of the turbulent mechanism). In some portions of the flow, the effective values may be increased manyfold over the static values. Since there was more or less turbulence in most of the experimental runs, it would be expected that there would be some discrepancy with laminar theoretical results on this account. Since the degree of turbulence appeared to increase with the strength of the non-dimensional heat source parameter, q_v , it would be expected that the discrepancy would increase as the non-dimensional heat source strength were increased. It would also be intuitively expected that the turbulent mixing would result in a reduced requirement for temperature differential to remove a given quantity of heat. Both of these expectations were observed.

Effect of Variable Temperature Upon Fluid Physical Properties

In a thoroughly exact analysis it would be necessary to consider all of the applicable fluid physical properties as functions of the fluid temperature. As previously pointed out, some of these properties, particularly viscosity, Prandtl's Number, and electrical conductivity, are quite sensitive to temperature. Since it would not be mathematically feasible to solve the governing fluid equations if they were written to include the temperature sensitivity of the fluid properties, it was necessary to define a mean temperature as applying to the entire vessel and to evaluate the properties in terms of this mean temperature. As was explained in an earlier section of the report, this

was the procedure was followed. However, it would be expected that there might be some discrepancy between theoretical and analytical results on this account.

Assumption of Axial Symmetry

The theoretical analysis is based upon the assumption of axial symmetry. The experimental method of measuring temperatures within the fluid involved the rotation of an eccentric thermocouple probe so that various wall distances were obtained for various angles of rotation. Consequently no real check on the authenticity of the axial symmetry assumption was obtained in this way. However, radial temperature profiles were obtained in this manner which indicated, without exception, a narrow boundary layer of severe radial temperature gradient adjacent to the wall and a fairly horizontal radial temperature distribution throughout the remainder of the cross-section. It does not seem likely that such profiles could have been obtained on all occasions for all the test sections which were used unless radial symmetry had substantially existed. From the physical viewpoint, there do not seem to be any important factors which would lead to the expectation of non-symmetrical conditions. As far as could be determined from visual observation of the velocity pattern, no non-symmetrical aspects of the flow pattern were apparent.

Effect of Center Probe

The existence of the eccentric center probe in the water-cooled facility could conceivably have an effect upon the experimental results in three ways. It could promote a non-symmetrical condition relative to the centerline due to its eccentric position, it could affect the

velocity profiles by the imposition of a zero velocity boundary condition on its own surface, and it could create an effect relative to the heat source distribution. As stated in the previous section, no evidence of non-symmetrical flow behavior was evident. The question of an effect upon the velocity regime due to an additional zero velocity boundary layer condition cannot be readily resolved. The additional shear area presented by the thermocouple probe is of the order of 15%. However, it is in the core region where the velocities are only of the order of, say 20% of the boundary layer velocity. Thus, considering a combination of these factors it is quite likely that no substantial effect would exist. Tests which were conducted in the air-cooled facility with no obstruction in the flow path did not show any observable difference in overall heat transfer characteristics from the tests with the various instrumentation fixtures (previously mentioned "Christmas Tree" for the air-cooled facility) in place.

The effect of the center probe upon the heat source distribution is believed to be negligibly small since the proportion of the total volume occupied by the probe (where no heat is generated) is only of the order of 5%.

In addition to the possible effects upon the rate of heat transfer mentioned in the foregoing there is also the possibility of an effect upon the initiation of turbulence, particularly in the case of the "Christmas Tree" arrangement used in the air-cooled facility, due to the vortices created by the obstructions posed to the flow. Since a detailed study of the initiation of turbulence was not included in the present investigation, no observations relative to the possible effect of these obstructions in this regard has been made.

Effect of End-Section Heat Losses

In the theoretical analyses it was assumed that there was zero heat loss from the test section ends. It is believed that this ideal was achieved to varying degree in the various tests. In the preliminary tests with the air-cooled facility, no attempt was made to seal the upper end from the atmosphere. As a result it was found in some cases that there was a substantial loss of fluid by evaporation. When this was reduced to a proportional heat loss, it was found that in the order of 20% of the heat input, in some cases, was escaping in this manner. Subsequently, the top was sealed with a thick rubber stopper so that evaporation was reduced to virtually zero. Due to the thermal resistance of the rubber, calculations showed that the proportionate conductive heat loss was negligible. Similar conditions existed at the bottom, since a heavy rubber stopper was used.

In the case of the water-cooled facility there was no question of evaporation loss of fluid since the end section is sealed. It was thermally insulated to prevent substantial heat loss. The temperature of the outside layer of insulation and of the surrounding air was measured so that an estimate could be made of the heat flow. It was found to be negligibly small compared to the total input. There is another possibility of end heat loss present in the water-cooled facility by conduction through the carbon steel electrodes to the water jacket. Order of magnitude calculations show that the proportionate heat loss in this manner is negligible. Since the table and other supporting apparatus at the bottom is substantially at cooling water temperature, no thermal insulation at the

bottom is required.

Although end heat losses appear to represent a negligible portion of the total heat input, they may have a significant effect upon the axial temperature gradient. This is not of great importance at the top since the velocities are large and the mixing thorough. At the bottom, however, the flow is quite stagnant and heat transfer is largely by conduction. Calculations show that if there is even a small heat leakage through the bottom end section, there may be a substantial effect upon the axial temperature gradient in this region. Measurements show a severe axial temperature gradient near the bottom. This is also predicted theoretically. However, it is likely that the severity of the gradient is materially increased by the end heat leakage, at least in the water-cooled facility. For this reason, little significance was attributed to temperature readings from thermocouples positioned within the vertical fluid passages in the bottom electrode.

Effects of Experimental and Theoretical Inaccuracies

The experimental accuracy relative to the temperature measurements and their location is believed to be quite good in the water-cooled facility so that the reported temperature differentials are probably accurate to about $\pm 5\%$. The lack of steady-state conditions over the length of a test is somewhat disturbing in this respect. It was found that a time period on the order of an hour would be required to make all required measurements in a given detailed test run. Often there would be some variation in cooling water temperature during this time or in electrical line voltage. Attempts to compensate for these effects were

made through a constant monitoring of the applicable instrumentation. Corrections were applied at the conclusion of a run if some variations in coolant temperature were noted. The order of magnitude of the variations, however, is not sufficient to cause an error in the overall temperature differentials greater than the limit above (i.e. $\pm 5\%$). Under these conditions it would seem desirable to proceed as rapidly as possible with a run. However, it was discovered that rapid movements of the thermocouple probe created fluid velocities and upset the temperature measurements (particularly in the stagnant region near the bottom) so that several minutes might be required for a return to equilibrium.

More serious than the inaccuracies in the temperature measurements were those in velocity measurement both with regard to location and magnitude. As previously mentioned it is believed that the velocity measurements cannot be regarded as more than semi-quantitative in nature, with a precision of the order of $\pm 30\%$.

In addition to the experimental inaccuracies discussed in the foregoing, there is also a degree of inaccuracy existent in the theoretical calculations. This is a result of the fact that the calculations were of the nature of trial and error so that the solutions are exact only to a predetermined degree of precision. To avoid excessive machine time, the specified precision was such that the overall temperature differentials were accurate to approximately $\pm 2\%$. As mentioned in a previous section, this rather minor lack of precision apparently has more substantial effects regarding some of the parameters. Velocity profiles and wall heat flux distributions seemed most severely

affected in this manner. The effect generally is concentrated near the bottom of the tube since the conditions fed into the calculation at the top are exact.

Theoretical Considerations

In order to allow a feasible mathematical approach to the problem it was necessary to postulate a simplified theoretical model for the fluid behavior and heat transfer. This model has been explained in detail in previous sections. It seems likely that some of the assumptions are responsible for discrepancies between the experimental and theoretical results. Among the most prominent in this regard are the following:

1. Laminar flow
2. Arbitrary assumption of velocity and temperature profiles
3. Neglect of inertia forces (Prandtl's Number very large)
4. Radial extent of velocity and temperature profiles equal (Prandtl's Number of unity)

The experimental evidence tends to support the validity of the second and last assumptions although it is not conclusive. It is not expected that the assumed velocity and temperature profiles should be duplicated in detail experimentally. It is important that they be approximated. This appears to have been the case as will be discussed further in a subsequent section. No statement regarding the importance of the second assumption can be made at this time. The question of the effect of turbulence has been previously discussed.

Detailed Comparisons Between Experimental and Theoretical Data

There are various areas of possible comparison between the experimental and theoretical data, and these will be examined in detail in the present section.

Overall Temperature Differential As Function of Volumetric Heat Source

The most direct comparison between the overall temperature differentials as a function of the volumetric heat source can be made between the experimental data for a value of the overall/radial temperature ratio of β and the computed results for the parabolic wall temperature distribution with uniform heat source distribution and overall/radial temperature distribution of β . Since the computed results for the parabolic and linear wall temperature distributions at the overall radial ratio of 3 are nearly identical with respect to overall temperature differential required for a given heat source, it is also possible to make a meaningful comparison between the experimental and calculated results at other overall/radial temperature differential ratios.

An examination of Figure 35 shows the comparison. In all cases the experimental non-dimensional temperature differential required for a given value of the non-dimensional heat source parameter is substantially less than the theoretical expectation. This difference becomes greater for the higher levels of q_v and there is some indication that the slope of the curves on a logarithmic plot, Figure 35, is also increasing for large q_v . These trends are similar to those reported by Martin⁽⁹⁾. Simplified relations based upon these slopes will be given in a later section both for the theoretical and experimental results. The discrepancy between theoretical and experimental t for given

q_v in this case is a factor of approximately 2.5 for the higher range of q_v investigated and about 1.5 for the lower.

Since the runs applying to the lower q_v range were made under far less turbulent conditions than the upper q_v range, it is felt that there is a basic discontinuity between these curves due to the initiation of substantial turbulence. For this reason they have not been connected in the curve-sheet and a transition region is assumed to exist in this region.

A similar comparison between experimental and theoretical results can be made from an observation of Figure 36 which shows the Nusselt's Number as a function of q_v for the same runs.

The correlation between experimental and theoretical results provided by this study is reasonable. The slopes of the experimental and theoretical curves in both low and high q_v ranges respectively are similar, the effect of increasing the overall/radial temperature differential ratio is the same, and the order of magnitude of the overall heat transfer characteristics over a range of approximately three decades of non-dimensional volumetric heat source for the experimental and theoretical data are the same. As mentioned above, there is a difference in Nusselt's Number, for instance, between experiment and theory over the range of q_v of between 1.5 and 2.5. However, this result is consistent with the observations of a previous investigator for a somewhat similar configuration⁽⁹⁾. The discrepancy is believed to be substantially the result of the turbulent mixing which occurs in the applicable range of non-dimensional heat source parameter; it will be noted that it is in the directions which would be intuitively expected - toward

a diminution of the required temperature differentials.)

Radial Temperature Profiles (Boundary Layer Behavior)

A comparison between the non-dimensional temperature differential between fluid along the centerline and the wall from the experimental and theoretical data is presented in Figure 20. A comparison is possible between the theoretical and experimental curves for an overall/radial temperature ratio of 1.0 (constant wall temperature case, extrapolated for experimental data) and for the overall/radial ratio of β where a calculation based upon a wall temperature distribution resembling that observed experimentally is available. It is noted in each case that the theoretical curve shows a greater initial decrease in the temperature differential with axial position than the experimental curve, which shows a more constant differential between the centerline and wall over a large portion of the vessel. This may be partially explained by the fact that the experimental temperature did not rise at the top as it theoretically should have because of heat loss through the top end section. However, the degree of agreement seems good and the trend observed with variation of overall/radial ratio is correct.

Figures 13-a and b and 14 show a comparison between the boundary layer thickness (based on temperature measurements since a location of the velocity boundary layer radial extent was not precise) observed experimentally and computed from the theory. There is some discrepancy between the theoretical and experimental boundary layer thicknesses. However, it does not appear excessive considering the degree of precision of the measurements and the trend toward reduced boundary layer thickness with higher q_v is observed experimentally.

Observation of Figures 12-a, b, and c show that the experimentally determined radial temperature profiles at various axial positions show a maximum near the inner extent of the boundary layer and decrease somewhat toward the centerline. The assumed profiles on the other hand showed constant temperature across the core (Figure 25). Theoretically, a reason for the location of this temperature maximum can be seen if it is considered that the fluid adjacent to the boundary layer is in retarded upward motion as compared with the fluid near the center. For this reason it is exposed to the internal heat source over a longer period than the fluid at the center before it reaches a cooling region, i.e. the descending boundary layer, and attains a higher temperature.

The above reasoning supposes an invalidation of the assumed velocity profile if it was assumed that velocity as well as temperature was constant across the core. Actually, the velocity maximum in the upward direction is probably achieved nearer the central portion (radially) and the flow adjacent to the boundary layer is retarded in its upward motion.

Axial Temperature Profiles

A comparison of the axial centerline temperature profile (normalized) is afforded by Figures 19-a and b. It is possible to compare the parabolic computed curve for overall/radial ratio of 3 with the experimental curve for the same ratio; and also to compare the curves for constant wall temperature, i.e.: overall/radial ratio of unity. It is noted in both cases that the experimental centerline

temperature profiles are above the computed curves over the entire vessel length. In other words, for a given overall/radial ratio and a given overall non-dimensional temperature differential, there is a greater differential between centerline and wall at any selected axial position from the experimental data than from the theoretical expectations. It is noted that the theoretical curves from the parabolic wall temperature distribution more closely approach the experimental profile than the linear distribution curves. This is as expected.

Figure 18 shows the experimental wall temperature axial distributions. The variation from the linear distribution which was assumed for many of the calculations is shown. The parabolic distribution upon which some of the calculations was based is taken from an average of these experimental distributions. It is noted that the effect of different overall/radial ratios is not large.

Normalized Wall Conduction Heat Flux

A comparison between the experimental and theoretical values of normalized wall heat flux is shown in Figures 32-d. Both theoretical computations and experimental measurements indicate a preponderance of the wall heat flux at the upper end of the vessel and a corresponding diminution at the lower end even though the internal heat source distribution is uniform as for the experimental measurements. Also, both experimental and theoretical results agree in the predictions of a decrease in the degree of non-uniformity as the overall/radial temperature differential ratio is increased. The calculations show a large increase and decrease of normalized heat flux adjacent to the top and

bottom of the test section respectively. The experimental measurements, based on the measured temperature differential across the test section wall, would not be adequate to show such an effect because of the possibility of substantial heat flow in the glass in the axial direction. This axial heat flow would smooth out large radial gradients imposed across the glass if they were of only small axial extent. Consequently, the experimental data has been assumed to apply only in the central 70% of the length and the curves have been so presented. It is noted that the agreement between the experimental and calculated data within these limits is quite good. The experimental curve for an overall/radial temperature differential ratio of 3 lies between the calculated curves for the same ratio for linear and parabolic wall temperature distributions respectively. The experimental curve was taken with an approximately parabolic temperature distribution.

Velocity Magnitudes

As previously explained, very approximate velocity measurements were made. It did not prove feasible to locate these measured points with sufficient precision so that reliable information regarding the velocity profiles could be obtained. The supposed location of the velocity reversal point for several of the experimental runs at different axial positions is listed in the experimental summary sheets, Tables A-IV through VII in the Appendix. However, it is felt that the uncertainty of these data is too great to merit further consideration.

The comparison between the experimental and computed non-dimensional boundary layer and core velocities is shown in Figure 23. The curves

agree in showing an increase of velocity in both core and boundary layer for increased non-dimensional heat source parameter q_v . However, the experimental results show considerably less differentiation between core and boundary layer than do the theoretical results, i.e: boundary layer velocity is smaller and core velocity greater in the experimental measurements, than the calculated values. This is partly a result of the fact that the theoretical boundary layer velocity is the maximum velocity of a parabolic profile while the observations would tend to reflect the mean. On the other hand, the theoretical core velocity profile is flat, whereas presumably the actual profile would show a maximum near the tube centerline. This is further evidenced, as mentioned in an earlier section, by the maximum temperature location near the inner extent of the boundary layer instead of the tube centerline. For these reasons, the measured core velocities would tend to be greater than those of the assumed flat profile.

In addition to the factors mentioned in the foregoing paragraph, the diminution of the experimental boundary layer velocity with respect to the theoretical value may be substantially a result of the greater (than laminar flow prediction) drag opposed to its motion by the turbulent mixing with the ascending core.

Summarization of Comparisons Between Experiment and Theory

The general velocity and temperature regimes and the general behavior of the flow and of the heat transfer phenomenon as derived from the theoretical model are quite well checked at numerous points by the experimental data. The agreements are not quantitatively precise in many

cases, but the trends and order of magnitudes of results over a very wide range of non-dimensional power inputs (3-4 decades) are in satisfactory agreement.

The overall heat transfer results are well correlated by the non-dimensional parameters which emerge from the theoretical analysis. The direction and magnitude of variations theoretically anticipated are indeed encountered experimentally. There is some difference in the absolute magnitude of the overall heat transfer parameters between theory and experiment. However, it is believed that this discrepancy is largely a result of turbulence which could not be properly considered in the analysis. This conclusion is strengthened by the fact that the experimental results vary from the analysis in the direction normally associated with turbulent conditions; i.e., toward increased heat transfer coefficients.

CHAPTER VIII

METHODS OF SOLUTION FOR OVERALL PROBLEM

Statement of Overall Problem

The discussions up to the present point in this dissertation have been concerned with the internal heat and mass transfer phenomena within the vessel when the boundary temperature conditions are specified. Under these conditions, within the simplifying assumptions of the theoretical analysis, the solution is uniquely specified if the boundary temperatures and also the strength and distribution of the heat source are specified. It is also true from the experimental viewpoint, if the wall temperature conditions are specified, then the velocity and temperature regimes (as averaged over the turbulent fluctuations) are uniquely fixed by the strength and distribution of the heat source. It is noted that the situation is somewhat different from that encountered with an ordinary heat exchanger in that the internal flow is in effect a closed loop so that the system's degrees of freedom are reduced. For example, if an ordinary heat exchanger is considered, it is possible to specify the boundary temperature conditions, the rate of heat transfer, and the mass flow rate (leaving inlet and outlet temperature as dependent variables). In the present instance, once the boundary temperatures are set, it is only possible to set one additional parameter, such as the rate of heat transfer, i.e.; overall heat source strength.

If the application to a homogeneous reactor is considered, then the overall problem facing the designer would be the provision of a suitable quantity of heat transfer area between the fissioning fluid and the

coolant to remove heat at a specified rate without exceeding limiting fluid temperatures for both coolant and internal fluid. In addition the maximum coolant flow rate would probably be specified as a function of erosion, velocity limitations, and/or pump work.

In other words, a coolant flow rate, inlet or outlet temperature, and heat transfer rate would be known. It would be required to design suitable heat transfer surface between fissioning fluid and coolant so that the maximum temperature of the heat transfer surface and/or of the fissioning fluid would not exceed a specified maximum. Additional requirements could involve a specified minimum temperature for the fissioning fluid in cases where molten metals are involved in order to prevent freezing. Also there might be questions of mass transport of the container material within the fissioning fluid and possible erosive effects. For these reasons it is important to know the velocity and temperature regimes of the internal system.

General Method of Solution

As is evident from an examination of the preceding discussion, it probably would not be possible in a practical case to specify the wall temperature distribution for the fissioning fluid container. It would be necessary to utilize this wall temperature distribution as a connecting link between the internal heat and mass flow parameters and the parameters of the cooling system, including the heat transfer characteristics of the vessel wall. It would be necessary that the wall heat flux into the wall from the internal system at a point be matched by the heat flux at the same point into the coolant system.

It would also be necessary that the temperature differential across the wall as specified by the internal flow and the coolant, be consistent with the wall thickness and material. In addition, the coolant temperature at any point must be consistent with the heat flow into the coolant before that point and the inlet temperature of the coolant.

In general, it is seen that a trial and error solution is required, using the inner wall temperature distribution as the connecting link between the requirements of the coolant system and of the internal natural convection system. For example, it would be necessary to make a preliminary estimate of the wall temperature distribution, estimate the wall heat flux distribution which results from either the experimental or theoretical curves presented in this report for the particular wall temperature distribution which had been assumed, and the applicable non-dimensional heat source parameter, q_v . With the resultant wall heat flux distribution, the coolant temperature distribution could be computed and it would be ascertained whether the assumed wall temperature distribution was correct. If it were not, then a revised assumption of wall temperature distribution would be necessitated and the process would be repeated. It may be instructive to examine several simplified examples in this regard to clarify the procedure.

Specific Examples

Infinite Coolant Flow Rate

For infinite coolant flow rate, the film coefficient for heat transfer of the coolant side would also be infinite (infinite Reynolds Number) and the temperature rise of the coolant as it passed through the

reactor would be zero. In this case, the temperature of the coolant side of the tube walls would be constant. If the wall heat flux were constant, then the inner wall temperature would also be constant. However, reference to Figure 32 showing the nomalized wall conduction distribution to be expected with various wall temperature distributions shows that for constant wall temperature there is a large preponderance of wall heat flux near the top of the vessel and a corresponding diminution at the bottom, leading to varying drop across the tube wall and hence a variable inner wall temperature. Therefore, the assumption of constant wall temperature of the tube inner surface is not compatible with the facts.

Since the wall heat flux is always greater near the top of the vessel, it is necessary that the inner tube temperature also be greater at the top to provide the increased differential between inner and outer tube wall necessitated by the heat flux distribution. It is thus necessary to assume wall temperature distributions of this sort, estimate the heat flux distribution from the curves of Figure 32-c, and check for compatibility. In a given case, it may be that the consistent wall temperature distribution cannot be approximated either by the linear or parabolic distributions which were calculated. In this case, further basic theoretical calculations would be required to provide an adequate network of curves.

Non-Infinite Coolant Flow Rates; Co-Flow and Counter-Flow

If the coolant flow rate is not infinite, it is apparent that there will be some rise in temperature in the coolant in the direction

of flow. Considering a configuration similar to the previously described water-cooled facility, it is evident that if the coolant flow is upward, the overall system has some of the elements of a counterflow heat exchanger. Heat is exchanged across the tube wall between the descending boundary layer within the test section and the ascending coolant stream. On the other hand, if the coolant is passing through the annular channel in a downward direction, then the system is in effect a co-flow heat exchanger. (The listing of the experimental runs in Tables A-IV through VII in the Appendix use this terminology).

With finite coolant flow rates, the direction of coolant flow has an effect upon the wall temperature distribution as does the flow rate. The co-flow (or downward coolant flow direction) arrangement tends to provide a reduced axial temperature gradient for the inner wall as compared with counter-flow. This is a result of the proportionately larger wall temperature differential which exists at the top by virtue of the rise in coolant temperature as it moves toward the bottom. This automatically allows a larger preponderance of heat flux at the top without large wall axial gradient than for the opposite case. An examination of Figure 32 shows that a larger unbalance of heat flux corresponds to a smaller axial temperature gradient. It will be noted from an examination of the summary tables for the experimental runs (Tables A-IV - VII) that co-flow did indeed produce a smaller axial wall temperature gradient than counter-flow ($t_{c_{L0}}/t_o$ of the order of 2 for co-flow; order of 5 for counter-flow in the water-cooled facility).

The rate of coolant flow also has an effect upon the overall/ radial temperature differential which will obtain within the test section. This is apparent from the fact that the coolant temperature rise for a given heat source strength is inversely proportional to the flow rate. For this reason, a small flow rate with co-flow will be more effective than a larger rate in producing a minimum axial temperature gradient within the test section. On the other hand, a low coolant flow rate with counter-flow will tend to increase the axial temperature gradient along the inner surface of the wall. This latter trend also is illustrated by the experimental data. However, the effect of coolant flow rate upon the axial temperature gradient within the test section is not apparent for co-flow from the more limited experimental results taken with this configuration.

To solve the overall problem for the various cases of finite coolant flow rate, it is again necessary to satisfy by trial and error the conditions of local wall heat flux values consistent with the requirements of both internal and coolant systems. The bridging parameter most convenient in this case is again the wall temperature distribution. As previously mentioned, an investigation of additional types of wall temperature distributions would probably be necessary to solve accurately problems of this type. Once the suitable distribution has been determined, of course, the solution is unique and all the flow parameters of interest become known (via the plots of this report).

The case of a very small coolant flow rate in the counter-flow direction would presumably provoke a very large internal axial wall temperature gradient, so the internal wall temperature would remain in excess

of the coolant temperature at all points and heat flow out of the facility would occur at all points. The case of a very small flow rate in the co-flow direction is more interesting. It would appear that if the internal heat source were sufficiently large, the discrepancy between temperature differentials across the tube wall at top and bottom would be too great for a consistent solution even with constant inner wall temperature. It would then apparently be required that the temperature should rise in the descending boundary layer, creating an inverse buoyancy gradient i.e; lighter fluid at a lower level in the boundary layer. Such a condition could lead to separation of the boundary layer from the wall, and perhaps the division of the tube into several axial lengths with more or less distinct circulation in each. Within the measureable coolant flow rates and feasible power inputs no such condition occurred within the test facilities.

Constant Wall Heat Flux

Constant wall heat flux is more closely approached as the overall/radial temperature differential ratio is increased. A similar trend is observed if a parabolic wall temperature distribution is substituted for a linear distribution. These effects are obvious from an examination of Figure 32-c. It is shown that a parabolic wall temperature distribution with an overall/radial temperature ratio of 3 produces a wall heat flux distribution similar to a linear distribution of between 10 and 40.

It can be shown that the method of solution for the flow regime with the theoretical model which was assumed cannot be applied

if constant wall heat flux is assumed. However, this case can be approached if very large overall/radial temperature ratios are assumed.

Approximate, Simplified Relations

The methods for solution of the overall problem of a natural convection cell and a forced convection coolant wherein it is required that continuity of heat flux between internal fluid and coolant be observed at the wall must rely upon complete information regarding temperatures, temperature distributions, and heat flux distribution. It is, however, possible to reduce the relationships between overall temperature differential and volumetric heat source for the internal fluid for various configurations of wall temperature and heat source distribution to approximate relationships - both for the experimental and theoretical results. This is easily accomplished because of the straight line relationship between non-dimensional heat source, q_v , and overall non-dimensional temperature differential, t_{E_0} . The applicable values for k and n for the relation




$$q_v = k t_{E_0}^n$$

are listed in Table II for various ranges of heat source and wall temperature distributions for the experimental data and for various wall temperature and heat source distributions for the computed data.

TABLE II

APPROXIMATE RELATIONSHIPS FOR NATURAL CONVECTION FLOW IN CLOSED VERTICAL CYLINDER WITH INTERNAL HEAT GENERATION - AQUEOUS FLUIDS

$$q_v = k t_{\phi}^n$$

<u>Experimental Data</u>		<u>k</u>	<u>n</u>
I <u>$q_v > 10^8$</u>			
$t_{\phi_{Lo}}/t_o = 1.0$	(Constant Wall Temp.)	0.00834	1.55
= 3.0		0.00834	1.53
= 10.0		0.146	1.33
= 20.0		0.298	1.27
= 40.0		0.484	1.24
II <u>$q_v < 10^8$</u>			
$t_{\phi_{Lo}}/t_o = 10.0$		0.0372	1.33
= 20.0		0.0647	1.27
<u>Theoretical Data</u>			
I <u>Uniform q_v, Linear Temp. Dist.</u>			
$t_{\phi_b}/t_o = 1.0$	(Constant Wall Temp.)	0.673	1.24
= 3.0	(Linear or Parabolic)	0.182	1.27
= 10.0		0.0757	1.25
= 20.0		0.0326	1.26
= 40.0		0.0209	1.24
II <u>Non-Uniform q_v, Uniform Wall Temperature</u>			
Uniform q_v		0.673	1.24
Lighthill Analogy, 		1.433	1.24
		1.143	1.24
		0.455	1.24
Sine Distribution		0.726	1.26

CHAPTER IX

RECOMMENDED SUBSEQUENT INVESTIGATIONS

There are numerous desirable extensions to the present study from the viewpoint of nuclear applications alone which are suggested. Among these in approximate order of priority might be listed the following. The order of priority to be assigned to the further investigations would depend largely upon the detailed practical application under consideration.

1. Extension to fluids with very low Prandtl Number such as liquid metals.
2. Extension to lower values of the heat source parameter for both aqueous-type fluids and liquid metals.
3. Extension to internal cells of differing geometries. Included might be non-circular vessels as well as circular vessels with a plurality of heat-transfer tubes inserted in the manner of a shell-and-tube heat exchanger. Additional degrees of freedom in the specification of heat source and temperature distribution; i.e., non-axisymmetry and/or radial qv variation.
4. Detailed investigation of laminar-turbulent transition applying to present case as well as all others mentioned above.
5. Investigation of effects upon heat and mass transfer of fission gas generation within the fluid.
6. Investigation of effects upon disposition and formation of fission gas bubbles of nuclear radiation as would be encountered within a nuclear reactor.
7. Investigation of feed-back parameters due to the heat and mass transport phenomena upon the nuclear parameters, affecting reactivity, stability, flux distribution, and burn-up ratios.

8. More detailed examination of velocity and temperature profiles to discover whether extent of velocity boundary layer is identical to that of temperature boundary layer, and to increase the precision of the experimental data in general.
9. Investigation of effects of fluid motion on the stability of the structural materials.

There are various additional investigations which would also be of interest for applications other than nuclear. Of this type are the following:

1. Extension of the Lighthill analysis using the digital computer program here originated to arbitrary wall temperature distribution. Application is to turbine-blade cooling, and other cases where there is no internal heat source.
2. Extension of the Lighthill analysis to non-steady state cases with arbitrary wall temperature distribution using the digital computer program modified to consider finite time steps. An application would be the external heating or cooling of closed vessels.
3. Experimental check of laminar theory under flow conditions guaranteeing laminar flow.
4. Modification of laminar theory here derived to turbulent flow conditions.

CHAPTER IX

CONCLUSIONS

A method has been developed for the theoretical analysis of the flow and temperature regimes existing under conditions of laminar flow within a closed vertical, cylindrical vessel filled with a fluid having a Prandtl's Number of the order of unity within which heat is generated with arbitrary axial distribution (uniform radial distribution). Heat is removed to a surrounding coolant so that steady-state exists. Such a physical configuration has application to homogeneous, aqueous, nuclear reactors. This method of solution has been programmed for an IBM-650 digital computer and results have been obtained for a variety of conditions of heat source and wall temperature distribution over a wide range of non-dimensional heat source values.

Under flow conditions ranging from near-laminar to highly turbulent, experimental data has been obtained for several of the temperature and heat source distributions theoretically investigated. The correlation between the theoretical and experimental results has been good in that the overall nature of the flow pattern has been verified; the detailed temperature, velocity, and wall heat flux distributions approximately verified; and the direction and degree of variation of the independent variables verified. The magnitude of overall temperature differential to remove a given quantity of heat was less than the theoretical anticipation by a factor of approximately 2.5 for the experimental results in the higher heat source ranges which were investigated. The factor was approximately 1.5 for the lower

heat source ranges. It is concluded that the varying discrepancy is a result of the highly turbulent conditions existing in the higher internal heat source experiments and the considerably less turbulent (nearly laminar) conditions existing in the lower.

Approximate simplified relations between the non-dimensional heat source parameter, q_v (which has been originated in the present study) and the overall non-dimensional temperature differential existing within the test section, primarily axial rather than radial, are presented in tabular form for both experimental and theoretical data for various boundary condition configurations. Such a simplified presentation is possible because of the straight-line relation existing between q_v and t_{G_0} in a logarithmic plot.

Finally it is concluded that the results of the present study regarding anticipated wall heat flux distributions, temperature distributions, temperature profiles, and temperature differentials are sufficient to allow at least the approximate analysis of the significant parameters for an overall system consisting of closed, natural-convection, heat-generating cell, and forced convection coolant system. Approximate methods for solving such cases are developed. Such methods are required for the realistic specification of a system of this type of which a homogeneous, aqueous nuclear reactor system is a possible example. No suitable data or information prior to the present investigation is available.

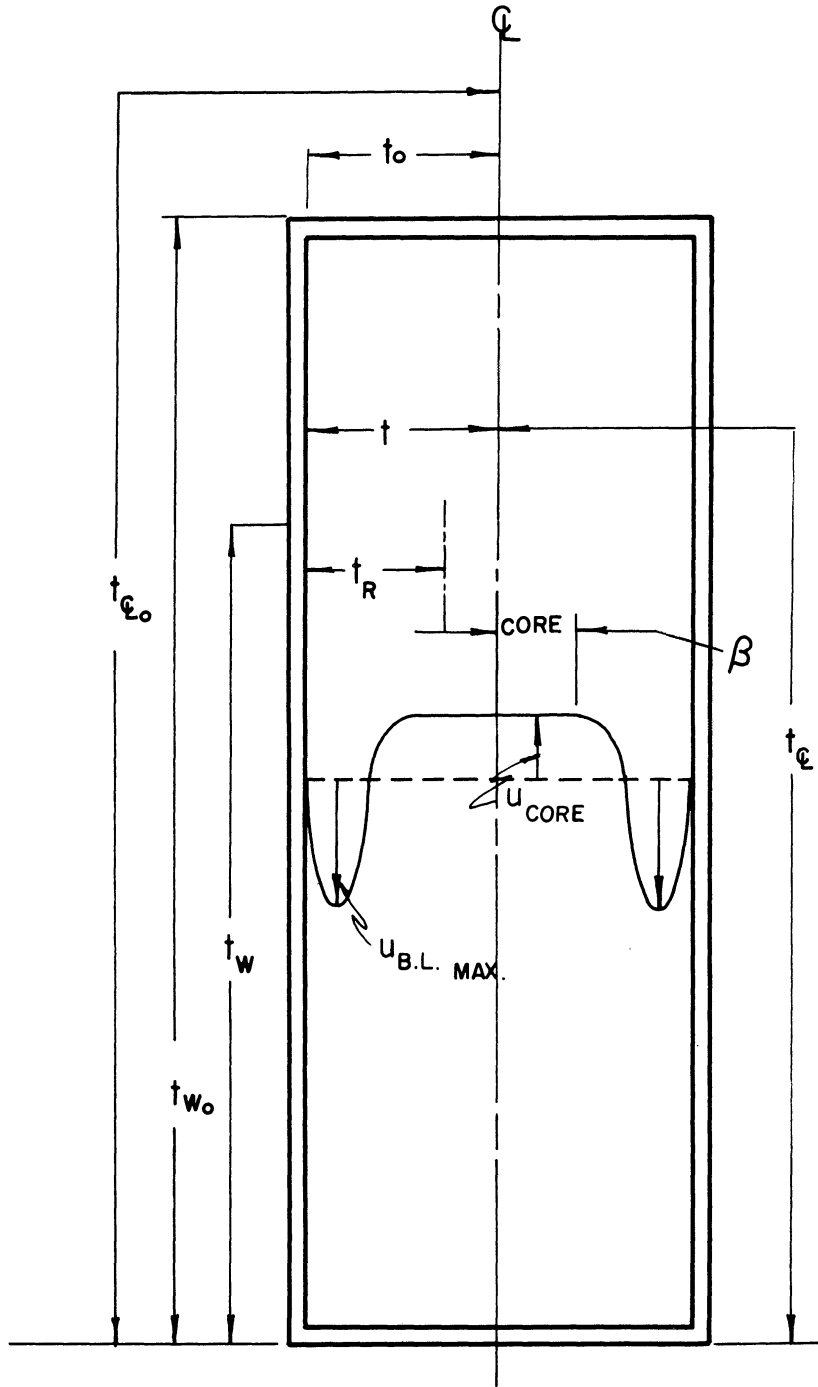


Figure 37. Test Section Nomenclature Schematic Diagram

APPENDIX

1-A Derivation of Energy Equation (see Chapter V)

Consider a disc as shown in Figure 26 and write an energy balance:

$$\rho c_v \left[\frac{\partial}{\partial x} \int_0^a UT2\pi R dR \right] \Delta x = k \left(\frac{\partial T}{\partial R} \right)_{R=a} \Delta x 2\pi a + Q_v \pi a^2 \Delta x \quad (1-a)$$

or

$$\frac{\partial}{\partial x} \int_0^a 2UTR dR = 2 \frac{k}{\rho c_v} a \left(\frac{\partial T}{\partial R} \right)_{R=a} + a^2 \frac{Q_v}{\rho c_v} \quad (2-a)$$

and

$$\kappa = \frac{k}{\rho c_v}$$

Make the substitutions as below to obtain non-dimensional relations.

$$X = xl$$

$$R = ra$$

$$T = T_{\text{wall min}} - \frac{\nu \kappa l}{\alpha g a^4} t$$

$$U = \frac{\kappa l}{a^2} u$$

$$\begin{aligned} \frac{1}{l} \frac{\partial}{\partial x} \int_0^1 \frac{2\kappa l}{a^2} u \left(T_{\text{wall min}} - \frac{\nu \kappa l}{\alpha g a^4} t \right) (ar) d(ar) &= \\ = \frac{2\kappa a}{a} \frac{\partial}{\partial r} \left(T_{\text{wall min}} - \frac{\nu \kappa l}{\alpha g a^4} t \right)_{r=1} + \frac{a^2 Q_v}{\rho c_v} & \quad (3-a) \end{aligned}$$

$$\frac{\partial}{\partial x} \int_0^1 2u t r dr = 2 \left(\frac{\partial t}{\partial r} \right)_{r=1} - \frac{a^2}{\rho c_v} \frac{\alpha g a^4}{\kappa^2 \nu l} Q_v \quad (4-a)$$

$$\frac{\partial}{\partial x} \int_0^1 u t r dr = \left(\frac{\partial t}{\partial r} \right)_{r=1} - \frac{q_v}{2} \quad (5-a)$$

$$\left(\frac{\partial t}{\partial r}\right)_{r=1} = -t(x) \left[2 \left(\frac{r-\beta}{1-\beta}\right) \left(\frac{1}{1-\beta}\right) \right]_{r=1} = -\frac{2t(x)}{1-\beta} \quad (6-a)$$

utilizing the assumed temperature profile (2') of Chapter V)

$$\begin{aligned} \frac{\partial}{\partial x} \int_0^1 r u t dr &= \frac{\partial}{\partial x} \left(\int_0^\beta r u t dr + \int_\beta^1 r u t dr \right) = \\ &= \frac{\partial}{\partial x} \left\{ \int_0^\beta -\gamma t(x) r dr - \gamma t(x) \int_1^\beta \left[1 - \left(\frac{r-\beta}{1-\beta}\right)^2 \right] \right\} \\ &\quad \left\{ 1 - \left(\frac{r-\beta}{1-\beta}\right)^2 [1 + \delta (r - 1)] r dr \right\} \end{aligned} \quad (7-a)$$

utilizing the assumed velocity profile (1'), and the assumed temperature profile (2') of Chapter V

Following the procedure of Lighthill (Reference 10) we should get

$$\frac{\partial}{\partial x} \int_0^1 r u t dr = \underbrace{\left[-\frac{2t(x)}{1-\beta} - \frac{q_v}{2} \right]}_{\substack{\text{from (5-a) and} \\ \text{(6-a)}}$$

and also

$$= 2 \underbrace{\frac{d}{dx} [t^2(x)F(\beta)]}_{\text{from (7-a)}} \quad (8-a)$$

where

$$F(\beta) = \frac{(1-\beta)^3 (3+\beta) (45 + 132\beta + 181\beta^2 + 62\beta^3)}{30,240 (3 + 4\beta + 3\beta^2)}$$

Integrating both sides of (8-a), and considering the disc of Figure 26,

we get

$$[t^2(x)F(\beta)]_{x_2}^{x_1} = - \int_{x_2}^{x_1} \frac{t(x)}{1-\beta} dx - \frac{q_v(x_1-x_2)}{4} \quad (9-a)$$

2-A Derivation of Centerline Temperature Gradient (see Chapter V)

In dimensional quantities, it was shown in the text (Equation 11):

$$\frac{dT_c}{dx} = - \frac{Q_v}{\rho c_v U_c} \quad (11)$$

Making the non-dimensionalizing substitutions of Section 1-A

$$\frac{\partial}{\partial(x/l)} \left[T_{wall\beta} - \frac{\nu\kappa l}{\alpha g a^4} t \right] = - \frac{Q_v}{\rho c_v \frac{\kappa l}{a^2} \gamma} \quad (10-a)$$

$$\frac{\partial t}{\partial x} = \frac{Q_v a^6 \alpha g}{\rho \nu \kappa^2 l c_v \gamma} = \frac{q_v}{\gamma} \quad (11-a)$$

3-A Derivation of Difference Equations (see Chapter V)

Equation (9) may be written in an approximate form as

$$\frac{t_N^2 F_N - t_{N-1}^2 F_{N-1}}{x_N - x_{N-1}} - \left(\frac{t_N + t_{N-1}}{2} \right) \left/ \left(1 - \frac{\beta_N + \beta_{N-1}}{2} \right) \right. + \frac{q_{vN}}{4} = \Delta \quad (13)$$

For a consistent solution,

$$\Delta \rightarrow 0$$

Equation (13) combined with (6) gives

$$\bar{G}(\beta) \bar{t}(x) \Delta t(x) = q_{vN} \Delta x$$

where

$$\bar{t} = t_{N-1} - \frac{\Delta t}{2}$$

or

$$\bar{t} \Delta t = \frac{q_{vN} \Delta x}{\bar{G}}$$

and

$$\Delta t \left(t_{N-1} - \frac{\Delta t}{2} \right) - \frac{q_{vN} \Delta x}{\bar{G}} = 0$$

or

$$\Delta t = t_{N-1} \pm \sqrt{t_{N-1}^2 - \frac{2q_{vN} \Delta x}{\bar{G}}}$$

where only the negative sign has physical significance;

so

$$(\Delta t)_{N,N-1} = t_{N-1} \left(1 - \sqrt{1 - \frac{2q_{vN} \Delta x}{\bar{G} t_{N-1}^2}} \right)$$

and

$$\Delta t = t_{N-1} - t_N ;$$

$$\bar{G} = \frac{G_N + G_{N-1}}{2}$$

so that

$$t_N = t_{N-1} \sqrt{1 - \frac{4q_v \Delta x}{t_{N-1}^2 [G_N + G_{N-1}]}}$$

or, as explained in the text,

$$(t + t_w)_N = (t + t_w)_{N-1} \sqrt{1 - \frac{4q_v (x_N - x_{N-1})}{(t + t_w)_{N-1}^2 [G_N + G_{N-1}]}} \quad (16)$$

4-A Relations Between Nusselt Number, q_v , t_g (see Chapter IV)

$$Nu_a = \frac{ha}{k} = \frac{Q_a}{A_s \Delta T_{\max} k} = \frac{Q_v \pi a^3 l}{2\pi l a \Delta T_{\max} k} = \frac{\bar{Q}_v a^2}{2\Delta T_{\max} k} \quad (12-a)$$

where

Q is total heat input rate

\bar{Q}_v is mean volumetric heat input rate

By definition:

$$\frac{q_v}{2(t'_o + t_{w_o})} = \frac{\frac{Q_v a^2 \alpha g}{\nu \kappa^2 c_v \rho l}}{\frac{\alpha g a^4 \Delta T_{\max}}{\nu \kappa l}} = \frac{\bar{Q}_v a^2}{2 \Delta T_{\max} k} = Nu_a$$

Table A-I Calculation Summary Sheet - Constant Wall Temperature

Run Number	I	II	III	IV	V	VI	VII	VIII	IX	X	XI	XII
x/L	unif. qv	unif. qv	unif. qv	unif. qv	unif. qv	unif. qv	qv, sine	qv, sine	qv, sine	qv, v	qv, Δ	qv, L
0	1.000	1.000	1.000	1.000	1.000	1.000	1.000	1.000	1.000	1.000	1.000	1.000
0.01	9.278	9.548	9.704	9.786	9.846	9.902	9.953	9.997	9.997	9.994	9.972	9.951
0.10	9.794	9.548	9.509	9.446	9.339	9.239	9.211	9.228	9.231	9.274	9.469	9.591
0.50	9.172	8.863	8.259	7.467	6.615	5.757	4.823	3.947	3.150	2.505	2.019	1.622
1.00	7.357	6.356	5.124	3.925	2.945	2.249	1.764	1.419	1.150	0.926	0.778	0.672
1.50	6.939	5.822	4.704	3.646	2.826	2.249	1.805	1.481	1.250	1.011	0.824	0.717
2.00	6.538	5.314	4.257	3.328	2.640	2.149	1.764	1.481	1.250	1.011	0.824	0.717
3.00	6.404	5.102	4.057	3.228	2.640	2.149	1.764	1.481	1.250	1.011	0.824	0.717
4.00	6.431	5.102	4.057	3.228	2.640	2.149	1.764	1.481	1.250	1.011	0.824	0.717
5.00	6.529	5.237	4.192	3.375	2.845	2.449	2.064	1.764	1.500	1.250	1.011	0.824
6.00	6.657	missing	5.504	3.948	3.184	2.640	2.249	1.949	1.650	1.350	1.050	0.850
1.000	1.000	1.000	1.000	1.000	1.000	1.000	1.000	1.000	1.000	1.000	1.000	1.000
0	14.20 x 10 ³	9.070 x 10 ⁴	5.885 x 10 ⁵	1.790 x 10 ⁶	6.500 x 10 ⁶	4.082 x 10 ⁷	7.24 x 10 ⁴	1.404 x 10 ⁶	3.225 x 10 ⁷	2.507 x 10 ⁸	1.154 x 10 ⁹	9.622 x 10 ⁵
0.01	13.628 x 10 ³	4.632 x 10 ⁴	4.653 x 10 ⁵	1.695 x 10 ⁶	5.492 x 10 ⁶	3.882 x 10 ⁷	7.232 x 10 ⁴	1.403 x 10 ⁶	3.229 x 10 ⁷	2.352 x 10 ⁸	1.152 x 10 ⁹	9.622 x 10 ⁵
0.10	12.401 x 10 ³	7.897 x 10 ⁴	4.257 x 10 ⁵	1.550 x 10 ⁶	4.622 x 10 ⁶	3.551 x 10 ⁷	7.219 x 10 ⁴	1.399 x 10 ⁶	3.220 x 10 ⁷	2.079 x 10 ⁸	1.151 x 10 ⁹	9.622 x 10 ⁵
0.50	10.924 x 10 ³	6.908 x 10 ⁴	3.721 x 10 ⁵	1.351 x 10 ⁶	4.925 x 10 ⁶	3.095 x 10 ⁷	7.085 x 10 ⁴	1.372 x 10 ⁶	3.157 x 10 ⁷	1.707 x 10 ⁸	1.139 x 10 ⁹	9.622 x 10 ⁵
1.00	9.899 x 10 ³	5.517 x 10 ⁴	2.964 x 10 ⁵	1.069 x 10 ⁶	3.885 x 10 ⁶	2.415 x 10 ⁷	6.355 x 10 ⁴	1.220 x 10 ⁶	2.794 x 10 ⁷	1.200 x 10 ⁸	1.076 x 10 ⁹	9.622 x 10 ⁵
1.50	7.312 x 10 ³	4.403 x 10 ⁴	2.352 x 10 ⁵	8.41 x 10 ⁵	3.034 x 10 ⁶	1.879 x 10 ⁷	5.112 x 10 ⁴	9.600 x 10 ⁵	2.178 x 10 ⁷	8.457 x 10 ⁷	4.652 x 10 ⁸	9.622 x 10 ⁵
2.00	6.008 x 10 ³	3.472 x 10 ⁴	1.856 x 10 ⁵	6.532 x 10 ⁵	2.334 x 10 ⁶	1.448 x 10 ⁷	3.664 x 10 ⁴	6.433 x 10 ⁵	1.478 x 10 ⁷	6.305 x 10 ⁷	3.204 x 10 ⁸	9.622 x 10 ⁵
3.00	4.569 x 10 ³	2.488 x 10 ⁴	1.244 x 10 ⁵	4.52 x 10 ⁵	1.620 x 10 ⁶	1.023 x 10 ⁷	2.081 x 10 ⁴	3.289 x 10 ⁵	1.264 x 10 ⁷	5.174 x 10 ⁷	6.449 x 10 ⁸	9.622 x 10 ⁵
4.00	3.847 x 10 ³	1.851 x 10 ⁴	1.041 x 10 ⁵	3.33 x 10 ⁵	1.194 x 10 ⁶	7.244 x 10 ⁶	1.399 x 10 ⁴	1.511 x 10 ⁵	5.743 x 10 ⁶	4.923 x 10 ⁷	4.579 x 10 ⁸	9.622 x 10 ⁵
5.00	3.358 x 10 ³	1.270 x 10 ⁴	8.043 x 10 ⁴	2.33 x 10 ⁵	8.592 x 10 ⁵	4.977 x 10 ⁶	1.164 x 10 ⁴	8.679 x 10 ⁴	2.128 x 10 ⁶	4.860 x 10 ⁷	3.040 x 10 ⁸	9.622 x 10 ⁵
6.00	2.739 x 10 ³	missing	5.97 x 10 ⁴	1.11 x 10 ⁵	5.121 x 10 ⁵	2.434 x 10 ⁶	0.0	1.743 x 10 ⁴	1.743 x 10 ⁶	4.348 x 10 ⁷	0.0	9.622 x 10 ⁵
1.000	0.0 x 10 ³	0.0 x 10 ⁴	0.0 x 10 ⁵	0.0 x 10 ⁶	0.0 x 10 ⁷	0.0 x 10 ⁸	0.0	0.0	0.0	0.0	0.0	0.0
0.001	39.949 x 10 ⁴	3.920 x 10 ⁶	3.227 x 10 ⁷	1.627 x 10 ⁸	9.271 x 10 ⁸	9.178 x 10 ⁹	3.094 x 10 ⁶	1.241 x 10 ⁸	6.576 x 10 ⁹	2.478 x 10 ¹⁰	9.699 x 10 ¹¹	7.1408 x 10 ⁶
0.01	13.448 x 10 ⁴	1.373 x 10 ⁶	1.132 x 10 ⁷	5.713 x 10 ⁷	2.8.902 x 10 ⁷	2.8.794 x 10 ⁸	1.142 x 10 ⁶	4.683 x 10 ⁷	2.371 x 10 ⁹	8.479 x 10 ⁹	3.664 x 10 ¹⁰	2.9.858 x 10 ⁶
0.10	7.689 x 10 ⁴	7.939 x 10 ⁵	6.472 x 10 ⁶	3.258 x 10 ⁷	1.6.527 x 10 ⁷	1.6.422 x 10 ⁸	7.276 x 10 ⁶	2.946 x 10 ⁷	1.520 x 10 ⁹	4.607 x 10 ⁹	2.355 x 10 ¹⁰	1.8.922 x 10 ⁶
0.50	4.434 x 10 ⁴	4.468 x 10 ⁵	3.682 x 10 ⁶	1.8.51 x 10 ⁷	9.376 x 10 ⁷	9.249 x 10 ⁸	4.786 x 10 ⁶	1.944 x 10 ⁷	9.866 x 10 ⁸	2.3.944 x 10 ⁹	1.3.974 x 10 ¹⁰	1.3.090 x 10 ⁶
1.00	3.793 x 10 ⁴	3.729 x 10 ⁵	3.045 x 10 ⁶	1.1.18 x 10 ⁷	5.626 x 10 ⁷	5.487 x 10 ⁸	3.175 x 10 ⁶	1.292 x 10 ⁷	6.437 x 10 ⁸	1.2.68 x 10 ⁹	1.1.37 x 10 ¹⁰	1.0.199 x 10 ⁶
1.50	3.011 x 10 ⁴	1.992 x 10 ⁵	1.638 x 10 ⁶	7.619 x 10 ⁶	3.711 x 10 ⁷	3.612 x 10 ⁸	2.181 x 10 ⁶	9.493 x 10 ⁶	4.150 x 10 ⁸	7.749 x 10 ⁹	9.739 x 10 ¹⁰	8.975 x 10 ⁶
2.00	2.543 x 10 ⁴	1.329 x 10 ⁵	1.072 x 10 ⁶	5.122 x 10 ⁶	2.801 x 10 ⁷	2.735 x 10 ⁸	1.366 x 10 ⁶	4.862 x 10 ⁶	2.314 x 10 ⁸	5.304 x 10 ⁹	6.565 x 10 ¹⁰	6.115 x 10 ⁶
3.00	1.492 x 10 ⁴	0.948 x 10 ⁵	0.764 x 10 ⁶	3.501 x 10 ⁶	1.695 x 10 ⁷	1.635 x 10 ⁸	8.076 x 10 ⁴	2.285 x 10 ⁶	1.087 x 10 ⁸	4.298 x 10 ⁹	4.800 x 10 ¹⁰	7.709 x 10 ⁶
4.00	1.042 x 10 ⁴	0.702 x 10 ⁵	0.594 x 10 ⁶	2.448 x 10 ⁶	1.212 x 10 ⁷	1.142 x 10 ⁸	5.704 x 10 ⁴	1.395 x 10 ⁶	5.493 x 10 ⁸	3.984 x 10 ⁹	3.447 x 10 ¹⁰	7.532 x 10 ⁶
5.00	0.803 x 10 ⁴	missing	0.458 x 10 ⁵	1.581 x 10 ⁶	0.821 x 10 ⁷	7.826 x 10 ⁷	missing	missing	missing	missing	missing	missing
6.00	0.599 x 10 ⁴	0.0 x 10 ⁵	0.0 x 10 ⁶	0.0 x 10 ⁷	0.0 x 10 ⁸	0.0 x 10 ⁹	0.0	0.0	0.0	0.0	0.0	0.0
1.000	1.0	1.0	1.0	1.0	1.0	1.0	1.0	1.0	1.0	1.0	1.0	1.0
0	1 x 10 ⁵	1 x 10 ⁶	9 x 10 ⁶	4 x 10 ⁷	2 x 10 ⁸	2 x 10 ⁹	1 x 10 ¹⁰	4 x 10 ¹¹	2 x 10 ¹²	4 x 10 ¹³	4 x 10 ¹⁴	4 x 10 ¹⁵
1.420 x 10 ⁴	9.07 x 10 ⁴	4.884 x 10 ⁵	1.780 x 10 ⁶	6.500 x 10 ⁶	4.082 x 10 ⁷	2.507 x 10 ⁸	7.24 x 10 ⁴	1.404 x 10 ⁶	3.225 x 10 ⁷	2.507 x 10 ⁸	1.154 x 10 ⁹	9.622 x 10 ⁵
2.52	5.52	9.18	11.23	15.4	24.5	43.5	6.92	14.23	31.0	7.97	17.3	20.8
1.420 x 10 ⁴	9.07 x 10 ⁴	4.884 x 10 ⁵	1.780 x 10 ⁶	6.500 x 10 ⁶	4.082 x 10 ⁷	2.507 x 10 ⁸	7.24 x 10 ⁴	1.404 x 10 ⁶	3.225 x 10 ⁷	2.507 x 10 ⁸	1.154 x 10 ⁹	9.622 x 10 ⁵
1.0	1.0	1.0	1.0	1.0	1.0	1.0	1.0	1.0	1.0	1.0	1.0	1.0

q_v
T_f
N_{max}
T_w
t_{9,9}/t₀

Table A-II - Calculation Summary Sheet - Variable Wall Temperature, Uniform q_v

Run Number	x/L	XIII	XIV	XV	XVI	XVII	XVIII	XIX	XX	XXI	XXII	XXIII	XXIV
		linear t	linear t	linear t	linear t	linear t	linear t	linear t	linear t	linear t	linear t	linear t	linear t
	0	1.000	1.000	1.000	1.000	1.000	1.000	1.000	1.000	1.000	1.000	1.000	1.000
	.001	9.516	9.483	9.473	9.471	9.475	9.470	9.473	9.476	9.474	9.474	9.474	9.474
	.010	9.319	9.199	9.189	9.181	9.184	9.180	9.184	9.187	9.186	9.186	9.186	9.186
	.050	8.965	8.871	8.880	8.867	8.862	8.864	8.867	8.869	8.872	8.872	8.872	8.872
	.200	8.449	8.529	8.474	8.465	8.453	8.456	8.459	8.461	8.462	8.462	8.462	8.462
	.400	8.109	8.332	8.454	8.614	8.824	9.102	9.473	9.820	9.966	9.984	9.984	9.984
	.600	8.049	8.326	8.473	8.634	8.832	9.072	9.422	9.682	9.817	9.847	9.847	9.847
	.800	8.051	8.347	8.509	8.639	8.849	9.073	9.452	9.654	9.730	9.730	9.730	9.730
	.960	8.067	8.355	8.531	8.640	8.826	9.083	9.478	9.654	9.730	9.730	9.730	9.730
	.999	8.073	8.389	8.426	8.423	8.423	8.423	8.423	8.423	8.423	8.423	8.423	8.423
	1.000	1.000	1.000	1.000	1.000	1.000	1.000	1.000	1.000	1.000	1.000	1.000	1.000
	0	6.244 x 10 ⁴	4.94 x 10 ⁴	4.13 x 10 ⁴	3.57 x 10 ⁴	3.35 x 10 ⁴	3.22 x 10 ⁴	3.05 x 10 ⁴	2.87 x 10 ⁴	2.68 x 10 ⁴	2.48 x 10 ⁴	2.28 x 10 ⁴	2.08 x 10 ⁴
	.001	6.281 x 10 ⁴	4.794 x 10 ⁴	4.108 x 10 ⁴	3.508 x 10 ⁴	3.338 x 10 ⁴	3.199 x 10 ⁴	3.032 x 10 ⁴	2.84 x 10 ⁴	2.64 x 10 ⁴	2.44 x 10 ⁴	2.24 x 10 ⁴	2.04 x 10 ⁴
	.010	6.022 x 10 ⁴	4.702 x 10 ⁴	4.065 x 10 ⁴	3.491 x 10 ⁴	3.256 x 10 ⁴	3.105 x 10 ⁴	2.928 x 10 ⁴	2.728 x 10 ⁴	2.528 x 10 ⁴	2.328 x 10 ⁴	2.128 x 10 ⁴	1.928 x 10 ⁴
	.050	5.614 x 10 ⁴	4.590 x 10 ⁴	3.997 x 10 ⁴	3.454 x 10 ⁴	3.242 x 10 ⁴	3.067 x 10 ⁴	2.871 x 10 ⁴	2.654 x 10 ⁴	2.437 x 10 ⁴	2.220 x 10 ⁴	2.003 x 10 ⁴	1.786 x 10 ⁴
	.200	4.993 x 10 ⁴	4.342 x 10 ⁴	3.982 x 10 ⁴	3.437 x 10 ⁴	3.231 x 10 ⁴	3.056 x 10 ⁴	2.850 x 10 ⁴	2.624 x 10 ⁴	2.407 x 10 ⁴	2.190 x 10 ⁴	1.973 x 10 ⁴	1.756 x 10 ⁴
	.400	4.419 x 10 ⁴	4.087 x 10 ⁴	3.921 x 10 ⁴	3.855 x 10 ⁴	3.816 x 10 ⁴	3.790 x 10 ⁴	3.764 x 10 ⁴	3.738 x 10 ⁴	3.712 x 10 ⁴	3.686 x 10 ⁴	3.660 x 10 ⁴	3.634 x 10 ⁴
	.600	3.842 x 10 ⁴	3.782 x 10 ⁴	3.616 x 10 ⁴	3.494 x 10 ⁴	3.453 x 10 ⁴	3.431 x 10 ⁴	3.414 x 10 ⁴	3.397 x 10 ⁴	3.380 x 10 ⁴	3.363 x 10 ⁴	3.346 x 10 ⁴	3.329 x 10 ⁴
	.800	3.068 x 10 ⁴	3.270 x 10 ⁴	3.235 x 10 ⁴	3.214 x 10 ⁴	3.219 x 10 ⁴	3.225 x 10 ⁴	3.231 x 10 ⁴	3.237 x 10 ⁴	3.243 x 10 ⁴	3.249 x 10 ⁴	3.255 x 10 ⁴	3.261 x 10 ⁴
	.960	2.519 x 10 ⁴	2.829 x 10 ⁴	2.972 x 10 ⁴	3.092 x 10 ⁴	3.180 x 10 ⁴	3.240 x 10 ⁴	3.281 x 10 ⁴	3.314 x 10 ⁴	3.347 x 10 ⁴	3.380 x 10 ⁴	3.413 x 10 ⁴	3.446 x 10 ⁴
	.999	1.520 x 10 ⁴	1.671 x 10 ⁴	1.502 x 10 ⁴	1.222 x 10 ⁴	—	1.642 x 10 ⁴	1.378 x 10 ⁴	1.178 x 10 ⁴	1.011 x 10 ⁴	1.000	1.000	1.000
	1.000	1.000	1.000	1.000	1.000	1.000	1.000	1.000	1.000	1.000	1.000	1.000	1.000
	.0001	2.409 x 10 ⁶	1.983 x 10 ⁶	1.582 x 10 ⁶	1.450 x 10 ⁶	1.310 x 10 ⁶	1.085 x 10 ⁶	9.772 x 10 ⁵	8.440 x 10 ⁵	6.857 x 10 ⁵	5.549 x 10 ⁵	4.416 x 10 ⁵	3.444 x 10 ⁵
	.001	2.415 x 10 ⁶	1.989 x 10 ⁶	1.587 x 10 ⁶	1.458 x 10 ⁶	1.319 x 10 ⁶	1.090 x 10 ⁶	9.778 x 10 ⁵	8.448 x 10 ⁵	6.861 x 10 ⁵	5.551 x 10 ⁵	4.418 x 10 ⁵	3.446 x 10 ⁵
	.010	2.002 x 10 ⁶	1.643 x 10 ⁶	1.276 x 10 ⁶	1.178 x 10 ⁶	1.041 x 10 ⁶	8.441 x 10 ⁵	7.143 x 10 ⁵	5.844 x 10 ⁵	4.545 x 10 ⁵	3.246 x 10 ⁵	1.947 x 10 ⁵	6.896 x 10 ⁴
	.050	1.200 x 10 ⁶	9.751 x 10 ⁵	7.511 x 10 ⁵	6.859 x 10 ⁵	6.041 x 10 ⁵	4.541 x 10 ⁵	3.243 x 10 ⁵	1.946 x 10 ⁵	6.857 x 10 ⁴	3.246 x 10 ⁴	1.947 x 10 ⁴	6.897 x 10 ³
	.200	8.000 x 10 ⁵	6.254 x 10 ⁵	4.944 x 10 ⁵	4.544 x 10 ⁵	3.944 x 10 ⁵	2.944 x 10 ⁵	2.144 x 10 ⁵	1.544 x 10 ⁵	1.044 x 10 ⁵	6.444 x 10 ⁴	3.444 x 10 ⁴	1.444 x 10 ⁴
	.400	5.000 x 10 ⁵	3.944 x 10 ⁵	3.044 x 10 ⁵	2.844 x 10 ⁵	2.444 x 10 ⁵	1.844 x 10 ⁵	1.344 x 10 ⁵	9.444 x 10 ⁴	6.444 x 10 ⁴	4.444 x 10 ⁴	3.444 x 10 ⁴	2.444 x 10 ⁴
	.600	3.000 x 10 ⁵	2.344 x 10 ⁵	1.844 x 10 ⁵	1.744 x 10 ⁵	1.544 x 10 ⁵	1.144 x 10 ⁵	8.444 x 10 ⁴	6.444 x 10 ⁴	4.444 x 10 ⁴	3.444 x 10 ⁴	2.444 x 10 ⁴	1.444 x 10 ⁴
	.800	1.433 x 10 ⁵	1.133 x 10 ⁵	8.844 x 10 ⁴	8.344 x 10 ⁴	7.144 x 10 ⁴	5.244 x 10 ⁴	3.744 x 10 ⁴	2.644 x 10 ⁴	1.844 x 10 ⁴	1.244 x 10 ⁴	8.444 x 10 ³	5.444 x 10 ³
	.960	1.142 x 10 ⁵	1.070 x 10 ⁵	1.000 x 10 ⁵	1.000 x 10 ⁵	1.000 x 10 ⁵	1.000 x 10 ⁵	1.000 x 10 ⁵	1.000 x 10 ⁵	1.000 x 10 ⁵	1.000 x 10 ⁵	1.000 x 10 ⁵	1.000 x 10 ⁵
	.999	1.142 x 10 ⁵	1.142 x 10 ⁵	1.142 x 10 ⁵	1.142 x 10 ⁵	1.142 x 10 ⁵	1.142 x 10 ⁵	1.142 x 10 ⁵	1.142 x 10 ⁵	1.142 x 10 ⁵	1.142 x 10 ⁵	1.142 x 10 ⁵	1.142 x 10 ⁵
	1.000	1.000	1.000	1.000	1.000	1.000	1.000	1.000	1.000	1.000	1.000	1.000	1.000
	3.06	11.97	26.71	1.414	1.940	3.12	6.95	12.46	27.35	59.59	3.249	13.319	

q_v

t₁

N_w

t₂

t₂/t₁

Table A-III Calculation Summary Sheet - Variable Wall Temperature, Uniform q_v concluded

Run Number	x/L	XXV Linear t	XXVI Linear t	XXVII Parabolic t	XXVIII Parabolic t	XXIX Parabolic t				
	0	1.000	1.000	1.000	1.000	1.000				
	.01	.9884	.9881	.9765	.9891	.9507				
	.010	.9824	.9821	.9625	.9826	.9208				
	.050	.9764	.9761	.9460	.9750	.8855				
	.200	.9704	.9701	.9280	.9669	.8464				
β	.400	.8694	.9727	.9191	.9639	.8289				
	.600	.9699	.9739	.9161	.9638	.8240				
	.800	.9727	.9772	.9177	.9672	.8288				
	.900	.9841	.9912	.9208	.9932	.8370				
	.950	.9899	.9955	.9237	.9983	.8452				
	.999	.9929	.9925	.9207	.9983	.8452				
	1.000	1.000	1.000	1.000	1.000	1.000				
	0	1.655×10^7	1.43×10^7	1.40×10^6	2.430×10^7	5.920×10^4				
	.001	1.646×10^7	1.426×10^7	1.110×10^6	2.363×10^7	5.766×10^4				
	.010	1.627×10^7	1.417×10^7	1.057×10^6	2.343×10^7	5.495×10^4				
	.050	1.594×10^7	1.400×10^7	9.826×10^5	2.274×10^7	5.120×10^4				
	.200	1.526×10^7	1.359×10^7	8.472×10^5	1.908×10^7	4.554×10^4				
t	.400	1.439×10^7	1.237×10^7	7.588×10^5	1.564×10^7	4.068×10^4				
	.600	1.315×10^7	1.202×10^7	6.777×10^5	1.318×10^7	3.612×10^4				
	.800	1.024×10^7	9.636×10^6	5.640×10^5	9.468×10^6	3.031×10^4				
	.900	5.046×10^6	4.042×10^6	4.752×10^5	2.486×10^6	2.569×10^4				
	.960	4.998×10^6	4.019×10^6	2.757×10^5	1.580×10^6	2.028×10^4				
	.999	4.940×10^6	3.961×10^6	1.742×10^5		2.354×10^3				
	1.000	0.0	1.00	1.00	1.00	1.00				
	.001	2.727×10^6	2.408×10^6	9.598×10^5	4.449×10^6	2.369×10^6				
	.010	1.119×10^6	9.565×10^5	3.559×10^5	1.633×10^6	9.763×10^5				
	.050	7.905×10^5	6.753×10^5	2.229×10^5	1.019×10^6	5.492×10^5				
	.200	5.758×10^5	5.441×10^5	1.468×10^5	6.076×10^5	3.610×10^5				
Wall	.400	4.919×10^5	4.908×10^5	1.070×10^5	4.869×10^5	2.656×10^5				
Conduction	.600	4.539×10^5	4.692×10^5	3.773×10^5	3.994×10^5	2.303×10^5				
	.800	4.098×10^5	4.480×10^5	2.471×10^5	3.292×10^5	1.914×10^5				
	.900	3.566×10^5	4.334×10^5	1.441×10^5	3.021×10^5	1.676×10^5				
	.960	1.763×10^5	1.514×10^5	6.479×10^4	4.413×10^5	1.447×10^5				
	.999	1.127×10^5	8.69×10^4	3.886×10^4		9.248×10^4				
	1.000									
		2×10^9	2×10^9	4×10^7	2×10^9	1×10^6				
q_v		4.935×10^5	9.682×10^5	3.74×10^6	8.49×10^7	1.919×10^5				
t/t_0		2.026	1.032	5.35	11.78	2.61				
N_{we}		1.655×10^5	1.43×10^5	1.140×10^6	2.43×10^7	5.92×10^4				
t_0/t_0		29.92	67.1	3.29	3.49	3.24				

Table A-IV Experimental Data Summary Sheet I, Water-Cooled Full length Run

Run Number	1	2	3	4	5	6	7	8	9	10	11	12	13	14
Facility	Water-Land	Water-Land	Water-Land	Water-Land	Water-Land	Water-Land	Water-Land	Water-Land	Water-Land	Water-Land	Water-Land	Water-Land	Water-Land	Water-Land
Coolant Direction	Counters	Counters	Counters	Counters	Counters	Counters	Counters	Counters	Counters	Counters	Counters	Counters	Counters	Counters
Coolant Flow Rate (gpm)	660	660	660	660	660	660	660	660	660	660	660	660	660	660
Power Input (watts)	400	490	550	594	830	950	1040	1140	1760	1920	2440	359.5	450	600
$t_{in} + t_{out} = t$	1.02 x 10 ⁷	1.06 x 10 ⁷	4.52 x 10 ⁶	4.58 x 10 ⁶	2.08 x 10 ⁷	1.68 x 10 ⁷	1.36 x 10 ⁷	1.02 x 10 ⁷	4.02 x 10 ⁷	3.68 x 10 ⁷	2.85 x 10 ⁷	5.72 x 10 ⁶	5.43 x 10 ⁶	1.13 x 10 ⁷
$(t_{out} - t_{in}) / t = \Delta t / t$	4.76	4.32	6.68	4.38	5.07	3.85	3.54	2.96	6.73	5.72	4.18	4.98 (?)	2.01	3.12
T mean (°F)	9.71	9.43	9.12	8.93	13.16	17.86	22.06	27.78	23.70	27.17	35.09	17.48	18.42	26.55
	107.0	99.45	90.3	87.47	133.9	122.52	114.27	111.19	182	170	146.1	112.4	101.6	143.3
Power Out (Coolant)	339	689	730	457	797	951	1200	1303	1389	1979	2622	206	615	636
Test Section length (ft)	1.855	1.855	1.855	1.855	1.855	1.855	1.855	1.855	1.855	1.855	1.855	1.855	1.855	1.855
Test Section Radius (ft)	0.156	0.156	0.156	0.156	0.156	0.156	0.156	0.156	0.156	0.156	0.156	0.156	0.156	0.156
length / Radius	11.9	11.9	11.9	11.9	11.9	11.9	11.9	11.9	11.9	11.9	11.9	11.9	11.9	11.9
μ_{top} / μ_{bot}	Top (1/0.015)	230/120	—	—	—	—	380/93	435/70	475/170	—	—	—	220/170	—
	Mid. (1/0.018)	230/77	—	—	—	—	1080/93	825/76	390/155	—	—	—	170/135	—
	Bottom (1/0.025)	230/30	—	—	—	—	220/93	505/70	475/140	—	—	—	170/90	—
β	Top (1/0.015)	1.90	—	—	—	—	963	—	833	—	—	—	—	—
	Mid (1/0.018)	1.90	—	—	—	—	963	—	833	—	—	—	—	—
	Bottom (1/0.025)	1.90	—	—	—	—	963	—	866	—	—	—	—	—
% Power Error	15.3	43.5	32.7	23.0	10.52	5.001	1.54	1.43	1.54	0.31	0.91	1.16	0.37	1.04
Turbulence	Core laminar	—	—	—	—	—	—	Everywhere turbulent except at bottom	—	—	—	—	—	—
	2/3 up, turb. at top	—	—	—	—	—	—	—	—	—	—	—	—	—
Normalized Wall Cond														
X/L = 0.25	1.445	1.145	1.13	1.206	1.33	1.156	1.085	1.064	1.351	1.160	1.057	1.14	1.139	1.252
X/L = 0.55	1.0	1.0	1.0	1.0	1.0	1.0	1.0	1.0	1.0	1.0	1.0	1.0	1.00	1.00
X/L = 0.78	5.60	7.42	8.4	9.4	5.75	9.4	9.1	8.6	6.55	8.59	8.72	8.17	9.93	7.75
Temp. Top (X/L = .25)	9.25	9.3	9.25	9.4	9.2	9.0	9.5	9.46	9.46	9.65	9.40	9.65	9.52	9.65
Temp. Mid (X/L = .55)	9.2	9.2	9.2	9.0	9.2	9.0	9.5	9.50	9.50	9.65	9.00	9.50	9.70	9.70
Temp. Bot. (X/L = .78)	9.3	9.2	9.4	9.0	9.2	9.2	9.4	9.40	9.40	9.40	9.20	9.50	9.52	9.70
Re _d	2.07 x 10 ⁴	2.13 x 10 ⁴	906 x 10 ⁴	920 x 10 ⁴	4.57 x 10 ⁵	3.37 x 10 ⁵	2.73 x 10 ⁵	2.17 x 10 ⁵	9.46 x 10 ⁵	7.38 x 10 ⁵	5.72 x 10 ⁵	1.145 x 10 ⁶	1.09 x 10 ⁶	2.27 x 10 ⁶

Table A-V Experimental Data Summary Sheet II, Water-Cooled Reduced Length Runs

Run Number	15	16	17	18	19	20	21	22	23	24	25	26	27	28
Facility	Water	Water	Water	Water	Water	Water	Water	Water	Water	Water	Water	Water	Water	Water
Coolest Direction	Max length Co-flow	Max length Co-flow	Max length Co-flow	Max length Co-flow	Max length Co-flow	Max length Co-flow	Min length Co-flow	Min length Co-flow	Min length Co-flow	Min length Co-flow	Min length Co-flow	Min length Co-flow	Min length Co-flow	Min length Co-flow
Coolant Rate (GPM)	1.0	10.0	6.58	2.0 x 10 ⁹	2.0 x 10 ⁹	2.0 x 10 ⁹	2.0 x 10 ⁹	2.0 x 10 ⁹	2.0 x 10 ⁹	7.60	1.0	10.0	16.0	2.0 x 10 ⁹
Power Input (Watts)	6.0 x 10 ⁸	6.0 x 10 ⁸	2.0 x 10 ⁹	2.0 x 10 ⁹	2.0 x 10 ⁹	2.0 x 10 ⁹	2.0 x 10 ⁹	2.0 x 10 ⁹	2.0 x 10 ⁹	6.0 x 10 ⁹	6.0 x 10 ⁹	6.0 x 10 ⁹	6.0 x 10 ⁹	6.0 x 10 ⁹
t _o + t _w + t _f	9.0	10.50	15.04	19.20	2.130	1.33	3.00	3.12	3.76	5.70	5.85	6.40	13.0	3.00
(t _o + t _w) / t _o + t _f	1.10 x 10 ⁷	1.095 x 10 ⁷	2.68 x 10 ⁷	2.70 x 10 ⁷	2.35 x 10 ⁷	1.65 x 10 ⁷	2.38 x 10 ⁷	3.09 x 10 ⁷	2.65 x 10 ⁷	6.46 x 10 ⁷	8.12 x 10 ⁷	5.92 x 10 ⁷	9.23 x 10 ⁷	1.95 x 10 ⁷
N _{max}	1.97	1.95	2.57	1.70	2.43	3.99	3.53	4.24	4.57	3.90	6.80	4.35	2.44	3.67
T _{mean} (°F)	27.27	27.40	27.31	27.04	42.55	9.39	42.02	32.36	37.67	46.44	36.95	50.68	22.5	51.38
Power Output (Watts)	126.9	116.0	191.54	171.8	158	8.8	112	110	100	144	—	—	88.5	111
Test Section length-ft.	1093	1201	1419	2305	1627	—	—	—	—	—	—	—	—	—
Test Section Radius-ft.	0.156	0.156	0.156	0.156	0.156	0.156	0.156	0.156	0.156	0.156	0.156	0.156	0.156	0.156
Length / radius	11.9	11.9	11.9	11.9	11.9	3.34	3.34	3.34	3.34	3.34	3.34	3.34	3.34	3.34
h _o / h _c Top (1/4" x 0.157)	790/67	435/220	585/96	—	—	—	—	—	—	—	—	—	—	—
Mid (1/4" x 0.118)	425/210	435/190	390/185	—	—	610/122	1156/578	—	—	2190/730	—	—	—	—
Bot. (1/4" x 0.181)	320/73	325/170	293/155	—	—	—	—	—	—	—	—	—	—	—
h _o / h _c Top (1/4" x 0.157)	977	—	983	—	—	—	—	—	—	—	—	—	—	—
Mid (1/4" x 0.118)	799	—	900	—	—	—	—	—	—	—	—	—	—	—
Bot. (1/4" x 0.181)	933	—	967	—	—	—	—	—	—	—	—	—	—	—
1/4 Power Error Elec-Cool	—	—	—	—	—	—	—	—	—	—	—	—	—	—
Turbulence	—	—	—	—	—	—	—	—	—	—	—	—	—	—
Normalized Wall Conductivity	—	—	—	—	—	—	—	—	—	—	—	—	—	—
k/L = 0.25	1.072	1.065	1.189	1.035	1.034	1.11	1.13	1.036	1.11	1.11	1.093	1.077	1.064	1.00
k/L = 0.55	1.00	1.00	1.00	1.00	1.00	1.00	1.00	1.00	1.00	1.00	1.00	1.00	1.00	1.00
k/L = 0.78	0.48	0.82	0.66	0.95	0.29	0.45	0.64	0.91	0.49?	0.45	0.79	0.92	0.61	0.73
h _o / h _c Top (1/4" x 0.25)	93	965	965	965	965	—	—	920	—	952	—	—	—	—
Mid (1/4" x 0.55)	965	965	972	975	952	—	—	965	—	965	—	—	—	—
Bot. (1/4" x 0.78)	955	965	972	965	930	—	—	952	—	972	—	—	—	—
h _o / h _c Top	2.21 x 10 ⁹	2.19 x 10 ⁹	5.38 x 10 ⁹	5.42 x 10 ⁹	4.72 x 10 ⁹	1.335 x 10 ⁹	2.99 x 10 ⁹	3.88 x 10 ⁹	3.33 x 10 ⁹	9.11 x 10 ⁹	1.02 x 10 ⁹	7.43 x 10 ⁹	1.16 x 10 ⁹	2.45 x 10 ⁹

Some turb. fluctuations of temperature

Some turb. fluctuations of temperature

Some turb. fluctuations of temperature

Some turb. fluctuations of temperature

Table A-VI Experimental Data Summary Sheet III Water-Cooled Reduced length & AEC Runs

Run Number	29	30	31	32	33	34	35
Facility	Water	Water	Water	Water	AEC	AEC	AEC
Coolant Direction	Min. length Co-flow	Min. length Co-flow	Min. length Co-flow	Min. length Co-flow	Water Cooled	Water Cooled	Water Cooled
Coolant Rate (CFM)	10.0	10.0	1.0	10.0	3.14	4.0	1.65
q_v	2×10^9	2×10^{10}	6×10^9	6×10^9	1.889×10^{10}	1.147×10^{10}	1.355×10^{10}
Power Input (Watts)	332	1400	585	645	2200	1900	2100
$t_w + t_{w2} + t_b$	2.44×10^7	1.75×10^9	6.56×10^7	6.33×10^7	2.64×10^8	1.98×10^8	2.40×10^8
$(t_w + t_{w2}) / t_w = 4.98$	3.98	4.76	4.76	4.43	42.1	48.8	32.4
Nusselt	40.98	57.14	45.73	47.39	26.31	30.34	28.23
Temperature $^{\circ}F$	106	182	145	133	178	174	191
Power Output (Coolant)	---	---	---	---	---	---	---
Test Section length - ft.	0.521	0.521	0.521	0.521	2.100	1.750	1.930
Test Section Radius - ft.	0.156	0.156	0.156	0.156	0.25	0.25	0.25
length / Radius	3.34	3.34	3.34	3.34	8.0	8.0	8.0
Wgt. Loc. Top ($x/L = 0.157$)	---	---	---	---	↑	↑	↑
Mid. ($x/L = 0.418$)	---	---	---	---	583 / 55.4	553 / 55.4	583 / 55.4
Bot. ($x/L = 0.787$)	---	---	---	---	↓	↓	↓
β Top ($x/L = 0.157$)	---	---	---	---	---	---	---
Mid. ($x/L = 0.418$)	---	---	---	---	---	---	---
Bot. ($x/L = 0.787$)	---	---	---	---	---	---	---
% Power Error Elec.	-2.41	-0.26	+0.24	---	+0.455	+0.079	+0.81
Turbulence	Turbulent	Very turbulent	Turbulent	Turbulent	Temperature fluctuations	Temperature fluctuations	Temperature fluctuations
Normalized Wall Cond.	1.057	1.072	1.005	1.014	1.013 @ 42	1.01 @ 46	---
$x/L = .25$	1.00	1.00	1.00	1.00	1.00 @ 48	1.00 @ 43	1.00 @ 467
$x/L = .75$.909	.919	.982	.947	.922 @ 23	.833 @ 23	.957 @ 23
β Temp Top ($x/L = .25$)	---	---	---	---	---	---	---
Mid. ($x/L = .5$)	---	---	---	---	---	---	---
Bot. ($x/L = .75$)	---	---	---	---	---	---	---
Re_x	3.06×10^9	2.20×10^{10}	8.24×10^9	7.95×10^9	1.11×10^{12}	7.92×10^{11}	1.007×10^{12}

Table A-VIII Experimental Data Summary Sheet IX - Air-Cooled Runs

Run Number	36	37	38	39	40	41	42	43	44	45	46	47	
Facility	Air	Air	Air	Air	Air	Air	Air	Air	Air	Air	Air	Air-Cooled	
Coilant	Max. length Natl. Conv. 5.42 x 10 ⁶	Max. length Natl. Conv. 1.693 x 10 ⁷	Max. length Natl. Conv. 2.1 x 10 ⁷	Max. length Natl. Conv. 3.11 x 10 ⁷	Max. length Natl. Conv. 1.607 x 10 ⁷	Max. length Natl. Conv. 1.617 x 10 ⁷	Max. length Natl. Conv. 2.99 x 10 ⁷	Max. length Natl. Conv. 2.99 x 10 ⁷	Max. length Natl. Conv. 2.01 x 10 ⁷	Max. length Natl. Conv. 16.4	Max. length Natl. Conv. 4.19 x 10 ⁷	Max. length Natl. Conv. 5.92 x 10 ⁷	Max. length Natl. Conv. 1.034 x 10 ⁸
Power Input (Watts)	30.4	72.7	79.2	92.0	30.6	24.3	46.9	67.8	16.4	27.0	31.4	43.0	
Flow rate = $\frac{Q}{\rho \cdot c_p \cdot \Delta T}$	1.513 x 10 ⁶	3.42 x 10 ⁶	6.42 x 10 ⁶	9.72 x 10 ⁶	3.77 x 10 ⁶	2.45 x 10 ⁶	6.02 x 10 ⁶	1.07 x 10 ⁷	3.81 x 10 ⁶	6.35 x 10 ⁶	1.005 x 10 ⁷	1.494 x 10 ⁷	
Nusselt	1.79	3.47	1.636	2.88	22.4	11.6	12.52	19.6	15.53	16.42	15.77	19.70	
Time - °F	119.7	138.0	161.5	180.1	138	122	160	188	121	129	159	187	
Test Section length-ft.	1.657	1.657	1.657	1.657	1.103	1.103	1.103	1.103	0.641	0.641	0.641	0.641	
Test Section Radius-ft.	0.1093	0.1093	0.1093	0.1093	0.1093	0.1093	0.1093	0.1093	0.1093	0.1093	0.1093	0.1093	
length / Radius	15.17	15.17	15.17	15.17	10.09	10.09	10.09	10.09	5.86	5.86	5.86	5.86	
$W_{b, 1/4} \text{ Top } (\frac{1}{4} \text{ in. } \times .25)$	31.9	167 / 33.4	167 / 33.4	167 / 33.4	99.3 / 22.2	99.3 / 22.2	99.3 / 22.2	99.3 / 22.2	22.8 / 11.4	22.8 / 11.4	22.8 / 11.4	22.8 / 11.4	
$W_{b, 1/4} \text{ Mid } (\frac{1}{4} \text{ in. } \times .5)$	21.9	17.0 / 17.0	110 / 46.6	41.3 / 41.3	16.5 / 23.3	15.7 / 15.7	25.2 / 15.5	22.8 / 11.4	22.8 / 11.4	22.8 / 11.4	22.8 / 11.4	22.8 / 11.4	
$W_{b, 1/4} \text{ Bot. } (\frac{1}{4} \text{ in. } \times .75)$	21.9	66.7 / 23.3	66.7 / 23.3	66.7 / 23.3	128.3 / 23.3	128.3 / 23.3	128.3 / 23.3	128.3 / 23.3	128.3 / 23.3	128.3 / 23.3	128.3 / 23.3	128.3 / 23.3	
β	Top ($\frac{1}{4} \text{ in. } \times .25$) Mid ($\frac{1}{4} \text{ in. } \times .5$) Bot. ($\frac{1}{4} \text{ in. } \times .75$)	0.686 0.286 0.286	0.686 0.286 0.286	0.686 0.286 0.286	0.686 0.286 0.286	0.686 0.286 0.286	0.686 0.286 0.286	0.686 0.286 0.286	0.686 0.286 0.286	0.686 0.286 0.286	0.686 0.286 0.286	0.686 0.286 0.286	
% Power Error	laminar	laminar	laminar	laminar	laminar	laminar	laminar	laminar	laminar	laminar	laminar	laminar	
Turbulence	laminar	Turbulent at exit top	Turbulent at exit top	Turbulent at exit top	All laminar	All laminar	All laminar	All laminar	All laminar	All laminar	All laminar	All laminar	
Normalized wall cond.	$\frac{1}{L} = .25$ $\frac{1}{L} = .50$ $\frac{1}{L} = .75$	1.20 1.15 1.15	1.07 1.13 1.13	.97 1.03 1.03	1.037 1.00 1.072	1.13 1.00 1.26	1.032 1.00 1.029	.892 1.00 0.882	1.08 1.00 0.889	.895 1.00 0.921	1.053 1.00 1.062	1.137 1.00 1.052	
β	Top ($\frac{1}{4} \text{ in. } \times .25$) Mid ($\frac{1}{4} \text{ in. } \times .50$) Bot. ($\frac{1}{4} \text{ in. } \times .75$)	.97 .97 .92	.96 .97 .95	.86 0.96 0.96	.90 .96 .96	.955 .975 .962	.940 .945 .960	.955 .950 .955	.960 .959 .950	.960 .960 .960	.962 .979 .979	.970 .960 .960	
Re_{α}	8.04×10^{10}	1.82×10^{11}	3.41×10^{10}	5.19×10^{11}	3.91×10^{10}	2.54×10^{10}	6.29×10^{10}	1.167×10^{11}	4.50×10^9	7.48×10^9	1.185×10^{10}	2.00×10^{10}	

BIBLIOGRAPHY

1. Schmidt, E. and Beckmann, W., *Tech. Mech. Thermod.* 1 (1930) 341-349 and 391-406.
2. Saunders, O. A., *Proc. Roy. Soc.* 157 (1936), 278-291.
3. Ostrach, S. "An Analysis of Laminar Free-Convection Flow and Heat Transfer About a Flat Plate Parallel to the Direction of the Generating Body Force", NACA Report 1111, 1953.
4. Ostrach, S. "Laminar Natural-Convection Flow and Heat Transfer of Fluids With and Without Heat Sources in Channels With Constant Wall Temperature", NACA Technical Note 2863, December 1952.
5. Ostrach, S. "Combined Natural-and Forced-Convection Laminar Flow and Heat Transfer to Fluids With and Without Heat Sources in Channels With Linearly Varying Wall Temperatures", NACA Technical Note 3141, April 1954.
6. Lighthill, M. J., "Theoretical Considerations on Free Convection in Tubes," Quarterly Journal of Mechanics and Applied Mathematics, Vol. 6, 1953, pp 398-439.
7. Ostrach, S., and Thornton, P. R. "On the Stagnation of Natural Convection Flows in Closed-End Tubes," ASME Paper No. 57-SA-2.
8. Murgatroyd, W., "Thermal Convection in a Long Cell Containing a Heat Generating Fluid", Atomic Energy Research Establishment ED/R 1559, Harwell, Berks, England, 1954.
9. Martin, B. W., "Free Convection in an Open Thermosyphen, with Special Reference to Turbulent Flow", *Proc. of Royal Society, Series A*, Vol. 230, 1955, pp 502-530.
10. Haas, P. A., and Langsdon, J. K, HRP-CP Heat Removal From a Proposed Hydroclone Underflow Pot Geometry for a Volume Heat Source, CF-55-10-7, Oak Ridge National Laboratory, October 5, 1955.
11. Hamilton, D. C., et al, "Free Convection in Fluids Having a Volume Heat Source," ORNL 1769, Oak Ridge National Laboratory, December 3, 1954.
12. Hamilton, D. C., and Lynch, F. E., "Free Convection Theory and Experiment in Fluids Having a Volume Heat Source, ORNL 1888, Oak Ridge National Laboratory, August 19, 1955.

13. Poppendiek, H. F., and Palmer, L. D., "Application of Temperature Solutions for Forced Convection Systems with Volume Heat Sources to General Convection Problems", ORNL 1933, Oak Ridge National Laboratory, October 25, 1955.
14. International Critical Tables, Volumes 3, 4, 5, 6, 7, 9.
15. Perry, J. H., Chemical Engineers Handbook, McGraw Hill Book Company, Inc. (1950).
16. Handbook of Physics and Chemistry, 35th Edition, Chemical Rubber Publishing Company (1953-4).